

N76-77707

PROCEEDINGS OF THE CONFERENCE ON PROPELLANT
TANK PRESSURIZATION AND STRATIFICATION
January 20, 21, 1965

VOLUME I
of
TWO VOLUMES

National Aeronautics and Space Administration



GEORGE C. MARSHALL SPACE FLIGHT CENTER

PROCEEDINGS OF THE CONFERENCE ON PROPELLANT
TANK PRESSURIZATION AND STRATIFICATION
January 20,21, 1965

Volume I
of
Two Volumes

PROPULSION DIVISION
PROPULSION AND VEHICLE ENGINEERING LABORATORY

TABLE OF CONTENTS **FOR VOLUME I**

	Page
FOREWORD.....	1
CHAIRMEN AND COMMITTEES.....	2
 SESSION I 	
Analytical Investigation of Some Important Parameters in the Pressurized Liquid Hydrogen Tank Outflow Problem WILLIAM A. ROUDEBUSH and DAVID A. MANDELL NASA/Lewis Research Center.....	3
Experimental and Analytical Studies of Cryogenic Propellant Tank Pressurization M. E. NEIN, NASA/George C. Marshall Space Flight Center J. F. THOMPSON, JR., Mississippi State University.....	29
Fast Response Thermocouple for the Measurement of Temperatures in Cryogenic Gases C. C. ROBINSON, A. R. LOWRIE, and T. BIELAWSKI Beech Aircraft Corporation.....	55
Propellant Tank Pressurization by Internal Combustion PAUL A. FRIEDMAN and RICHARD J. KENNY Martin Company.....	69
A Cryogenic Helium Pressurization System for the Lunar Excursion Module J. C. SMITHSON and W. R. SCOTT NASA/Manned Spacecraft Center.....	109
Bulk Liquid Interfacial Mass Transfer with Variable Ullage Pressure; Dimensionless Mass Transfer Alignment Chart for Suddenly Pressurized Liquid-Vapor Systems JOHN R. O'LOUGHLIN, Consultant to The Boeing Company, Associate Professor of Mechanical Engineering, Tulane University.....	125
 SESSION II 	
Thermal Analysis and Description of Liquid Hydrogen Tank Fluid Line Fittings JOSEPH M. FOWLER The Boeing Company.....	157

TABLE OF CONTENTS

	Page
Thermal Design of Cryogenic Heat Exchangers for Space Vehicle Pressurization Systems	
J. H. HARGIS, Brown Engineering Company, Inc.	
H. A. STOKES, Chrysler Corporation.....	189
Weight Optimization of a Gas Generator/Heat Exchanger Subsystem During the Initial Design of a Pressurization System: Two Computer Programs	
DR. W. A. MUTH, Martin Company.....	215
Digital Computer Analysis of Pneumatic Pressure Regulator Dynamics	
JAMES G. ABSALOM, Rocketdyne Division North American Aviation, Inc.....	245
Servomechanism Approach to Facility Tank Pressurization	
SANFORD M. GOLDSTEIN and KURT J. SCHURMAN Rocketdyne Division, North American Aviation, Inc.....	297
Cryogenic Storage of Helium for Propellant Tank Pressurization	
J. S. TYLER, AiResearch Manufacturing Company.....	327

TABLE OF CONTENTS **FOR VOLUME II**

SESSION III

	Page
A Theoretical Model for Predicting Thermal Stratification and Self-Pressurization of a Fluid Container	
R. W. ARNETT and D. R. MILLHISER	
Institute for Material Research, National Bureau of Standards.....	1
Investigation of Stratification Reduction Techniques	
B. D. NEFF	
Martin Company.....	21
Stratification Reduction by Means of Bubble Pumps	
D. C. PEDREYRA	
Martin Company.....	43
Experimental Investigation of the Effects of Baffles on Natural Convection Flow and on Stratification	
G. C. ULIET and J. J. BROGAN	
Lockheed Missiles and Space Company.....	61
Transient Laminar Free Convection Heat and Mass Transfer in Two-Dimensional Closed Containers Containing Distributed Heat Source	
HUSSEIN Z. BARAKAT	
University of Michigan.....	87
Transient, Laminar, Free-Convection Heat and Mass Transfer in Closed, Partially Filled, Liquid Containers	
DR. JOHN A. CLARK and HUSSEIN Z. BARAKAT	
University of Michigan.....	119

SESSION IV

A Hypothesis for Helium Adsorption/Desorption in Slush Hydrogen	
CLARENCE A. SCHALLA	
Lockheed Missiles and Space Company.....	191
Selecting Liquid Level Transducers for Cryogenic Service	
D. A. BURGESSON	
National Bureau of Standards.....	205

FOREWORD

The Conference on Propellant Tank Pressurization and Stratification, sponsored by the Propulsion and Vehicle Engineering Laboratory, George C. Marshall Space Flight Center, was held to promote the direct exchange of technical information between government agencies and industries. Emphasis was on propellant tank pressurization and stratification; the presentations covered significant topics on propellant tank thermodynamics, pressurization system and component design, mechanics of stratification, stratification reduction, instrumentation, and the behavior of propellants under conditions of reduced gravity.

The conference was planned to inform those organizations that are in a position to benefit from the information discussed. Some 200 engineers and scientists, having major responsibilities in the design and development of propellant feed systems for launch and space vehicles, attended this conference, representing industry, NASA, and other government agencies.

The sponsors of the conference wish to thank all companies and individuals who contributed toward the success of the meeting. The special interest and guidance of Mr. Hans G. Paul, Mr. Charles C. Wood and Mr. Max E. Nein, Propulsion Division, Propulsion and Vehicle Engineering Laboratory, are gratefully acknowledged.


F. B. CLINE

Acting Director, Propulsion and
Vehicle Engineering Laboratory

1

CHAIRMEN AND COMMITTEES

Conference Chairman, MAX E. NEIN, Technical Assistant,
Fluid Mechanics and Thermodynamics Branch

Session Chairmen

- Session I - C. C. WOOD, Chief, Fluid Mechanics and
Thermodynamics Branch
- Session II - FRANK COMPITELLO, Liquid Propulsion Technology
Office, OART, Headquarters, National Aero-
nautics and Space Administration
- Session III - SID GLASSER, Supervisor, S-II Stage Pressurization
Systems, S&ID, North American Aviation, Inc.
- Session IV - DR. ROBERT R. HEAD, Chief, Applied Mechanical
Research Branch

Review Committee

- Chairman - MAX E. NEIN, Technical Assistant, Fluid
Mechanics and Thermodynamics Branch
- C. DAVID ARNETT, Fluid Mechanics and Thermo-
dynamics Branch

Welcoming Address - HANS G. PAUL, Chief, Propulsion Division

ANALYTICAL INVESTIGATION OF SOME
IMPORTANT PARAMETERS IN THE PRESSURIZED
LIQUID HYDROGEN TANK OUTFLOW PROBLEM

by

William H. Roudebush and David A. Mandell
Lewis Research Center
Cleveland, Ohio

ANALYTICAL INVESTIGATION OF SOME IMPORTANT PARAMETERS
IN THE PRESSURIZED LIQUID HYDROGEN TANK OUTFLOW PROBLEM

by William H. Roudebush and David A. Mandell

Lewis Research Center
National Aeronautics and Space Administration
Cleveland, Ohio

INTRODUCTION

Many factors influence the amount of gas required to pressurize a cryogenic propellant tank during the period of outflow. Besides the tank volume and the temperature and pressure of the incoming gas, other factors such as outlet flow rate, gas-to-wall heat-transfer coefficient, mass and specific heat of the tank wall, and the gas specific heat must be considered. A systematic experimental investigation of these individual factors is very difficult for liquid hydrogen. It is desirable, therefore, to attempt analytically to determine the relative significance of the various parameters.

An analysis of the tank pressurization problem for a cylindrical tank was made at Lewis Research Center (ref. 1). A simple one-dimensional model was used, based on a rather restrictive set of physical assumptions. Even for the simple model the resulting differential equations were quite complex and a numerical solution was clearly indicated. The details of the numerical solution were worked out and a computer program was developed. Results of the analysis were compared with experimental results for a number of cases and the agreement was shown to be surprisingly good in view of the restrictive assumptions.

The good agreement appeared to justify the use of the computer program for investigating systematically the various parameters affecting the pressurization problem. This investigation was carried out and the results are presented in detail in a forthcoming report (ref. 2). A brief discussion of these results and of the assumptions involved is given in the present paper.

ANALYSIS

The analysis is restricted to the cylindrical portion of the tank (fig. 1) and only the period of time during which outflow occurs is considered. Certain assumptions are made in an attempt to simplify the analysis and shorten the subsequent numerical solution while still retaining the most important features of the problem. A list of the assumptions and a discussion of their validity follows:

- (1) The ullage gas is nonviscous.
- (2) The velocity of the ullage gas is parallel to the tank axis and varies only in the axial direction.

- (3) The tank pressure varies only with time.
- (4) The ullage gas temperature varies only in the axial direction.
- (5) The tank wall temperature varies only in the axial direction.
- (6) No heat is transferred axially in either the gas or the wall.
- (7) No condensation or evaporation occurs.
- (8) No heat is transferred at the liquid interface or at the top of the tank.

With these assumptions the problem is reduced to a one-dimensional, nonsteady, nonviscous flow of the ullage gas with heat transfer to the tank wall.

Although the problem is clearly not one-dimensional (radial flow must take place as the gas enters the tank), it is necessary to simplify the equations. Therefore, assumptions (1) and (2) stipulate that the pressurizing gas enters the tank uniformly at $x = 0$ (fig. 1) and proceeds downward with a velocity that varies with time and axial location only; that is, no mixing of the ullage gas occurs.

Assumption (3) is likely to be satisfied closely because of the low gas density and small change in gas momentum from top to bottom of the tank.

Assumption (4) arises from experimental results obtained at Lewis with a cylindrical tank having a low heat leak. The assumption may not be valid for other circumstances.

Assumption (5) is adequate for thin metal tank walls.

Assumption (6) arises from the low conductivity of the ullage gas and the small thickness of the tank wall.

Assumption (7) appeared to be justified by early data taken at Lewis. Recently taken data, however, put the assumption in doubt. More experimental results, especially on larger tanks, are needed to evaluate this assumption properly.

Assumption (8) has not been verified. There are likely to be some cases in which the heat transfer to the top of the tank, at least, cannot be ignored.

With these assumptions, the differential equations that govern the pressurization problem can be written (see ref. 1 for details)

$$\frac{\partial T}{\partial t} = \frac{2hZRT}{rMPc_p} (T_w - T) - u \frac{\partial T}{\partial x} + \frac{RT}{MJPc_p} \left(Z + T \frac{\partial Z}{\partial T} \right) \frac{\partial P}{\partial t} + \frac{RTZCq_I}{\pi r^2 MPc_p} \quad (1)$$

$$\frac{\partial T_w}{\partial t} = \frac{h}{l_w \rho_w c_w} (T - T_w) + \frac{q_o}{l_w \rho_w c_w} \quad (2)$$

$$\frac{\partial u}{\partial x} = \frac{1}{ZT} \left(Z + T \frac{\partial Z}{\partial T} \right) \left(\frac{\partial T}{\partial t} + u \frac{\partial T}{\partial x} \right) - \frac{1}{ZP} \left(Z - P \frac{\partial Z}{\partial P} \right) \frac{\partial P}{\partial t} \quad (3)$$

(All symbols are defined in the appendix.) In addition to these three differential equations in the three unknowns T , T_w , and u , the following initial and boundary conditions are also required to determine a solution:

(1) At the start of outflow, the gas and wall temperature distributions must be given.

(2) The variation during outflow of the incoming gas temperature, the tank pressure, the outlet flow rate, and the gas and wall temperatures at the interface must be prescribed.

Furthermore, the heat-transfer coefficient must be supplied, either by an equation relating it to fluid properties or by using appropriate experimental values.

NUMERICAL SOLUTION

A finite difference solution of equations (1) to (3) was programmed in Fortran IV for use on an IBM 7094-II computer. Backward difference equations were used resulting in a nonlinear set of algebraic equations that were explicit in the unknown variables.

The time step Δt is related to the space step Δx by the requirement that

$$\Delta t = \frac{\Delta x}{u_L(t)}$$

where $u_L(t)$ is the velocity of the liquid surface. This restriction on Δt is used to keep the net spacing Δx constant as the solution progresses. (It is not a condition for stability of the numerical solution and it does not result in unusually small values of Δt). The program has been run over a very wide range of problems and no numerical instability has been encountered.

The output of the computer program is the distribution of gas and wall temperatures at any desired time during outflow. The pressurant mass required at each instant is also determined. A typical solution uses about 200 net points in the x -direction for covering the entire length of the tank. The 19 solutions presented in reference 1 averaged 24 seconds of computer time per solution.

EXPERIMENTAL AND CALCULATED RESULTS

In reference 3 the authors report some of the results of a systematic series of liquid hydrogen expulsion experiments. The tank used was 27 inches in diameter and 89 inches in overall length with dished head ends. A gas diffuser was used at the inlet. The tank was constructed of 5/16-inch 304 stainless-steel plate and was vacuum jacketed. The instrumentation, described in detail in reference 3, provided a relatively significant heat sink in some of the experiments.

Ten experiments (some of which were not discussed in ref. 3) were selected to check the analysis. These covered a wide range of outlet flow rates, tank pressures, and inlet gas temperature variations. Helium was used to pressurize in four of the cases. The detailed input data necessary to carry out the calculation is given in reference 1 for each of the experiments. Some of the principal data are given in table I.

TABLE I. - LEWIS EXPERIMENTAL DATA

Example	Pressure, lb/sq in.	Outflow time, sec	Outflow rate, cu ft/sec	Experimental average heat-transfer coefficient, Btu/(sq ft)(hr)(°R)	Pressur- izing gas
1	160	350	0.0669	13.75	H ₂
2	161	93	.2375	12.25	H ₂
3	57	284	.0780	7.09	H ₂
4	58	101	.2238	6.67	H ₂
5	164	95	.2340	11.34	H ₂
6	40	88	0.2550	5.13	H ₂
7	159	355	.0634	12.31	He
8	159	90	.2598	11.15	He
9	159	100	.2365	10.45	He
10	40	309	.0703	5.25	He

Figure 2 shows the gas and wall-temperature distributions calculated at the end of outflow and the corresponding experimental values for each example. The agreement generally is good.

Reference 4 reports the results of hydrogen experiments carried out at Lockheed-Georgia Company using a 40-inch-diameter test tank 100 inches in overall length. The test tank was 0.090-inch-thick stainless steel and was enclosed in a 60-inch-diameter vacuum-tight carbon steel tank. A gas diffuser was in the top and an antivortex baffle was in the bottom. Perforated conical slosh baffles were located at various axial positions. The heat sink effect of the internal hardware could not be well estimated from the information reported.

Nine tests are reported in reference 4 for which the system vacuum was maintained. These cover two values of inlet gas temperature and a range of values of

initial ullage. The outflow time and tank pressure varied only slightly from test to test. Helium was used to pressurize in one case. Sloshing of the liquid was induced in all but one case. The detailed input data for the calculations is given in reference 1. Some of the principal data are shown in table II.

TABLE II. - LOCKHEED-GEORGIA EXPERIMENTAL DATA

Example	Pressure, lb/sq in.	Outflow time, sec	Outflow rate, cu ft/sec	Experimental average heat-transfer coefficient, Btu/(sq ft)(hr)(°R)	Pressur- izing gas
1	45.5	89	^a 0.672	11.5	H ₂
2	47.6	103	.560	^b 12.0	H ₂
3	46.5	120	.511	11.3	H ₂
4	46.5	87	.607	12.0	H ₂
5	45.5	99	.609	12.1	He
6	47.0	95	.644	12.3	H ₂
7	45.0	111	.530	11.8	H ₂
8	46.2	97	.632	11.7	H ₂
9	45.5	105	.565	13.9	H ₂

^aFlow rates are computed from reported outflow time, tank volume, and percent initial ullage.

^bEstimated value; not given in reference 4.

For the Lewis and the Lockheed-Georgia experiments pressurant mass requirements were obtained from the analysis. Table III shows these calculated values along with the experimental value in each case. The percent difference is also shown. The average difference for the Lewis experiments is about 5 percent. The average difference for the Lockheed-Georgia experiments is about $4\frac{1}{2}$ percent. This agreement is better than might be expected from the simple description of the problem used for the analysis.

TABLE III. - PRESSURANT MASS REQUIREMENTS

Example	Experimental mass, lb	Calculated mass, lb	Percent differ- ence	Example	Experimental mass, lb	Calculated mass, lb	Percent differ- ence
Lewis data				Lockheed-Georgia data			
1	3.98	3.95	-0.75	1	2.61	2.81	7.67
2	2.72	2.60	-4.41	2	2.13	2.24	5.17
3	1.76	1.68	-4.54	3	2.86	3.05	6.64
4	1.24	1.27	2.42	4	2.57	2.65	3.11
5	3.76	3.51	-6.65	5	5.79	5.89	1.73
6	.83	.93	12.04	6	2.47	2.58	4.45
7	8.14	7.61	-6.51	7	2.81	2.86	1.78
8	5.59	5.57	-.36	8	2.81	2.95	4.98
9	9.24	8.48	-8.23	9	2.88	3.00	4.17
10	2.70	2.56	-5.18				

It should be noted that experimental average values of heat-transfer coefficient were used and that the gas and wall temperature distributions at the start of outflow were obtained from the data. The variation of inlet gas temperature with time at the position $x = 0$ is also from the experiments.

PARAMETRIC ANALYSIS

The agreement shown between calculated and experimental values of pressurant mass requirement in the preceeding section encourages the use of the analytical method for examining the effect of the various parameters entering the pressurization problem. A method for doing this and the results obtained are described briefly in this section.

Dimensionless Parameters

The following additional assumptions are made to simplify the differential equations (1) to (3) and the initial and boundary conditions:

- (9) The ullage gas is a perfect gas with constant specific heat.
- (10) The gas-to-wall heat-transfer coefficient is constant in space and time for a given example.
- (11) The inlet gas temperature, the tank pressure, and the outflow rate are constant.
- (12) The gas and wall temperatures at the liquid interface are constant and equal throughout the outflow period.
- (13) The gas and wall temperatures at the start of outflow are equal and vary linearly in the direction of the tank axis from the temperature at the liquid interface to a temperature at the top of the tank equal to the average of the inlet gas temperature and the liquid surface temperature.

The last assumption is obviously an arbitrary choice for the initial gas and wall temperatures. The effect of this assumption and the others will be considered later.

Using these assumptions and introducing the dimensionless variables

$$\hat{t} = \frac{t}{t_f}$$

$$\hat{x} = \frac{x}{L_f - L_0}$$

$$\hat{u} = \frac{u}{u_L}$$

$$\begin{aligned}\hat{T} &= \frac{T}{T_g} \\ \hat{T}_w &= \frac{T_w}{T_g}\end{aligned}\tag{4}$$

into equations (1) to (3) gives

$$\frac{D\hat{T}}{Dt} = 2 St_g (\hat{T}_w - \hat{T})\hat{T}\tag{5}$$

$$\frac{\partial \hat{T}_w}{\partial t} = St_w (\hat{T} - \hat{T}_w)\tag{6}$$

$$\frac{\partial \hat{u}}{\partial x} = \frac{1}{\hat{T}} \frac{D\hat{T}}{Dt}\tag{7}$$

where

$$St_g \equiv \frac{hRt_f T_g}{rMPc_p} = \frac{ht_f}{r\rho_g c_p} = \frac{1}{\hat{x}} \left(\frac{h}{\rho_g c_p u_L} \right)\tag{8}$$

$$St_w \equiv \frac{ht_f}{l_w \rho_w c_w} = \frac{1}{\hat{l}_w} \left(\frac{h}{\rho_w c_w u_L} \right)\tag{9}$$

The numbers St_g and St_w have the form of Stanton numbers modified by the presence of the dimensionless lengths \hat{x} and \hat{l}_w , respectively. The use of a parameter St_w , containing both fluid and wall properties, is unusual. The ratio

$$\frac{St_g}{St_w} = \frac{l_w \rho_w c_w}{r\rho_g c_p}$$

which is equal to one-half the ratio of the heat capacity of the wall to the heat capacity of the gas, could be used in place of St_w . However, St_w has been retained since it arises naturally in the development of the equations.

It is seen that St_g and St_w completely determine the differential equations for the dimensionless dependent variables \hat{T} , \hat{T}_w , and \hat{u} . It is shown in reference 2 that the dimensionless constants

$$\hat{L}_0 \equiv \frac{L_0}{L_f - L_0}\tag{10}$$

$$\hat{T}_L \equiv \frac{T_L}{T_g}\tag{11}$$

enter the initial and boundary conditions for the dimensionless equations. Within the assumptions made thus far St_g , \hat{L}_0 , and \hat{T}_L are constant for a given problem. The St_w will vary only if c_w is allowed to vary.

Pressurant Mass Ratio

Defining an ideal pressurant mass

$$m_1 = \pi r^2 (L_f - L_0) \rho_g$$

it can be shown that the mass ratio (sometimes called collapse factor) is given by

$$\frac{m}{m_1} = \int_0^{\hat{L}_f} \frac{\partial \hat{x}}{\hat{T}(\hat{x}, 1)} - \int_0^{\hat{L}_0} \frac{\partial \hat{x}}{\hat{T}(\hat{x}, 0)} \quad (12)$$

The mass ratio is, therefore, known when the solution of equations (4), (5), and (6) for the dimensionless temperature variation $\hat{T}(\hat{x}, \hat{t})$ is known. These considerations lead to the following conclusion: With the assumptions stated in the analysis, and with the further assumption that the wall specific heat is constant, the mass ratio is completely determined by the specification of four dimensionless constants St_g , St_w , \hat{L}_0 , and \hat{T}_L .

This conclusion is not restricted to any particular liquid, pressurizing gas, or tank wall material. The constant \hat{L}_0 is determined by the initial ullage ratio, and the constant \hat{T}_L is determined by the saturation temperature and the pressurizing gas temperature. All other characteristics of the problem, for example tank wall material, wall thickness, tank radius, density, and specific heat of the pressurizing gas and tank pressure, enter only through the constants St_g and St_w . Within the assumptions of the analysis, therefore, a complete parametric investigation can be done by examining the effects on the mass ratio of variations in St_g , St_w , \hat{L}_0 , and \hat{T}_L .

For hydrogen problems, however, the assumption that c_w is constant is not very good. If this assumption is dropped, the preceding conclusion no longer holds. The specific heat c_w then varies with temperature T_w and the form of the variation may change from one wall material to another. This leads to the following conclusion: With the assumptions stated in the analysis, and confining attention to a single wall material, the mass ratio is completely determined by the specification of four dimensionless constants St_g , St_w , \hat{L}_0 , and \hat{T}_L and the inlet gas temperature T_g .

Effect of Parameters

The parametric investigation is then continued as follows. Values of \hat{L}_0 , \hat{T}_L , and T_g are fixed and computer solutions of equations (5), (6), and (7) for a wide range of values of St_g and St_w are obtained. From these solutions (in particular, the temperature distributions) the mass ratios are computed. The results of these calculations are shown in figure 3.

For fixed values $\hat{L}_0 = 0.0526$ (corresponding to an initial ullage of 5 percent), $T_L = 0.074$, and $T_g = 500^\circ \text{R}$, figure 3 enables the prediction of pressurant mass ratio (collapse factor) for a wide range of design conditions, within the assumptions of the analysis.

The effect of the arbitrarily chosen values of T_g , \hat{T}_L , and \hat{L}_0 is examined next. Representative curves ($St_g = 5.0$ and $St_w = 2.5$) are taken from figure 3. With these curves for comparison the value of T_g is changed to 300° and 700°R with T_L and L_0 held at their original values. Again mass ratios are obtained from computer solutions and the results are compared with the original results (fig. 3) for $T_g = 500^\circ \text{R}$. Figure 4 gives an indication of the effect of T_g on the mass ratio. The effect is large only for large values of St_g .

In a similar manner the effect of \hat{T}_L is found by holding T_g and \hat{L}_0 fixed at the values used for figure 3 and changing \hat{T}_L to 0.12 ($\hat{T}_L = 0.12$ corresponds to $T_L = 60^\circ \text{R}$ and $T_L = 0.074$ corresponds to $T_L = 37^\circ \text{R}$). The results are shown in figure 5. The effect on the mass ratio is small.

The dimensionless initial ullage height \hat{L}_0 is treated similarly, changing it from the value 0.0526 (corresponding to an initial ullage volume of 5 percent) used in figure 3 to the value 0.25 (corresponding to an initial ullage volume of 20 percent). As shown in figure 6 the initial ullage effect is small for values of initial ullage up to 20 percent.

Figures 4 to 6 indicate that the reference Stanton number map (fig. 3) has a wider range of validity than was first evident. In particular, the use does not appear to be restricted to the particular values of T_g , \hat{T}_L , and \hat{L}_0 that were used to obtain figure 3. This conclusion will be checked against experimental data in a later section.

Effect of Assumptions

It is possible to examine, in a similar manner, the effect of some of the assumptions entering the analysis. Figure 7 shows results obtained using a variable gas specific heat. The difference is negligible. Figure 8 shows the relatively large effect, on the other hand, of choosing wall specific heat to be constant. It was this latter result that led to the inclusion of varying wall specific heat in determining the reference Stanton number map. It is interesting that changing the wall material from stainless steel to aluminum has

little effect on the mass ratio (fig. 9). The reason for this is given in reference 2.

It is shown in reference 2 that the choice of initial values of gas and wall temperatures affects the mass ratio little for initial ullages up to 20 percent. The effects of initial transients in outflow rate and inlet gas temperature are shown in that report to be small. Transient pressure effects are more important.

Comparison with Experiment

An analysis of the tank pressurization problem has indicated that the primary parameters affecting the mass required to pressurize a cylindrical tank during outflow can be combined into two dimensionless groups having the form of modified Stanton numbers, one associated with the gas and one with the tank wall. This enables approximate values of mass ratio (collapse factor) to be determined from a single figure for a large range of design variables. To test this conclusion the experimental data used previously in the paper will be used again.

In the case of the Lewis experiments and the Lockheed-Georgia experiments described before, the experimental average values of heat-transfer coefficient are available. Using these values of h the gas and wall Stanton numbers can be determined for each set of data. Using these Stanton numbers and figure 3, an estimated value of mass ratio can be obtained.

Values of mass ratio determined in this way for the Lewis experiments are shown in table IV. One of the Lockheed-Georgia experiments was omitted since it contained helium in the initial ullage space and was subsequently pressurized

TABLE IV. - COMPARISON OF EXPERIMENTAL VALUES OF MASS RATIO WITH VALUES DETERMINED FROM THE REFERENCE STANTON NUMBER MAP

Example	Experi- mental mass ratio	Mass ratio determined from Stanton number map	Percent differ- ence	Example	Experi- mental mass ratio	Mass ratio determined from Stanton number map	Percent differ- ence
Lewis data				Lockheed-Georgia data			
1	2.58	2.76	-6.5	1	1.72	1.54	11.7
2	1.77	1.84	-3.8	2	2.14	2.16	-0.9
3	3.09	3.31	-6.7	3	1.79	1.61	11.2
4	3.20	2.25	-2.2	4	1.71	1.68	1.8
5	1.47	1.35	8.9	5	1.81	1.69	7.1
6	2.37	2.56	-7.4	7	1.80	1.71	5.3
7	2.73	2.86	-4.5	8	1.75	1.59	10.0
8	1.86	1.93	-3.6	9	1.83	1.69	8.3
9	1.38	1.25	10.4				
10	3.92	4.25	-7.8				

with hydrogen, a situation not covered by figure 3. Values of mass ratio determined from figure 3 for the other eight Lockheed-Georgia experiments are shown in table IV. Also shown are the experimental values of mass ratio for all the experiments. In the case of the Lewis data the actual experimental values are modified to eliminate the heat sink effect that is not accounted for in figure 3.

The percent difference between calculated and experimental values of mass ratio is also shown in table IV. The average value of the absolute differences for the Lewis data is about 6 percent. For the Lockheed-Georgia data the average is about 7 percent. These results bear out the implications of the parametric analysis.

It should be remembered, however, that to compute Stanton numbers for design purposes a value of heat-transfer coefficient h must be estimated. In reference 2 a simple method of estimating h from a free convection formula is examined. For the experiments considered here such a simple method appears to be adequate. Its general use, however, is open to serious question and the determination of heat-transfer coefficient for arbitrary conditions remains an unsettled question.

APPENDIX - SYMBOLS

C	effective perimeter of internal hardware
c_p	specific heat of gas
c_w	specific heat of tank wall
h	heat-transfer coefficient
J	mechanical equivalent of heat
L_f	ullage height at time $t = t_f$
\hat{L}_f	dimensionless ullage height, $L_f/(L_f - L_0)$
L_0	ullage height at time $t = 0$
\hat{L}_0	dimensionless initial ullage height, $L_0/(L_f - L_0)$
l	height of ullage (see fig. 1)
l_w	thickness of tank wall
\hat{l}_w	dimensionless thickness of tank wall, $l_w/(L_f - L_0)$
M	molecular weight

m	mass of pressurant gas added during outflow
m_1	mass of pressurant gas required assuming no heat transfer
P	pressure in tank
q_i	heat flow rate to gas from internal hardware
q_o	heat flow rate to tank wall from outside
R	universal gas constant
r	radius of tank
\hat{r}	dimensionless radius of tank, $r/(L_f - L_o)$
St_g	modified gas Stanton number, $\frac{1}{Pr} \frac{h}{\rho_g c_p u_L}$
St_w	modified wall Stanton number, $\frac{1}{\hat{r}_w} \frac{h}{\rho_w c_w u_L}$
T	gas temperature
\hat{T}	dimensionless gas temperature, T/T_g
T_g	gas temperature at tank inlet
T_L	gas temperature at liquid interface
\hat{T}_L	dimensionless temperature, T_L/T_g
T_w	temperature of tank wall
\hat{T}_w	dimensionless temperature, T_w/T_g
t	time
\hat{t}	dimensionless time, t/t_f
t_f	time at end of outflow
Δt	time increment for finite difference equations
u	velocity of gas
\hat{u}	dimensionless gas velocity, u/u_L
u_L	velocity of gas at liquid interface
x	space coordinate in direction of tank axis
\hat{x}	dimensionless space coordinate, $x/(L_f - L_o)$

Δx space increment for finite difference solution
 Z compressibility factor
 ρ_g density of gas
 ρ_w density of tank wall

REFERENCES

1. Roudebush, William H.: An Analysis of the Problem of Tank Pressurization During Outflow. Proposed NASA Technical Note.
2. Mandell, David A., and Roudebush, William H.: Parametric Investigation of Liquid Hydrogen Tank Pressurization During Outflow. Proposed Technical Note.
3. Gluck, D. F., and Kline, J. F.: Gas Requirements in Pressurized Transfer of Liquid Hydrogen. Advances in Cryogenic Engineering, vol. 7, 1962, pp. 219-233.
4. Main Propellant Tank Pressurization System Study and Test Program. Lockheed-Georgia Co. Rep. ER-5238, Aug. 1961.

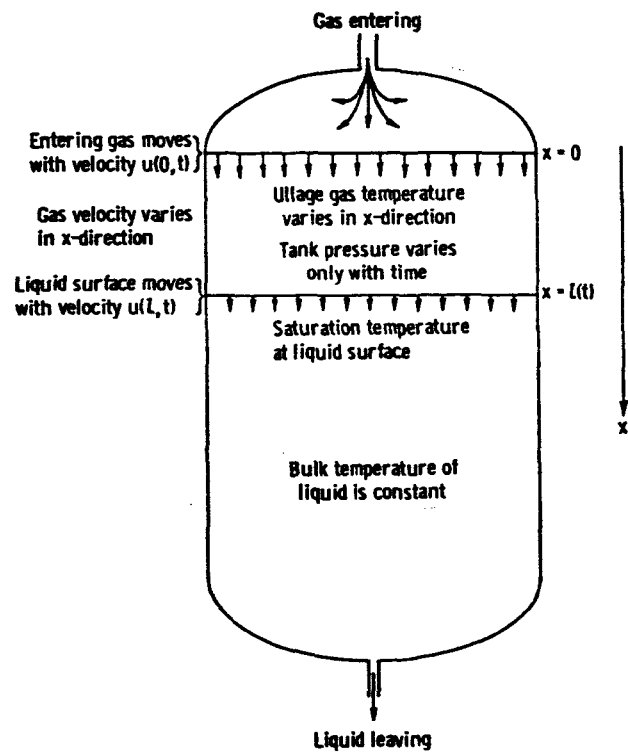


Figure 1. - Schematic drawing of cylindrical tank.

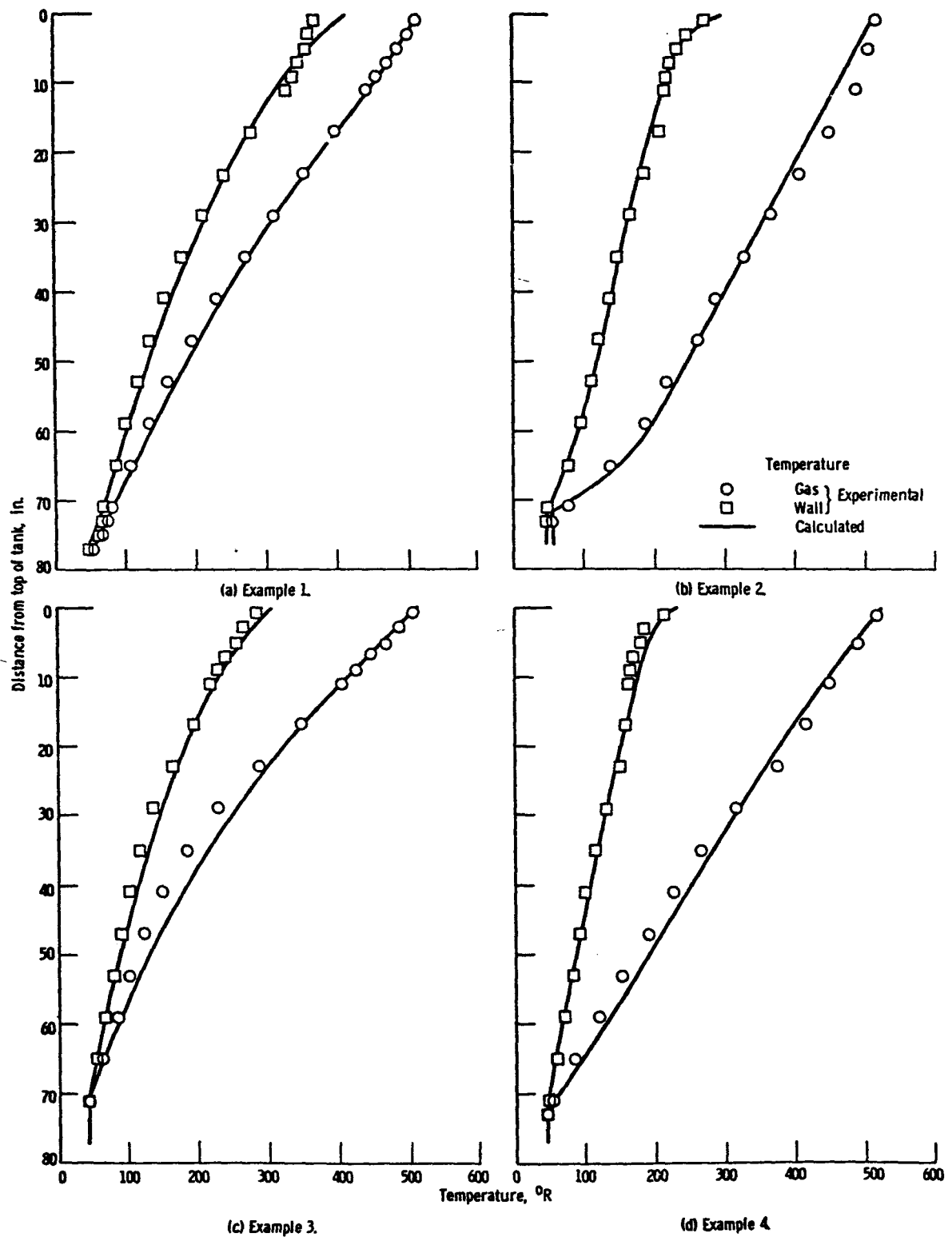


Figure 2. - Comparison of calculated and experimental gas and wall temperatures at end of outflow.

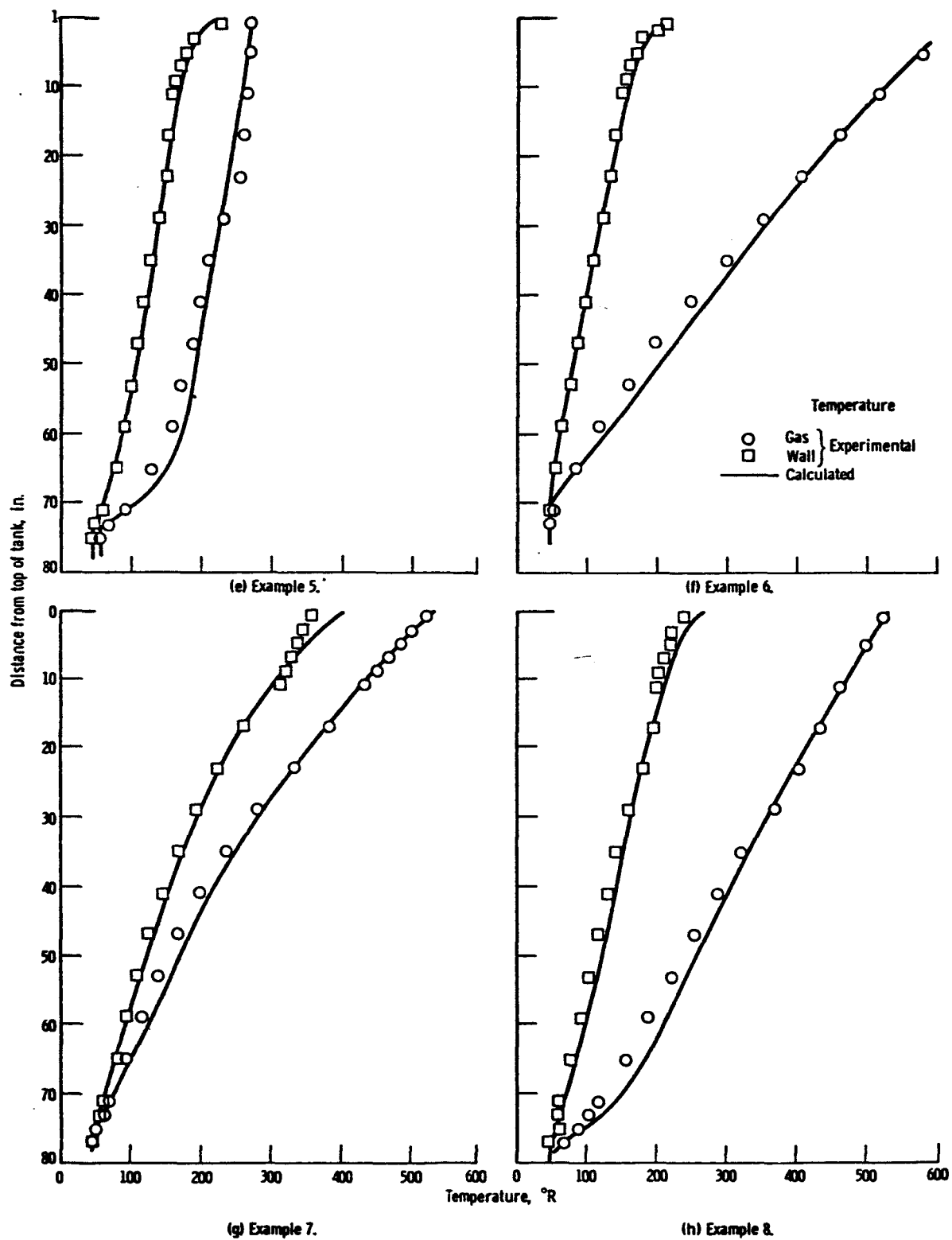
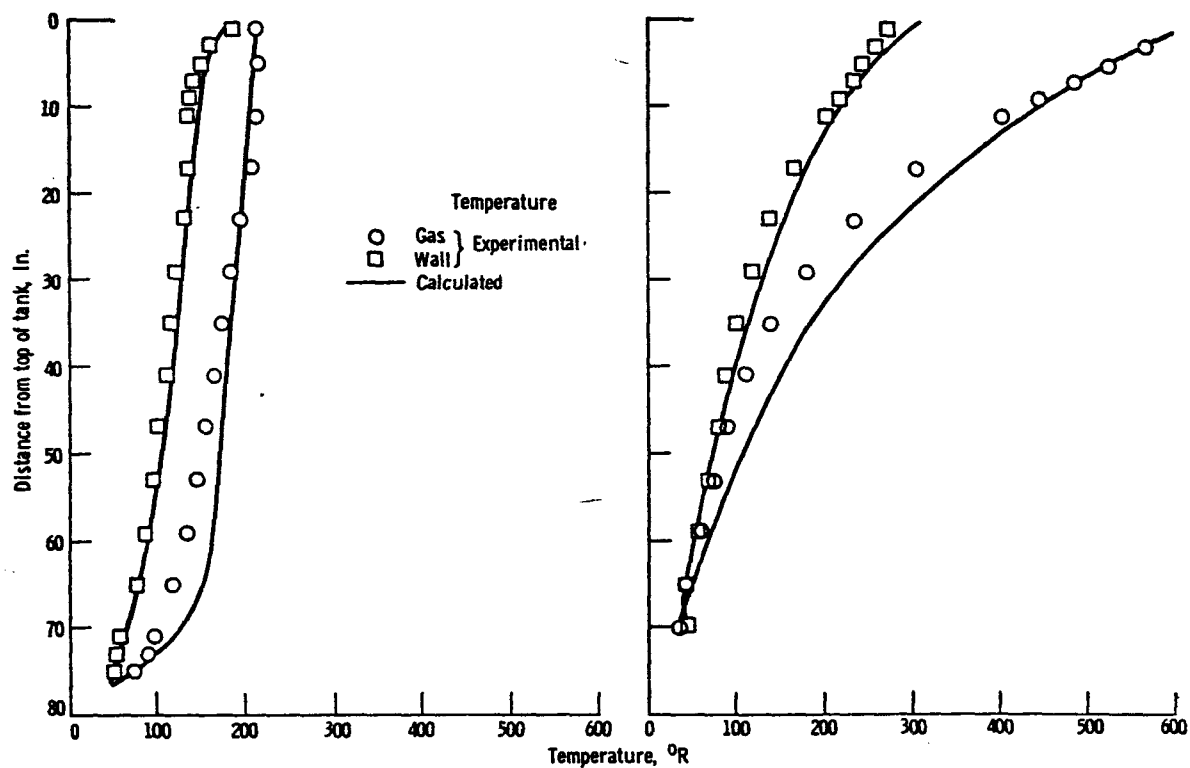


Figure 2 - Continued. Comparison of calculated and experimental gas and wall temperatures at end of outflow.



(i) Example 9.

(j) Example 10.

Figure 2. - Concluded. Comparison of calculated and experimental gas and wall temperatures at end of outflow.

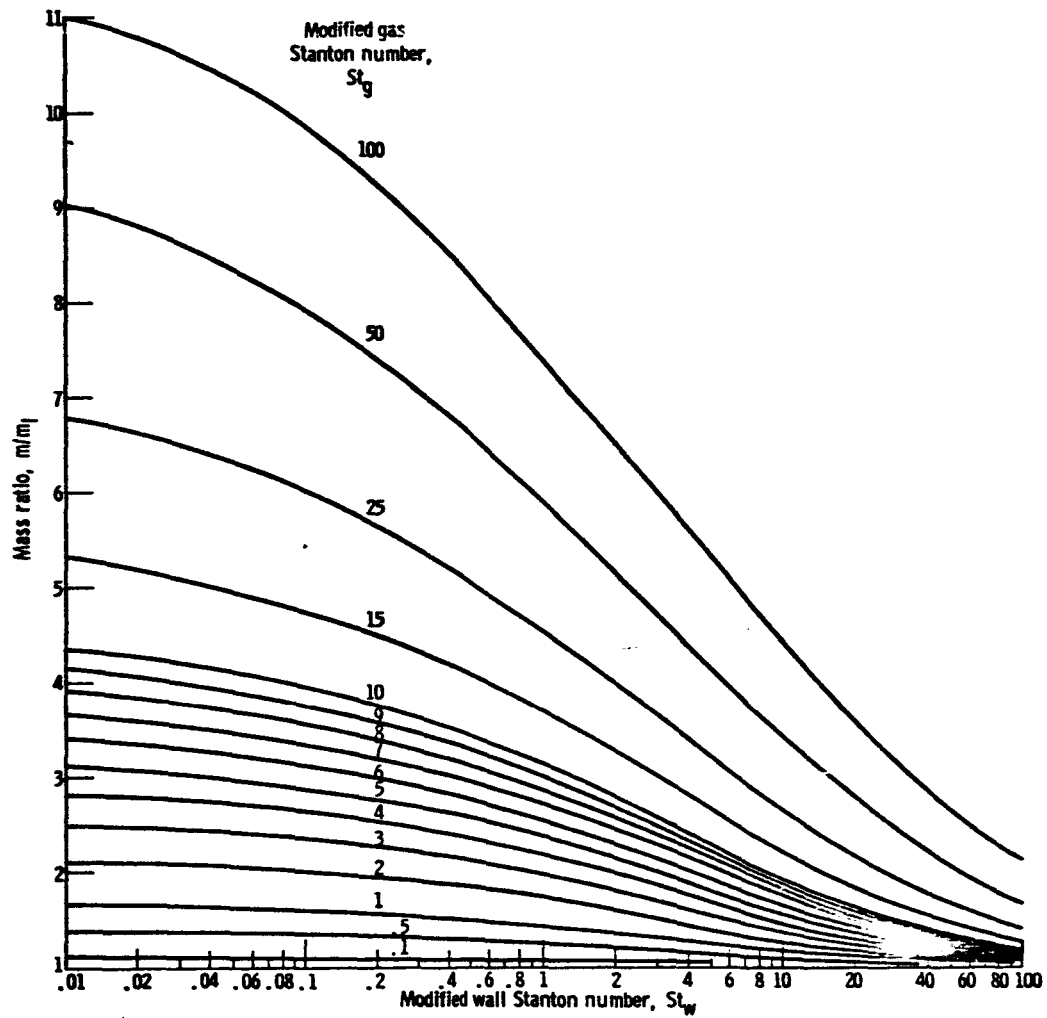


Figure 3. - Stanton number map showing values of mass ratio for range of gas and wall Stanton numbers. Initial ullage ratio, 0.05; dimensionless interface temperature, 0.074.

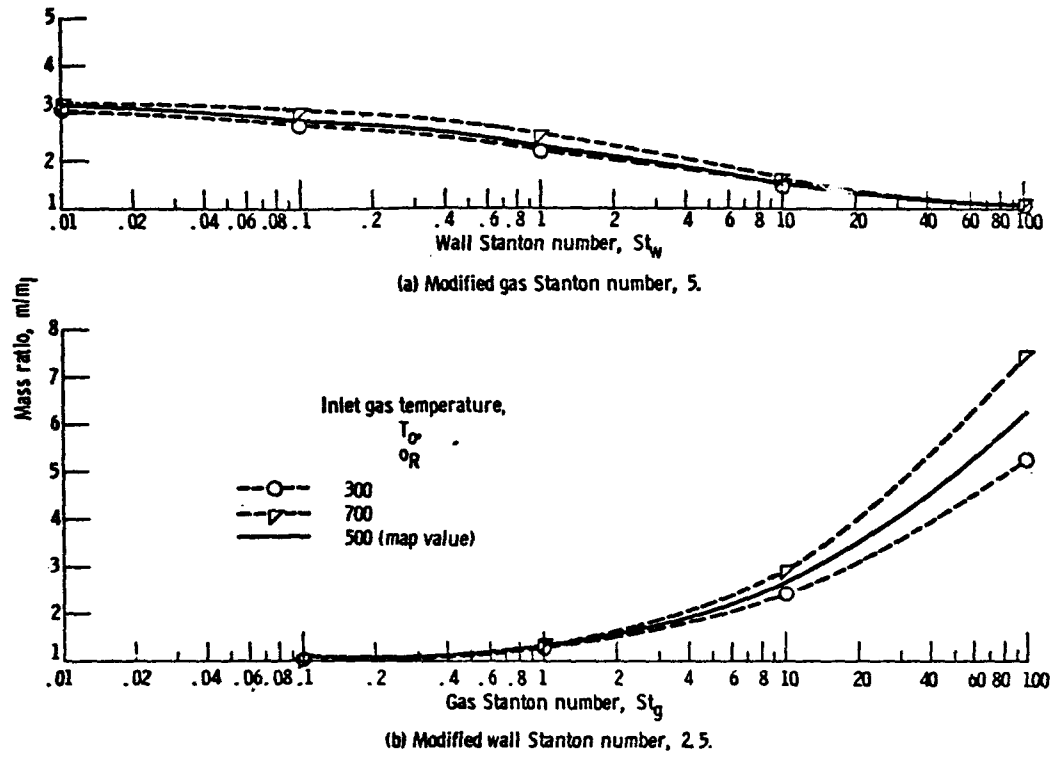


Figure 4 - Effect on mass ratio of changing the inlet gas temperature. Dimensionless interface temperature, 0.074; dimensionless initial ullage height, 0.0526.

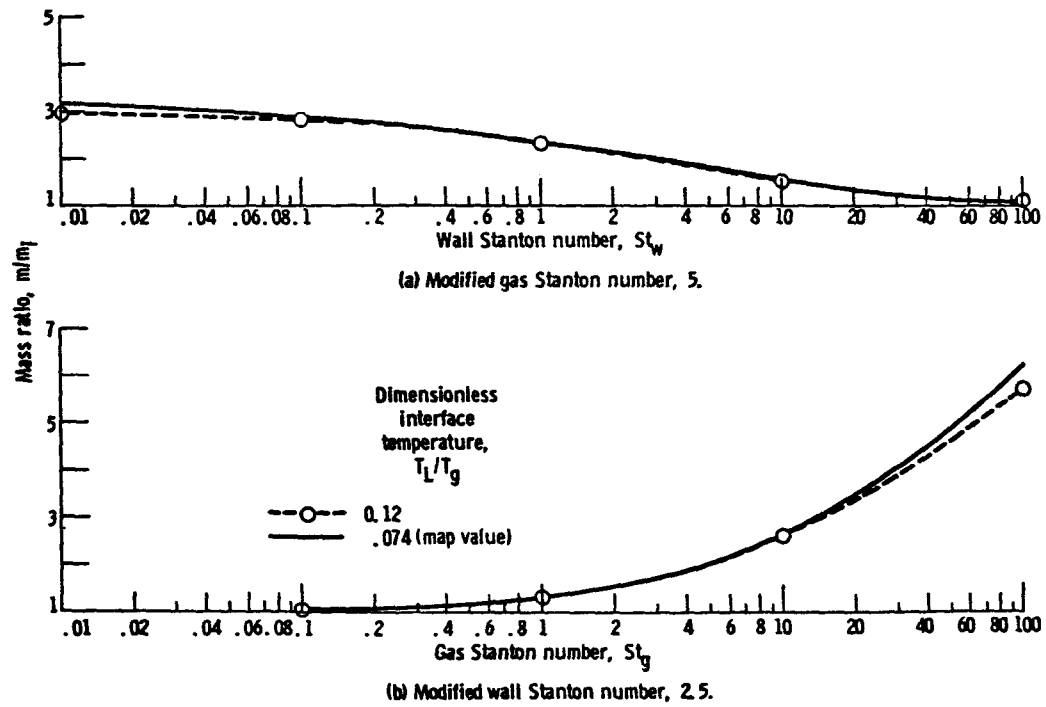


Figure 5 - Effect on mass ratio of changing the dimensionless interface temperature. Inlet gas temperature, $500^{\circ}R$; dimensionless initial ullage height, 0.0526.

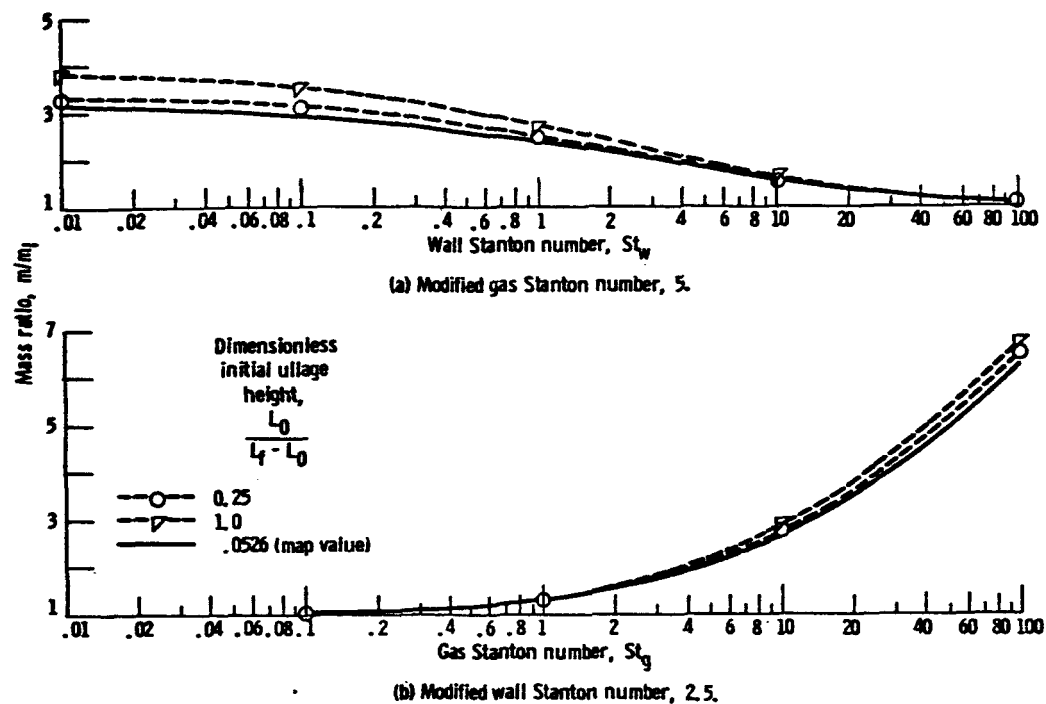


Figure 6. - Effect on mass ratio of changing the dimensionless initial ullage height. Inlet gas temperature, $500^\circ R$; dimensionless interface temperature, 0.074.

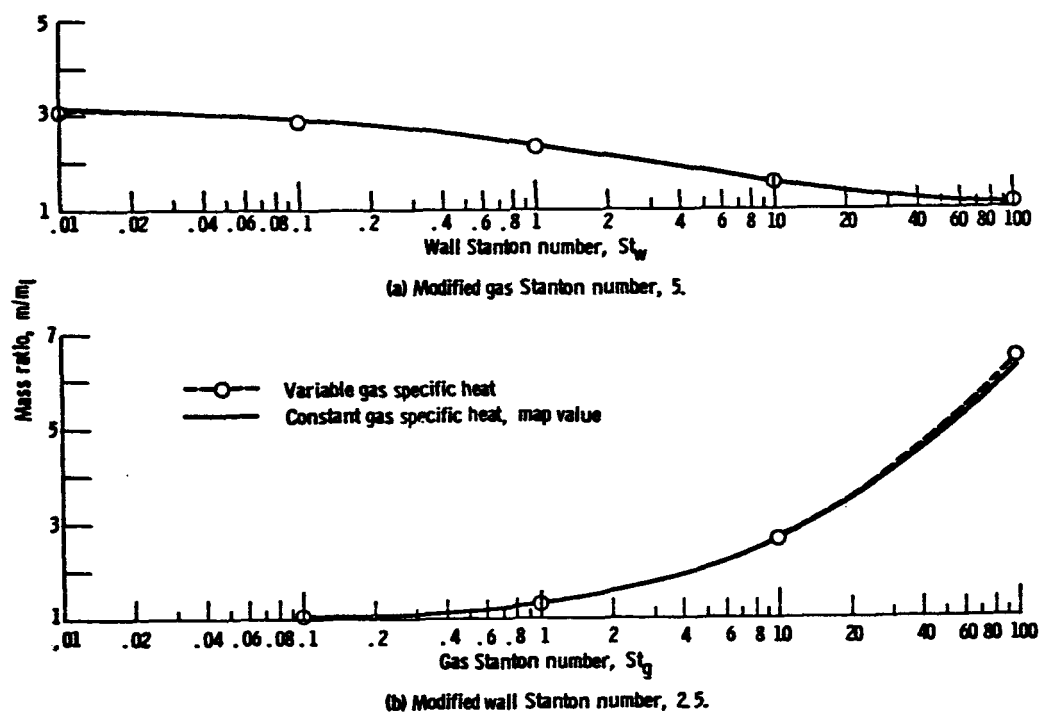


Figure 7. - Effect on mass ratio of allowing gas specific heat to vary with temperature. Inlet gas temperature, $500^\circ R$; dimensionless interface temperature, 0.074; dimensionless initial ullage height, 0.0526.

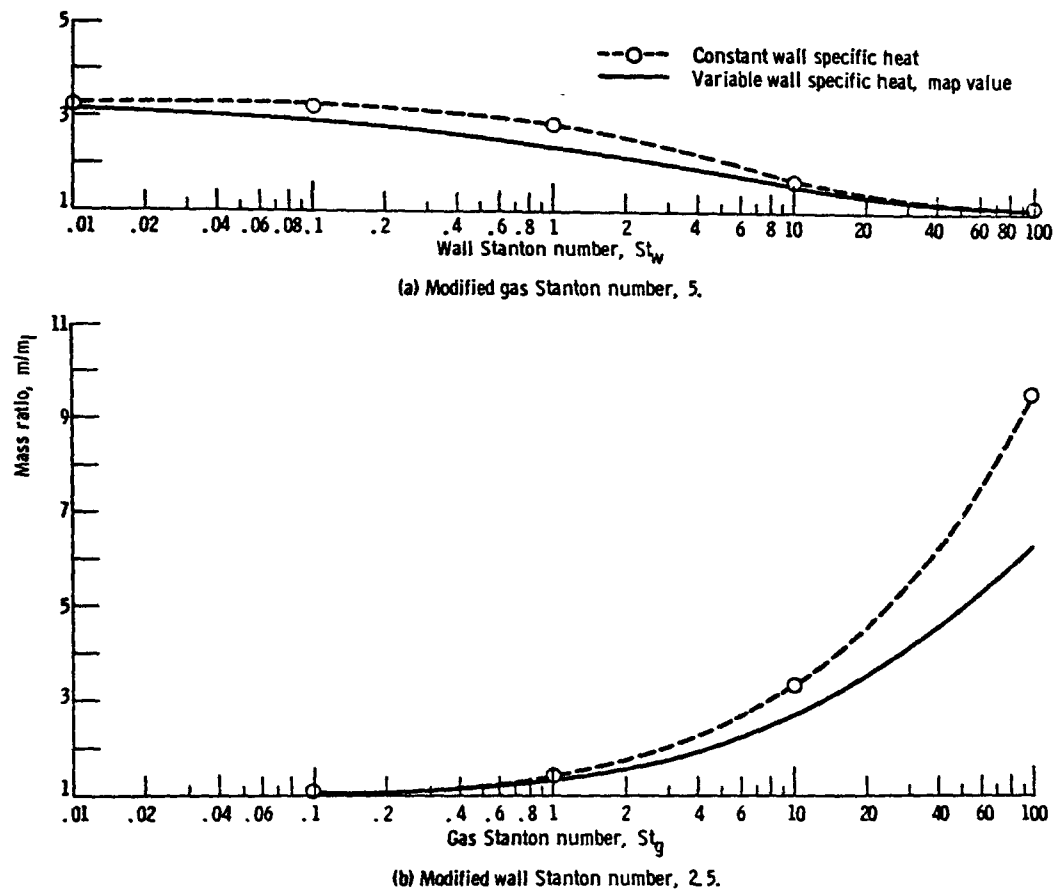


Figure 8. - Effect on mass ratio of holding wall specific heat constant. Inlet gas temperature, $500^\circ R$; dimensionless interface temperature, 0.074; dimensionless initial ullage height, 0.0526.

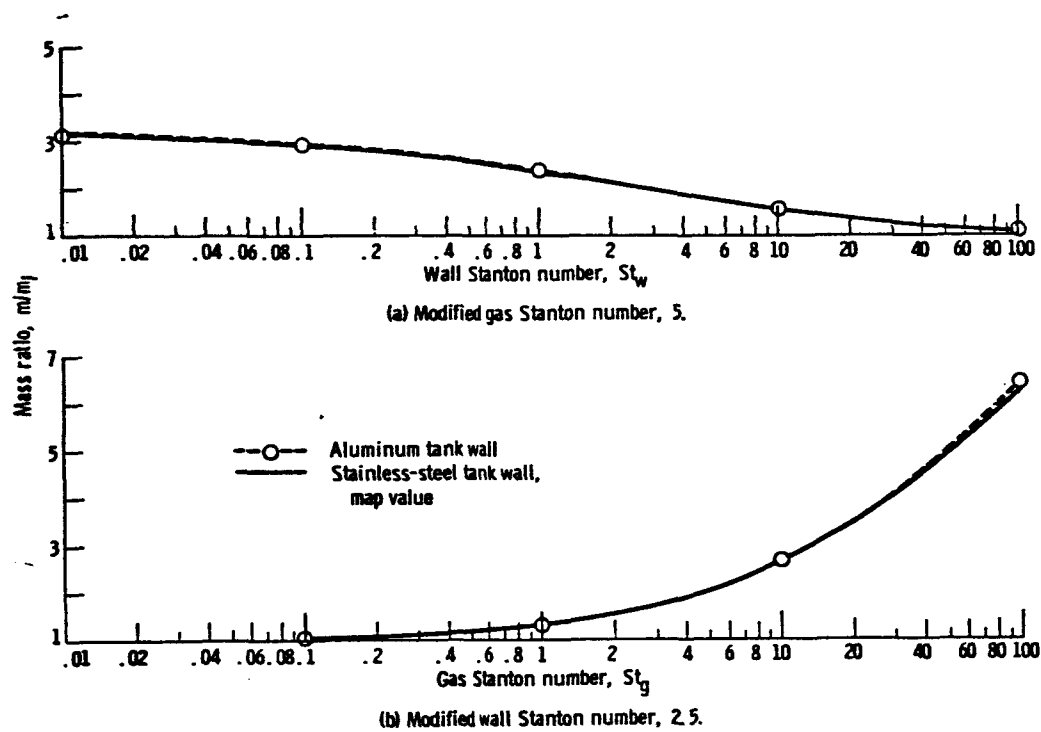


Figure 9. - Effect on mass ratio of changing tank wall temperature from stainless steel to aluminum. Dimensionless interface temperature, 0.074; dimensionless initial ullage height, 0.0526.

EXPERIMENTAL AND ANALYTICAL STUDIES
OF CRYOGENIC PROPELLANT TANK
PRESSURIZATION

by

M. E. Nein and J. F. Thompson, Jr.*
George C. Marshall Space Flight Center
Huntsville, Alabama

* Assistant Professor at Mississippi State University, Aeronautical
Engineering Department; formerly with MSFC

NS
PAGE INTENTIONALLY BLANK

EXPERIMENTAL AND ANALYTICAL STUDIES OF CRYOGENIC PROPELLANT TANK PRESSURIZATION

INTRODUCTION

Determination of the pressurant gas weight for cryogenic propellant tanks is complex and defies exact analytical treatment because of the interdependent transient phenomena of heat and mass transfer that occur simultaneously in a propellant tank. Mathematical models describing the internal thermodynamics of tank pressurization have been developed by various investigators.

The experimental data on pressurization obtained by the Marshall Space Flight Center during the SATURN launch vehicle development were applied to several pressurization analyses and some of the results are presented in this paper.

Although the most accurate method of predicting pressurant requirements is with a computer program that has been varified by experiments, it is advantageous to have a fast, reasonably accurate method to determine the total mass of pressurant gas required without resorting to the computer. This type of analysis is necessary in comparison and optimization studies for preliminary design where the number of possibilities to be considered precludes a detailed computer analysis of each case. Therefore, a dimensional analysis of a large number of pressurization tests and computer runs was applied to develop an equation that predicts pressurant requirements for cylindrical and spherodial propellant tanks.

EXPERIMENTAL PROGRAM

Test Facilities

The experimental work was conducted on five tank configurations at Marshall Space Flight Center:

- A. Saturn I, S-I Stage, Multiple Interconnect LOX Tanks
- B. Saturn I, S-IV Stage, LOX and LH_2 Tanks

- C. A 6.5 x 39 foot (DxL) cylindrical LOX Tank
- D. A 13 x 26 foot (DxL) cylindrical LOX Tank
- E. A 1 x 3 foot (DxL) cylindrical LOX Tank

The test parameters for these tank configurations are compared in Table I. Configurations A and B were flight vehicles and thus contained the standard test instrument of the Saturn propellant feed system. Configurations C, D, and E were equipped with many thermocouples along the tank axis. Thermocouples, mounted at several radii at three elevations in these tanks, allowed measurement of radial temperature gradients. Special calorimeter plates were mounted in tanks C and D for determination of gas-to-wall heat transfer coefficients. Finally, gas sampling devices were placed at several locations to measure ullage gas concentration gradients.

The pressurant gas was introduced at the top of the container through a distributor to minimize inlet velocities and disturbances of the liquid surface by impinging gas jets.

The tank Configurations C, D, and E could be sloshed at rotational or translatory oscillation in excess of the first critical frequency of the tank. The results of some of these pressurization tests conducted with the five tank configurations are presented in FIG 1 through 9.

Test Results

a. Heat Transfer Coefficients

Heat transfer between pressurant and tank side walls was measured during pressurization tests in Configuration C by two plate calorimeters. Each calorimeter was a 12 x 12 inch, 30 gage copper plate mounted from teflon spacers parallel to and at a distance of four inches from the tank wall.

For determination of heat transfer coefficients, it was assumed that heat transfer to the back side of the plate (towards tank wall) was by free convection because of the shielding effect of the plate-to-wall arrangement.

The free convection heat transfer coefficient was calculated for two component mixtures based on the time and space dependent helium-oxygen concentration in the tank. The total heat transfer to the calorimeters was then corrected using the calculated free convection effect on the back side. The heat transfer coefficients to the front of the calorimeter plates measured in Tests 130-9, -10, -15 are presented in FIG 1 and FIG 2 using gaseous oxygen and helium as pressurants. Ullage gas-to-wall heat transfer was also evaluated from wall temperature measurements at a location 3.5 ft from the top of the tank. Wall measurements at locations initially below the liquid surface produced erroneous readings and were discarded. These coefficients were corrected by subtracting the effect of external heat flux from the measured wall temperature rise.

Inspection of FIG 1 and FIG 2 shows very good agreement between measured and calculated heat transfer coefficients. It is noted that the gas-to-wall heat transfer coefficient is definitely within the forced convection regime for the oxygen tests, but in the free convection regime for the helium test. Although the heat transfer coefficient by forced convection diminishes with increasing distance from the pressurant distributor, the free convection contribution compensates for this decay to such a degree that a nearly constant heat transfer coefficient is obtained along the tank bulkhead and side wall.

b. Sloshing Effects

Pressurization studies conducted at MSFC have shown that the use of helium as a main pressurant for cryogenic propellants does not always result in the lightest pressurization system. However, it was determined experimentally that prepressurization with helium reduces pressure decay during liquid sloshing near the critical frequency. It is assumed that the helium acts as a buffer zone between the splashing cryogenic liquid and the condensable pressurant, suppressing excessive mass transfer.

FIG 3 shows a typical tank pressure history for a stationary liquid oxygen test tank as compared to a pressure history in which the liquid sloshes near the first critical mode of oscillation (Ref. 1). The tank was prepressurized, with either helium or nitrogen, followed by main pressurization during liquid expulsion with super-heated oxygen. The tank pressure history during the slosh test (using helium as a prepressurant) is nearly identical to the pressure history of the non-sloshing expulsion test.

In contrast, prepressurization with gaseous nitrogen resulted in a marked pressure decay during the sloshing of the liquid, which was not evident during a non-sloshing expulsion test with gaseous nitrogen prepressurization.

c. Ullage Gas Concentration Gradients

Gas flow conditions and the concentration of helium gas in a cryogenic propellant tank during pressurization discharge were studied in test Configurations C and D. Spectrographic analyses were made of gas samples taken at various positions in the tanks. Samples taken at various elevations in tank Configuration C just before the end of the tests yielded the results shown in FIG 4. In the test in which helium was used for prepressurization and oxygen as the main pressurant, the helium concentration is maximum at 12 ft above the liquid, and gradually decreases in both directions.

The concentration of oxygen near the liquid surface is probably caused by accumulation of the gaseous oxygen that is initially in the ullage before prepressurization. For comparison, FIG 4 also shows the concentration of helium above the liquid oxygen for the case in which helium prepressurization is followed by pressurization with helium during liquid expulsion. The oxygen concentration at 10 ft above the liquid interface was only 6 percent by volume. The total amount of gaseous oxygen in the ullage was only slightly larger than the amount of oxygen in the ullage before prepressurization (0.77 moles versus 0.73 moles). This indicates that interfacial mass transfer, although small under these conditions, was in the form of evaporation.

d. Mass Transfer

A comparison of mass transfer results obtained in Configuration C with results obtained by Clark (Ref. 2) is shown in FIG 5. Condensation in excess of 30 percent of the pressurant flow was found by Clark during liquid nitrogen expulsion tests with a 1 x 3 ft cylindrical tank. Similar results were obtained with the MSFC test Configuration E, also shown in FIG 5. The mass transfer measured in test Configuration C indicates that condensation was 5-10 percent. Condensation in the larger facility is less because of the smaller wall-area/volume ratio of a larger tank.

Comparing the condensation in the small tank with that in the large tank on the basis of wall-area/volume ratio, the values are approximately equal. During tests at high pressurant inlet temperature, initial evaporation noted in Configuration C diminished as the test proceeded. However, Clark had found increased condensation at higher pressurant inlet temperatures in small tanks. These conflicting results point out the incomplete knowledge of mass transfer.

e. Axial Ullage Temperature Gradients and Pressurant Flowrates

The axial ullage temperature gradients obtained in tests 130-6 and 130-7 with Configuration C (FIG 6 and 7) became approximately linear as the test proceeded. These two tests were conducted at 48 psia and 30 psia tank pressure with oxygen as pressurant at about 550°R. There was a rapid increase in temperature of about 30°R immediately above the liquid interface in these tests, indicating that mass transfer was small.

Pressurant flowrates to the LOX tanks of the SATURN I, S-I stage, during static test and flight are presented in FIG 8 and 9.

PRESSURIZATION ANALYSES

Pressurized discharge from cryogenic liquid containers was studied analytically and experimentally by several investigators and their results are presented in the literature. The method by Epstein (Ref 3), was chosen by MSFC for pressurization system analyses, because this approach makes maximum use of the techniques of digital computer calculations and is not subject to the restrictive assumptions that are made in other programs. However, extensive comparisons of the program with test data were required to evaluate the physical parameters and constants initially contained in the program as indeterminate identities. The equations were modified when necessary and the relative importance of each of the parameters involved in the program determined.

The pressurant flowrate and ullage temperature gradients predicted by the computer program after modification are compared with test data in FIG 6 - 9. In all comparisons, the ullage pressure, liquid drain rate, ambient heat transfer coefficients, and ambient temperature were input to the computer as functions of time. Either the pressurant inlet temperature or the heat exchanger performance curve was also input.

The agreement between the computer predictions and the test data is generally good. Prediction of ullage temperature gradient and total pressurant mass is important for overall vehicle layout. However, the design of the pressurization systems require that pressurization analysis can predict transient flowrates within close tolerances to avoid flow instabilities in heat exchanger which can occur under certain flow conditions. It is seen from FIG 8 and FIG 9 that good agreement between computer predictions and test data of pressurant flowrate is obtained. The irregularities in the computed pressurant flowrate, are caused by the over-sensitivity of the program to changes in the slope of the ullage pressure curve.

Based on these and other comparisons of test results and computer predictions, it is concluded that pressurant gas requirements for launch and space vehicles may be accurately predicted by this model of the pressurization process.

However, preliminary design studies require a fast and reasonably accurate method of prediction without resorting to computer programs. Therefore, dimensional analysis was applied to a large number of pressurization tests and computer runs to develop a single equation that predicts pressurant requirements for cylindrical and spheroidal propellant tanks.

a. Dimensional Analysis

The total mass of pressurant gas required is a function of the ullage mean temperature at cutoff derived with the gas equation of state:

$$W_{\text{Total}} = \frac{PV}{\alpha NRT_m} \quad (1)$$

The total pressurant mass required may be calculated if the ullage mean temperature at cutoff can be determined. In the most general case, the ullage mean temperature at cutoff will be a function of twelve system design variables, seven physical properties, the mechanical equivalent of heat, and the gravitational constant:

$$T_m = f(J, g_c, M_w, k, \mu, C_p, r, T_o, T_L, \theta_T, V, A, h_a, T_a, C_{pw}, \rho_w, d_w, P, V_i, \dot{V}_L, A_D) \quad (2)$$

The 19 variables can be expressed in six fundamental dimensions, length (L), mass (M), time (θ), temperature (T), heat (H), and force (F).

The two dimensional constants, J and g_c , are included because heat and force can be expressed in terms of the other four dimensions. The dimensions of each variable are given in the nomenclature.

Since any equation representing physical phenomena must be dimensionally homogeneous, it must be possible to write equation 2 in a nondimensional form. Therefore, using π as a symbol for a dimensionless group, equation 2 may be written as follows:

$$\pi_1 = f(\pi_2, \pi_3, \dots, \pi_i) \quad (3)$$

Developing the dimensionless groups according to Buckingham's theorem, the following ten π terms were obtained containing the design variables and physical properties of a pressurization system.

$$\pi_1 = \frac{T_m - T_L}{T_o - T_L}$$

$$\pi_6 = \frac{g_c M_w P V_i}{\mu^2 r^4}$$

$$\pi_2 = \frac{J g_c M_w^2 k (T_o - T_L)}{\mu^3 r^4}$$

$$\pi_7 = \frac{g_c M_w P}{\mu^2 r}$$

$$\pi_3 = \frac{T_o - T_L}{T_L}$$

$$\pi_8 = \frac{h_a r}{k}$$

$$\pi_4 = \frac{\mu r \theta_T}{M_w}$$

$$\pi_9 = \frac{T_a - T_L}{T_o - T_L}$$

$$\pi_5 = \frac{M_w k}{\mu r^2 (C_{p_w} \rho_w d_w)}$$

$$\pi_{10} = \frac{M_w \dot{V}_L}{A_D \mu r^2}$$

Curve Fit of Dimensionless Equation

These ten dimensionless groups can be used to correlate the results of tests and computer runs according to equation 3. In most cases, equation 3 would be written in the following form:

$$\pi_1 = \alpha \pi_2^\beta \pi_3^\gamma \pi_4^\delta \pi_5^\epsilon \pi_6^\xi \pi_7^\lambda \pi_8^\tau \pi_9^\sigma \pi_{10}^\zeta \quad (4)$$

However, in this case, it is necessary to satisfy certain boundary conditions that cannot be satisfied by equation (4). The ullage mean temperature at cutoff must remain finite and not equal to zero as the ambient heat transfer approaches zero. This boundary condition cannot be satisfied by equation (4), unless the functional dependence on π_8 and π_9 is exponential. Also, as the distributor Reynolds number π_{10} approaches zero, the heat transfer in the tank approaches free convection. Therefore, the boundary condition of finite, non-zero mean temperature, when π_{10} is zero is imposed dictates an exponential functional dependence on π_{10} . Thus, these boundary conditions can be satisfied by writing equation (4) in the form:

$$\pi_1 = \alpha_1 \pi_2^\beta \pi_3^\gamma \pi_4^\delta \pi_5^\epsilon \pi_6^\xi \pi_7^\lambda e^{\alpha_2' \pi_8^\tau} \pi_9 e^{\alpha_3' \pi_{10}} \quad (5)$$

The coefficients and exponents in this equation were evaluated by a curve-fit to the data from the computer runs and tests.

It was found that the data could be correlated by equation (5) if the coefficients, α_2' and α_3' , in the exponentials were taken as functions of π_2 and π_3 :

$$\alpha_2' = \alpha_2 \pi_2^\omega \pi_3^\psi \quad (6)$$

$$\alpha_3' = \alpha_3 \pi_2^\phi \quad (7)$$

Equation (5) then becomes

$$\pi_1 = \alpha_1 \pi_2^\beta \pi_3^\gamma \pi_4^\delta \pi_5^\epsilon \pi_6^\xi \pi_7^\lambda e^{\alpha_2 \pi_2^\omega \pi_3^\psi \pi_8^\tau \pi_9} e^{\alpha_3 \pi_2^\phi \pi_{10}} \quad (8)$$

where all the coefficients and exponents are constants.
From the curve-fit, the following values were obtained for the coefficients and exponents in equation 8.*

$\alpha_1 = 0.424$	$\xi = 0.01416$
$\alpha_2 = 0.00210$	$\lambda = 0.0620$
$\alpha_3 = -0.0292$	$\omega = 0.415$
$\beta = -0.1322$	$\psi = 1.174$
$\gamma = -0.1688$	$\tau = 0.765$
$\delta = -0.1146$	$\phi = 0.1510$
$\epsilon = 0.0780$	

* Note: Use of these exponents requires that
 π_2 be divided by 10^{14}
 π_8 be divided by 10^3
 π_{10} be divided by 10^5

This equation is general and is capable of predicting the ullage mean temperature, and thus pressurant mass at cutoff, within $\pm 10\%$ for cylindrical tanks and oblate spheroids.

FIG 10 shows total pressurant requirements obtained by various investigators for a wide range of tank sizes and system parameters compared with the pressurant weights calculated by Equation (8). Excellent agreement is obtained over the entire range of conditions for hydrogen and oxygen pressurization. Evaluating the test results of (REF 4) by this method resulted in a large, but constant deviation from actual observed pressurant weight. This is probably due to the fact that the test parameters such as heat leak through the vacuum chamber and pressurant inlet temperature had to be assumed. Additional information about these tests are required to re-evaluate the conditions. The equation is limited in its application to conditions of constant ullage pressure, pressurant inlet temperature, and ambient heat transfer. The studies indicated that the equation is inaccurate at inlet temperatures less than 100°R above the saturation temperature, at ullage pressure below propellant saturation, and for very short expulsion times of less than 50 seconds.

. The restriction to cylindrical tanks can be removed by proper choice of the characteristic tank radius. Studies have shown that the characteristic tank radius for oblate spheroids, used in equation 8, should be about two thirds of the maximum tank radius. This assumption is justified because a cylinder having the same volume and surface area as an oblate spheroid has a radius equal to 0.63 times its maximum radius. Further test data and analytical studies are necessary to select the characteristic radius for other geometries.

Recently, Epstein (Ref 5) has developed a similar correlation predicting pressurant requirements. A comparison of these two methods is presently being made.

THE EFFECTS OF SYSTEM PARAMETERS ON PRESSURANT REQUIREMENT

In designing a launch or space vehicle pressurization system, vehicle parameters such as tank volume, engine flowrate, tank material, etc., determined by vehicle mission profile, are fixed input values.

However, there are various controllable parameters in a pressurization system that can be used to optimize the system without affecting basic vehicle characteristics. The relative significance of various parameters on pressurant requirements has, therefore, been investigated. The results of these studies are presented in FIG 11.

From a central origin, representing a reference condition (SATURN V, S-IC Stage) for all parameters, the increase (+Y) and decrease (-Y), of the ullage mean temperature at cutoff is shown as a function of variation of the parameters on the abscissa. The parameters were varied over a range expected for vehicle design. Thus, pressurant inlet temperature can increase or decrease by a factor of 2 from the reference condition, pressure by a factor of 3, tank radius by a factor of 2, expulsion time by a factor of 3, etc. It was indicated that the pressurant inlet temperature exerts the greatest influence on the ullage mean temperature. Diminishing return of this effect did not exist within the range of investigation (530°R to 1200°R). The mean temperature increased as the ullage pressure was increased and also as the tank radius was increased. Increasing the tank wall thickness, heat capacity, or density caused a decrease in the mean temperature. The pressurant distributor flow area (A_D) that controls the gas-to-wall forced convection heat transfer coefficient had a significant effect on the mean temperature when A_D was reduced, but no effect at all when the flow area was increased. This indicates that the pressurant inlet velocity for the reference systems was chosen at an optimum point. FIG 11 also indicates that helium pressurant must be introduced into a tank at a temperature about 1.1 times higher than oxygen pressurant to obtain the same ullage mean temperature.

CONCLUSIONS AND RECOMMENDATIONS

a. Pressurization data from cylindrical and spheroidal tanks ranging in size over four orders of magnitude have been applied for development or checkout of analytical pressurization models.

b. Heat transfer between pressurant and tank walls can differ significantly from free convection, depending on tank geometry and distributor design.

c. An equation derived by dimensional analysis provides a reasonably accurate method for prediction of pressurant requirements for cylindrical LOX and hydrogen propellant containers.

d. The strongest influence on pressurant weight is exerted by pressurant inlet temperature, for which no diminishing return occurs within a temperature range compatible with tank materials. Other important influencing factors are tank radius, distributor flow area, expulsion time and aerodynamic heating. The effect of wall heat capacity is not as significant as might be expected.

DEFINITION OF SYMBOLS

Symbol

A_D	Distributor area, L^2	(Ft^2)
J	Dimensional constant, FL/H	$(lb_f Ft/Etu)$
M_W	Pressurant molecular weight, M	(lb_m)
T_a	Ambient temperature, T	$(^{\circ}R)$
T_L	Propellant temperature, T	$(^{\circ}R)$
T_m	Ullage mean temperature at cutoff, T	$(^{\circ}R)$
T_o	Pressurant inlet temperature, T	$(^{\circ}R)$
V	Propellant tank volume, L^3	(Ft^3)
V_i	Initial ullage volume, L^3	(Ft^3)
\dot{V}_L	Propellant volumetric drain rate, L^3/θ	(Ft^3/Hr)
d_w	Wall thickness, L	$(Btu/lb_m^{\circ}R)$
c_p	Pressurant specific heat, H/MT	$(Btu/lb_m^{\circ}R)$
c_{pw}	Wall specific heat, H/MT	$(Btu/lb_m^{\circ}R)$
g_c	Dimensional constant, $ML/F\theta^2$	$(lb_m ft/lb_f Hr^2)$
h_a	Ambient heat transfer coefficient, $H/\theta TL^2$	$(Btu/Hr Ft^2 ^{\circ}R)$
k	Pressurant thermal conductivity, $H/L\theta T$	$(Btu Ft/Hr Ft^{2\circ}R)$
p	Ullage pressure, F/L^2	(lb_f/Ft^2)

DEFINITION OF SYMBOLS (CONCLUDED)

r	Propellant tank characteristic radius (maximum radius for cylindrical tanks), L	(Ft)
θ_T	Time of pressurization, θ	(Hr)
μ	Pressurant viscosity, M/L θ	(lb _m /ft hr)
ρ	Wall density, M/L ³	(lb _m /ft ³)

REFERENCES

1. Moses, J. L., and Nein, M. E., Evaluation of Propellant Sloshing on Pressurant Requirement for Large Scale Cryogenic Containers, presented at the 1962 Cryogenic Engineering Conference, Los Angeles, California.
2. Clark, J. A. et al, Pressurization of Liquid Oxygen Containers, The University of Michigan under contract with the Department of the Army # DA-20-018-or D-254, March 1961.
3. Fortran Program for the Analysis of a Single Propellant Tank Pressurization System, Rocketdyne, Division of North American Aviation, Inc., R-3936-1, September 1963.
4. Cox, E. and Tatum, John, Main Propellant Tank Pressurization System Study and Test Report, Lockheed-Georgia Company, Contract AF 04 (611)6087.
5. M. Epstein- Prediction of Liquid Hydrogen and Oxygen Pressurant Requirements, Cryogenic Engineering Conference, Philadelphia, Pennsylvania, 1964.

BIBLIOGRAPHY

J. E. Myers, C. O. Bennet: "Momentum, Heat and Mass Transfer," McGraw Hill, New York (1962).

R. B. Scott: "Cryogenic Engineering," D. Van Nosrand Company, Inc., Princeton (1959).

V. J. Johnson: "A Compendium of the Properties of Materials at Low Temperature (Phase I) Part I Properties of Fluids," National Bureau of Standards Cryogenic Laboratory (July 1960).

J. H. Hargis: "Thermophysical Properties of Oxygen and Hydrogen, . . ." NASA-MSFC Internal Note In R-P&VE-P-63-13, (October 1963).

TANK CONFIGURATIONS AND TEST PARAMETERS

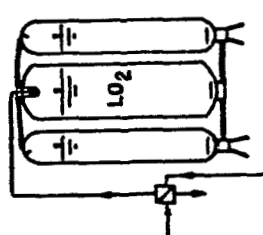
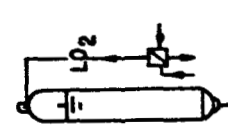
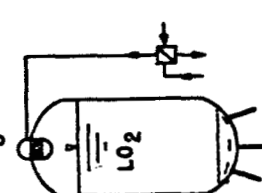

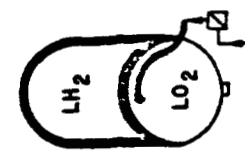
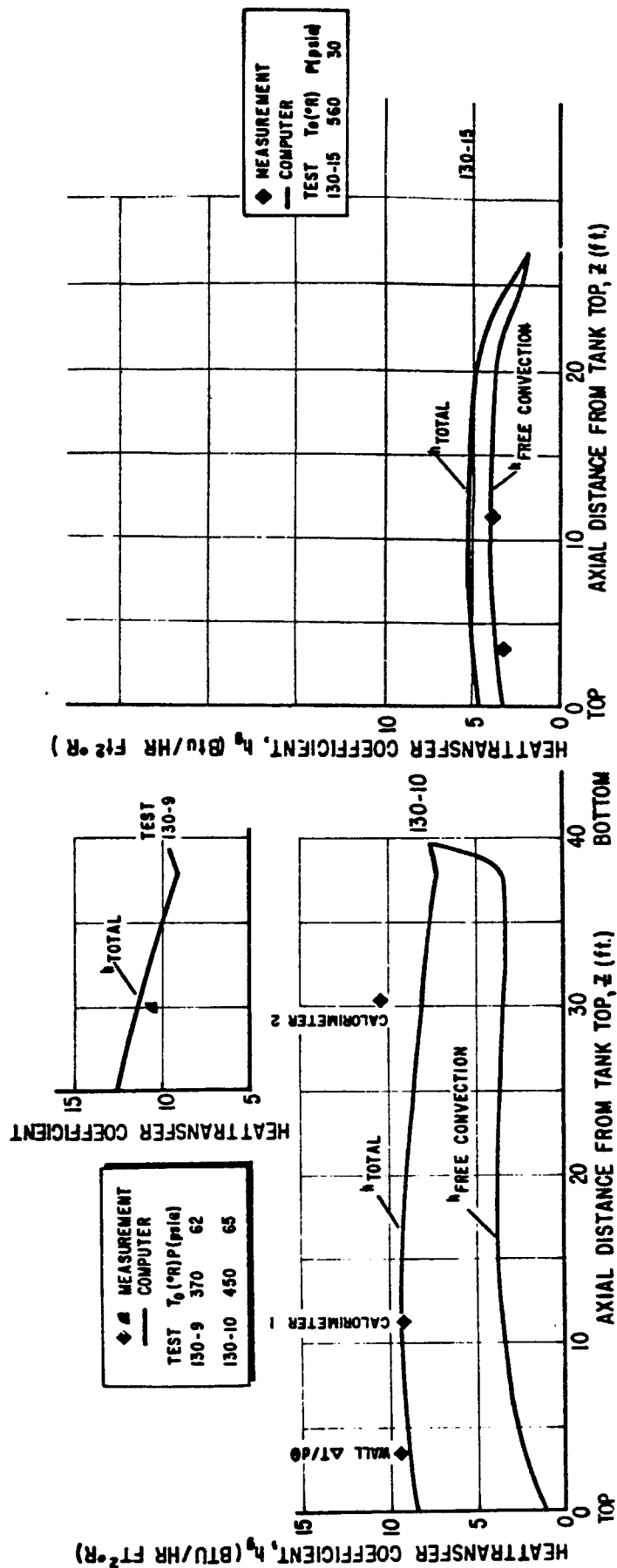
FACILITY		1	2	3	4	5
HEAT EXCHANGER						
PARAMETER	SATURN I	CTL 114	SIC 1/3	1x3 MODEL	SIV (LOX)	
TEST						
INITIAL ULLAGE VOLUME %	2 - 30	5 - 30	3 - 7	5		
PREPRESSURANT	He	O ₂ , He	He	GN ₂ , He	He	
PRESSURANT	O ₂	O ₂ , He	O ₂ , He	GN ₂	He	
TANK PRESSURE (psia)	60	14.7 - 60	20 - 40	14.7 - 60	46	
TIME OF DISCHARGE (sec.)	150	150	150 - 300	150 - 400	478	
PRESSURANT TEMP (°R)	800	370 - 800	460 - 960	510	400 - 265	
PRESS. INLET VELOCITY (FT/sec)	40 radial	35 down	13 radial	1 radial	50 ^{up} radial down	
TANK						
TOTAL VOLUME FT ³	8980	1396	3058	2.36	151	
DIAMETER (in.)	1 @ 105 4 @ 70	78	156	12	260	
L/D (APPROX.)	7	6	2	3	0.45	
TANK MATERIAL	ALUM.	SS	SS	SS	ALUM.	
INSULATION	NONE	NONE	NONE	ALL	COMMON BLKH.	
DISTRIBUTOR FLOW AREA (FT ²)	2.92	2.1	2.5	0.0436	0.05	

FIG. 1

COMPARISON BETWEEN EXPERIMENTAL AND COMPUTED HEAT TRANSFER COEFFICIENTS CONFIGURATION C



TESTS 130-9 AND 130-10 OXYGEN AS PRESSURANT

TEST 130-15, HELIUM AS PRESSURANT

FIG. 2 COMPARISON BETWEEN ULLAGE PRESSURE LOSS FOR H_2 AND GN_2 PRE-PRESSURANTS
UNDER LIQUID SLOSH AND NON-SLOSH CONDITIONS IN TANK CONFIGURATION C

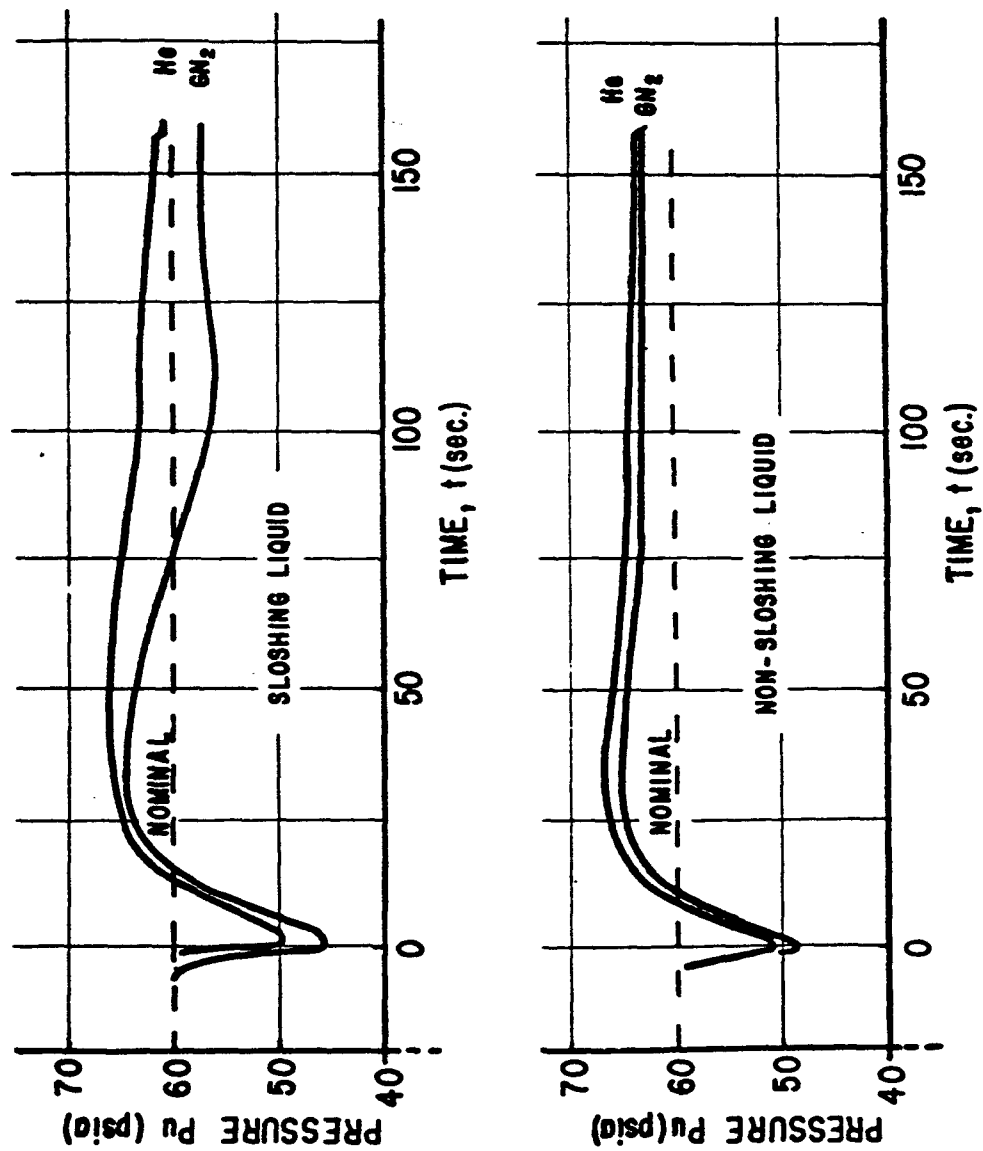


FIG. 3 MEASURED ULLAGE GAS CONCENTRATION GRADIENTS

TANK CONFIGURATION C

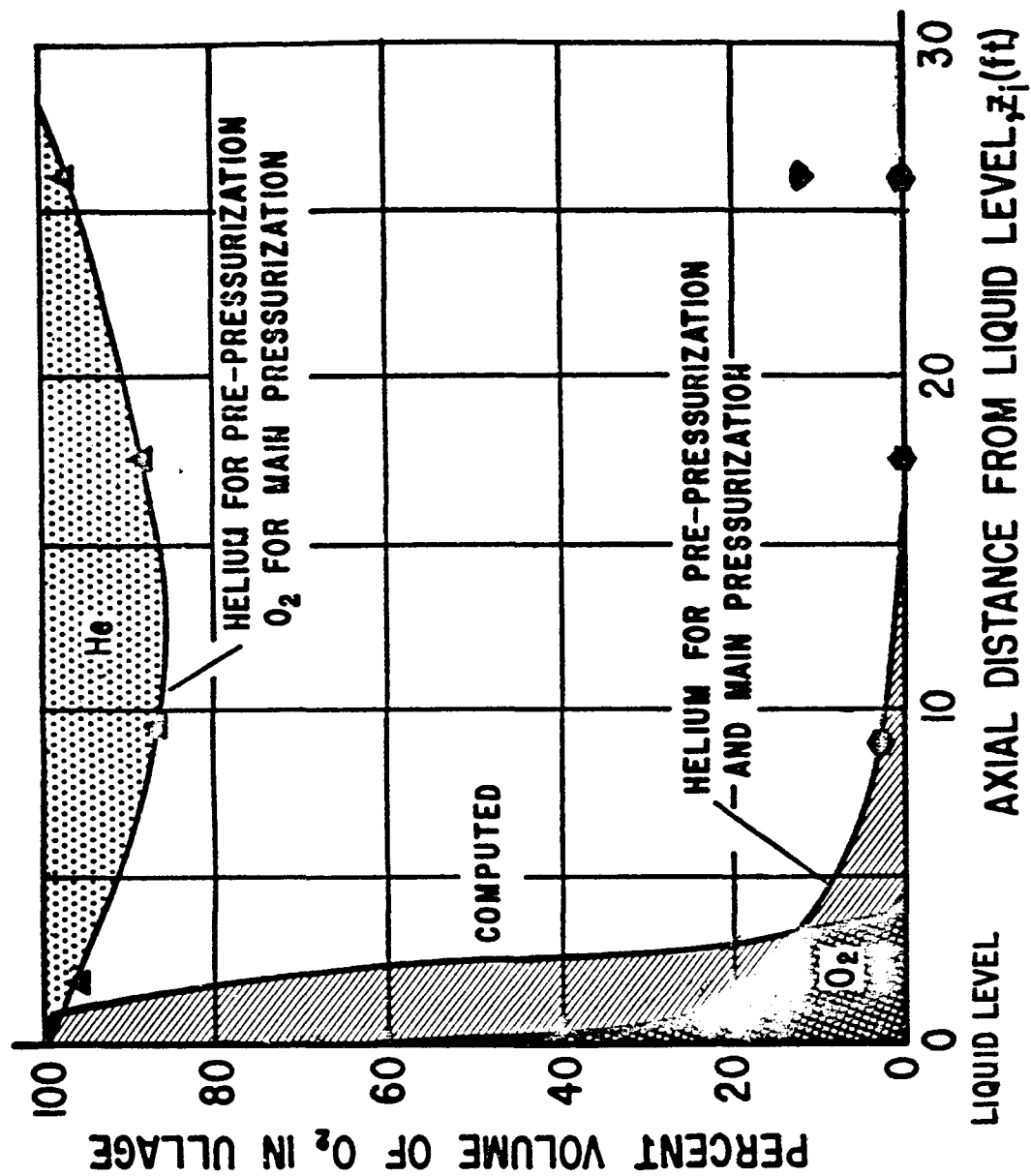


FIG. 4 EXPERIMENTALLY DETERMINED MASS TRANSFER

MT/ ΔM (LB/LB) VS TIME T (SEC)

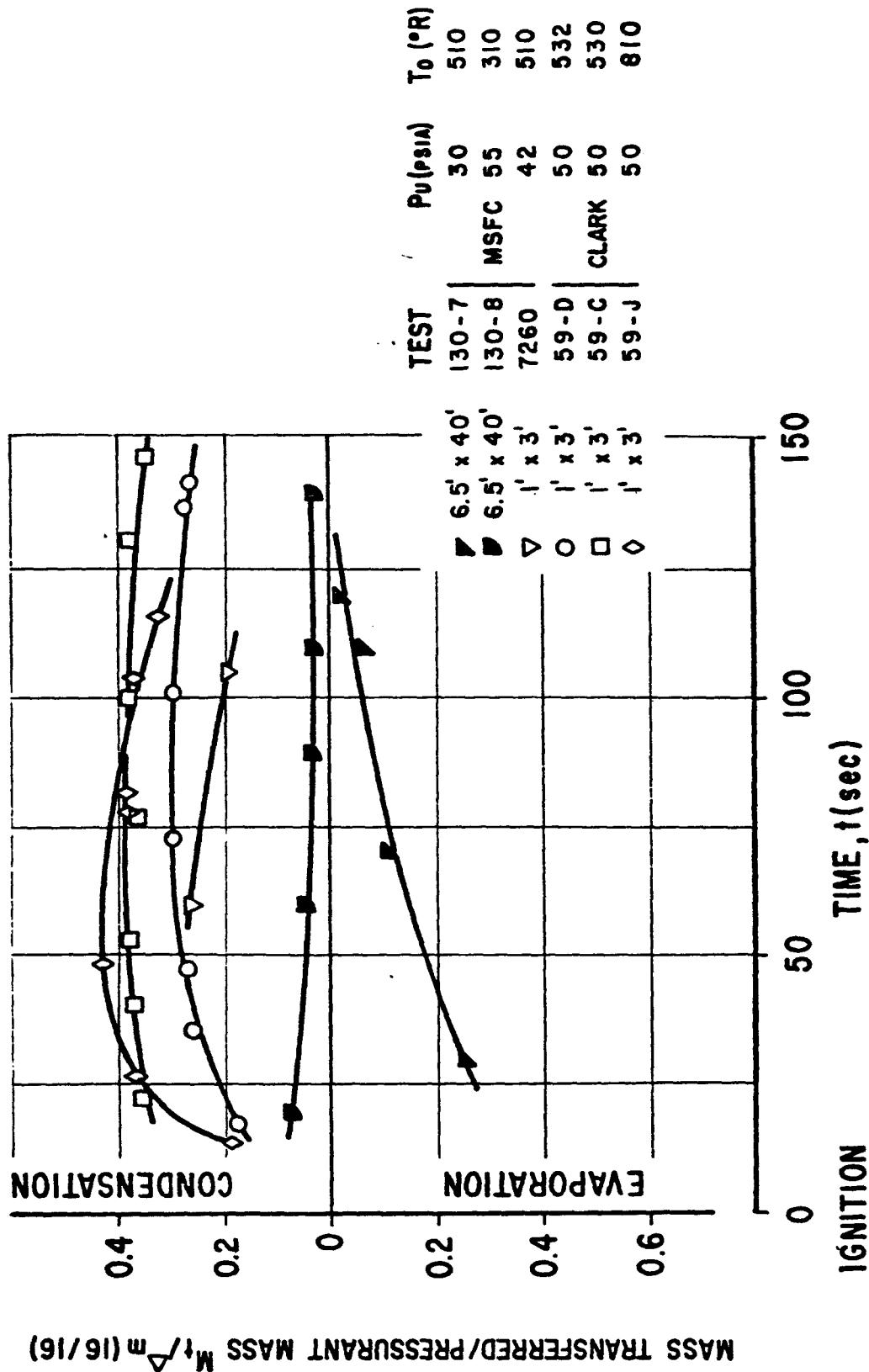
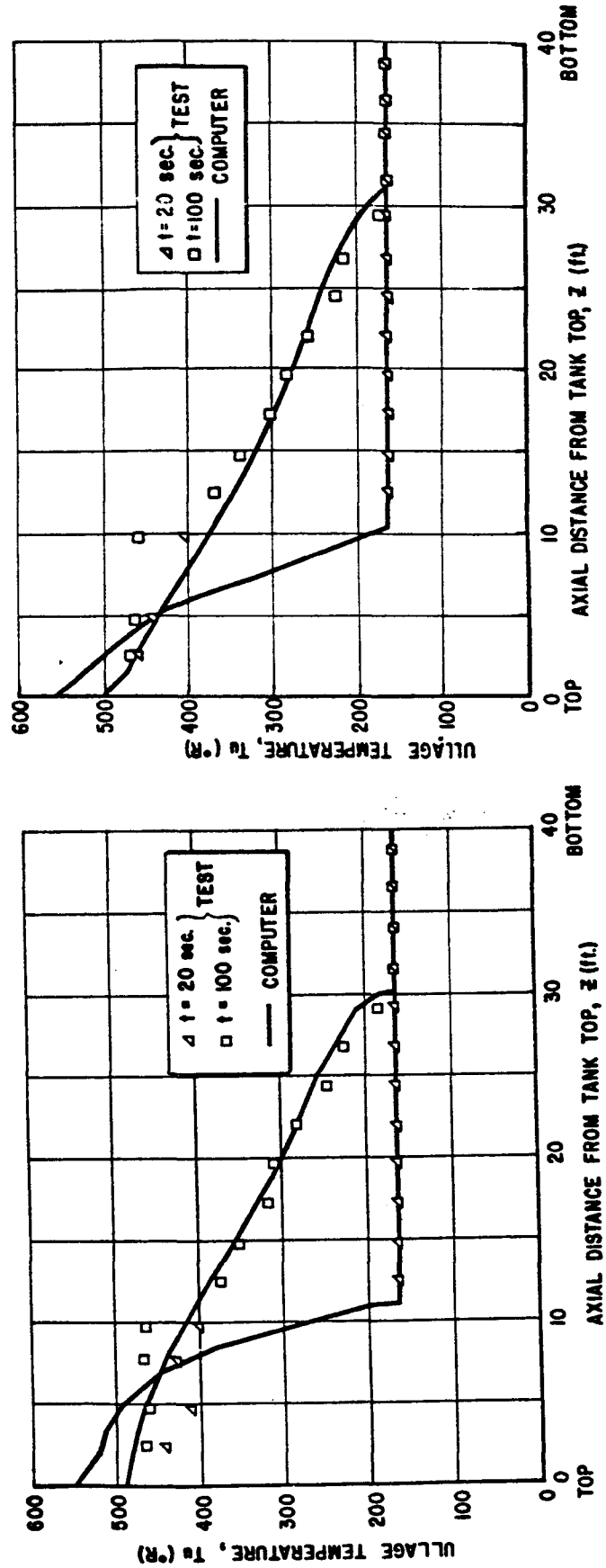


FIG. 5 COMPARISON BETWEEN EXPERIMENTAL AND COMPUTED ULLAGE TEMPERATURE GRADIENT
TANK CONFIGURATION C, OXYGEN AS PRESSURANT



TEST 130-7

TEST 130-6

**FIG. 6 COMPARISON BETWEEN EXPERIMENTAL AND COMPUTED PRESSURANT FLOWRATE
S-I STAGE LOX TANKS, OXYGEN AS PRESSURANT**

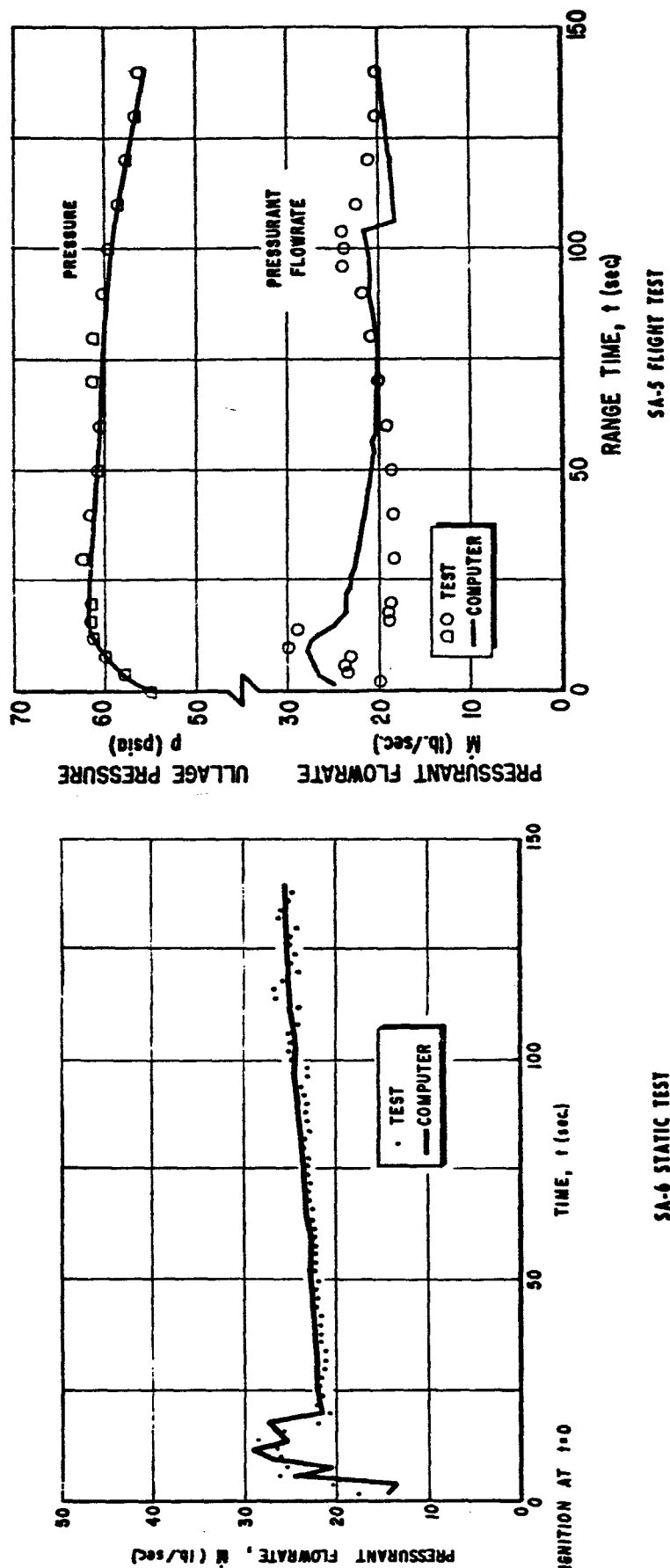
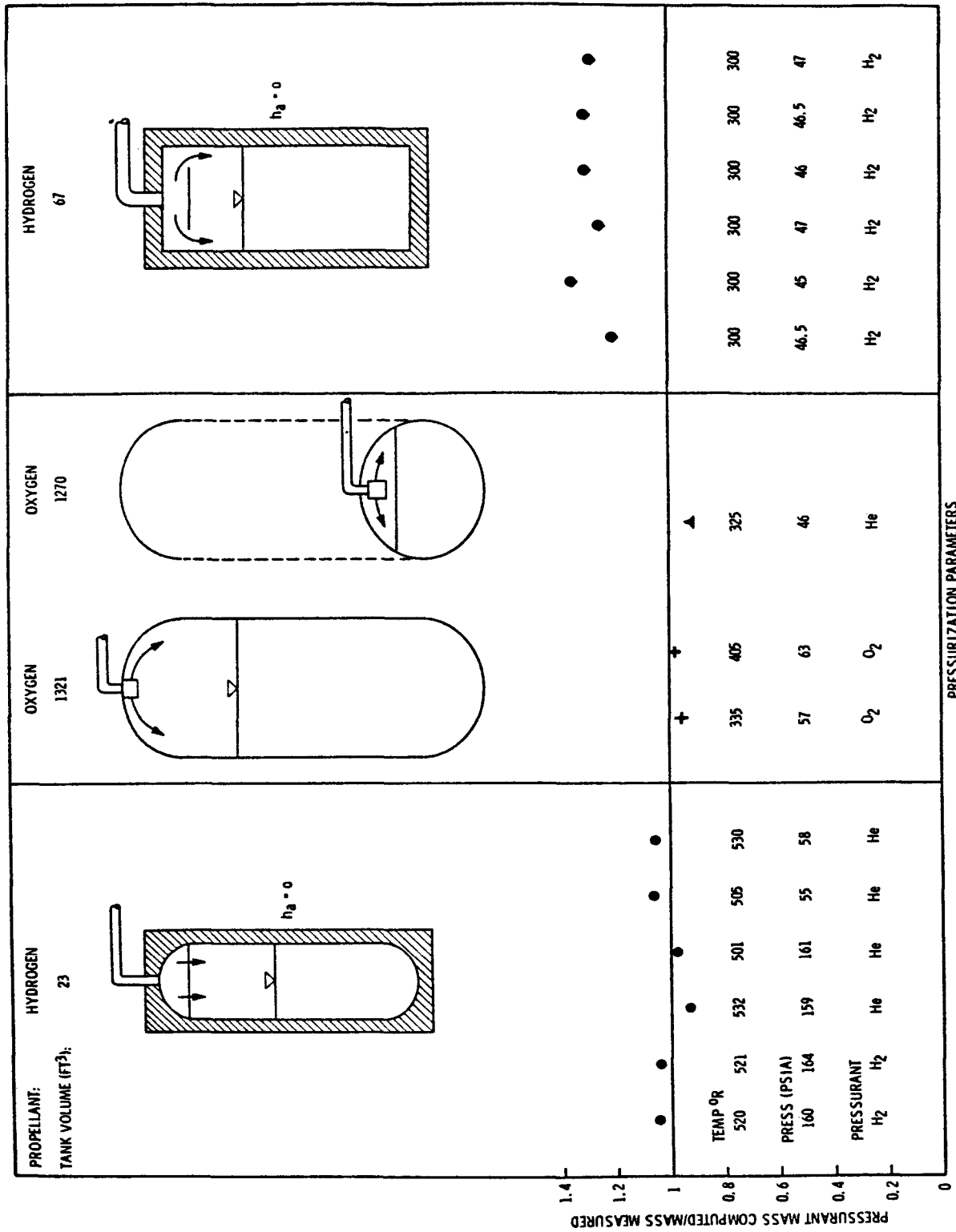
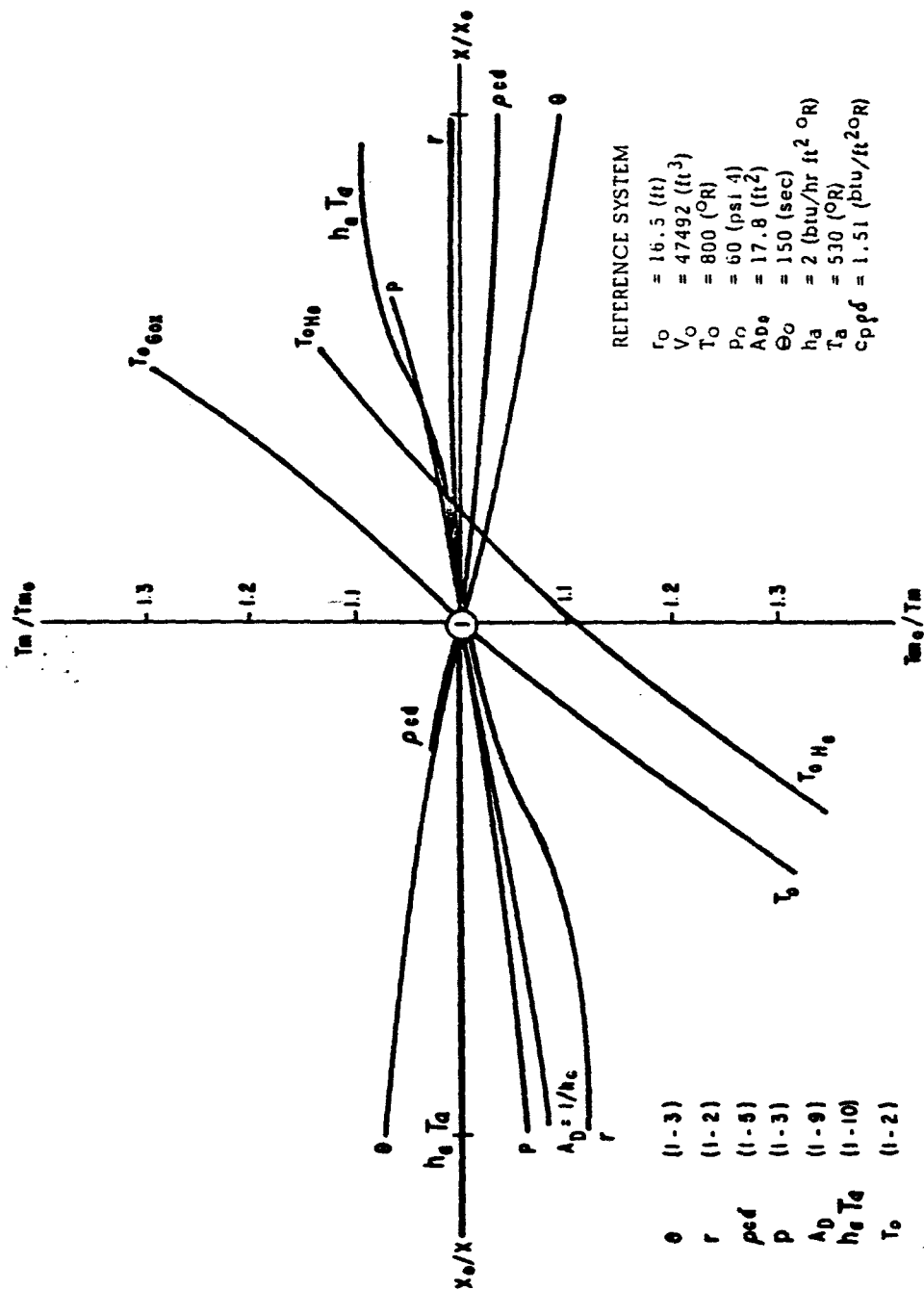


FIG. 7 COMPARISON OF CALCULATED AND MEASURED PRESSURANT MASS FOR VARIOUS TEST PARAMETERS



**FIG. 8 THE EFFECTS OF VARIOUS DESIGN PARAMETERS
ON THE MEAN TEMPERATURE AT CUTOFF**



FAST RESPONSE THERMOCOUPLE
FOR MEASUREMENT OF
TEMPERATURES IN CRYOGENIC GASES

by

C. C. Robinson, A. R. Lowrie, T. Bielawski
Beech Aircraft Corporation
Wichita, Kansas

ABSTRACT

Available thermocouples had inadequate response characteristics for an intended application. Computer studies and model tests by the Fluid Mechanics and Thermodynamics Branch of NASA Marshall Space Flight Center indicated that the "slingshot" thermocouple would give the necessary response time.

An investigation of certain variables in the "slingshot" thermocouple configuration was conducted in an attempt to develop an optimum design.

The final design decreased response time under test conditions from 4 seconds to .65 second and was satisfactory in all respects for the intended application.

INTRODUCTION

A thermocouple development program was initiated after an unsuccessful search for a suitable thermocouple to measure ullage gas temperatures. The program was funded by National Aeronautics and Space Administration, George C. Marshall Space Flight Center Contract Number NAS-8-5531, in support of a study on pressurization of liquid hydrogen missile tanks. The tests required a temperature sensor with a time constant of two seconds or less in hydrogen gas at two atmospheres pressure and cryogenic temperatures. Most time response data on temperature sensors are for high heat capacity fluids or for gases at relatively high velocities. Previous work indicated that the sensitivity of thermocouples fabricated from small diameter wire was acceptable and work was begun to optimize the design and determine the time constant for these specific conditions.

THEORETICAL APPROACH

To obtain a fast response from a temperature sensor the heat capacity of the sensing element must be small in relation to the heat transfer to the element. Also, the element must be thermally isolated from its supports. The first of these requirements is met by a small diameter thermocouple wire. The second requirement can be met by making the leads of sufficient length so the heat conduction down the leads is small and by assuming that the leads adjacent to the junction are subjected to the same thermal conditions. On other sensors that were considered, the mountings were generally large and thermally too close to be considered acceptable. Platinum wire resistance probes were considered but require a four-wire lead system to eliminate the error due to lead resistance changes. Also the sensor element "averages" the temperature between the sensor wire supports and is affected to a considerable degree by heat transfer to the supports. Although the smallest thermocouple wire used will give the fastest response time, this program was restricted at the onset to a wire size considered large enough to withstand gas velocities up to 30 feet per second.

The rate of response of a thermocouple to a step change in the temperature of the surroundings is essentially a heat transfer problem. The energy balance of the thermocouple junction may be written as:

$$Q_r + Q_k + Q_c = Q_s \text{ where:}$$

Q_r is the rate of heat transfer from environment to the junction by means of radiation.

Q_k is the rate of conductive heat transfer.

Q_c is the rate of convective heat transfer (the junction is assumed to have a finite length, and for practical purposes includes segments of the wires).

Q_s is the rate at which heat is stored in the junction.

For purposes of simplification, assume the thermocouple to be cylindrical and of sufficient length that Q_k becomes insignificant.

As the absolute temperatures of the radiating surfaces are relatively low, Q_r is also insignificant. Therefore, by setting $Q_k = Q_r = 0$, the energy balance equation reduces to:

$$Q_s = Q_c$$

This equation, when written in terms of the temperature difference with gas and thermocouple parameters constant, shows that the time constant, τ , is the time interval required for the junction to respond to 63.2% of the step change in temperature of the media surrounding the couple.¹ The time constant is defined by

$$\tau = \frac{\rho_w c_w V}{hA} \quad \text{where:}$$

- ρ_w = density of the thermocouple wire
- c_w = specific heat of the thermocouple wire
- V = volume of the thermocouple wire per unit length
- A = surface area of the thermocouple wire per unit length
- h = heat transfer coefficient which is further defined as

$$h = \frac{Nu K_g}{D} \quad \text{where:}$$

- D = diameter of the wire
- K_g = coefficient of thermal conductivity of the gas
- Nu = Nusselts Number

Assuming a gas velocity of 5 feet per second and solving the above equations for τ resulted in time constants of .149 for hydrogen gas and .817 for nitrogen gas under the conditions of these tests. The actual velocity of the convection currents in the experiment was not measured and the velocity of 5 feet per second was arbitrarily chosen in order to define the response parameters.

EXPERIMENTAL APPROACH

A step function of temperature in a non-flowing gas requires that the sensor be moved from one temperature region to another or that the sensor be

conditioned to an "artificial" temperature in the reference gas. The conditioning may be done by heating or cooling the sensor to a nonequilibrium temperature.² After consideration of the actual test conditions it was decided to condition the sensor in the saturated liquid and move it to a second position in the warmer ullage gas several inches above the liquid. This also simulated draining of a test liquid to below the level of a sensor which leaves the sensor wet. The resultant "drying" time of the sensor was also of interest for the pressurization study program. The temperature of the ullage gas was not disturbed by the presence of the cold thermocouple nor is any appreciable velocity imparted to the ullage gas by the 5 feet per minute velocity of the thermocouple. The start of warm-up is assumed to be the point at which the sensor is no longer cooled by the vaporizing liquid. This point can be used as zero time for the response time in gas only. The response times presented in the data do not include this "drying" time which is a function of shape, orientation, and wettability of the couple as well as the heat of vaporization of the test liquid.

The basic configuration to be tested is known as the slingshot type and consists of a Y-shaped frame supporting the thermocouple and its leads. Figure 1 shows some of the configurations tested.

The following is a list of variables which were investigated for their effects on response time.

1. The thickness of a teflon slingshot frame.
2. A slingshot frame made of 18 gauge cu/con thermocouple wire.
3. Dimensions of the slingshot frame.
4. Thermocouple junction weld.
5. Welds on lead wires in relation to the frame.
6. Angles formed by the thermocouple junction.
7. Relation of the thermocouple to the horizontal during testing.
8. Effect of insulation and varnish.
9. Cleaning of the thermocouple wire at the junction.
10. Speed of probe being removed from liquid.

EXPERIMENTAL APPARATUS

The schematic of the test apparatus is shown in Figure 2. The cryostat is a flanged 35 liter Hoffman Liquified Gas Dewar. Figure 3 shows the general configuration of the cryostat and the mechanism used to position the probes relative to the liquid level. Schedule requirements of the program dictated

that a relatively simple mechanism be fabricated to position the test probe and manual operation was used in lieu of a more refined mechanical system.

The four-point liquid level probe was installed through a compression seal which permitted adjustment of the probe to determine the actual liquid level in the dewar. A reference temperature sensor was mounted on this same probe at such a position that it could be lowered into the liquid or raised to a point 5.5 inches above the nominal liquid level.

The test probe support was constructed from 3/8" diameter tubing through which the test probe leads were brought out of the dewar. This tube was installed through a compression seal and a support arm on the dewar cover. Two (2) microswitches were used to indicate the extreme positions of the support at either end of its eleven inch travel. The microswitches provided a record of the time that the probe was moving and provided a means for determining the time that the probe entered the ullage gas from the liquid.

The test probe was attached to a bar on the end of the support and adjusted so that the thermocouple junction was located within one-fourth inch of the reference sensor and in the same horizontal plane when both were in the "raised" position 5.5 inches above the liquid level.

The necessary plumbing was attached to the top cover of the dewar and consisted of a liquid fill system and a vent relief system.

Figure 4 is a photograph of the experimental apparatus removed from the dewar.

EXPERIMENTAL PROCEDURE

The thermocouple to be tested was installed on the support so that the junction was located properly in relation to the reference couple and the horizontal plane. The cover was then secured and the cryostat filled with liquid hydrogen or liquid nitrogen until the second liquid level sensor indicated covered.

Both the test probe and the reference probe were then immersed into the liquid and allowed to stabilize for five minutes. At the conclusion of this period the millivolt output for both probes was read and recorded. Both probes were then raised to the gaseous media, the five minute stabilization period repeated, and the millivolt output of both probes read and recorded. At this time the test probe was lowered into the liquid and allowed to thermally stabilize. The recorder is started and the test probe is raised to the gaseous atmosphere.

Each thermocouple was tested ten times and the average response time was determined. The ullage pressure was ambient during all response tests.

RESULTS

The first variable investigated was the mass of the teflon support frame. The frame, with arms of 1/4 inch square cross-section, was tested with a 30 gauge Cu/Con thermocouple. The response time was 2.2 seconds. The frame thickness was reduced to 1/8 inch by removing material from the outside edge and keeping the distance between arms at 3 inches. This caused no change in the response time and it was felt that the mass of the frame was still excessive. A frame was then constructed of 14 gauge stranded and insulated thermocouple wire. Similar metal solder joints were made between the 30 gauge wires of the thermocouple under test and the thermocouple wire that formed the frame. The response time for this configuration was 4.6 seconds. The configuration of a frame of 18 gauge wire and a 30 gauge thermocouple had an approximate time of 2 seconds.

The second variable investigated was the size of the frame. The length of the two arms was the same as the length of the base. The response time of 30 gauge thermocouples mounted on various size frames of 18 gauge wire are as follows:

- 1 inch frame - 5.0 seconds
- 2 inch frame - 2.0 seconds
- 3 inch frame - 1.1 seconds

The thermocouple leads were in a straight line between the ends of the frame arms. The third variable investigated was the configuration of the weld made at the thermocouple junction. The welding was done with a Weldomatic welder, model 1026-C using two pound electrode pressure and 5 watt-seconds of heat. A copper chromium alloy, Class 2 electrode and a Tungston base inert Class 2 electrode were used. The wires were overlapped for welding. To check weld repeatability a junction was first broken, the ends trimmed back, and the junction rewelded. The response time of the rewelded thermocouple was within 2% of the original thermocouple. It was observed that apparently identical thermocouples had a widely varying response time. Careful examination of the junction showed a small length of wire extending beyond the weld. Trimming of this wire resulted, in some cases, in a decrease in response time from 3.8 to 0.5 seconds. All welds were carefully trimmed to avoid erratic data.

The fourth variable investigated was the included angle between the thermocouple leads. The response time of 30 gauge thermocouples mounted on 18 gauge frames with varying included angles are as follows:

- 74° angle, 1.2 seconds average for 14 tests.
- 98° angle, 1.3 seconds average for 14 tests.
- 118° angle, 2.0 seconds average for 14 tests.
- 143° angle, 2.8 seconds average for 14 tests.

The fifth variable investigated was the angle which the plane of the frame arms made with the horizontal. The response time with varying mounting angles are as follows:

- 45° angle above horizontal, .78 second.
- 30° angle above horizontal, .63 second.
- 15° angle above horizontal, .90 second.
- 0° horizontal, 1.1 seconds.
- 15° angle below horizontal, 1.2 seconds.
- 30° angle below horizontal, 1.5 seconds.
- 45° angle below horizontal, 1.8 seconds.

The sixth variable investigated was the effect of insulating varnish. Removal of the varnish on a 24 gauge thermocouple by careful scraping resulted in approximately 20% reduction in thermocouple response time. The 30 gauge thermocouples used in this work were fabricated from bare wire. The removal of varnish from the frame wires resulted in an additional decrease of approximately 10%.

The seventh variable investigated was the cleaning of the thermocouple. Several probes that were cleaned in Freon had only a slight change in response time. Cleaning is not felt to be an important variable.

The eighth variable investigated was the speed of thermocouple withdrawal from the hydrogen bath. The 11 inch movement was made in an average time of 0.6 second with small response time variations at other speeds.

The investigation of the above variables was the basis for design of thermocouples used in a hydrogen tankage pressurization study for NASA. Forty-five welded thermocouples were fabricated. Their calibration of output versus temperature was close to that of Powell, Caywood, and Bunch.³ The average time constant in hydrogen was approximately 0.5 second, and in nitrogen was approximately 1.2 seconds. Typical time response curves are shown in Figure 5. Some thermocouple locations required that they withstand liquid velocities

of 32 feet per second and gas velocities of 50 feet per second. These thermocouples performed satisfactorily.

CONCLUSION

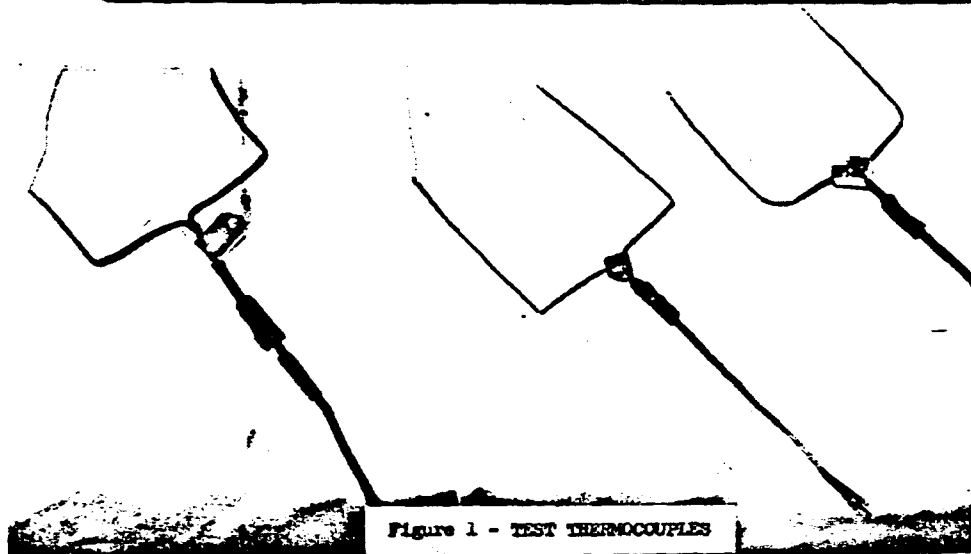
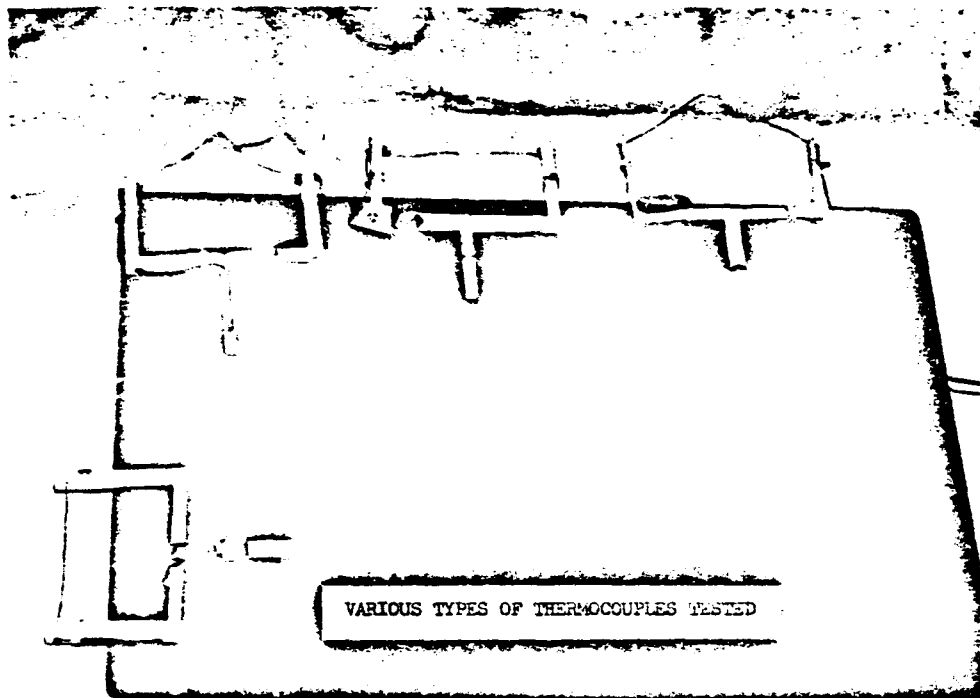
The results indicate that durable thermocouples can be made in quantity and have fast reproducible response times. Such thermocouples should be fabricated from uninsulated small diameter wire. The thermocouple should be mounted in a lightweight wire slingshot frame with support distance 3 inches or more. The thermocouple leads should form an included angle of about 75° (the bead about 2 inches beyond the ends of the frame arms). The frame should be mounted so the plane of the supports is about 30° above horizontal. The thermocouple junction should be made by welding with excess wire carefully trimmed away.

ACKNOWLEDGEMENTS

This program was begun by the Fluid Mechanics and Thermodynamics Branch of Marshall Space Flight Center in 1962. Computer studies and model tests indicated that the "slingshot" thermocouple would give the necessary response time. Beech Aircraft Corporation continued the NASA program to optimize the design for the particular test criteria.

REFERENCES

1. Baldwin-Lima-Hamilton Technical Data 4336-1.
2. Marvin D. Scadron and Isidore Warshawsky, "Experimental Determination of the Time Constants and Nusselt Number for Bare Wire Thermocouples." NACA Technical Note 2599, 1952.
3. Robert L. Powell, Lindsay P. Gaywood, Jr., and M. D. Bunch. "Low Temperature Thermocouples." Temperature, Its Measurement and Control in Science and Industry, Volume III, Part 2, 65 (1962).



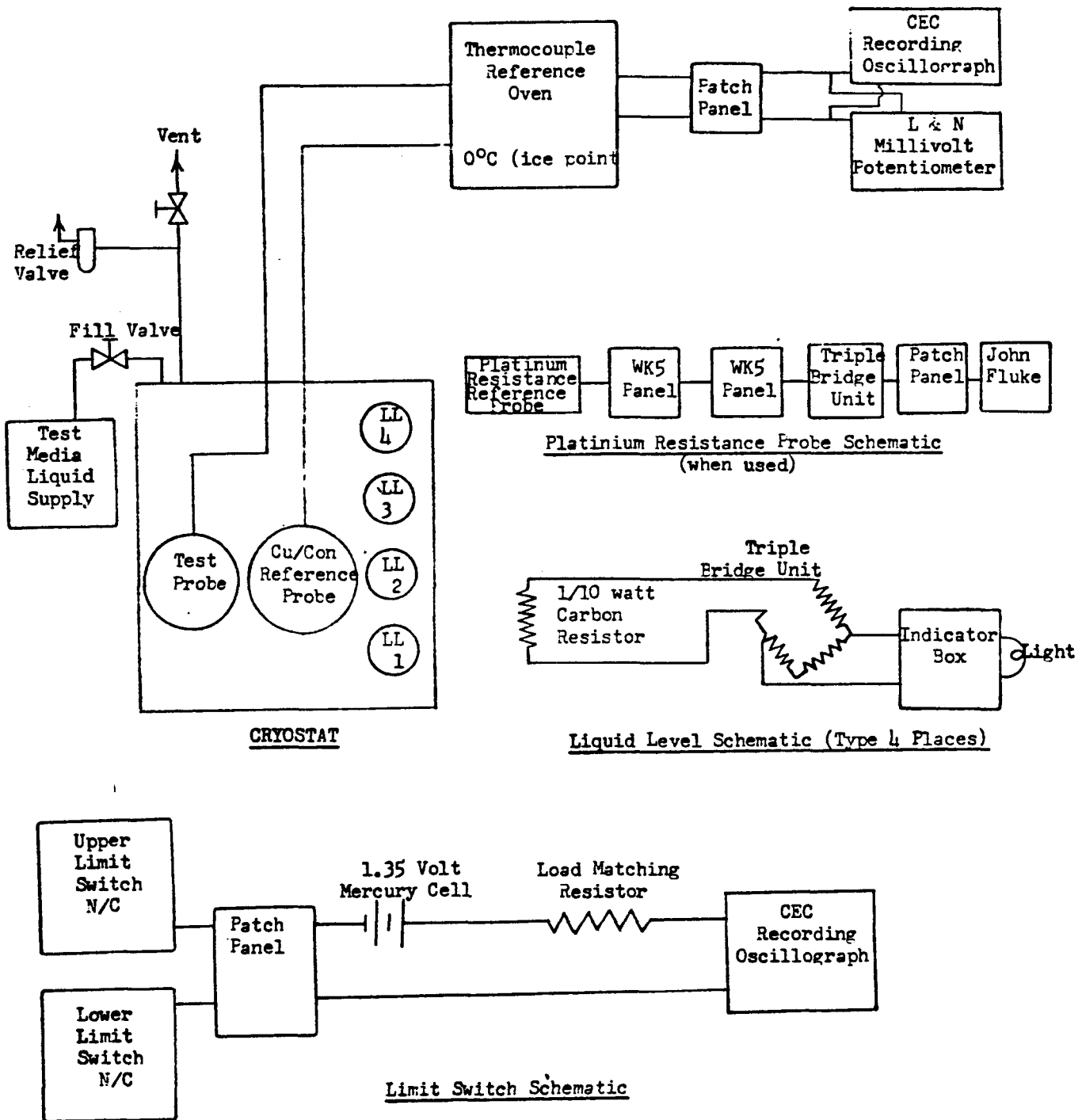


FIGURE 2
SCHEMATIC TEST SETUP

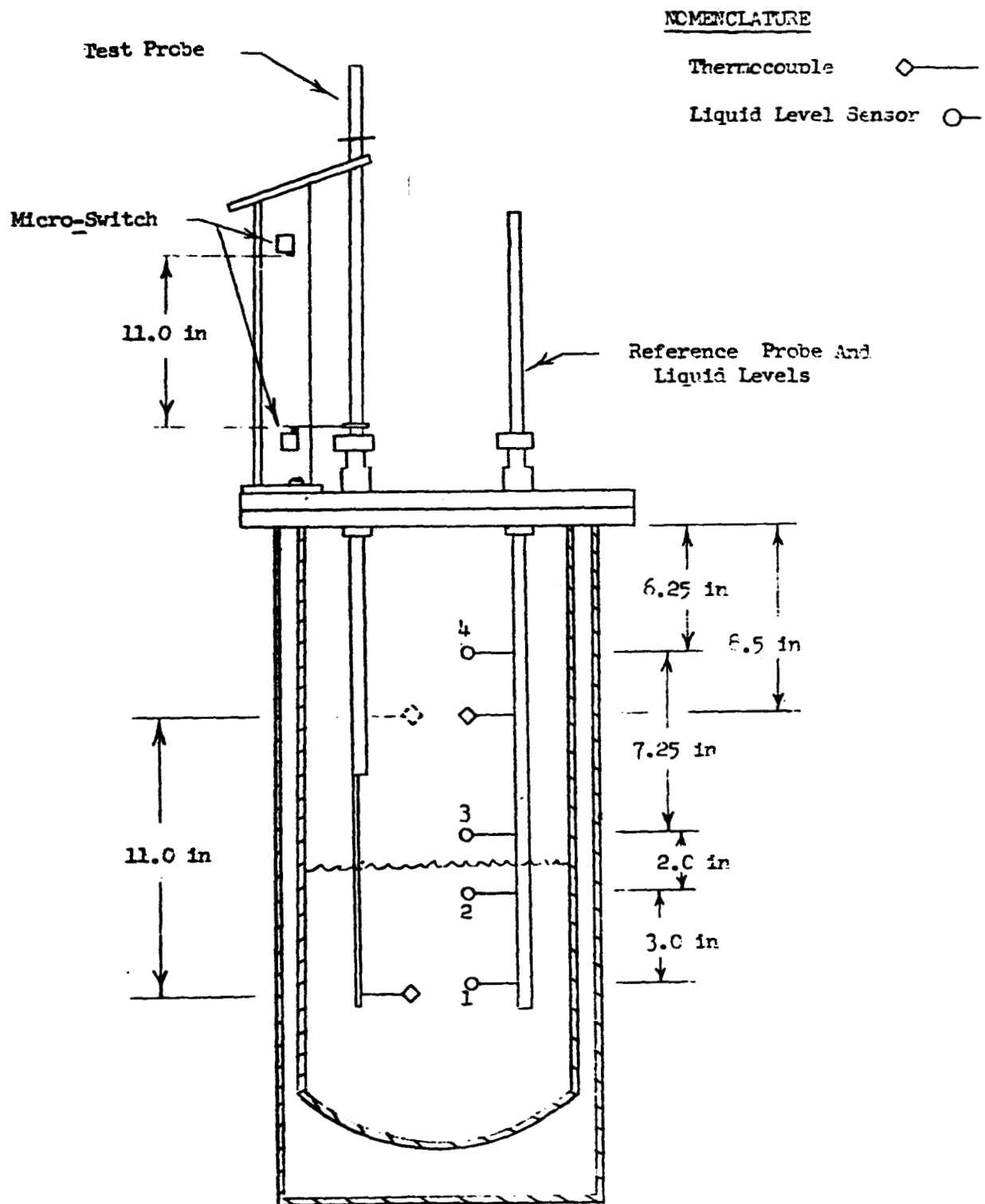


FIGURE 3. CRYOSTAT

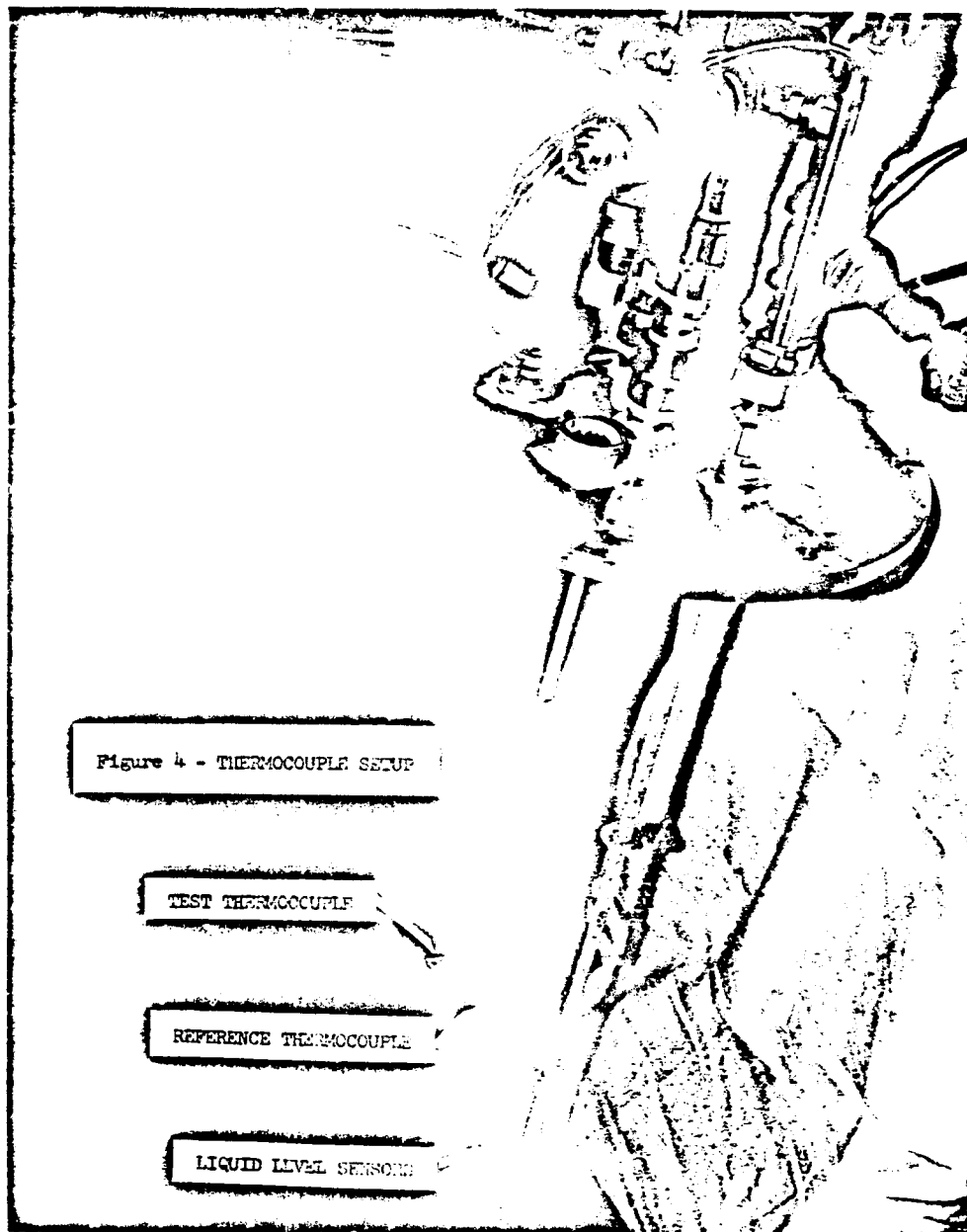


FIGURE 4. THERMOCOUPLE SETUP

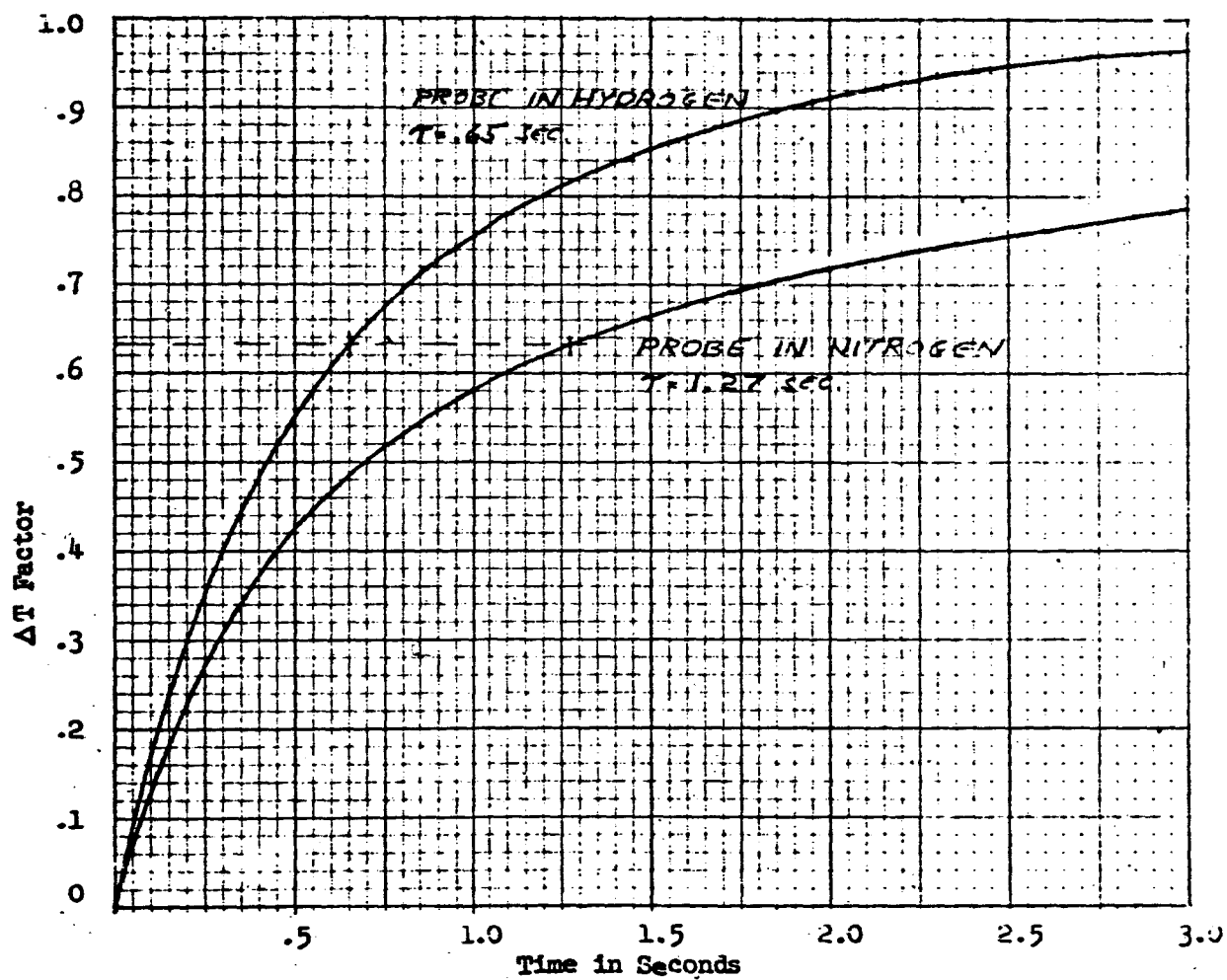


Figure 5 - TYPICAL THERMOCOUPLE RESPONSE CURVE

$$\Delta T = \frac{\text{Thermocouple Temperature} - \text{Liquid Temperature}}{\text{Gas Temperature} - \text{Liquid Temperature}}$$

PROPELLANT TANK PRESSURIZATION
BY INTERNAL COMBUSTION

by

Paul A. Friedman and Richard J. Kenny
Martin-Marietta Corporation
Martin Company
Denver, Colorado

PROPELLANT TANK PRESSURIZATION BY INTERNAL COMBUSTION

Paul A. Friedman and Richard J. Kenny

Martin Marietta Company, Denver, Colorado

A highly efficient method of propellant tank pressurization has been developed recently by the Martin Company, under Air Force sponsorship, employing the storable hypergolic liquid propellants nitrogen tetroxide and a 50/50 fuel blend of hydrazine and dimazine. The basic pressurization concept employs a controlled reaction inside of the main propellant tanks to generate the pressurizing gas for propellant expulsion. Over 100 subscale system tests were performed to develop the process and provide data up to 200 psia. Based on the results of this initial investigation, a mathematical model computer program was formulated for predicting pressurization system performance characteristics. This analytical model was used to predict full-scale system performance and aid in the design of a flight-weight ground-test article. Subsequent 15 second duration demonstration tests were performed on the full-scale system at 37 ± 0.25 psia to verify concept feasibility and establish system capability. Both the experimental and theoretical work are described, and technical considerations pertinent to this pressurization method are discussed. In addition, recent experimental tests are summarized and future programs outlined.

Introduction

With the advent of the Titan II storable hypergolic liquid propellants (nitrogen tetroxide and 50/50 hydrazine-unsymmetrical dimethyl hydrazine mixture), considerable interest developed in the possibility of a chemical reaction inside the main propellant tank for ullage pressurization. The possible elimination of a heat exchanger and reduction in pressurant storage tank requirements results in a lower propulsion system weight, thereby improving the overall vehicle mass fraction (usable propellant weight/lift-off weight). The primary advantages of high-density pressurant storage at low pressures and moderately low pressurizing gas density have been known for some time, but the feasibility of such a system installed in a flight-type propulsion system was first demonstrated this past year. The specific system developed employs fuel injection in the oxidizer tank (or vice versa) with the controlled combustion process providing the pressurizing gas for propellant expulsion. Pulse-mode pressure control with solid-stream reagent injection and propellant surface impingement are employed.

Specific objectives of this program were to effect the pressurization process with precise pressure control and tolerable thermal levels in both the tank wall and the liquid propellant, with a minimum of propellant degradation. To achieve this goal, extensive experimentation was performed on a 5.33-ft³ research test tank at 36, 100, and 200 psia to study the process in detail and establish an optimum configuration. Based on the knowledge acquired, a mathematical model was formulated on the IBM 7094 digital computer for full-scale system performance prediction. This program describes the thermodynamic history of a specific liquid rocket pressurization system during normal operation. The culmination of the experimental and theoretical programs was the generation of full-scale system design criteria and the demonstration of reliable system operation at 37 psia in a 279-ft³ flight-weight aluminum propellant tank.

Process Description

The basic concept of a propellant tank chemical pressurization system involves the direct injection of a hypergolic reactant into the main propellant with the combustion gases used as the pressurant. Figure 1 is a pictorial representation of the pressurization phenomenon associated with the system developed. The reactant is stored under pressure and intermittently injected by a pressure switch-controlled pneumatic valve. Flow of the reactant is initiated by a propellant tank low-limit pressure switch that opens the injector valve, causing the reactant to be forced into the propellant tank by a 100- to 200-psi injector differential pressure. The reaction occurs in a concentrated area below the propellant surface because of the penetration capability of the solid-stream surface injection technique. This method was selected for optimum performance. The energy of the reaction is partially absorbed by the liquid propellant, enabling moderate pressure rise rates in the propellant tank. Reagent injection is terminated when the propellant tank high-limit pressure switch deenergizes the normally closed injector. Experimentation established the capability of such a pulse-type injection pressurization system to control tank pressures within $\pm 1\%$ at an injection frequency of 2 to 5 cycles per sec with a 5% initial ullage volume.

During the research program, it became apparent that the injection technique was of primary importance in establishing pressurization process characteristics. Because of the availability of one of the reactants in a relatively infinite quiescent quantity, the nature of the injected reactant is the major factor in determining the reaction mixture ratio, mass oxidizer/mass fuel consumed (with associated combustion temperature and reaction product composition), and the amount of heat transferred to the propellant as a result of subsurface combustion. A precise definition of the combustion process is required because of the need to dissipate approximately 75% of the thermal energy to the liquid propellant in order to obtain moderate operating temperatures.

The pressurization process is further complicated by the fact that the quantity of gas generated depends not only on the apparent reaction mixture ratio (R_m) but also the condensation ratio (R_c). The quantity of injected reagent required can be expressed as:

for the fuel tank,

$$W_o = \frac{W_{cp}}{1 - R_c} \left(\frac{R_m}{R_m + 1} \right) \quad (1)$$

and for the oxidizer tank,

$$W_f = \frac{W_{cp}}{1 - R_c} \left(\frac{1}{R_m + 1} \right) \quad (2)$$

where

R_m = reaction mixture ratio (mass oxidizer/mass fuel),

R_c = reaction condensation ratio (mass condensibles M_{cp} /total products (M_{tp}),

W_o = mass oxidizer injected,

W_f = mass fuel injected,

W_{cp} = mass gaseous products.

The mass of gaseous combustion products required is readily determined by the ideal gas law with recognition of the partial pressure of propellant vapor and possible presence of an initial inert pressurant. The quantity of condensed products and the reaction mixture ratio were determined experimentally. Based on the extent of experimental investigation performed, the mixing phenomenon associated with the reaction indicated that a considerable variation in the reaction mixture ratio is possible. For the solid-stream surface injection technique, however, this ratio is always in favor of the main propellant for the nitrogen tetroxide - 50/50 hydrazine-dimazine combination (i.e., fuel-rich in the fuel tank and oxidizer-rich in the oxidizer tank). Consequently, a minimum quantity of injected reagent is required to pressurize a given volume.

Analysis

A mathematical model of the chemical pressurization process was developed for the IBM 7094 digital computer. The model was based on thermodynamic analysis of the experimental system, empirical relationships derived from photographic observation of the combustion phenomenon, and interpretation of ullage gas and propellant composition data. The solution of simultaneous mass and energy differential equations on an incremental time basis permits the prediction of transient pressurization system characteristics for either a nonvolatile or volatile propellant whose vapors may dissociate. Only the internal thermodynamics of the propellant tank with environmental influence is considered, and process gas data and reagent supply information must be furnished. Unique features of the model include:

- 1) the solution of developed equations for either liquid or vapor phase reaction inside the main propellant tank;
- 2) capability for common ullage pressurization;
- 3) variation in system configuration, mode of operation, and process parameters.

Comparisons of predicted reagent consumption, injector frequency, and operating temperature histories with full-scale system test results show encouraging agreement. But because of the complex nature of the reaction process, further investigation is planned to allow performance prediction for propulsion systems with extensive variations in configuration or propellant composition.

General Logic

The Mathematical Model considers pressurization of a single tank, or two tanks in series, with ullage gas from the primary tank used to pressurize the secondary tank. A flow diagram of the general computation sequence and subroutines is presented in Fig. 2. Injection of reactant into the primary tank may be controlled by a pressure-actuated on-off valve or by a constant-flow orifice. For constant-flow operation, a time increment is input, and transient conditions are calculated at the end of each interval until shutdown occurs. For cyclic or pulse (on-off) operation, a high- and low-pressure value for the primary tank is input, and the dependent time interval is calculated for either pressure decay to the low level (injector off) or pressure increase by reaction to the high level. The time and transient conditions are calculated at the end of each interval until shutdown occurs.

If two tanks are pressurized in series (common ullage configuration), gas crossflow may occur only from the primary to the secondary tank, and then only if the primary tank ullage pressure is sufficiently above the ullage pressure in the secondary tank. The crossflow is just sufficient to maintain a specific pressure in the secondary tank, and no heat loss or pressure drop effects in the transfer line are considered. Pressure-sensing points may be either at tank top or bottom. If at bottom, the pressure is the sum of ullage gas pressure plus propellant head.

Heat is transferred by convection between the gas and the adjacent tank wall, the liquid and the adjacent tank wall, the outside wall and the adjacent atmosphere, and across the tranquil portion of the gas-liquid interface. For subsurface reaction, heat transfer is also considered between the combustion zone and the liquid. Evaporation and subsequent vapor dissociation can be treated in either tank, with heat and mass transfer across the ullage gas-liquid interface. The computer program assumes homogeneous mass and energy distribution in both the liquid and gaseous phases and homogeneous temperature distribution in the tank wall adjacent to the gas and liquid. It also assumes the ideal gas law applies to the ullage constituents. For the range in temperature and pressure normally encountered in propellant tank pressurization systems, the compressibility effects may be neglected for noncryogenic applications.

Time Increment

With a constant-flow orifice, the time increment is an input constant to the program. For pulse-flow injection, however, the injector is actuated when ullage pressure drops to or below a specified level, and is deactivated when the pressure reaches or is above a particular level. To simulate this with the mathematical model, the required pressure change (ΔP) is calculated and compared with the pressure change rate ($dP/d\theta$) to arrive at the required time interval ($\Delta\theta$). The program assumes the ideal gas law, and that for small time intervals $dP/d\theta$ is equal to $\Delta P/\Delta Q$.

For a combustion cycle, $\Delta P = P_h - P$, and for a pressure-decay cycle $\Delta P = P - P_l$, where P is ullage gas pressure and P_h and P_l are, respectively, the high-pressure and low-pressure levels controlling the injection cycle.

For the ideal gas law,

$$P = \frac{WRT}{MV}$$

Differentiating with respect to time, we get

$$\frac{dP}{d\theta} = \frac{WR}{MV} \frac{\partial T}{\partial \theta} + \frac{RT}{MV} \frac{\partial W}{\partial \theta} - \frac{WRT}{MV^2} \frac{\partial V}{\partial \theta} - \frac{WRT}{M^2 V} \frac{\partial M}{\partial \theta}$$

The change rates of ullage gas temperature, weight, volume and molecular weight are evaluated on the basis of calculations over a 1-sec interval, and $dP/d\theta$ is determined.

Then

$$\Delta \theta = \frac{\Delta P}{(dP/d\theta)}$$

For the case of dissociating propellant vapors that require an iterative solution, the new ullage pressure is calculated from this $\Delta \theta$ and the method of false position used in two iterations to provide greater accuracy for $\Delta \theta$.

At the end of each cycle, the remaining propellant is compared with an input low-level volume and shutdown initiated when the propellant volume is equal to or less than this value. Injection is terminated, and a polytropic ullage-gas expansion takes place until the propellant is completely expelled. During the shutdown sequence, transient conditions are periodically output until program termination due to complete evacuation of the propellant tank.

Gas Properties

The composition of the ullage varies with time, consisting of inert pressurizing gas, propellant vapor, and gaseous combustion products. Empirical propellant vaporization rates and dissociation constants are used. To determine the bulk gas properties at any instant, the average molecular weight and quantities of each constituent are calculated.

Then

$$\bar{M} = \frac{\sum MF_i \mu_i \sqrt{MW_i}}{\sum MF_i \sqrt{MW_i}}$$

$$\bar{C}_p = \sum WF_i C_{p_i}$$

$$\bar{k} = \sum MF_i k_i$$

$$\bar{\beta} = \sum MF_i \beta_i$$

where

MF = mole fraction,

MW = molecular weight,

WF = weight fraction,

μ = viscosity,

C_p = heat capacity,

k = thermal conductivity,

β = volumetric coefficient of thermal expansion,

⁻ (superscript) = bulk property,

_i (subscript) = constituent property.

The composition of the gaseous combustion products is best determined by mass spectrometer quantitative analysis. However, good correlation has been obtained between actual data and calculated results from available combustion programs. Because of the quenching nature of the subsurface reaction, frozen product composition quenched to ambient tank conditions should be used (rather than a shifting equilibrium composition) as the product temperature is reduced from the adiabatic flame temperature to the ullage gas temperature. Condensible constituents should be considered to liquify and remain in the liquid-phase propellant. Some properties of the gaseous combustion products for the fuel tank reaction are presented in Fig. 3.

Heat Transfer

Heat transfer is considered between the gas and the adjacent wall, the tank wall and the outside environment, the gas and the liquid, the liquid and the adjacent tank wall, and the tank wall and the outside environment.

External heat transfer is calculated by $Q = h A_{\text{wall}} (T_{\text{aw}} - T_{\text{wall}})$ where T_{aw} is the adiabatic wall temperature. Both h and T_{aw} are tabular input to the program, and are based on aerodynamic heating calculations for particular mission profiles, or they may reflect simple heat transfer from the ambient environment.

Calculations of internal heat transfer between the liquid and adjacent wall are based on the natural convection relationship,

$$h \frac{D}{k} = \frac{1}{\alpha} \left(\frac{D^3 \rho^2 g \beta \Delta T}{\mu} \right)^M \left(\frac{C_p \mu}{k} \right)^N$$

By assuming $m = n$ and simplifying,

$$h = C \left(\frac{k}{D} \right) \left(\frac{D^3 \rho^2 g \beta \Delta T C_p}{\mu k} \right)^X$$

where C and X are approximately 0.25.

Because of the intermittent pressurization process, the ullage gas experiences some degree of forced convection. To account for this heat transfer from the ullage gas, C and X are empirically modified to fit test data.

Combustion Theory

The reaction mixture ratio, R_m , and the ratio of condensible combustion products to total combustion products, R_{cl} , are required to calculate a material balance around the combustion zone. The injected reagent flow rate is determined by the injector orifice and the pressure drop across the orifice. A material balance was performed for the reaction by comparing the amount of combustion products, based on ullage gas analyses, with the measured quantity of injected reagent. Estimation of the condensible combustion products was keyed to an oxygen balance for the fuel tank reaction and a hydrogen and nitrogen balance in the oxidizer tank. In the particular system evaluated in this study, the reaction was always fuel-rich in the fuel tank, and oxidizer-rich in the oxidizer tank. For lack of more precise information, the same equivalence ratios in the fuel and oxidizer tanks, respectively, may be used when evaluating other propellant combinations (where equivalence ratio, E_r , is defined as the ratio of the actual reaction mixture ratio to the stoichiometric mixture ratio). When the reactant's composition differs from the storable propellants tested, this assumption is not expected to be valid.

Convective heat transfer between the hot combustion gases in the combustion zone and the surrounding liquid is calculated by the standard relationship

$$Q = hA (T_f - T_1)$$

where T_f is the reaction adiabatic flame temperature and T_1 is the bulk liquid temperature.

By relating the unit flow rate of the injected reagent to the area of the combustion zone - liquid interface, we obtain

$$A_c = C_a \left(\dot{w}_r \right)^{2/3}$$

and for the film heat transfer coefficient, we use

$$h = C_h \left(\dot{w}_r \right)^{0.2}$$

where

A_c = interface area,

h = film heat transfer coefficient,

C_h, C_a = empirically derived constants,

\dot{w}_r = injected reagent weight flow rate.

Simplifying, the heat transferred between the hot combustion gases and the surrounding liquid,

$$Q = C_h C_a \left(\dot{w}_r \right)^{0.87} (T_f - T_1). \quad (3)$$

Total condensation of the condensible combustion products occurs in the combustion zone with a resultant enthalpy increase in the liquid

$$Q = W_{cl} \left(\Delta H_v + \int_{T_1}^{T_f} C_{pcl} dT \right) \quad (4)$$

where

W_{cl} = weight of condensibles,

ΔH_v = condensibles' latent heat of vaporization at T_1 ,

C_{pcl} = condensibles' constant pressure specific heat (vapor).

The remainder of the energy liberated by the combustion reaction goes into the ullage with the gaseous combustion products.

In the oxidizer tank, the heat of reaction for the actual mixture ratio is approximately -2,500 Btu/lb reactants, and the energy distribution for the total quantity of 28,000 Btu is shown in Fig. 4. In the fuel tank, the heat of reaction is approximately -2,100 Btu/lb reactants, because the reaction occurs at a mixture ratio considerably less than stoichiometric. Although the heat of reaction/lb of reactants is less in the fuel tank, the quantity of reactants increases, causing the total amounts of energy released in each system to be more nearly equal. The net effect on the energy distribution in the fuel tank is to increase the heat to the propellant and the ullage gases, because propellant vaporization is insignificant.

Material Balance

Calculated values derived during a material balance are summarized in Table 1. The summary was based on oxidizer injection into fuel for a subscale system test. Mass spectrometer analysis of the ullage gas indicated that 4.02 standard cu ft (equivalent to 0.313 lb) of gaseous combustion products had been generated while a measured 0.151 lb of fuel had been injected.

All quantities were converted to standard cubic feet, regardless of their actual state during the process, and their atomic constituents related to these volumes. After determining these atomic volumes for the gaseous combustion products and the injected fuel, a hydrogen balance was used to determine the amount of water condensed in the propellant. The consumed oxidizer was then calculated, based on an oxygen balance. Any atomic reactants unaccounted for were attributed to the condensible products. Excluding the unaccounted carbon and nitrogen, a weight balance (products/reactants) of 94.7% was obtained.

The reaction mixture ratio, R_m (weight of oxidizer/weight of fuel), was calculated to be 2.34, and the ratio of condensible liquid, R_{cl} (total weight of condensibles/weight of reactants), was 0.384. These two constants are required in the IBM 7094 mathematical model for calculating the reaction products distribution.

Injection Dynamics

A study of the injection phenomenon was undertaken because the mixing technique associated with the reaction has a significant influence on the reaction mixture ratio, product composition, heat transfer to the bulk propellant, and system response. This study was aimed at establishing penetration rate and maximum depth of penetration of the injected stream into the main propellant by an analogy with a nonreacting process. The amount of penetration of the injected reagent into the main propellant is of primary significance in determining the combustion zone area and related heat transfer to the bulk liquid. (See Fig. 5). In an attempt to define the primary factors influencing this phenomenon, a theoretical and experimental examination of the nonreacting solid-stream surface injection process was performed. An examination of the well-known basic flow equation shows the primary influencing factors:

Mass flow rate of injected reagent

$$\dot{M}_r = C_d A_\phi \sqrt{2g_c \rho_r \Delta P}, \text{ lb}_m/\text{sec} \quad (5)$$

and injection velocity

$$V_j = C_d \sqrt{\frac{2g_c \Delta P}{\rho_r}}, \text{ ft/sec} \quad (6)$$

where

C_d = injector discharge coefficient,

A_ϕ = orifice area (ft^2),

ρ_r = reagent density (lb_m/ft^3),

ΔP = injector differential pressure (lb_f/ft^2),

g_c = gravitational constant ($32.17 \text{ lb}_m \text{ ft}/\text{lb}_f \text{ sec}^2$).

As shown in Eq (5) and (6), the injection velocity is independent of the orifice size for a given fluid, and the mass flow is directly proportional to the square of the orifice diameter. Both characteristics are a function of injector differential pressure to the 0.5 power. The injection velocity, however, is limited to a 200-psi maximum injector differential pressure to avoid atomization of the solid stream. Consequently, injector orifice diameter is of primary importance in controlling penetration characteristics and system response. To achieve maximum system response, a small injector orifice diameter and high injector differential pressure are required.

A finite depth of penetration for a nonreacting process can be readily determined from an energy balance when the sum of the potential and kinetic energy of the stream, diminished by the energy dissipated in frictional, inertial, and drag forces, is equal to zero. This relation is expressed as:

$$WL + \frac{WV^2}{2g_c} - \left(f \frac{\rho V^2}{2g_c} A_s + \frac{g\rho}{g_c} A_c + C_d \frac{\rho V^2}{2g_c} A_c \right) L = 0 \quad (7)$$

where

W = weight of fluid injected (lb_m),

L = penetration distance (ft),

$f \frac{\rho V^2}{2g_c} A_s$ = energy loss due to skin friction (ft lb),

$\frac{g\rho}{g_c} A_c$ = energy loss due to inertial of the displaced fluid (ft lb),

$C_d \frac{\rho V^2}{2g_c} A_c$ = drag loss (ft lb).

By neglecting the frictional effects, the penetration rate can be derived by relating pressures at the stagnation point of a jet impinging on a target. Thus:

$$\frac{1}{2} \rho_j (V_j - U)^2 = \frac{1}{2} \rho U^2 \quad (8)$$

where ρ_j and ρ are the densities of the injected and penetrated fluid and U is the penetration rate.

If $\rho_j = \rho$, Eq (8) reduces to,

$$U = V_j/2. \quad (9)$$

If $\rho_j \neq \rho$, Eq (8) can be expanded and solved for U , the average penetration rate giving,

$$U_A = \frac{V_j \rho_j \pm \sqrt{V_j^2 \rho_j^2 - \rho_j - \rho_j V_j^2 (\rho_j - \rho)}}{2 (\rho_j - \rho)} \quad (10)$$

To assess the relative importance of injection velocity and mass flow rate on penetration characteristics for the non reaction process, an experimental program was conducted to provide a comparison with the theoretical analysis and data accumulated during the experimental program conducted with the hypergolic propellants. The non reacting process study was performed by the downward injection of colored water into a water-filled, 5-gal. cylindrical glass container calibrated with a $\frac{1}{2}$ -in. grid. The process was analyzed by inspecting motion pictures taken at 200 fps. Water was injected through orifices 0.006, 0.035, 0.015 and 0.040 in. in diameter at differential pressures of 75 and 150 psi. The data obtained are summarized in Table 2. All data reported were determined from photoanalysis except the injection velocity, which was computed. Particularly significant was the penetration distance, which increased linearly with the orifice diameter for a given injection velocity and was approximately proportional to the square root of the injector differential pressure. The average penetration rate was approximately 50% of the theoretical maximum and independent of orifice size, as expected from an inspection of the influencing parameters. See Eq (10).

Table 3 compares the actual and expected velocities computed from Eq (6) and (10) for water, a 50/50 blend of hydrazine and unsymmetrical dimethylhydrazine, and nitrogen tetroxide for 75-psi injector differential pressure. Since the combustion process in the oxidizer tank did not permit photography because of the dark color of the liquid propellant, there is no identification of the actual penetration rate or distance. Although the penetration processes are significantly different, the actual penetration rate for the combustion process appears to be 50% of the theoretical average for a nonreacting process. Particularly interesting was the fact that a maximum penetration distance was reached in each nonreacting test, as opposed to a reacting type process that appears to be limited only by the injection duration or the physical boundary of the system. Based on the lack of correlation with theory, more extensive investigation of the penetration phenomenon with the reacting process is required to include propellant and injectant combustion rates and to identify the effects of combustion zone counter flow currents induced in the main propellant.

Experimental Program

The experimental program consisted of more than 100 subscale tests, including both single-tank and common-ullage configurations. Testing was performed in a special scale model test fixture that was 2% as large as the full size system. A nominal 2½-minute propellant expulsion was used, based on typical rocket vehicle mission durations. All tests were fully instrumented, and gas composition data and motion pictures of the combustion process were obtained on approximately 80 runs. During this portion of the program, the pulse mode injection system was developed and experimental data acquired for variations in injector nozzle type, size, and location and at operating pressures of 36, 100 and 200 psia. Satisfactory system operation was achieved with injection pressurization of the initial ullage, during variable outflow and restart, and with induced random vibration. The basic test program described herein pertains to single-tank pressurization only. The common-ullage configuration was not recommended because of several special design considerations required for stable pressure control.

Test Configuration

To evaluate the effects of injection technique and acquire necessary data for full-scale system design, special 5-1/3 ft³ test tanks were fabricated from 5/8-in. wall 6061-0 aluminum helium spheres. Figure 6 shows the general equipment arrangement and Fig. 7 flow schematic. Each tank contained two 3-in. diameter x 3/4 in. Tuf-flex camera ports for combustion photography and a 1-in. diameter pyrex propellant outlet for visual observation of the expelled propellant. The tank outlets were contoured to prevent cavitation and dropout, and baffled to reduce vortexing and allow containment of the subsurface combustion zone. Figure 8 shows the propellant outlet and baffle arrangement. Additional ports were provided for reagent injection, overpressure protection, propellant level sensors, common ullage, instrumentation, and propellant and ullage gas sampling.

A pulse-mode pressurization system was selected and developed, based on positive shutoff, moderate

operating temperatures, and precise pressure control with emphasis on system versatility. The injector was fabricated from a commercial-type chemical spraying device with a 0.0135-in. diameter orifice, and was pneumatically operated. A Belleville-type pressure switch control of the 4-way solenoid valve was used. This design allowed interchangeability of injector nozzles and permitted surface or subsurface reagent impingement by adjusting the length of insertion into the test tank. Reagent was supplied from a 1-in. diameter x 18-in. calibrated pyrex reservoir pressurized to maintain a 75-psi injector differential pressure. Overpressure protection was provided by dual 2-in. diameter burst discs and a pressure switch-actuated 2-in. diameter vent and relief valve. Control console logic included automatic test sequencing, malfunction detection, and automatic corrective actions with capability for manual override. All systems were remote operated and fail safe, with high response isolation valves provided in the reagent supply and common ullage lines.

Test Procedure

The scope of the experimental program included an evaluation of solid-stream and 15 deg fan spray reagent injection with surface and subsurface impingement and a determination of common ullage feasibility. Preliminary experimentation at a 36-psia tank pressure established injector size and desirable injection methods. Subsequent tests were performed with the common ullage configuration and single-tank system at 36, 100, and 200 psia to establish operating pressure influences on the pressurization process. To determine system capability, tests were performed with a minimum 5% initial ullage pressurized by the injection system with the pressure maintained during zero, constant, and variable propellant outflow. All tests were 2½-minutes long except for demonstrations simulating restart capability when an unpressurized 10-minute coast period was included.

Although a variety of configurations were investigated and several different test series were performed, the operating procedures and test conditions were duplicated for each run. The initial subscale injection system evaluation tests were performed in the fuel tank, with the ullage gas used to pressurize a water-filled oxidizer tank. Common ullage tests were also performed with a live oxidizer; however, an emphasis has been placed on the recommended single-tank system (i.e., separate reagent injection into each tank). Ambient pressure was generally 11.7 psia with a 60 ± 10°F temperature range. A few tests, however, were performed at a 35°F minimum and a 90°F maximum ambient temperature without a noticeable change in reaction characteristics.

The normal loading sequence first required filling the calibrated injectant reservoir and then pressurizing it to the desired level with nitrogen. The initial load was recorded after entrained vapor was bled from the injection system, which was then placed in a manual mode for safety. Gas sampling, instrumentation, photographic, and television equipment was then readied and a propellant sample procured. Propellants were loaded to the identical ullage (either 5 or 30%) for each test, by monitored ultrasonic liquid level sensors. Prepressurization was generally accomplished by the automatic injection

system; however, early tests used helium initially for safety. Propellant outflow was automatically initiated by the control console and manually adjusted using remote operated modulating type propellant valves. The pressurization process maintained the tank ullage pressure within $\pm 1\%$ during the expulsion of 95% of the initial propellant load. A propellant low level sensor automatically terminates injection and sequences the propellant valves closed. Final propellant sample and ullage gas sample were taken immediately after each test.

Data Acquisition

The instrumentation monitoring system employed CEC oscillographs and Sanborn and Bristol recorders with all systems calibrated to ensure a 1% data accuracy. A schematic of the instrumentation system for the subscale test program is shown in Fig. 9. Pressures were measured by calibrated CEC unbonded strain-gage, bridge-type transducers and were temperature compensated. Tank wall temperatures were measured by copper-constantan type T thermocouples bonded to the external surface in three locations. Shielded chromel-alumel type K thermocouples were used for measuring liquid temperatures and the ullage gas temperature profile by use of a thermocouple rake inside the tank. Propellant flow rates were obtained from Cox turbine-type flowmeters with either a Dynac digital readout or continuous Sanborn recording. The subscale test fixture was suspended on wire ropes to allow acquisition of vibration data, which was obtained by triaxial crystal-type Statham accelerometer.

In addition to photographic and television observation of the combustion process and discharged propellant, gas samples were obtained during and after each test. A schematic of the gas sampling system is shown in Fig. 9. Approximately 120 specimens were acquired in evacuated glass bottles. Each sample was analyzed at operating temperatures within 48 hours by the National Bureau of Standards at Boulder, Colorado, on a mass spectrometer to an accuracy of ± 200 parts per million. Propellant analysis was performed by combinations of wet chemistry and thermal conductivity methods at the Martin Company Quality Control Laboratories to determine the quantity of water and other contaminants formed in addition to identifying any changes in chemical composition. Condensate obtained from the full tank ullage was analyzed by mass spectroscopy, X-ray diffraction, infrared, and wet chemistry. A positive identification of the condensed products formed in the full tank was not obtained because of the complex nature of the reddish brown substance; however, the primary constituents included UDMH and ammonia.

Experimental Test Results

Based on data and process information acquired during the subscale program, the feasibility of the chemical pressurization method was verified and considerable knowledge acquired for incorporation in the mathematical model used for predicting fullscale system performance. One of the most significant discoveries relating to this pressurization process was the effect of injection method on operating characteristics shown in Table 4 for the fuel tank. Each of the four injection methods produced a characteristic gaseous product composition and flame temperature as a result of the variation in apparent reaction mixture ratio. Because of the complex

nature of the reaction, some empirical techniques are required for system performance prediction.

Figure 10 shows the theoretical and actual variation in combustion product molecular weight and adiabatic flame temperature as a function of reaction-mixture ratio. Actual flame temperatures were determined from an energy balance and supported by a qualitative comparison of combustion photos, which are shown in Fig. 11 for each of the four injection methods in the fuel tank. The variation in system operating temperatures (Table 4) was primarily influenced by the location of the combustion zone and the extent of reaction quenching. A similar thermal behavior was also apparent from a limited number of tests performed in the oxidizer tank, but the combustion product gas composition and reaction mixture ratio were relatively constant. Table 5 summarizes typical pressurizing gas composition for either tank as determined by mass spectrometer.

Solid-stream injection with surface impingement was selected as the optimum method for pressurizing the N_2O_4 /UDMH- N_2H_4 propellant combination because of the low molecular weight gas obtained and desirable system operating temperature experienced. The resultant low density pressurant is required to reduce system weight in flight applications. Subsurface injection was not considered practical for missile use because of the $\pm 3g$ vibration levels encountered in the longitudinal axis. With the injection method selected, an average of 0.3% by weight water is formed in the propellants with an insignificant change in composition or viscosity for a 36-psia, 150-sec test. The slight effects of contaminated propellants on specific impulse are shown in Fig. 12, based on theoretical performance of a typical rocket engine operating at sea level with a 500-psia chamber pressure and an area ratio of 5.69. Visual observation of the propellant during expulsion verified the absence of entrained gases or solid contaminants.

Typical data for the subscale system at a 36-psia tank pressure are shown in Fig. 13 with a detailed presentation of the temperature stratification in the ullage shown in Fig. 14 and 15. The pressurization system exhibited stable pressure control during initial pressurization of the 5% ullage volume, rapid start transients, pressurization after a 10-minute coast period, and during normal operation with an induced random horizontal vibration of $\pm 1/4$ in. at a frequency between 1 and 3 cps. The performance of the subscale system at higher pressures is summarized in Table 6 with the pertinent parameters plotted in Fig. 16.

In general the reagent consumption is slightly higher in the oxidizer tank because of the lower operating temperatures and change in reaction characteristics. The increase in system operating temperatures at higher pressures appears to present a limitation for this injection method; however, further experimentation may alleviate excessive temperatures by subsurface injection during the first portion of propellant outflow. The temperatures are relatively moderate because of the large heat capacity of the thick-walled test vessel and small quantity of pressurant generated.

Demonstration Program

Primary objectives of the full-scale demonstration test program were 1) to demonstrate system capability in flight weight propellant tanks; 2) To accumulate sufficient data for verifying reliability, repeatability, and performance predictions; 3) To provide design information for future system development. Demonstration of the chemical pressurization process was performed in identical fuel and oxidizer tanks at 37 psia (Fig. 17). The tanks were 279 ft³ capacity, chem-milled aluminum missile propellant tanks, acquired from salvage, and modified slightly to accommodate the requirement of the demonstration test program. A top view of the test tank (Fig. 18) displays the injector, relief valve, pressure switch, propellant high level sensors, and miscellaneous instrumentation. The general test procedure, data acquisition, and system configuration were identical to that used in the experimental program, except for the reagent supply and measuring system (Fig. 19). For the demonstration tests, reagent was stored in a 0.523-ft³ spherical steel tank suspended from a load cell. The differential reagent weight recorded provided a direct readout that showed good correlation with reagent consumption determined by an integration of the injector switch trace and known flow capacity of the injector.

Demonstration Test Results

Four tests were performed on the fuel tank and two on the oxidizer tank to achieve the program objectives. All tests were completed successfully, including one restart test with a 10-minute coast period for each tank. Precise pressure control of 37 ± 0.25 psia was achieved for all tests with the experimental system injector incorporating a 0.047-in. diameter orifice tube. Reagent consumption and operating temperatures were within allowable predetermined values. No entrained gas was observed in the propellant outflow line sight glass, and there was no noticeable tank vibration or pressure surges. A sound recording made of the combustion process, however, indicated a very high rate of gas generation. The most significant observation concerning the full-scale system data was the change in reaction mixture ratio encountered from the small-scale test program. Table 7 compares the experimental and demonstration systems' performance.

A complete explanation for the change in process characteristics is not known, but the increase in injector size was probably a significant influence parameter. The gas composition was relatively unaffected and agreed with the experimental system data.

Figures 20 and 21 compare actual and predicted data for the fuel and oxidizer tanks, respectively. The predicted reagent consumption was adjusted to reflect the actual variation in reaction mixture ratio. A segment of typical fuel tank pressure trace is shown in Fig. 22. The initial injector frequency was 2.5 cycles/sec maximum in the fuel tank and 5 cycles/sec maximum in the oxidizer tank with pressure controlled to within ± 0.7 psia. Each test was performed with helium prepressurization of the 5% initial ullage, 750-gpm propellant outflow rate, and a 2½-minute test duration (except for the restart tests with a 10-minute coast period).

Design Considerations

Although a satisfactory technique has been developed for predicting the thermodynamic performance of a chemical pressurization system for the Titan II storable propellants, a considerable amount of additional investigation is needed to identify process influence parameters. Based on the extent of testing performed, empirical techniques have been developed to satisfactorily describe a good portion of the physical-chemical phenomenon. A more detailed examination of the injection and combustion process, however, will improve the accuracy for performance prediction of various full-scale system configurations.

Adiabatic Flame Temperature

The adiabatic flame temperature normally is determined by a separate IBM 7094 propellant performance program developed by NASA, since a wide variety of operating conditions can be examined in a relatively short period of time. This parameter can also be determined by a hand computation based on the heats of reaction of products and reactants, as was previously described for calculating the actual flame temperature from test data. Although the theoretical value has never been verified by a test measurement, the energy balance appears to support this method. The adiabatic flame temperatures at 36 psia for a range in reaction mixture ratio are shown in Fig. 10. These values will increase slightly with pressure and vary with the particular propellant combination under consideration. Errors in the assumed reaction mixture ratio, needed in the mathematical model developed, will affect the amount of heat released to the system.

Reaction Mixture Ratio and Condensation Ratio

The verification or direct measurement of the reaction mixture ratio (W_O/W_F) or the condensation ratio, $[W_O/(W_O + W_F)]$ has not been possible because of the relatively small quantities involved in the reaction and inconsistent chemical determinations. Consequently, a material balance technique, previously described, was selected. This method was originally based on a knowledge of the quantity and composition of gaseous products formed and the amount of injected reagent consumed. At present, these parameters must be determined by test because of unknown influence factors. In the absence of test data, the NASA computer program is employed at the inverse equivalence ratio (stoichiometric mixture ratio/actual mixture ratio) previously established for the Titan II propellants. These values are shown in Table 8 for two sizes of systems that do not appear to be significantly affected by operating pressures below the 200-psia maximum test pressure. The equivalence ratio is now considered the best assumption for predicting reaction characteristics for other propellants. This theory, however, has not been verified by test. The quantity of condensed products is generally determined by assuming that the state of the fluid is dictated by the bulk liquid propellant temperature. The amount of condensibles for the Titan II propellants are generally less than 0.3% and not considered an engine performance detriment. The quantity of injected reagent required must be increased to compensate for this condition. To determine maximum possible quantities of condensate formed, a material balance can be

written that assumes all available hydrogen and oxygen combines to form water. These values for the Titan II propellants are 1.1615 lb H_2O /lb fuel injected in the oxidizer tank and 0.7826 lb H_2O /lb N_2O_4 injected in the fuel tank.

Propellant Vaporization

Experimental data have shown a negligible quantity of propellant vapor in the fuel tank. Oxidizer vaporization amounted to approximately 30% for a range in tank operating pressure of 36 to 200 psia. This condition apparently results from the high rate of propellant vaporization in the combustion zone. In the case of nitrogen tetroxide, the large quantity of heat required for vaporization reduces the operating temperature of the system, causing a greater quantity of reactants to be consumed. The additional propellant required for both the reaction and vaporization must be considered in assessing the pressurization system weight penalty and determining vehicle propellant load requirements. This weight penalty, however, may not be a significant disadvantage in certain cases where the propellant has a low vapor molecular weight, such as for liquid hydrogen.

Zero Gravity Pressurization

Although no reduced gravity tests were performed, an observation of the pressurization process characteristics allows some speculation for space vehicle application.

Since the heat generated by the reaction is an important factor in improving pressurization system performance by reducing the ullage gas density and consequently system weight, injection during a coast period is not recommended. Further, pressurization before a restart can be accomplished in a minimum time interval because of the exceptional gas-generating capability of this type of pressurization method. If continuous pressurization during the coast period is required, special precautions may be required to ensure positive reaction control. Two situations warrant careful consideration:

- 1) The reaction may be affected at the tank wall or critical areas inside the propellant tank where heat damage would result.
- 2) The reagent may be allowed to vaporize and not react inside the tank, causing a fuel/oxidizer atmosphere that could be detonated by a liquid phase reaction.

To eliminate these two possibilities, the recommended propellant tank design would incorporate surface tension principles to establish positive propellant orientation and to ensure a liquid phase reaction at all times. A nonvolatile reagent or an inert gaseous product would be desirable in this situation to improve system reliability.

Propellant Tank Pressure Control

Fundamental pressure control can be achieved by pressure-switch actuation of an electrically operated solenoid valve of low-current drain. The present state-of-the-art limits the maximum injector frequency attainable to approximately 35 cps. By adjusting the injector orifice size and pressure control band, this pressurization method will

generally exceed present modulating-type pressure control systems. Overpressure protection for a chemical-type pressurization system should include an injector isolation valve to terminate reagent supply in the event of control system or injector malfunction. Normal pressure relief valves should be incorporated in the propellant tank with sufficient flow capacity and response to accommodate a failed open injector.

Additional Experimental Programs

Two additional propellant combinations have been investigated for application of the chemical pressurization technique:

- 1) Aluminum hydrazine thixotrope and nitrogen tetroxide
- 2) Liquid hydrogen and fluorine

The thixotropic experimentation was confined to open container tests. Nitrogen tetroxide was injected for 5 seconds through a 0.014 inch diameter injector into the fuel surface. A well-defined brilliant white reaction zone several inches across developed at and below the propellant surface with a shower of white flowing sparks generated in addition to gaseous combustion products formed. The process indicated the possibility of stable pressure control, and no solid combustion products were detected when the propellant was passed through a 16 mesh sieve. Figure 23 contains photos of the reaction taken at 0.035 second intervals. This propellant combination will be further investigated by the Martin Company under Edwards Air Force Base Contract AF 04(611)-9952

The cryogenic investigation was performed in a research test apparatus similar to that used for the storable propellant test program, but with a 1 minute test duration. Liquid hydrogen in a 5 1/3 cu. ft. insulated tank was pressurized to 150 psia by injecting fluorine into the LH₂ surface. Although a few successful tests were performed, combustion was unreliable and therefore requires some positive ignition. Subsequent investigation in a glass dewar confirmed the reactants were non-hypergolic in an extremely clean system. This work was performed at Martin-Denver in conjunction with the Advanced Pressurization Study, NAS 3-2574. Although testing has been terminated, some consideration is being given to the use of an activating agent in the system. (See references 8 and 9).

Future Programs

The following is a summary of current status of chemical pressurization studies at the Martin Company:

Main Tank Injection Feasibility Study for Sled Test Vehicles - AF 04(611)-10214

This program involves scale model testing of pressurizing two propellant systems of current interest for rocket sled application:

- 1) Nitrogen tetroxide - Unsymmetrical dimethyl hydrazine at 900 psig.
- 2) Inhibited red fuming nitric acid - 50/50 JP-4/UIMH at 600 psig.

A theoretical and test fixture design study have been completed under AF 04(611)-9887.

The fabrication and system development effort has been completed and testing is now in its final stages.

Main Tank Injection Pressurization of High Energy Propellants - AF 04(611)-9952

An investigation of five high energy propellant combinations of current interest to Edwards Air Force Base is now in process. This program involves analytical and experimental work at 25, 150, and 300 psig, considering four injection methods with several reactants and common ullage pressurization in two directions. The test propellants are:

- 1) Nitrogen tetroxide - aluminum thixotrope
- 2) Compound A - hydrazine
- 3) Compound A - MBF-5
- 4) FLOX - RP-1
- 5) Liquid Fluorine - Coolant hydrazine

A theoretical and design effort is underway with test programs scheduled for a mid February start. A pulse mode pressure control system will be used in the test fixture. The primary objective of this program is to determine the feasibility of pressurizing the above propellant combinations by the chemical pressurization method.

Conclusions

The feasibility of applying the M.T.I. pressurization process to missile propellant tanks has been established. Precise pressure control and moderate operating temperatures of the chemical pressurization system promote consideration of this process for a variety of applications, including missiles, rocket sleds, facility propellant supply systems, and possibly as a means of petroleum recovery. The feasibility of this pressurization method for missile applications considered propellant degradation and vibration in addition to system weight, safety, reliability, simplicity and other operating characteristics. The exceptional capability and promise of this type of pressurization process has been established under a variety of operating conditions. In addition, the development of a suitable method of predicting chemical pressurization thermodynamic performance will extend the range of application eventually to other system configurations or propellant combinations. At present, pressurization of cryogenic propellants, high pressure applications, and thixotropic propellant pressurization is being studied. Although considerable potential is apparent from an investigation of weight reductions achieved with this pressurization method, additional study of the reaction kinetics and process influence parameters is required before this technology can be applied to future vehicles that require high levels of performance and reliability.

Bibliography

1. Development and Demonstration of Main Tank Injection (MTI) Pressurization System, Final Report. RDT-TDR-63-1123. Martin Company, Denver Division, Denver, Colorado. December 1963.
2. Binkhoff, G. and Zarentovelle, E.: Jets, Wakes and Cavities. Academic Press, New York, N. Y. 1957.
3. Morey, T. F.: N₂O₄ Thermodynamic Properties. TM 0431-302, The Martin Company. October 1960.
4. Main Propellant Tank Pressurization System Study and Test Program. SSD-TR-61-21 (Vol III) Design Handbook, Lockheed Aircraft Corp, Marietta, Georgia. December 1961.
5. Heaton, T. R. and Roberts, F. L.: "In-tank Reaction for Propellant Pressurization." Paper Presented at Fifth Liquid Propellant Information Agency Symposium. Martin Company, Denver, Colorado. 1962.
6. Allen, Charles H.: "In-tank Reaction for Propellant Pressurization." Paper Presented at Fifth Liquid Propellant Information Agency Symposium. Rocket Propulsion Laboratories, Edwards AFB, California. 1962.
7. Kenny, R. J. and Friedman P. A.: "Chemical Pressurization of Hypergolic Liquid Propellants". Paper presented at the 1st AIAA annual meeting Washington, D. C. July 1964.
8. Journal of Physical Chemistry, V. 67, p. 2156, 1963.
9. Engineering, Journal of American Chemical Society 1930.

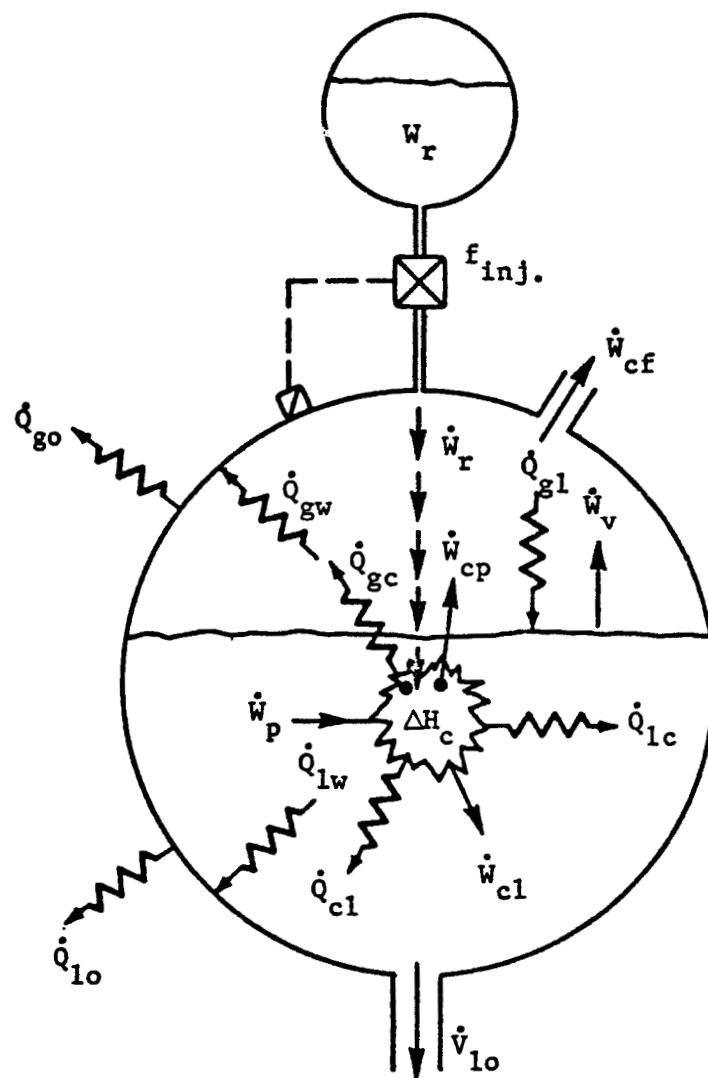


Fig. 1 Chemical Pressurization Process Schematic

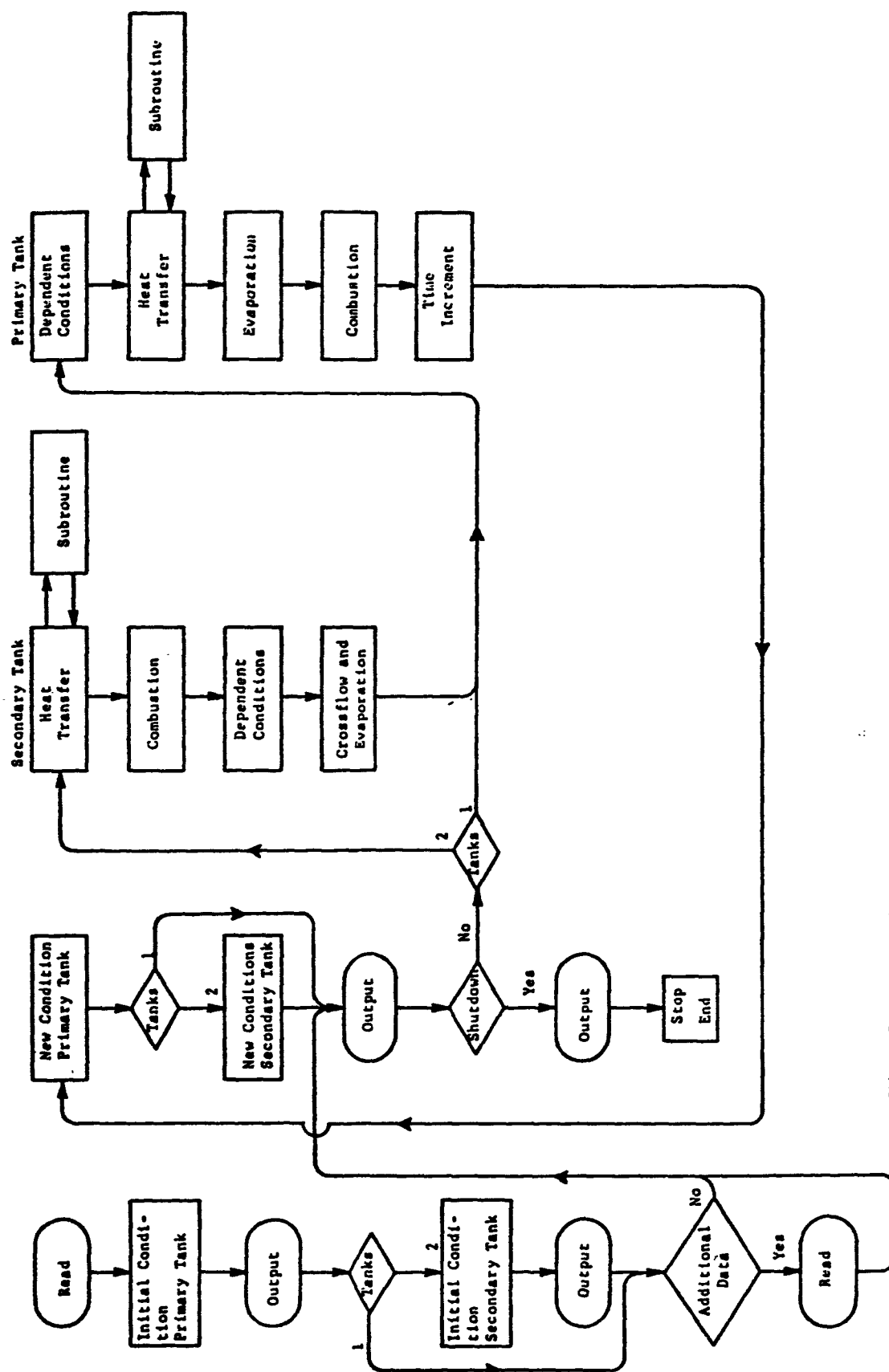


Fig. 2 General Logic Sequence - Pressurization Process Mathematical Model

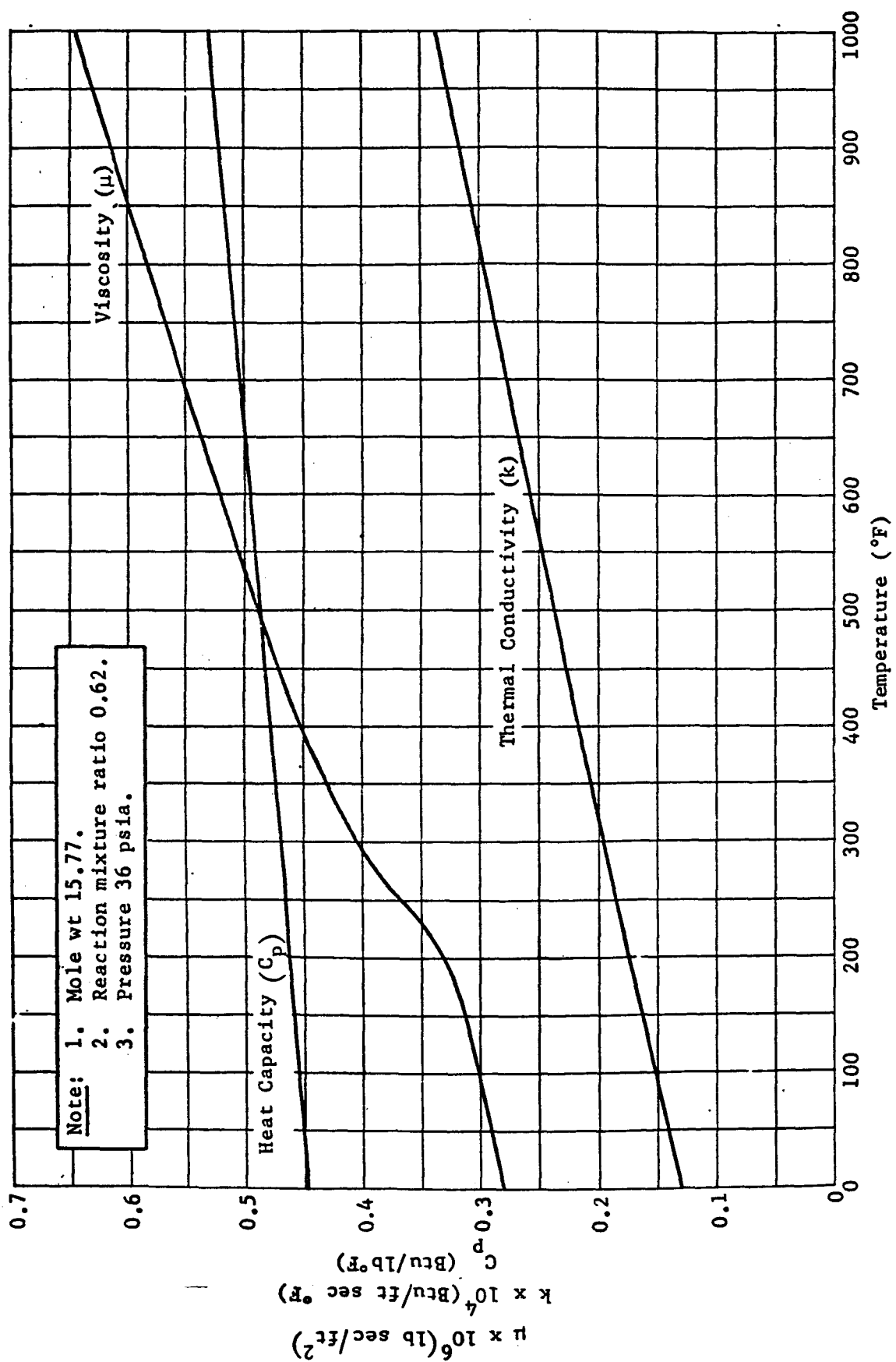


Fig. 3 Properties of Combustion Gases, Fuel Tank Reaction, N_2O_4 Injection

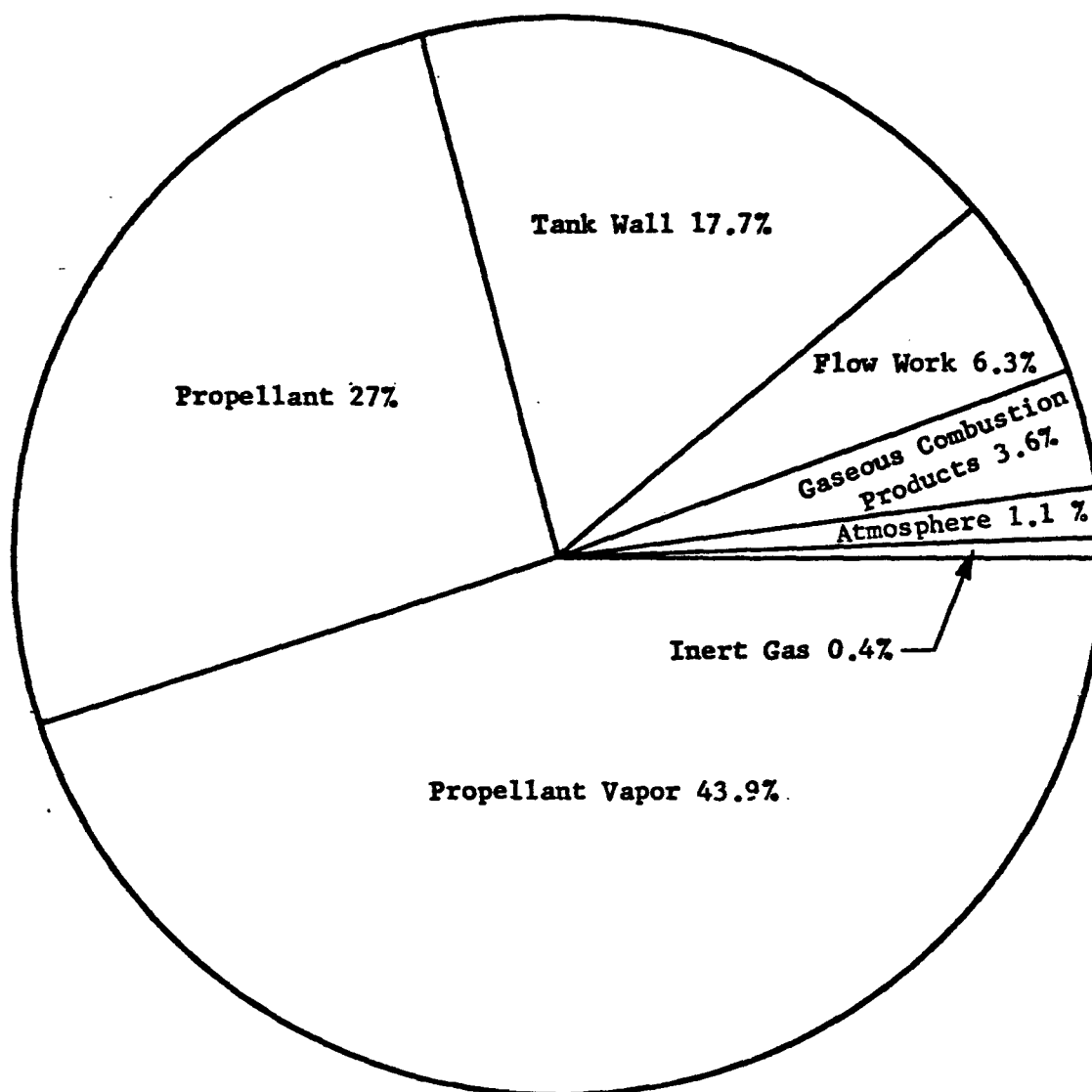


Fig. 4 Final Distribution of Energy Released in Typical Reaction

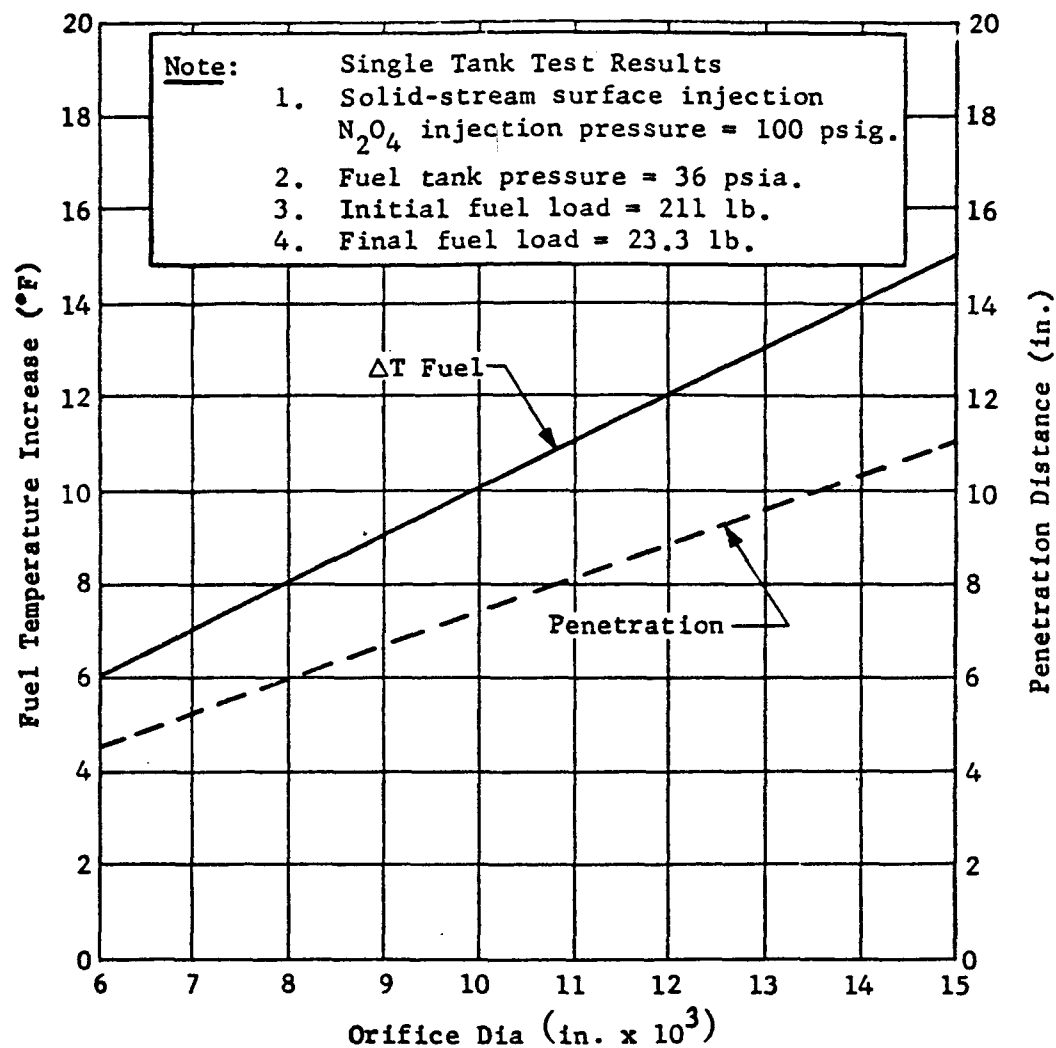


Fig. 5 Injector Orifice Size Effects on Fuel Tank Combustion Process

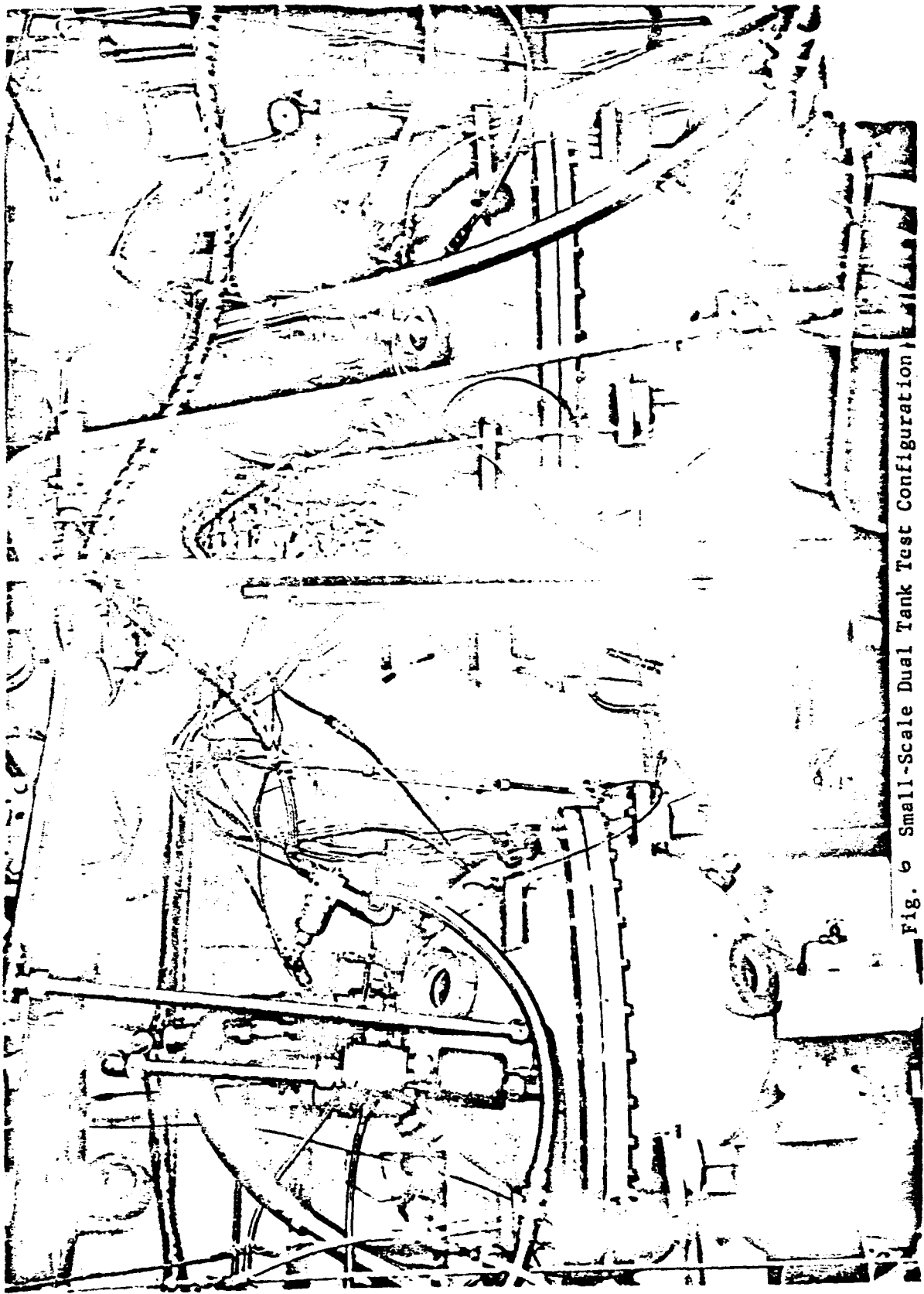


Fig. 6 Small-Scale Dual Tank Test Configuration

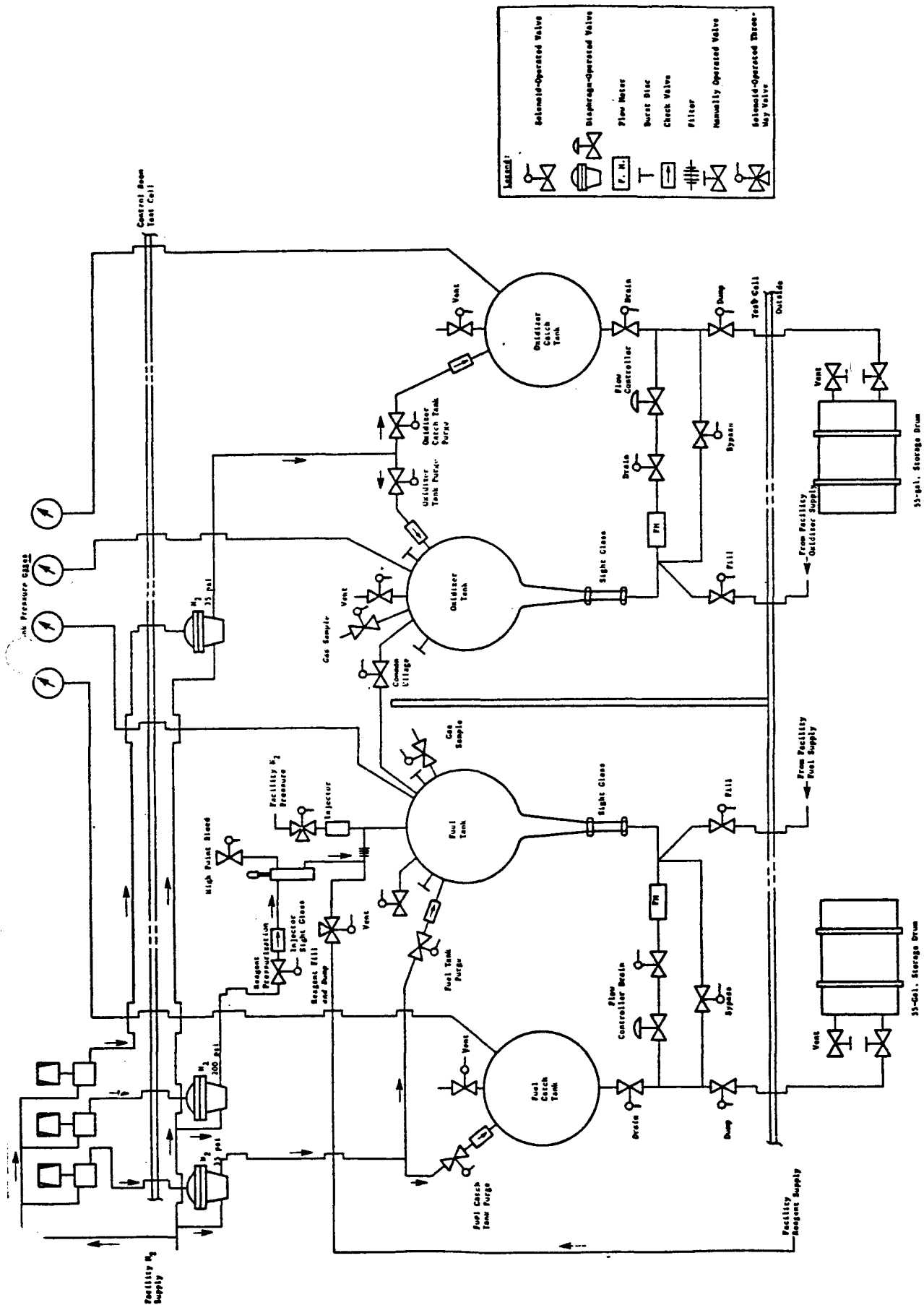


Fig. 7 Chemical Pressurization Test System Schematic

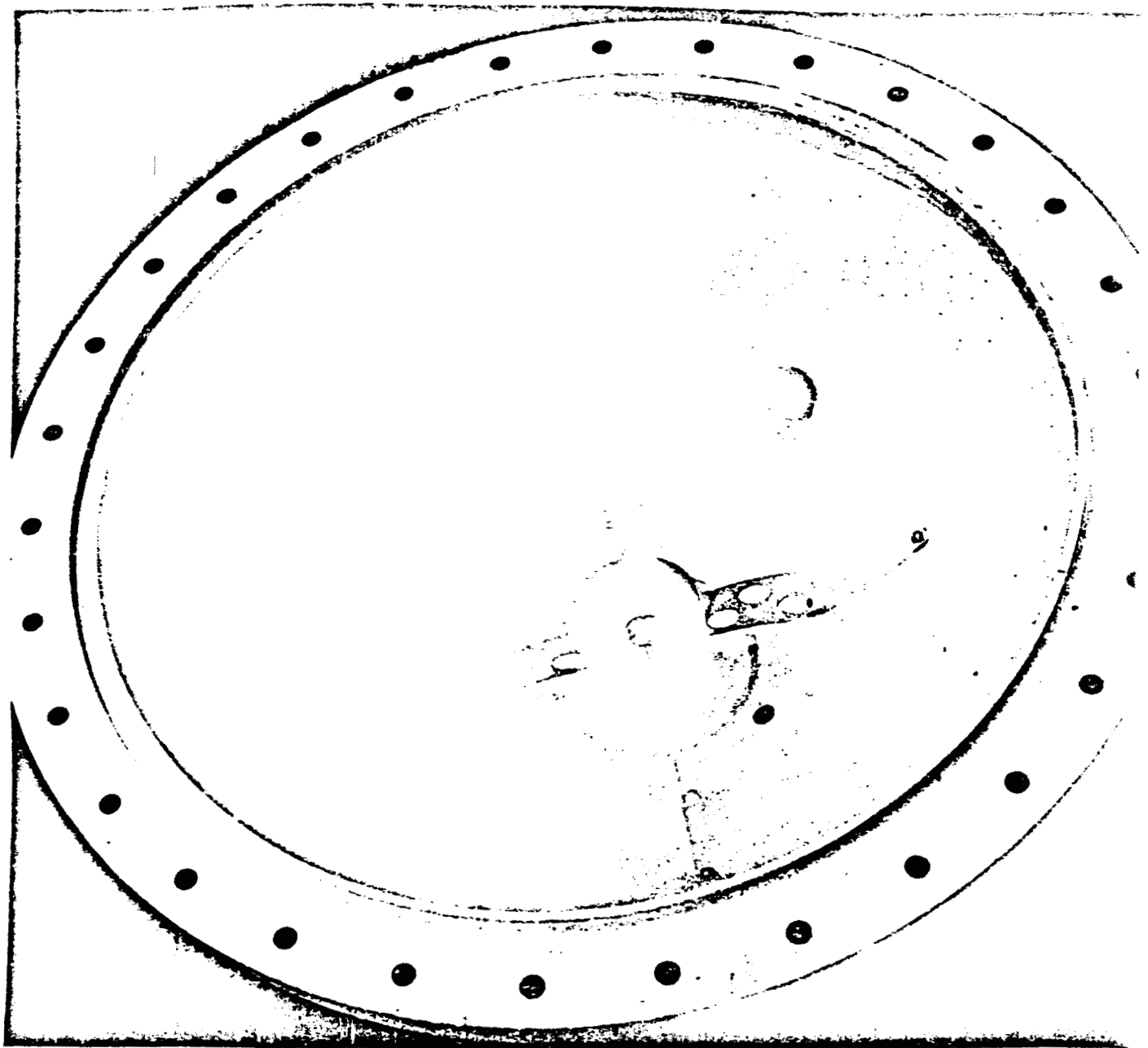
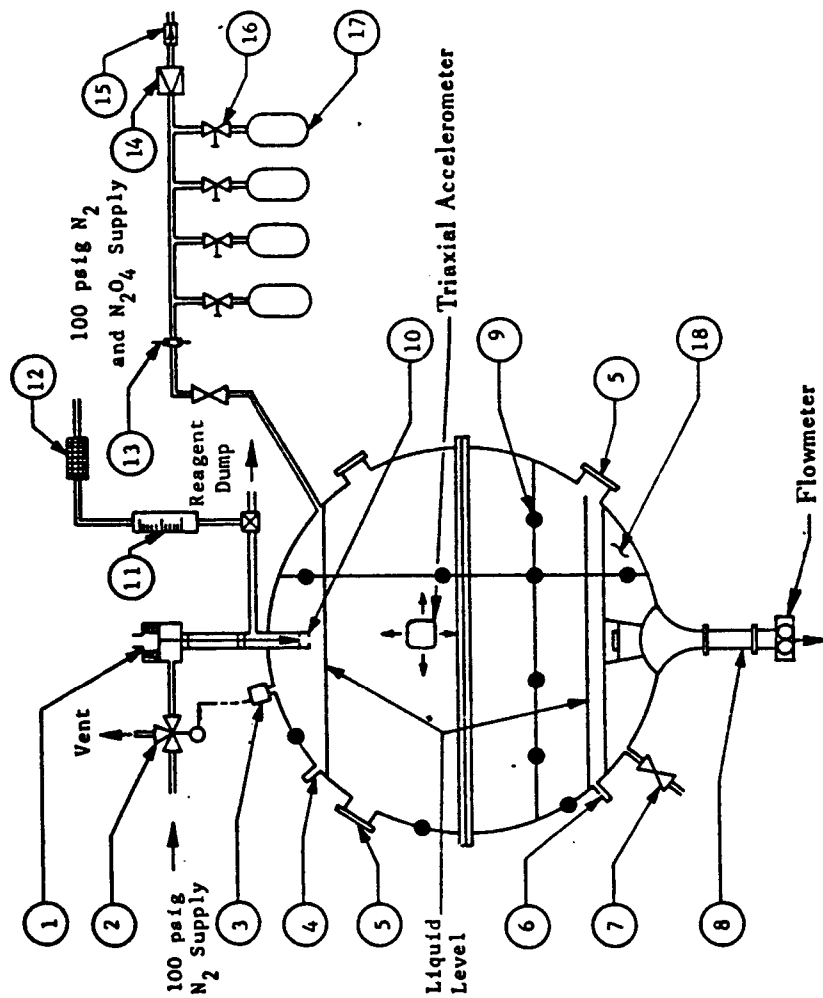


Fig. 8 Research Fixture Inside Lower Dome



Component	
No.	Title
1	Injector
2	Three-Way Valve
3	Pressure Switch
4	High-Level Liquid Sensor
5	Photographic or TV Camera Ports
6	Low-Level Liquid Sensors
7	Propellant Sample Valve
8	Sight Glass
9	Thermocouples
10	Orifice Spray Tip
11	Reagent Measuring Device
12	Filter
13	Orifice
14	2-psig Back Press Regulator
15	Check Valve
16	Bottle Stop Cocks
17	Gas Sample Bottles
18	Propellant Baffles and Combustion Container

Fig. 9 Subscale System Fuel Tank Test Schematic

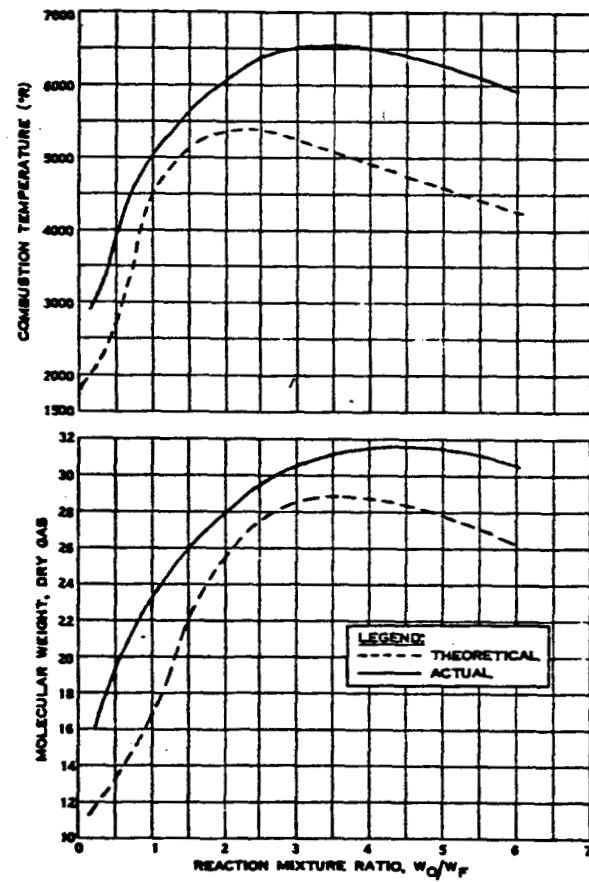


Fig. 10 Combustion Product
 Properties at 36 psia
 50-50 UDMH and N_2H_4

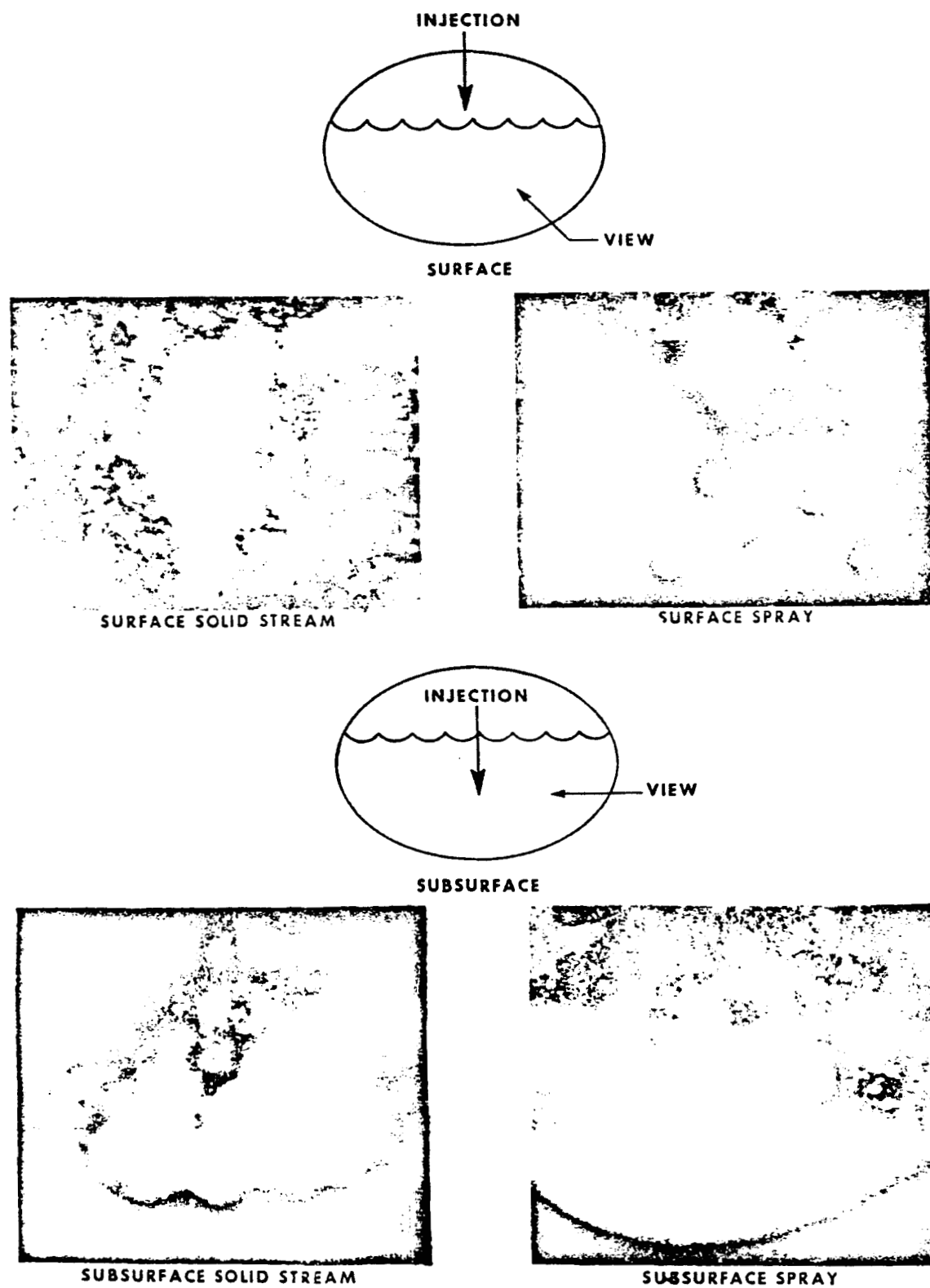


FIG. 11 COMBUSTION PHOTOGRAPHS,

N_2O_4 INTO 50-50 MIXTURE OF UDMH AND N_2H_4

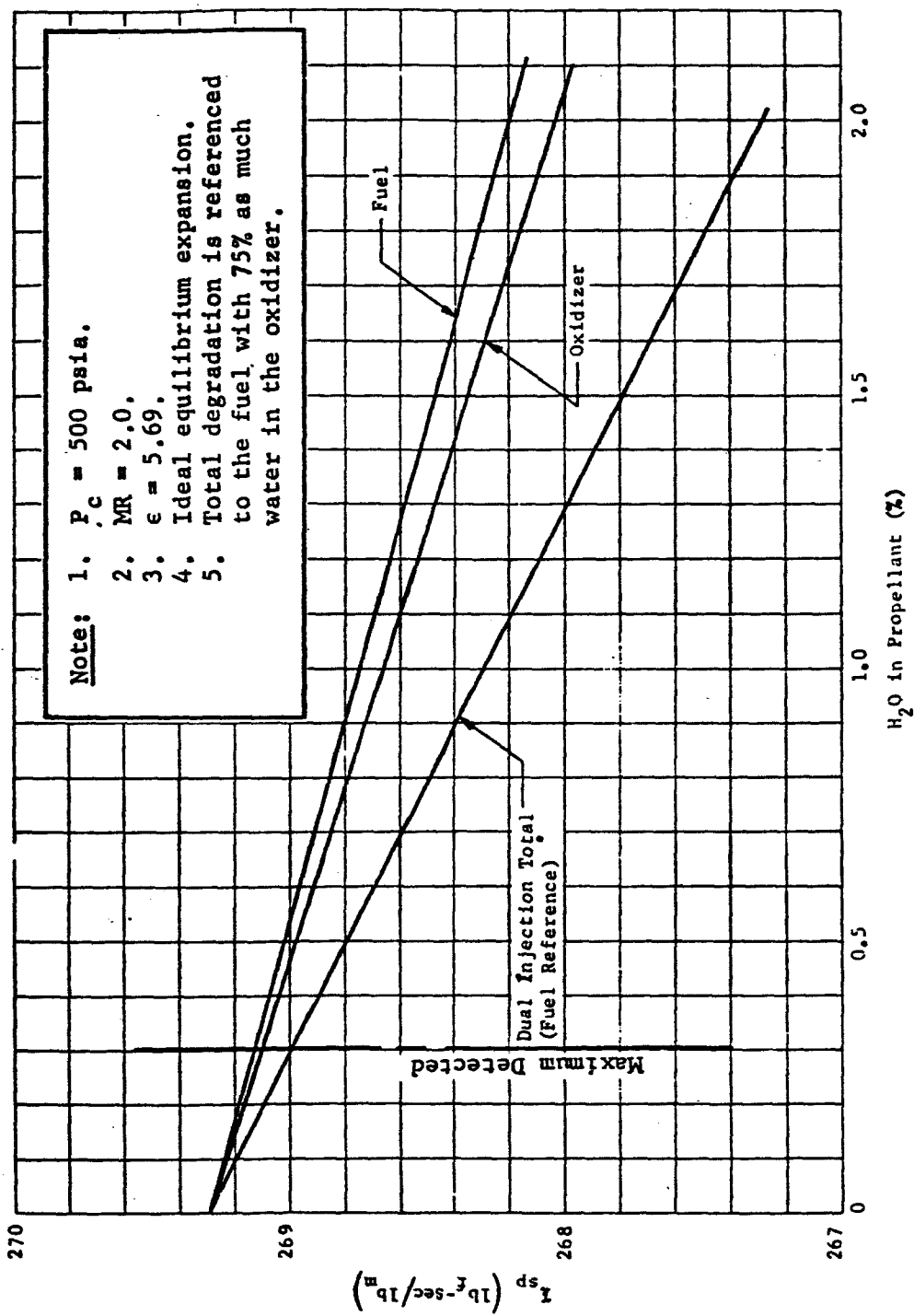


Fig. 12 Effect on I_{sp} of Water in N_2O_4/N_2H_4 -UDMH

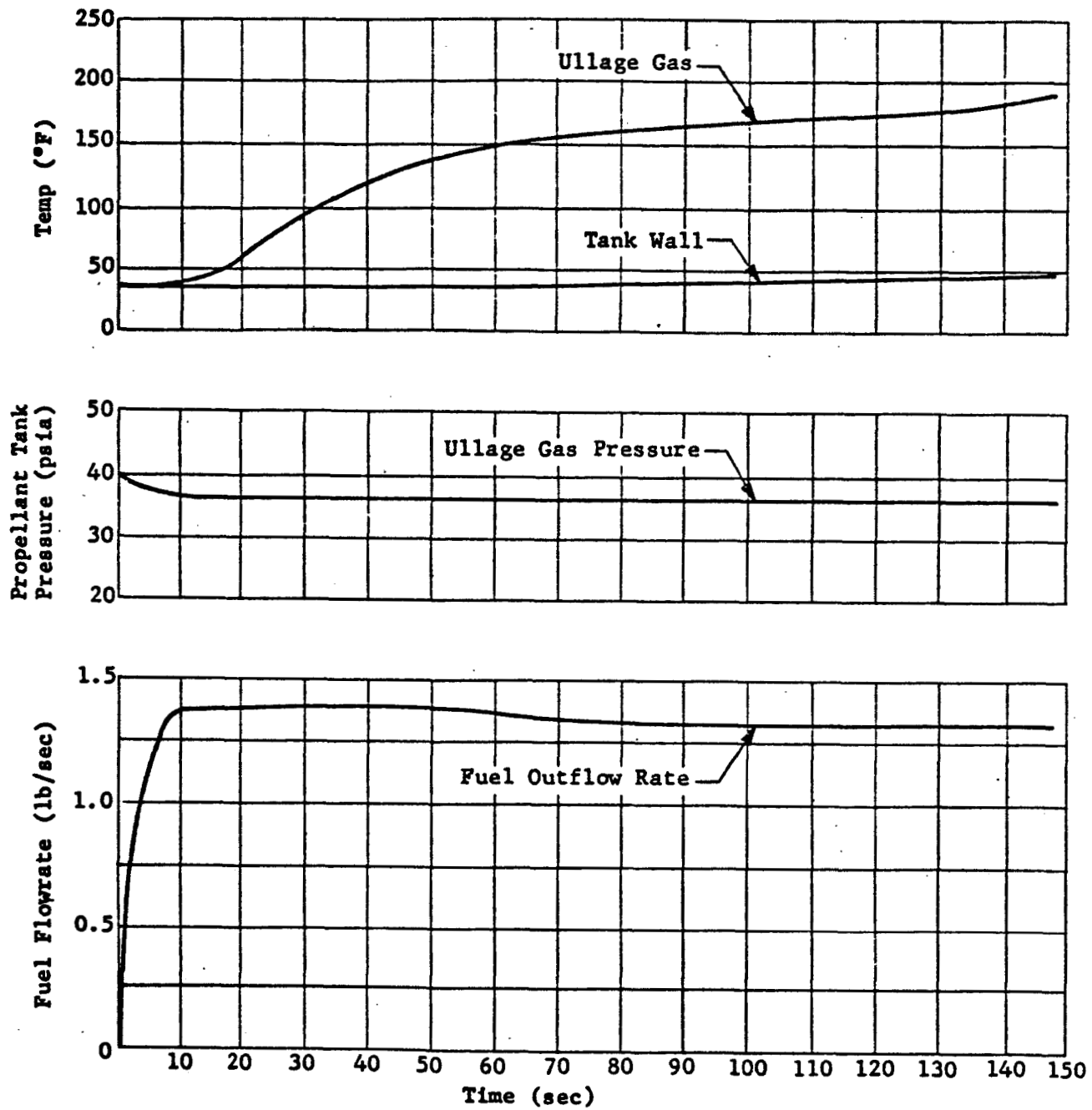


Fig. 13 Typical Single-Tank Pressurization System Performance with Solid-Stream Surface Injection

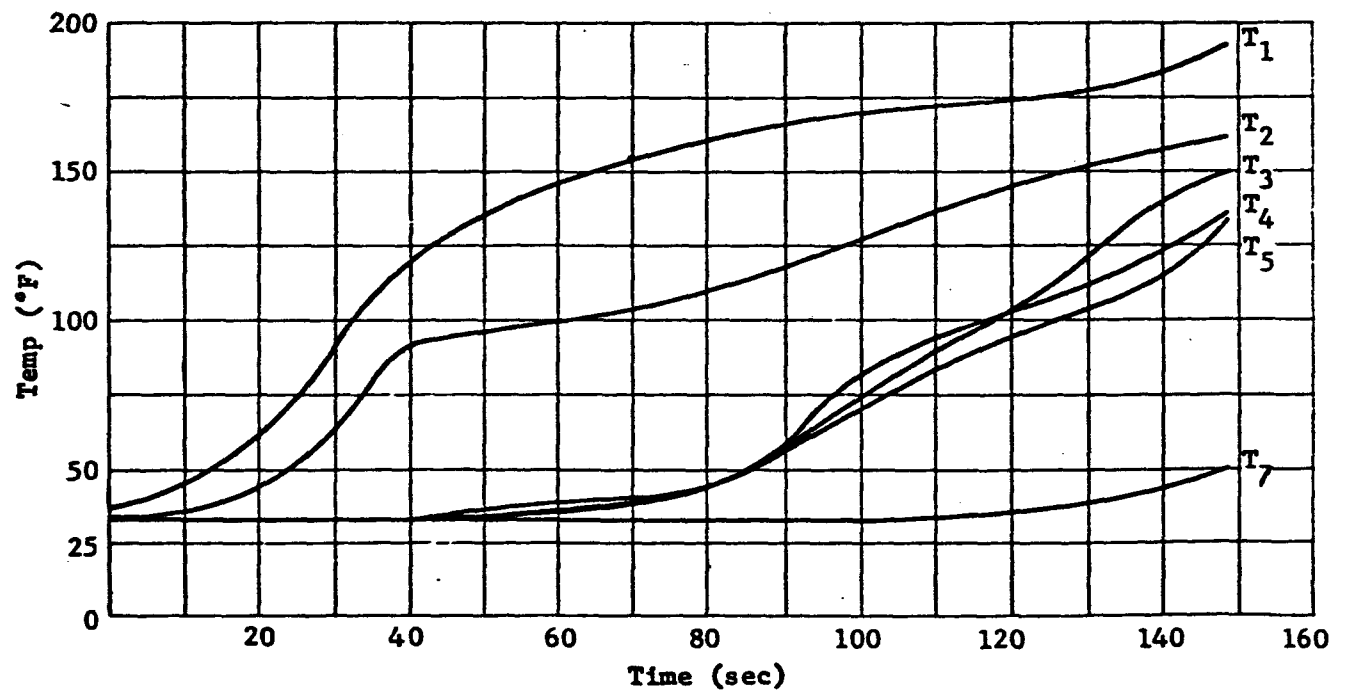
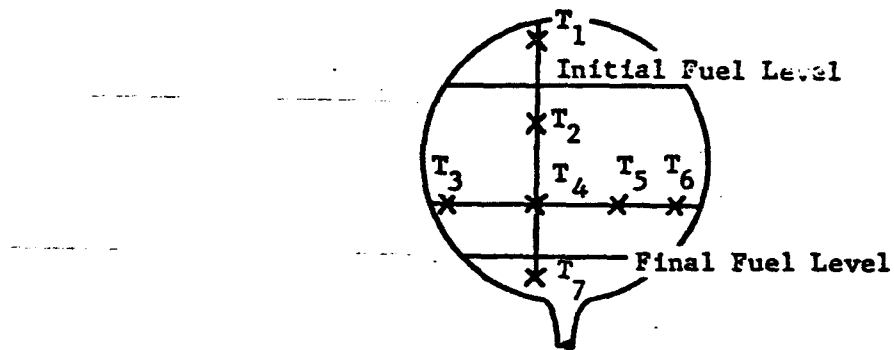


Fig. 14 Fuel Tank Internal Temperature Profile

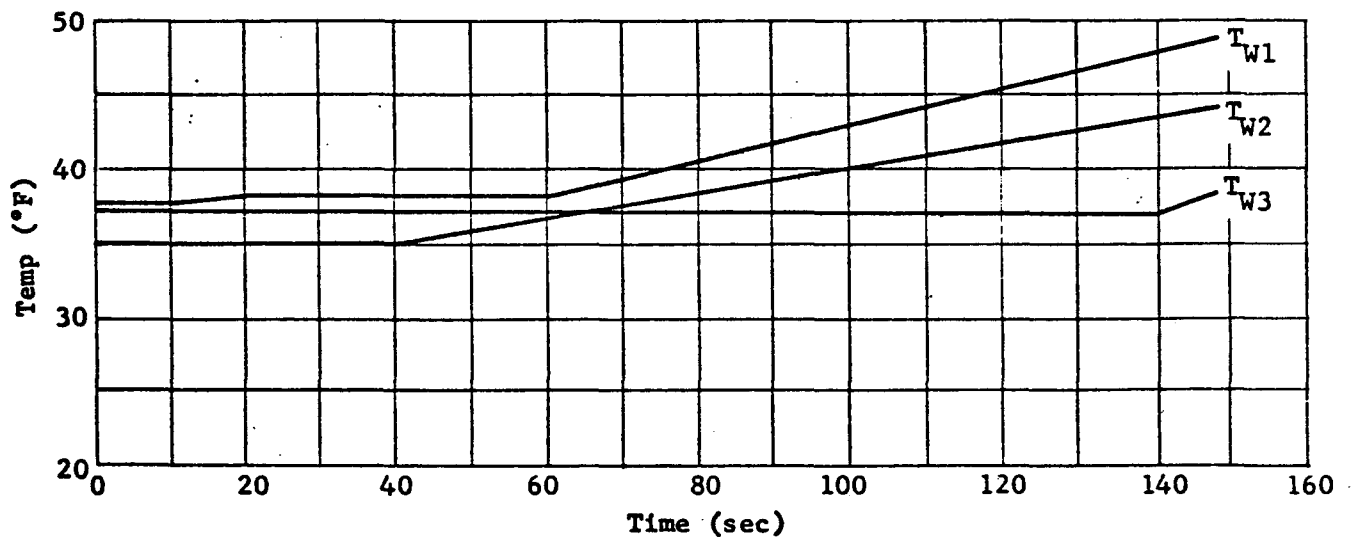
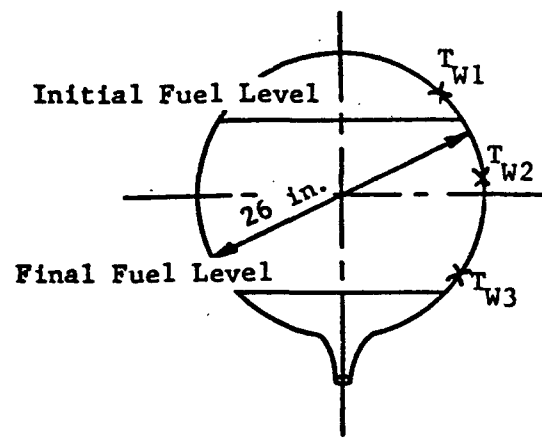


Fig. 15 Fuel Tank Wall Temperature Profile

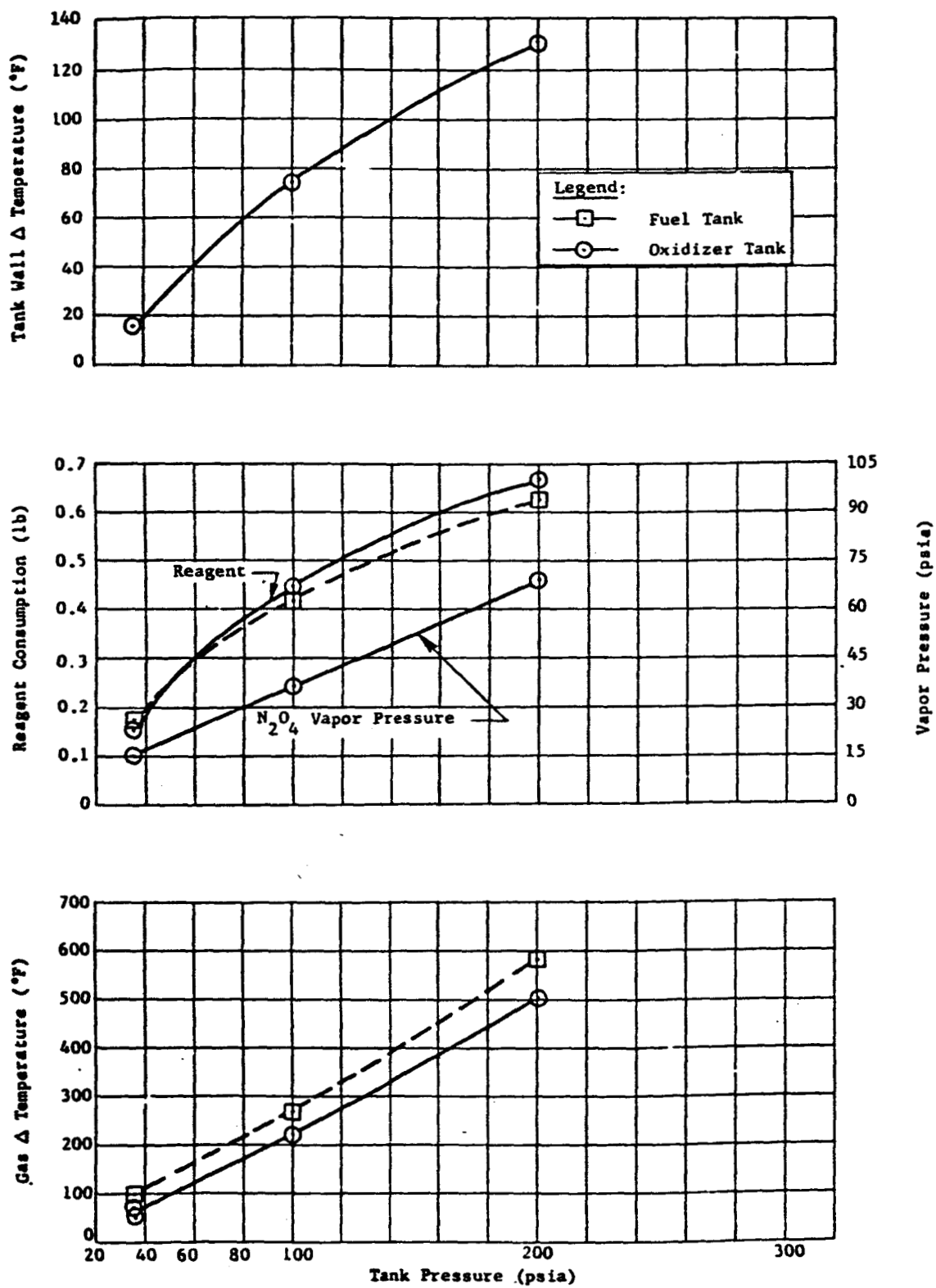


Fig. 16 Parametric Test Data Summary

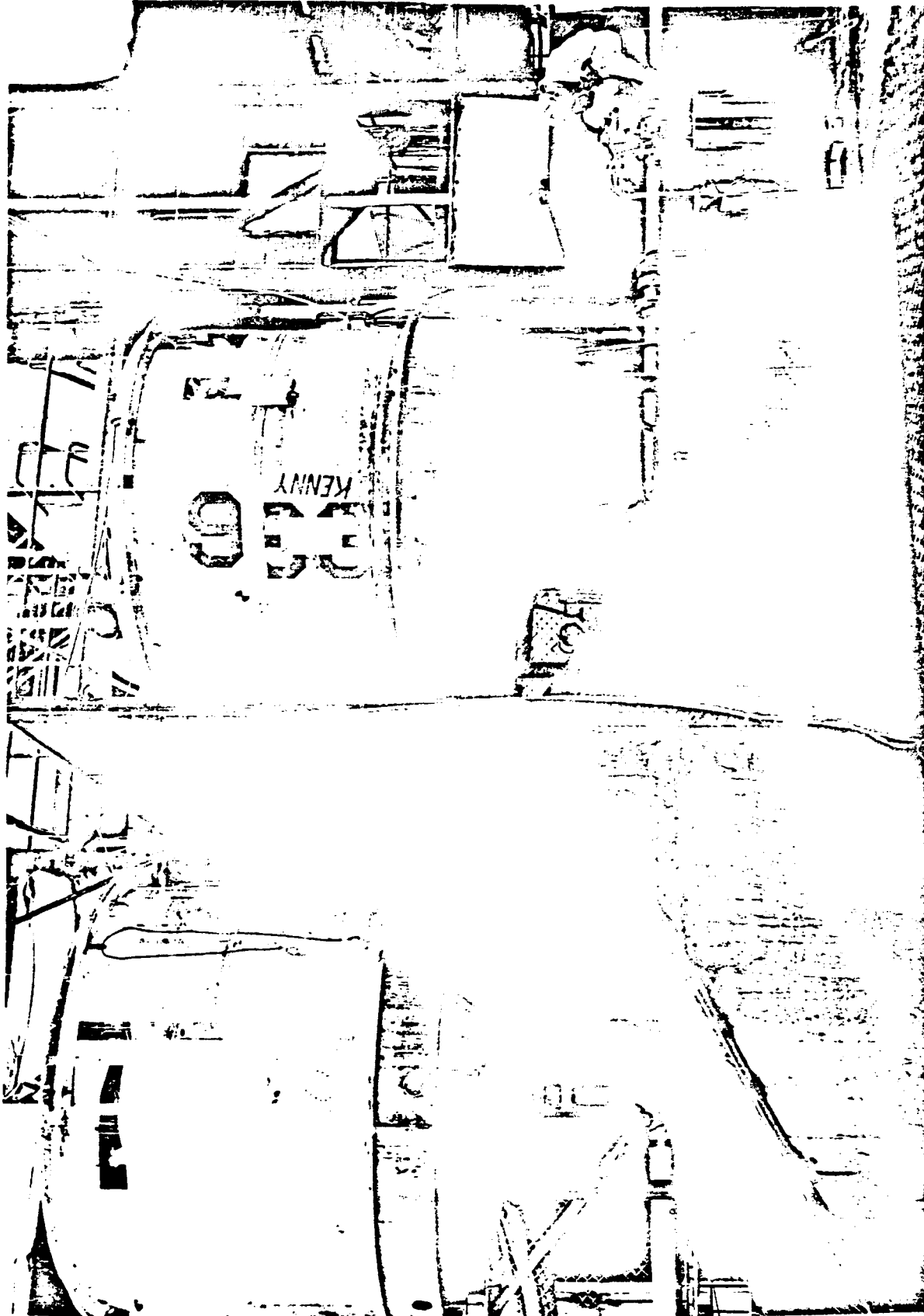


Fig. 17 Full-Scale System Test Article



Fig. 18 Full-Scale System Reagent Injection and Pressure Relief Systems

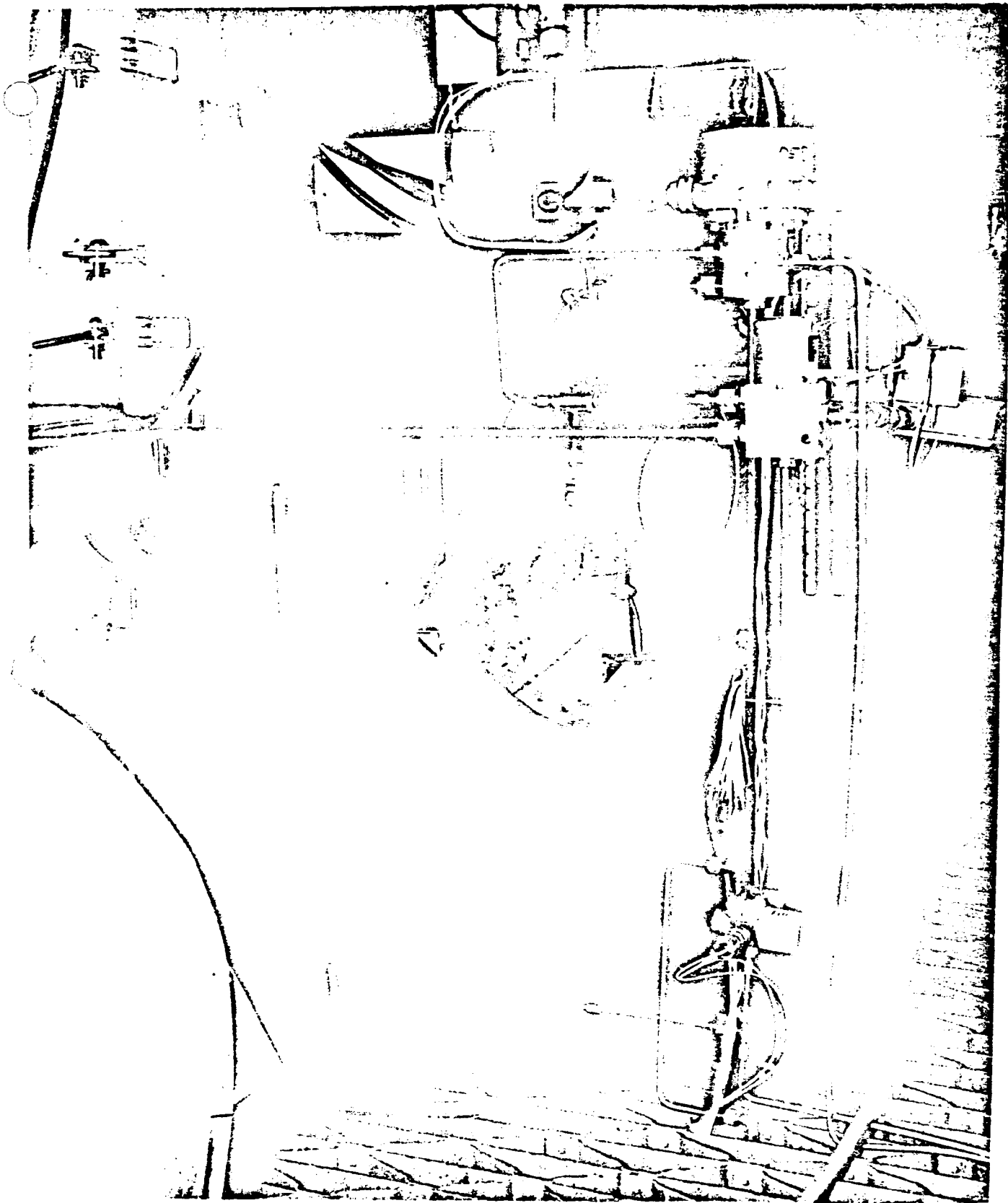


Fig. 19 Full-Scale System Reagent Weighing Fixture

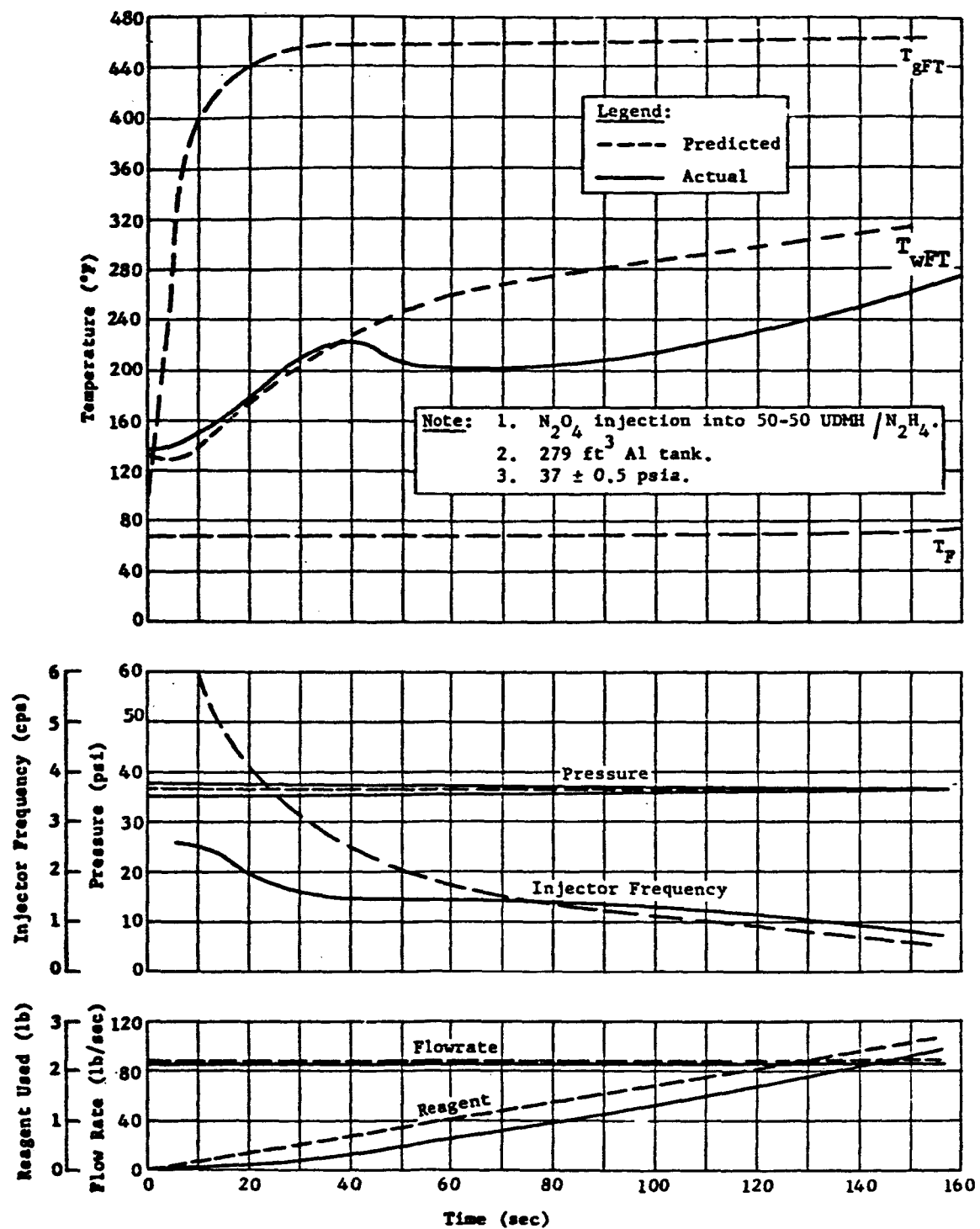


Fig. 20 Full-Scale System Fuel Tank Performance

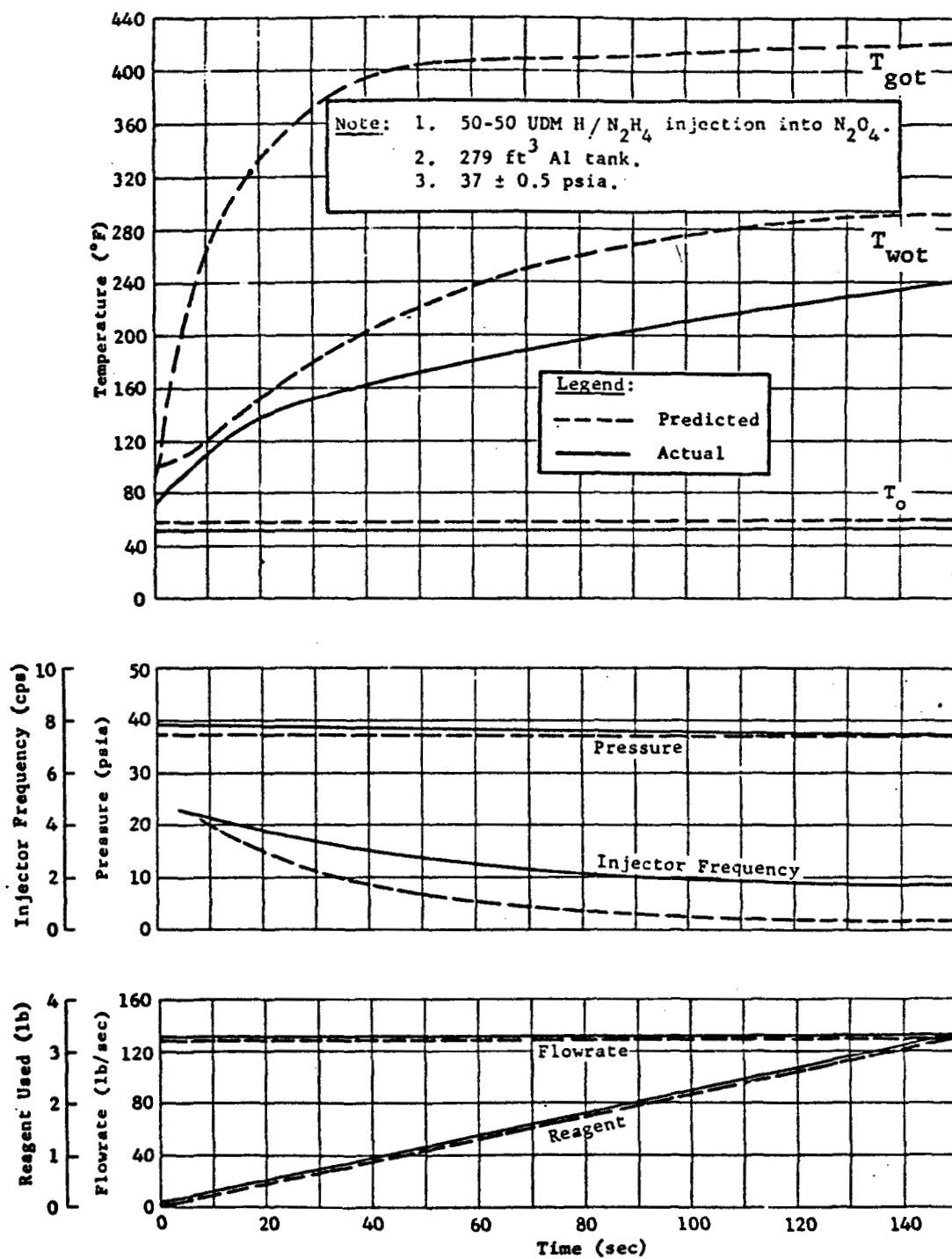


Fig. 21 Full-Scale System Oxidizer Tank Performance

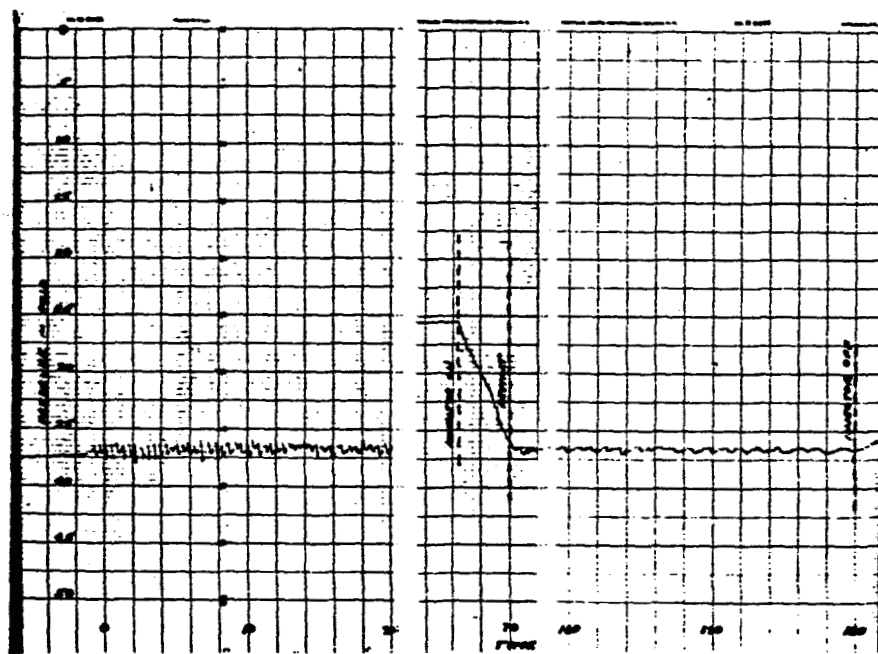
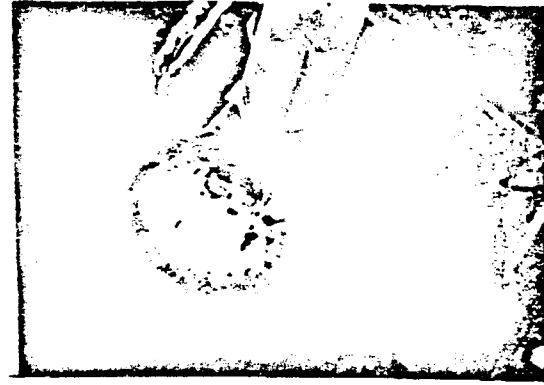


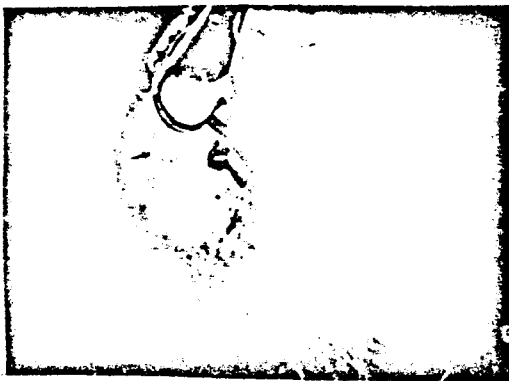
Fig. 22 Full-Scale System Actual Pressure History



(a)



(b)



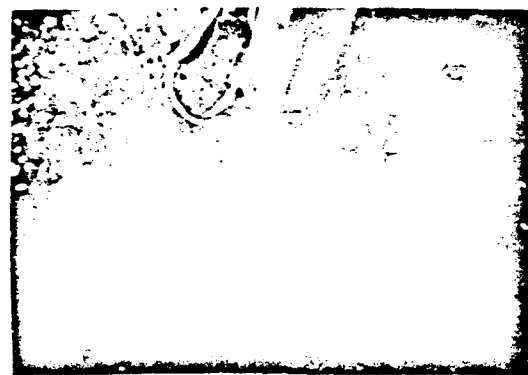
(c)



(d)



(e)



(f)

Fig. 23 Nitrogen Tetraoxide Injection Into Aluminum Thixotrope

**Table 1 Material Balance Tabulation for Subscale Oxidizer
Tank at 36 psia**

I Gaseous Combustion Products	Component	Weight (lb)	Volume SCF	Atomic Volumes			
				N	H	O	C
	H ₂		0.07	-	0.14	-	-
	N ₂		2.65	5.30	-	-	-
	CH ₄		0.03	-	0.12	-	0.03
	NH ₃		0.03	0.03	0.09	-	-
	CO ₂		0.46	-	-	0.92	0.46
	H ₂ O		0.13	-	0.26	0.13	-
	O ₂		0.65	-	-	1.30	-
	Total Gas	0.313	4.02	5.33	0.61	2.35	0.49
II Condensibles and un- accounted	H ₂ O	0.165	3.47	-	6.94	3.47	-
	N	0.014	0.38	0.38	-	-	-
	C	0.015	0.49	-	-	-	0.49
	Total Liquids	0.194		0.38	6.94	3.47	0.49
III Totals, Products		0.507		5.71	7.55	5.82	0.98
IV Injected Fuel	N ₂ H ₄		0.91	1.82	3.64	-	-
	N ₂ H ₂ (CH ₃) ₂		0.49	0.98	3.92	-	0.98
		0.151	1.40	2.80	7.56	-	0.98
V Oxidizer Reacted (III-IV with O/N-2)	N ₂ O ₄	0.354	1.46	2.92	-	5.84	-
VI Totals, Reactants			0.505	5.72	7.56	5.84	0.98

Table 2 Nonreaction Injection Penetration Test Data

Orifice Dia (in.)	Injector ΔP (psi)	Penetration (in.)	Time to Maximum Penetration (sec)	Penetration Rate Average (in./sec)	Injection Velocity (in./sec)
0.006	75	3.5	N/A	N/A	945
0.015	75	6.0	0.030	222	945
0.0135	75	6.0	0.030	222	945
0.0135	150	8.0	0.025	320	1340
0.040	75	13.0	0.053	244	945
0.040	150	15 (est)	0.048 (est)	315	1340

Table 3 Penetration Rate Comparison for Reacting and Nonreacting Process, $\Delta P = 75$ psi

Injected Fluid	Penetrated Fluid	Density Ratio (ρ_j / ρ)	Theoretical Injection Velocity (ft/sec)	Theoretical Average Penetration Rate (in./sec)	Actual Penetration Rate (in./sec)
Water	Water	1	78.8	472	222
Fuel	Oxidizer	0.628	82.8	438	N/A
Oxidizer	Fuel	1.59	66.0	442	100

Table 4 Fuel Tank Injection System Evaluation at 36 psia

	ΔT Gas (°F)	ΔT Fuel (°F)	ΔT Wall (°F)	Reagent Consumed (lb)	Mixture Ratio, W_o/W_f	Weight Gas (lb)	M W Gas, $*P_v = 0$
Surface Solid	266	27	37	0.412	0.62	0.579	13.4
Surface Spray	707	2	82	0.634	2.6	0.755	22.7
Subsurface solid	45	33	4	0.468	0.8	0.778	15.6
Subsurface Spray	37	29	2	0.412	1.0	0.900	17.5
$*P_v$ = Propellant vapor pressure							

Table 5 Gaseous Combustion Product Characteristics at 36 psia for Various Injection Methods

Injection Technique		Combustion Products Analysis (Vol %)									Ullage Gas Molecular Weight		
Fuel Tank	Oxidizer Tank	N ₂	H ₂	CH ₄	NH ₃	NO	CO ₂	CO	H ₂ O	O ₂	*P _v =0	*P _v =Actual	
Surface Solid	--	30.0	47.4	11.1	9.2	1.6	0.4	-	-	-	13.4		13.4
Surface Spray	--	60.0	11.8	18.8	3.4	3.1	3.0	-	-	-	22.9		22.9
Subsurface Solid	--	28.1	41.3	10.1	4.9	1.0	0.4	14.5	-	-	15.6		15.6
Subsurface Solid	--	35.8	37.5	13.0	3.4	1.0	0.2	9.5	-	-	16.4		16.4
--	Surface Solid	58.6	1.9	1.0	-	-	17.9	-	14.1	6.7	29.11		38.52
--	Surface Spray	59.8	3.5	0.6	1.4	-	11.4	-	8.4	15.0	28.45		34.77
*P _v = Propellant vapor pressure													

Table 6 - Subscale System Parametric Data Summary, Pressure Effects

Tank	Pressure (psia)	Temperature (°F)	Reagent Consumed (lb)	Mixture Ratio W_o/W_f	Ullage Gas Molecular Weight	
					$P_v = 0$	$P_v = \text{actual}$
Fuel	36	163	0.188	0.62	16.0	16.0
Oxidizer	36	154	0.151	2.34	29.5	36.53
Fuel	100	349	0.421	0.34	21.5	21.5
Oxidizer	100	300	0.448	2.34	29.87	35.79
Fuel	200	660	0.629	0.34	20.46	20.46
Oxidizer	200	580				

Table 7 Process Mass Balance Comparison

Configuration	Tank Pressure (psia)	Mole Weight (lb/lb mole.)	Combustion Product (lb gas)	Water Weight (lb)	Total Condensate (lb)	Reagent Weight (lb)	Reaction Mixture, W_o/W_f
<u>Experimental Program</u>							
Fuel Tank	36	15.77	0.412	0.208	0.316	0.278	0.62
Oxidizer Tank	36	29.51	0.313	0.165	0.192	0.151	2.34
<u>Demonstration Program</u>							
Fuel Tank	37	15.98	17.9	1.9	3.6	2.9	0.16
Oxidizer Tank	37	30.5	20.8	3.27	16.54	3.3	10.32

A CRYOGENIC HELIUM PRESSURIZATION SYSTEM
FOR THE LUNAR EXCURSION MODULE
by
J. C. Smithson and W. R. Scott
NASA-Manned Spacecraft Center
Houston, Texas

A CRYOGENIC HELIUM PRESSURIZATION SYSTEM
FOR THE LUNAR EXCURSION MODULE

J. C. Smithson and W. R. Scott
NASA-Manned Spacecraft Center
Houston, Texas

In order to effect a large weight reduction on the Lunar Excursion Module, the Grumman Aircraft Engineering Corporation has proposed the use of a cryogenic helium pressurization system. Since the LEM utilizes a pressure-fed propulsion system, relatively high tank pressures (225 psia), with attendant large pressurant masses are required. The use of helium stored in the supercritical state, because of its high density and low molecular weight (with a subsequent storage vessel size reduction), can provide the pressurization cycle required for the LEM while affecting a large weight decrease from the currently employed ambient system. Here, "supercritical" is used in the terminology of cryogenics, implying that the system is operating in the region of the critical temperature, but well above the critical pressure.

At the critical temperature, the specific volumes of the liquid phase and the gas phase are equal. Above this temperature, a fluid will not separate into two phases of different densities during an isothermal compression from large volumes. In other words, the liquid phase will not separate out. This phenomena is illustrated best with the aid of the P-v-T surface shown in Figure 1.

Consider that a system is initially in the thermodynamic state shown by point A. Now, if an isothermal compression was carried out in a transparent cylinder, one would observe the beginning of condensation into the liquid phase at the point where the isotherm meets the saturated vapor surface. As the compression process continues, the quantity of the liquid phase increases, while the vapor phase decreases. At the thermodynamic state represented by point B one would be sure that the fluid in the cylinder was wholly in the liquid phase. Now, another possibility exists; one could start with the system initially in the same state as shown previously (state point A) and carry out the process represented by the path from state point A to state point B, which curves around the critical point. (Of course, this process is not isothermal.) Although the end state of the system is the same in both processes, at no time in the second process did the fluid separate into two phases. Certainly, the fluid would be described as a liquid at the end of the second process as well as at the end of the first, for the end points (state point B) of the processes coincide. However, in the second process, the properties of the fluid changed continuously from those associated with a vapor, at state point A, to those associated with a liquid, at state point B. A system whose state point lies above the critical isotherm and critical isobar can exhibit characteristics identical to those described in the second process. Herein lies the advantage of a supercritical storage system. The fluid may be stored at a very high density (normally associated with a liquid) and utilized without ever encountering a two-phase region.

The critical point of helium is at pressure of 33.8 psia (2.26 atms), a temperature of 9.57°R (5.25°K), and a density of 7.81 lb/ft^3 .

Thus, the storage of supercritical helium for use on the Lunar Excursion Module presents a unique method of weight reduction because of the high fluid density with the resulting decrease in storage vessel volume.

In pressurization systems there exist many thermodynamic processes which the fluid in the storage vessel may undergo during expulsion. Of course, the most familiar is that of the isentropic expansion. This process is very closely approximated in the very rapid blow-down of high pressure bottles. However, this ideal process cannot be employed for a supercritical helium pressurization system since the rapidly decreasing temperature and pressure would leave an excessive amount of residual fluid in the vessel.

A second process is that of constant pressure expulsion. This is truly the "ideal" process, in that the residuals are a minimum, and the ideal process is time-independent. However, this type expulsion system would require a closely controlled, variable heat input. In a real system, it is highly questionable if the heater could handle the high transients required for maintaining a constant pressure. Further, a system requiring this close control has serious implications from the standpoint of system reliability.

A final system is one of almost constant heat input. This is the method which is utilized in the proposed LEM supercritical helium

pressurization system, and will be discussed in depth shortly.

The concept of low temperature, high pressure (supercritical) helium is not new. It was successfully employed in the Titan I, with the helium storage vessel immersed in the LOX tanks. The S-IV & S-IVB stages employ the same method, with the exception that the bottles are immersed in the liquid hydrogen tank. However, there is one basic dissimilarity: the stand-by time of the pressurization system used in these vehicles is not important. In a sense, one could consider that the helium (once temperature equilibrium is attained) is located in an infinite, low-temperature heat sink, i.e., the LH₂ tank at -423°F. The LEM does not possess this advantage, and the helium must be stored in a vacuum-jacketed Dewar.

The LEM supercritical helium system is shown schematically in Figure 2. For the sake of brevity, only the LEM descent stage will be discussed. The initial conditions at the time of helium withdrawal are approximately 1500 psia and 38°R, at a density of approximately 10 lb/ft³. The helium is withdrawn from the storage vessel, and passed through the primary helium-to-fuel heat exchanger. (The fuel is a blend of equal parts by weight of hydrazine and UDMH.) The temperature of the helium is raised from the storage vessel temperature (initially at approximately -428°F) to approximately -100°F. The warm helium is then returned to the storage vessel where an internal heat exchanger transfers heat from the effluent helium stream to the stored fluid, raising its temperature and consequently

its pressure. The helium, again at very low temperature, exits from the storage vessel and passes through the secondary helium-to-fuel heat exchanger, where the temperature is raised to approximately -50°F . The helium then flows through the regulator package to the propellant tanks.

The maximum helium flow rate is approximately 0.070 lb/sec, compared to a fuel flow rate of approximately 13 lb/sec at full thrust. Because of this wide variance in flow rates, no freezing of the fuel is encountered.

As was pointed out earlier, the helium vessel is a vacuum-jacketed Dewar. The addition of an internal heat exchanger further complicates the design. Figure 3 is a cross-sectional view of one proposed storage Dewar. The inner vessel is approximately 24 inches in diameter; the construction is of titanium - 6Al-4V(ELI). The annular volume contains super insulation. The withdrawal lines are routed circumferentially in the usual manner, to provide long heat conduction paths.

The internal heat exchanger in this design is a hollow copper sphere, with tubes wrapped around it. The sphere is pierced for minimum weight and to provide fluid ingress and egress. The copper sphere acts essentially as an extended surface for the heat exchanger.

The loading conditions place important and significant constraints on the design of a supercritical storage system. The system weight

is a direct function of the loading pressure and temperature. Thus, the higher the loading density, the lower the system weight because of a smaller storage vessel.

Figure 4 is the P-v-T surface for helium. Plotted on this figure are the loading conditions for the LEM supercritical helium pressurization system. (The figure is a qualitative representation and the coordinates do not necessarily correspond to the following quoted values.) The critical density (specific volume) is shown for reference. The vessel is loaded with liquid helium at approximately 3 psig and 8°R, shown on Figure 4 as state point 1. Then, chilled, high pressure helium (approximately 400 psia and 10°R) is used to bring the fluid to a supercritical state. The fluid is circulated through a liquid helium boiler, lowering its temperature, hence lowering its specific volume (from v_1 to v_2). When the temperature and pressure stabilize, the system is in a state represented by state point 2. The current LEM system is designed for a 142 hour standby time. During this time, the fluid is subject to a heat leak of approximately 6.5 Btu/hr. This heating, at constant density along the path from state point 2 to state point 3, brings the system to its operating conditions, represented by state point c, viz., 1500 psia and approximately 38°R, (but still at v_2).

Another condition which affects the system weight is the allowable heat leak. If the heat leak requirement is reduced from its present value of 6.5 Btu/hr to a value of 5.0 Btu/hr, the insulation

thickness for the Dewar increases approximately two inches. Since the weight is a function of the diameter cubed (D^3), the attendant weight increase is substantial.

Although one may be enthusiastic about the possible weight reduction offered by this method of storage, the magnitude of some of the potential problems associated with the development of a system of this nature should not be underestimated.

One of the most outstanding and pressing problems is the lack of basic thermodynamic properties of helium in the low temperature, high pressure regime. (This is especially true for the LEM ascent stage, which has been proposed as a 3000 psia system.) The size or weight of a Dewar is a function of the required pressure, temperature, and useable fluid mass. In view of the lack of P-v-T data in the regions of interest, the amount (mass) of fluid stored at a given pressure and temperature in a given volume cannot be accurately determined. Further, the weight of residual fluid cannot be easily established. Consequently, an accurate weight prediction is extremely difficult to make. Some preliminary experimental work to determine the required P-v-T data has been accomplished by the LEM contractor.

The passive temperature control of a low-temperature fluid system continues to be a critical area. This must be a very low heat leak system, to prevent over pressurization. As was pointed out earlier, the proposed design will permit a maximum heat leak of 6.5 Btu/hr.

Other programs utilizing supercritical storage systems are having difficulty meeting their stand-by time requirement, which is governed by a heat leak requirement much higher than the one required for the LEM.

Another area of concern is the design of both internal and external heat exchangers. The internal exchanger is a critical item. If the heat rejection rate of the internal exchanger is too high, overpressurization, with subsequent system venting, occurs early in the mission duty cycle. If the heat exchanger is too small, sufficiently high pressure and temperature is not available near the completion of the duty cycle, resulting in an excess of non-useable helium remaining in the storage vessel near the end of the duty cycle. Consequently, close design tolerances must be maintained on the internal heat exchanger. As was seen previously, one proposed design was the use of a spherical heat exchange surface. Another proposed exchanger is merely a pipe coil inside the pressure vessel.

The external heat exchanger appears to present major development problems. The exchangers must operate over a wide range of temperatures (from approximately -430°F to 0°F) at relatively high pressures. They must also be light-weight exchangers or much of the weight reduction potential afforded by this storage concept will be lost. There is, however, one more serious constraint. Recalling Figure 2, it is noted that the two external heat exchangers operate in series on the fuel side of the exchangers. Since the LEM employs

a pressure-fed engine, the propulsion system is quite sensitive to adverse pressure changes. The present LEM propulsion system can tolerate only a 10 psi ΔP increase. Thus, to allow a margin of safety, the external heat exchangers must be designed for a maximum fuel side ΔP of 2.5 psi each, or 5 psi ΔP for the two exchangers in series. For the propellant flow rates encountered on the LEM, this low ΔP requirement may well be a major problem area.

One final area of concern in the development and utilization of this system is in the field of ground support equipment (GSE). Due to its low heat capacity and low temperatures, liquid helium cannot be pumped over long distances without interstage refrigeration. Portable Dewars and a specially designed fill system will be employed for charging the storage vessel. Due to the stand-by time constraint, the system must be loaded just prior to launch; this dictates that the GSE must be at the LEM level, on the mobile arming tower. This introduces considerations of both weight and space on the arming tower.

In conclusion, it should be pointed out that the system is feasible, but that it is not without some problems. As was noted earlier, lack of P-v-T data is a serious shortcoming. The consistent achievement of a very low heat leak will be difficult. The sizing of the internal heat exchanger is critical. The pressure drop on the fuel side of the external exchangers present development problems. The GSE requirements for this system may be pacing items for a flight

system that must meet a strict launch schedule.

The seemingly endless number of problems of this system are countered by two great advantages: 1) large potential weight reduction, and 2) a smaller bottle package. This system offers a potential weight reduction of 500 to 1000 pounds (effective or separation weight), depending on whether the system is used on just the descent stage or on both ascent and descent stages. The weight saving is realized primarily in reduced bottle weight, since this constitutes over 80% of the pressurization system weight for an ambient, high pressure storage system. The fact that the volume of the bottle is much smaller (because of the high density), means that a smaller bottle package results. In fact, on the proposed LEM descent stage system, the 3500 psia ambient system, consisting of two storage vessels approximately 33 inches in diameter, is replaced by a supercritical helium pressurization system, consisting of one storage vessel, only 30 inches in diameter (O.D. of the vacuum jacket).

Thus the use of a cryogenic helium pressurization system for the Lunar Excursion Module appears to be an attractive method by which to reduce the overall LEM weight, which in turn increases the potential payload capability of the Lunar Excursion Module.

P-V-T SURFACE FOR HELIUM

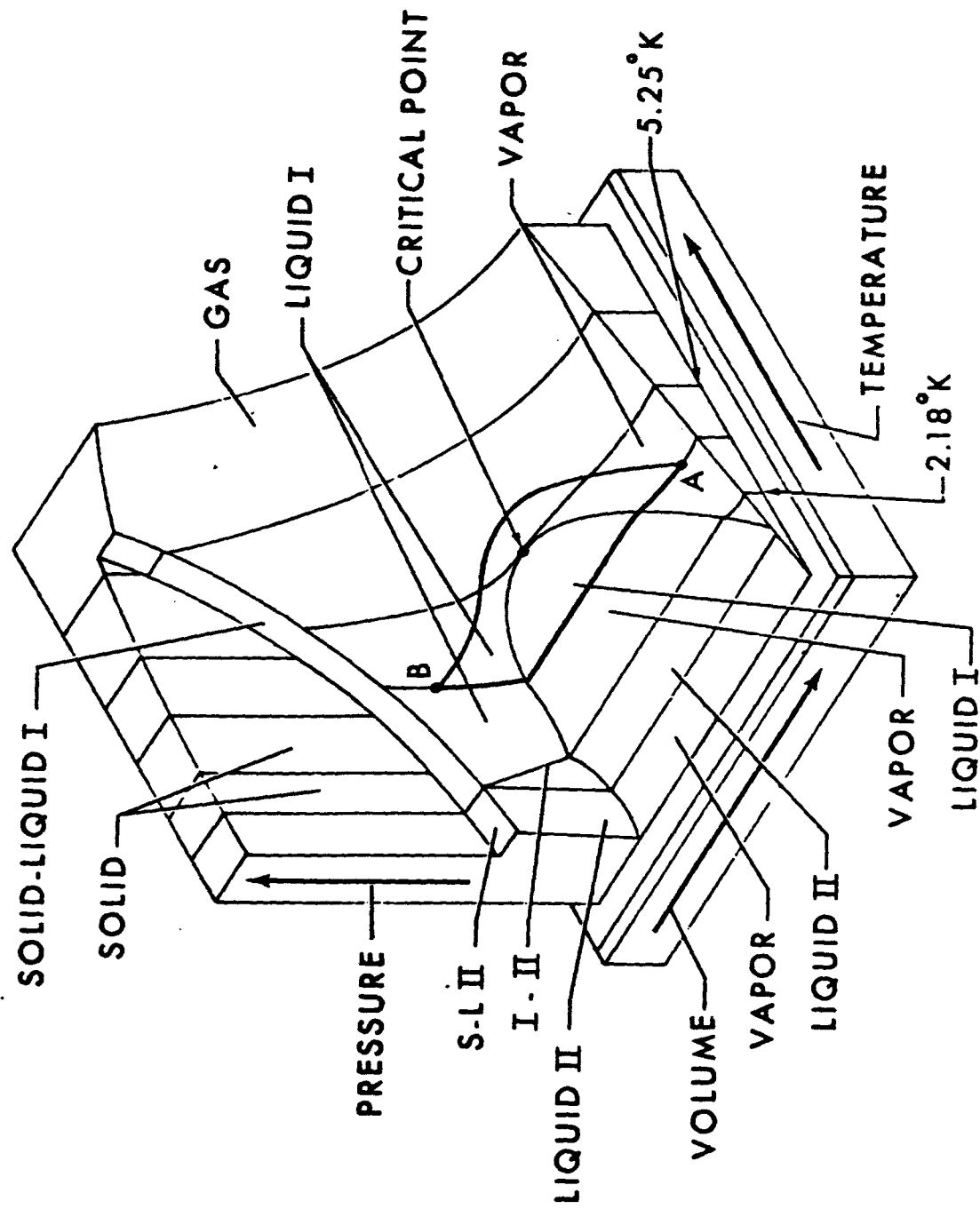


FIGURE 1

SUPERCritical HELIUM PRESSURIZATION SYSTEM FLOW SCHEMATIC

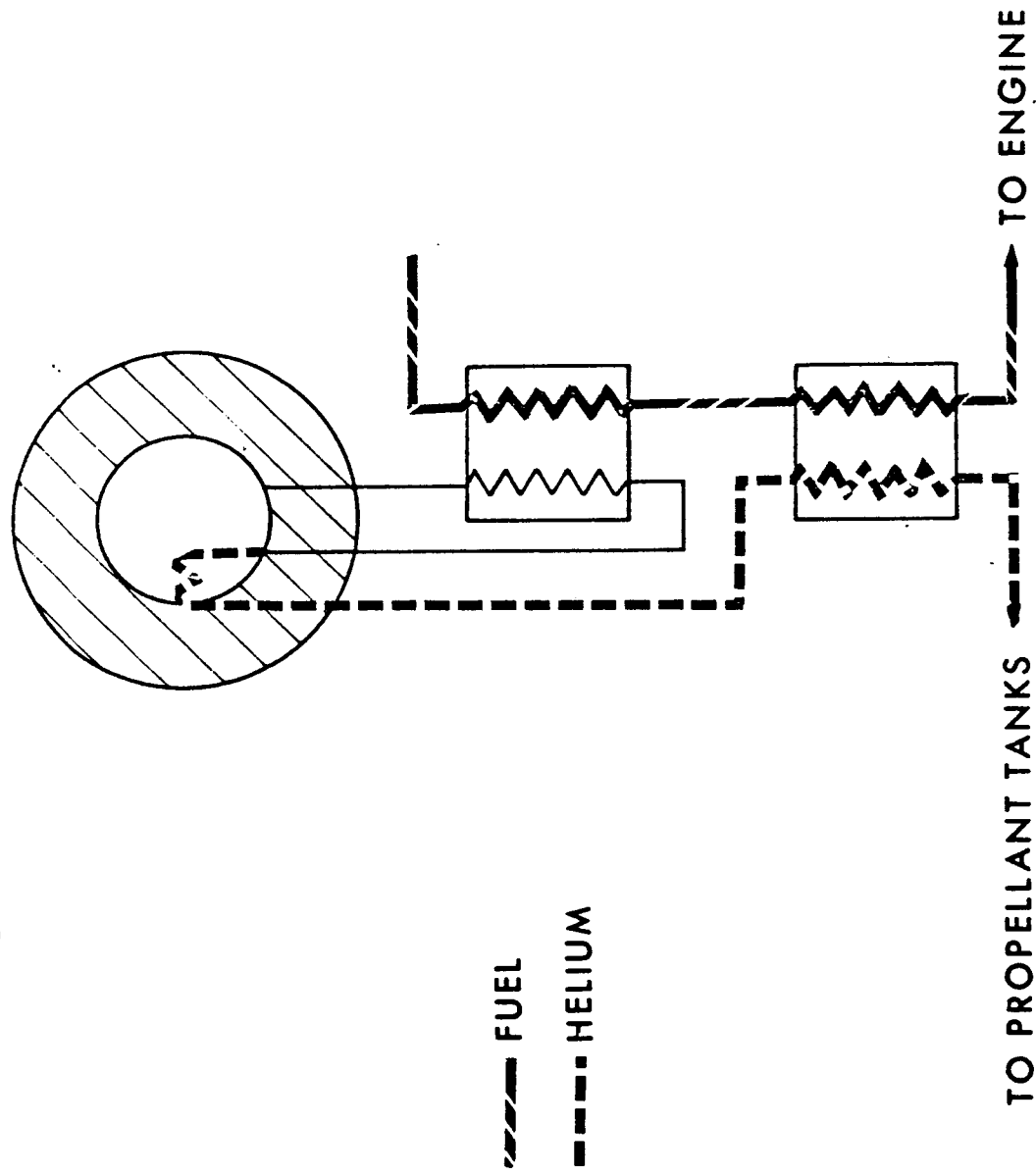


FIGURE 2

CROSS-SECTIONAL DRAWING OF HELIUM STORAGE VESSEL

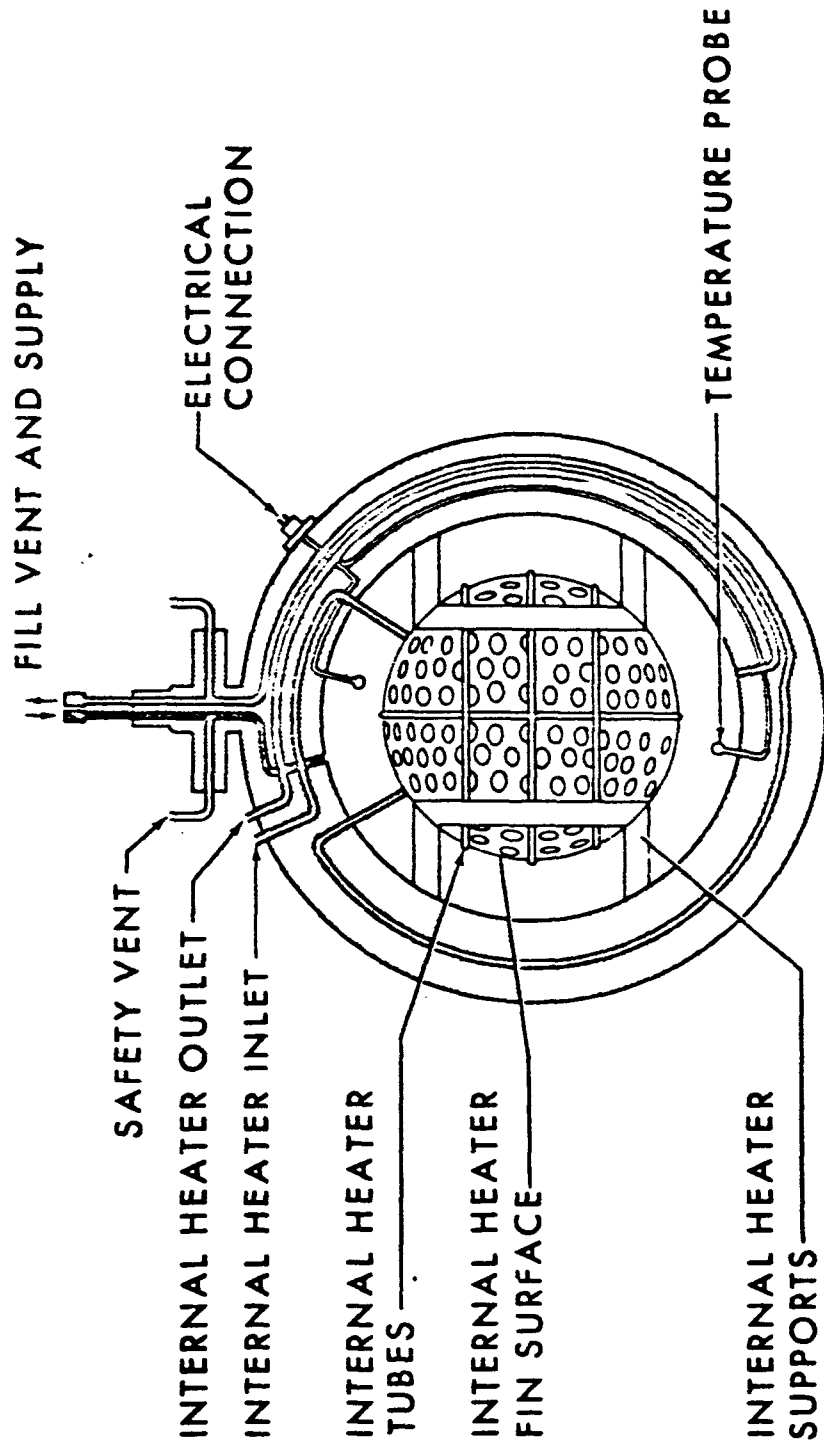


FIGURE 3

P-V-T SURFACE FOR HELIUM

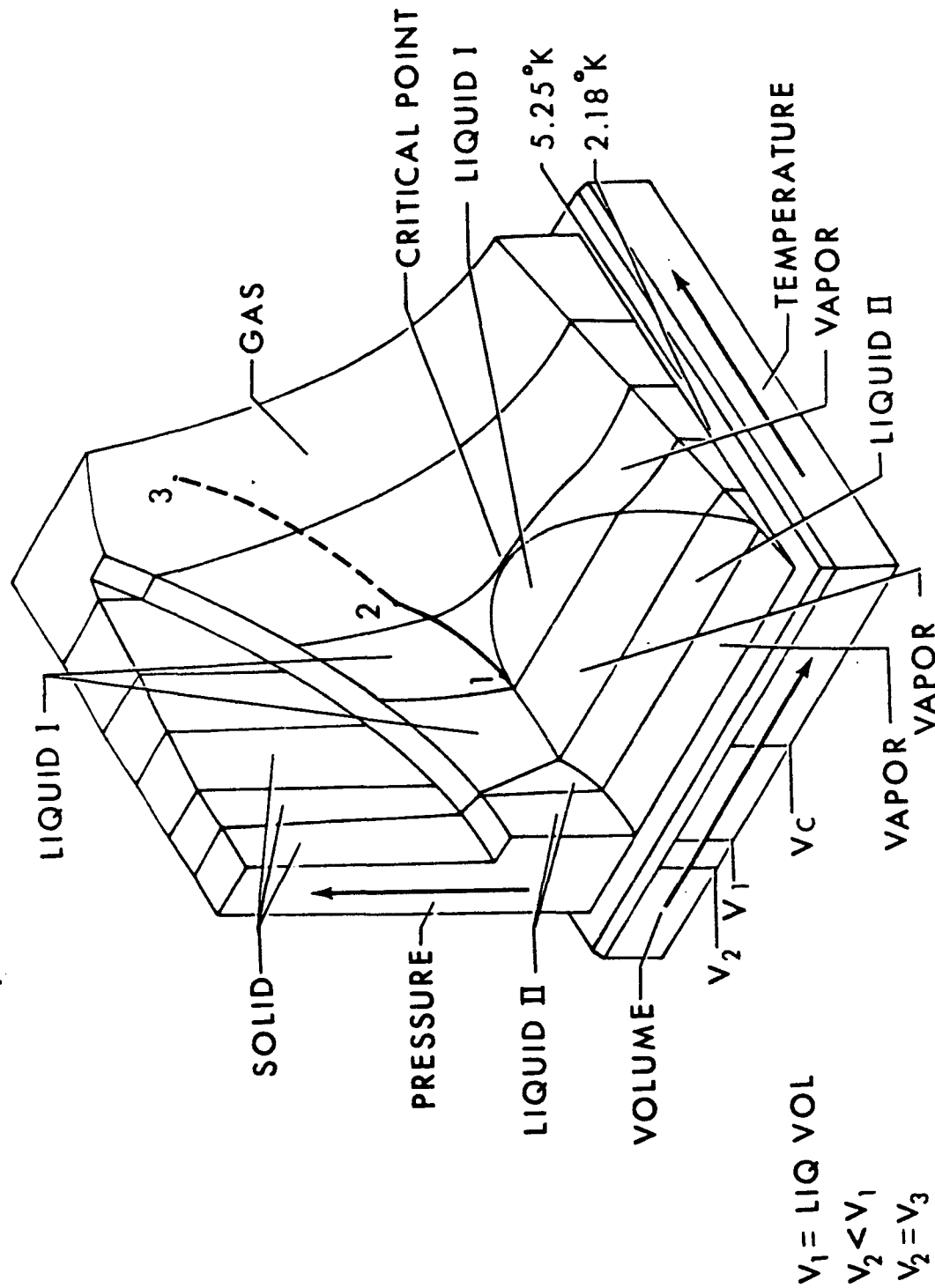


FIGURE 4

BULK LIQUID INTERFACIAL MASS TRANSFER
WITH VARIABLE ULLAGE PRESSURE

by

John R. O.'Loughlin* and Howell Glenn
The Boeing Company
New Orleans, Louisiana

* Associate Professor of Mechanical Engineering, Tulane University, New Orleans, Louisiana; consultant to The Boeing Company

BULK LIQUID INTERFACIAL MASS TRANSFER WITH
VARIABLE ULLAGE PRESSURE

John R. O'Loughlin *

Howell Glenn **

Abstract

A numerical program has been prepared which calculates the interfacial mass transfer for the cases of gradual initial pressurization and variable pressure after initial pressurization of a liquid-vapor system. The output of this program agrees well with the analytical results for the case of sudden pressurization followed by constant pressure. It is shown that the output of the program for sudden pressurization followed by variable pressure can be bracketed by the analytical results for sudden pressurization followed by constant pressure. The use of variable properties, possible in the numerical program but not in the analytical work, changes the mass transfer results only slightly from those found with constant properties.

* Consultant, Launch Systems Branch, The Boeing Company, also Associate

Professor of Mechanical Engineering, Tulane University, New Orleans, Louisiana

** Associate Engineer, Launch Systems Branch, The Boeing Company, Huntsville, Alabama.

Introduction

A considerable amount of work (1-4) has been done on the problem of interfacial phase change for a suddenly pressurized liquid-vapor system. These studies have examined the phase change for a system which is suddenly pressurized and then held at that pressure. Should the pressurization be gradual or the pressure vary in an arbitrary manner after the sudden pressurization, the problem becomes considerably more complex. The present paper describes a numerical method designed to handle such problems.

Analysis

Although the numerical method used here will accommodate any stable initial temperature profile, the present discussion will cover the case of an initially saturated liquid and vapor as shown in Figure 1a. For purposes of describing the program, examine the suddenly pressurized case. The thermal profile for this situation is shown in Figures 1b and 1c while the pressure-time history is shown in Figure 1f. Note however that the numerical program will handle gradual pressurization as well as sudden.

The method used to handle the variable ullage pressure is to approximate the given pressure-time history by segments of constant pressure connected by instantaneous pressure changes as shown after the sudden pressurization in Figure 1f.

The constant pressure segments of the pressure-time history are handled with a variable property version of the energy equations used in reference (1). These equations are based on a moving coordinate system mounted on the liquid-vapor interface.

$$\frac{\partial T_L}{\partial t} = \frac{1}{\rho_L c_L} \left\{ \left(\frac{\partial T_L}{\partial x} \right)^2 \left(\frac{dk_L}{dT_L} \right) + k_L \left(\frac{\partial^2 T_L}{\partial x^2} \right) \right\} - \frac{\epsilon}{\rho_L} \left(\frac{\partial T_L}{\partial x} \right) \quad (1)$$

$$\frac{\partial T_v}{\partial t} = \frac{1}{\rho_v c_v} \left\{ \left(\frac{\partial T_v}{\partial x} \right)^2 \left(\frac{dk_v}{dT_v} \right) + k_v \left(\frac{\partial^2 T_v}{\partial x^2} \right) \right\} - \frac{\epsilon}{\rho_v} \left(\frac{\partial T_v}{\partial x} \right) \quad (2)$$

where

$$\rho_v = \frac{P_v}{z R T_v} \quad (3)$$

The vapor and liquid are assumed to be at a uniform pressure throughout. This is accurate for the vapor where the density is low. In the liquid, however, consideration of the static pressure head causes the saturation temperature to vary with depth. This factor influences the amount of liquid flashed to vapor during an instantaneous pressure decrease but it is not currently included in the program.

During the constant pressure segments of the pressure-time history, the rate of condensation or evaporation is given by the following interfacial energy balance where $\epsilon < 0$ means condensation and $\epsilon > 0$ indicates evaporation.

$$\epsilon = \frac{1}{h_{fg}} \left\{ k_v \left(\frac{\partial T_v}{\partial x} \right)_{x=0} - k_L \left(\frac{\partial T_L}{\partial x} \right)_{x=0} \right\} \quad (4)$$

The instantaneous pressure changes are handled in an entirely different manner than the constant pressure segments of the pressure-time history. The problem is basically the same, however, in that the temperature profile must be continuously updated and a record of the interfacial mass transfer must be kept.

The following factors must be considered as a result of an instantaneous pressure change: (1) expansion or compression of the ullage vapor, (2) interfacial phase change caused by the imposed requirement that equilibrium be maintained in liquid and vapor at all times and, (3) displacement of the interface and of the vapor itself caused by phase change.

Taking the processes in (1) above as isentropic, the new temperature, T' , caused by a small change in pressure from P to P' is

$$T' = T \left(\frac{P'}{P} \right)^{zR/c_v} \quad (5)$$

For an ideal gas ($z = 1$), this reduces to the more familiar form

$$T' = T \left(\frac{P'}{P} \right)^{\frac{\gamma-1}{\gamma}}$$

In using equation (5), the pressure difference between P and P' is small. Therefore the temperature change is small and z and c_v can be taken as constants.

Consider a pressurization schedule such as shown in Figure 1f. The sequence of temperature profiles is as shown in Figures 1a, b and c. This is the same as discussed in reference (1). A sudden drop in pressure then occurs

at time t_i . This is required to follow the given pressure-time history. As a result of this drop in pressure, the interfacial temperature is reduced as it always equals the saturation temperature corresponding to the current ullage pressure. The vapor also expands with this pressure drop. In the numerical program, both vapor and liquid are divided into slabs by imaginary planes parallel to the interface and the new temperature of each vapor slab is now calculated from equation (5). The temperature profile at this time is as shown by the solid line of Figure 1d. It is apparent that non-equilibrium conditions exist in the vapor between the interface and x'_i and in the liquid between the interface and x_o . Based on the imposed requirement that such non-equilibrium conditions are forbidden, they are removed by an energy balance written for the non-equilibrium fluid. For example, the liquid between the interface and x_o contains an amount of energy over and above that of saturated liquid at temperature $(T_i - \Delta T)$. This liquid is therefore superheated. The excess energy is used to flash a certain portion of the superheated liquid and the temperature of the remaining liquid between the interface and x_o is reduced to $(T_i - \Delta T)$ since its excess energy has been utilized. The amount of superheated liquid flashed in this process is calculated from

$$E = \frac{1}{h_{fg}} \int_{x_o}^0 \rho_L (h_L - h_{sp}) dx \quad (6)$$

where $E > 0$ indicates evaporation.

The same non-equilibrium situation exists in the vapor following this pressure decrease. This non-equilibrium condition consists of the presence of supersaturated vapor and it is eliminated by an energy balance similar to that given above. That is, the energy deficiency of the supersaturated vapor is calculated. Such energy is then supplied by condensing a fraction of this vapor. The temperature of the remaining supersaturated vapor is then increased to $(T_2 - \Delta T)$ as the energy required to accomplish this has been supplied by the condensation. The amount of supersaturated vapor condensed is

$$E = \frac{1}{h_{t_2}} \int_0^{x'_0} \rho_v (h_v - h_{s,p}) dx \quad (7)$$

where $E < 0$ implies condensation.

The program will handle increasing pressures as well as decreasing. Figure 1e indicates that equilibrium is maintained for the increasing case thereby simplifying the calculations.

The total mass condensed or evaporated between $t = 0$ and any later time t must be calculated by adding together the phase changes which take place during the instantaneous pressure changes as well as those which occur during the constant pressure processes.

$$m = \sum \epsilon (\Delta t) + \sum E \quad (8)$$

The program will accommodate variable ullage temperature as well as variable ullage pressure. The technique for accomplishing this is to assume that the thermal layer in the vapor adjacent to the liquid-vapor interface is

not influenced by changes in the temperature of the bulk vapor. Thus a change in the bulk vapor temperature is assumed to change the temperature of only the top two slabs of the thermal vapor layer. This technique is open to criticism but treatment of the situation from a more rigorous standpoint immediately introduces considerable complexity.

There are limits on the allowable changes in ullage pressure and temperature. No change is allowed which would cause the entire bulk of liquid or vapor to be in a non-equilibrium state. That is, no change is allowed which would cause the temperature at the interface (T_2) to become less than the bulk liquid temperature (T_1) or greater than the bulk vapor temperature (T_3). This would exclude, for example, a pressure drop from the initial saturated state as given in Figure 1a.

Numerical Method

The computer program is written for the IBM 7094 in the Fortran IV programming language. The following finite difference equation is used to approximate the partial differential equations (1) and (2).

$$T_i^{n+1} = T_i^n + \frac{\Delta t}{\rho_i^n c_i^n} \left\{ \frac{dk_i^n}{dT_i^n} \left[\frac{T_{i+1}^n - T_{i-1}^n}{2 \Delta x} \right]^2 + k_i^n \left[\frac{T_{i+1}^n - 2 T_i^n + T_{i-1}^n}{(\Delta x)^2} \right] \right\} - \frac{(\Delta t) \epsilon}{\rho_i^n} \left[\frac{T_{i+1}^n - T_{i-1}^n}{2 \Delta x} \right] \quad (9)$$

where $T_i^n = T(x_i, t_n)$

$T_{i+1}^{n+1} = T(x_i + \Delta x, t_n + \Delta t)$

Equation (9) is used during periods of constant pressure to calculate the new temperature at each x location in liquid and vapor with the exception of the interface. For an instantaneous pressure change, the new temperature at each x location is calculated from equation (5) and then adjusted to account for vapor motion caused by interfacial phase change and vapor compression or expansion.

Equation (6) is approximated by the following summation.

$$E = \frac{1}{h_{fj}} \sum_{i=1}^{x_0} [\rho_v (h_v - h_{sp})]_i [x_{i-1} - x_i] \quad (10)$$

A similar form is used to approximate equation (7).

The numerical method takes into account the variation of fluid properties with temperature. Therefore in the finite difference equations, the properties are evaluated at the temperature of each slab.

Some instability difficulties were encountered with equation (9). It is apparent that large discontinuities in the temperature profiles caused by instantaneous pressure changes required small time steps until the profile became smooth again. Consequently, the time step was reduced after each pressure change and then allowed to increase later after the profile had been somewhat smoothed.

A flow diagram for the numerical program is shown in Figure 2.

Results and Discussion

The results of several runs with the numerical program are shown in Figure 3. This figure also shows results obtained by the exact technique of Reference 1. The oxygen system was used for these calculations. For all curves, the liquid and vapor oxygen are initially saturated at 16.7 psia. At time = 0, the ullage temperature is suddenly changed to 200°R for all curves. The other pressurization conditions are as follows.

- Curve 1: Sudden pressurization to 30 psia at $t = 0$ and hold at this pressure for 160 seconds. Solution by the exact method of Reference 1 which requires constant properties evaluated at an average temperature.
- Curve 2: Sudden pressurization to 30 psia at $t = 0$ and hold at this pressure for 160 seconds. Solution by the present numerical program with variable properties.
- Curve 3: Sudden pressurization to 30 psia at $t = 0$ and hold at this pressure for 160 seconds. Solution by the present numerical program with constant properties evaluated at an average temperature.
- Curve 4: Sudden pressurization to 30 psia at $t = 0$ and hold at this pressure for 80 seconds then drop linearly to 20 psia at 160 seconds. Solution by the present numerical program with variable properties.
- Curve 5: Sudden pressurization to 30 psia at $t = 0$ and hold at this pressure for 5 seconds then drop linearly to 20 psia at 160 seconds. Solution by the present numerical program with variable properties.
- Curve 6: Sudden pressurization to 20 psia at $t = 0$ and hold at this pressure for 160 seconds. Solution by the exact method of Reference 1 which requires constant properties evaluated at an average temperature.

Several useful results are apparent from an examination of Figure 3.

The fact that curves 2 and 3 fall on top of each other indicates that the consideration of variable properties has little effect for these conditions. The actual results from which curves 2 and 3 were plotted indicate that the use of variable properties yielded slightly lower results than the use of constant properties. The difference, however, is too small to show on Figure 3. Notice that all cases examined have an ullage temperature of 200°R . Should a higher ullage temperature be used, it is expected that the difference in the results using variable and constant properties would be more significant.

Ideally, curves 1 and 3 should fall on top of each other. The discrepancy is due to inaccuracy in the numerical program. Note that curve 3 follows curve 1 very well after the first 5 seconds. Apparently the inaccuracy is introduced in the numerical program between $t = 0$ and $t = 5$ seconds. A possible explanation of this is as follows. The exact analytical method of Reference 1 yields infinite temperature gradients and consequently an infinite mass transfer rate at $t = 0$. The numerical program yields large temperature gradients and a large, but finite, mass transfer rate at $t = 0$. Consequently the mass transfer from the numerical program starts off low and although it follows the exact solution very well thereafter, it always remains slightly low due to the situation at $t = 0$. It is apparent that the rates of mass transfer, as given by the slopes of the curves, are practically identical for curves 1 and 3 for time greater than about 5 seconds.

Curve 4 follows curves 2 and 3 until 80 seconds as it should since conditions are the same until that time. After $t = 80$ seconds, the ullage pressure drops linearly with time. The numerical program follows this linear drop with a series of steps as shown in Figure 1f. Between $t = 80$ and 110 seconds, the evaporation caused by instantaneous pressure drops is less than the condensation during periods of constant pressure. The result is continuing condensation but at a lesser rate during this period. The peaking of curve 4

and its subsequent gradual drop indicates that after 110 seconds the mass evaporated during the instantaneous pressure drops exceeds that condensed during the constant pressure segments of the pressure-time history. The result is a net evaporation between 110 and 160 seconds. This evaporation is less, however, than the mass condensed between $t = 0$ and $t = 110$ seconds so that the net mass transfer between $t = 0$ and $t = 160$ seconds is 2.15×10^{-2} lb_m/ft² condensation as shown in Figure 3.

Curve 5 drops away from curves 2 and 3 after about 10 seconds. Its maximum occurs near the maximum for curve 4.

It is reasonable that curves 4 and 5 be bracketed between curves 1 and 6 because the pressure-time histories of the latter bracket the pressure-time histories of the former.

Conclusions

The numerical program satisfactorily checks the analytical results for the case of sudden pressurization followed by holding at that pressure. Possibly smaller time steps near $t = 0$ would yield even a closer check.

Use of the numerical program with constant and variable properties indicates that this difference causes only a small change in mass transfer. Higher ullage temperature than used here could increase this difference.

The results indicate that for the variable pressure conditions studied, the mass transfer is bracketed by the analytical results of Reference 1 if pressures are used with that analytical method which bracket the pressure-time history for the variable pressure case.

Nomenclature

c	specific heat at constant pressure
E	mass transfer per unit of interfacial area caused by an instantaneous change in ullage pressure ($E < 0$ for condensation; $E > 0$ for evaporation)
h_{fg}	heat of vaporization
k	thermal conductivity
m	total mass transfer per unit of interfacial area between time zero and any later time t ($m < 0$ for condensation; $m > 0$ for evaporation)
P	pressure
R	gas constant
T	temperature
t	time
x	coordinate perpendicular to the liquid-vapor interface
z	compressibility factor
γ	ratio of specific heats
ϵ	rate of mass transfer per unit of interfacial area during periods of constant ullage pressure ($\epsilon < 0$ for condensation; $\epsilon > 0$ for evaporation)
ρ	density

Subscripts

L	liquid
o	condition where temperature equals saturation temperature
sp	saturation condition corresponding to current ullage pressure
V	vapor

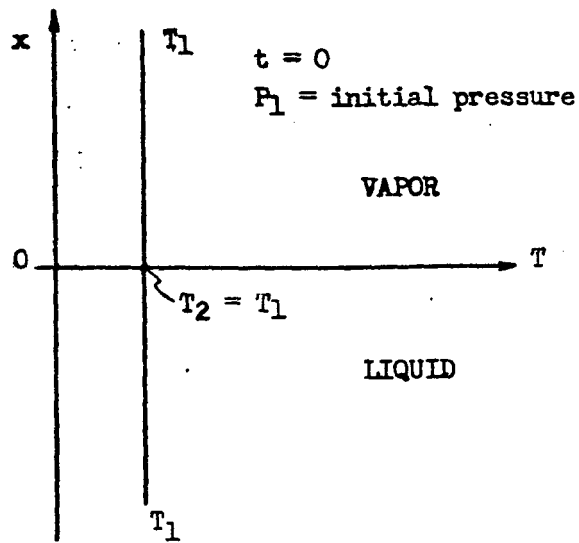


Figure 1a

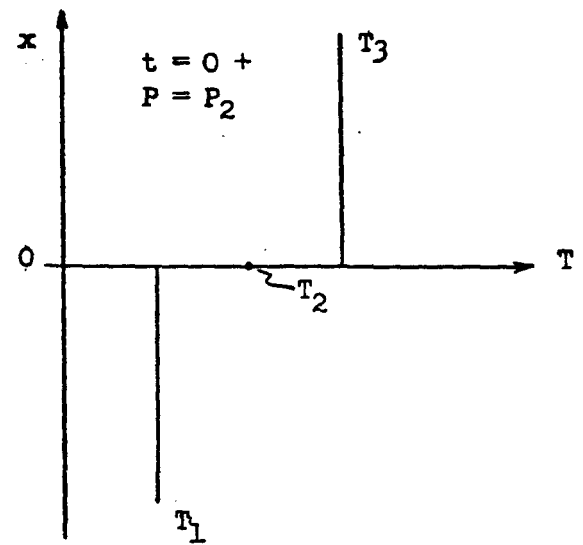


Figure 1b

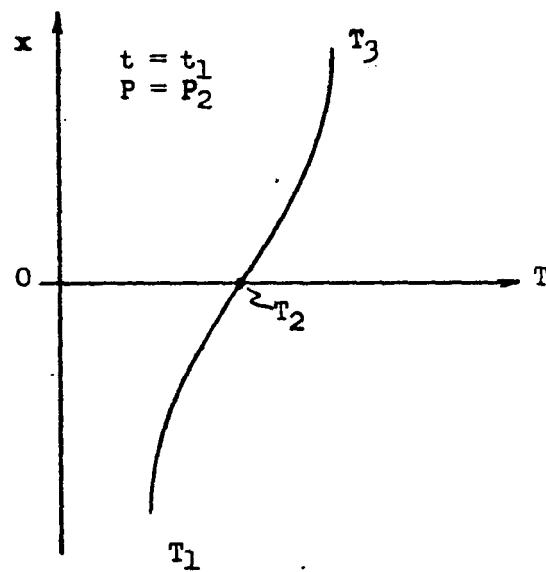


Figure 1c

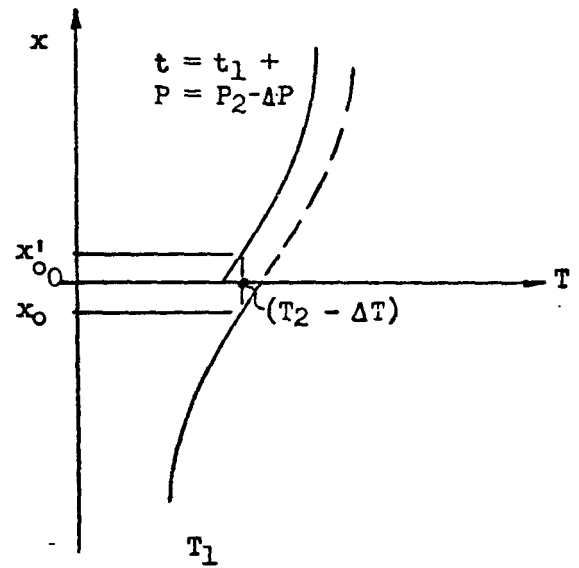


Figure 1d

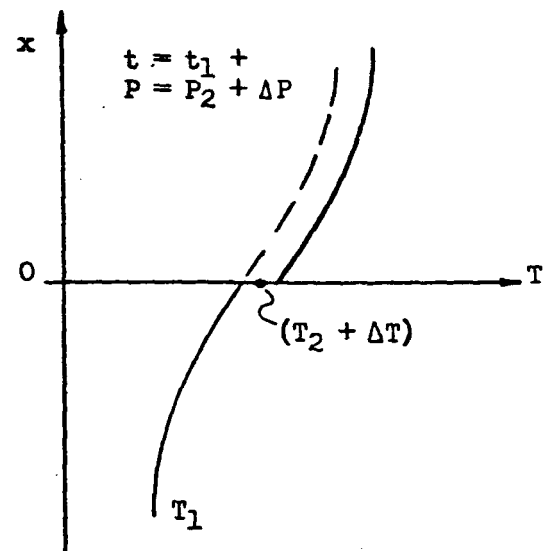


Figure 1e

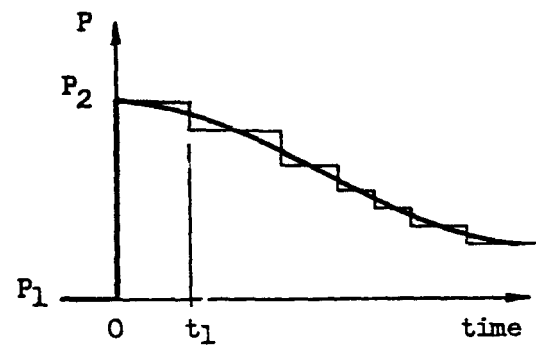


Figure 1f

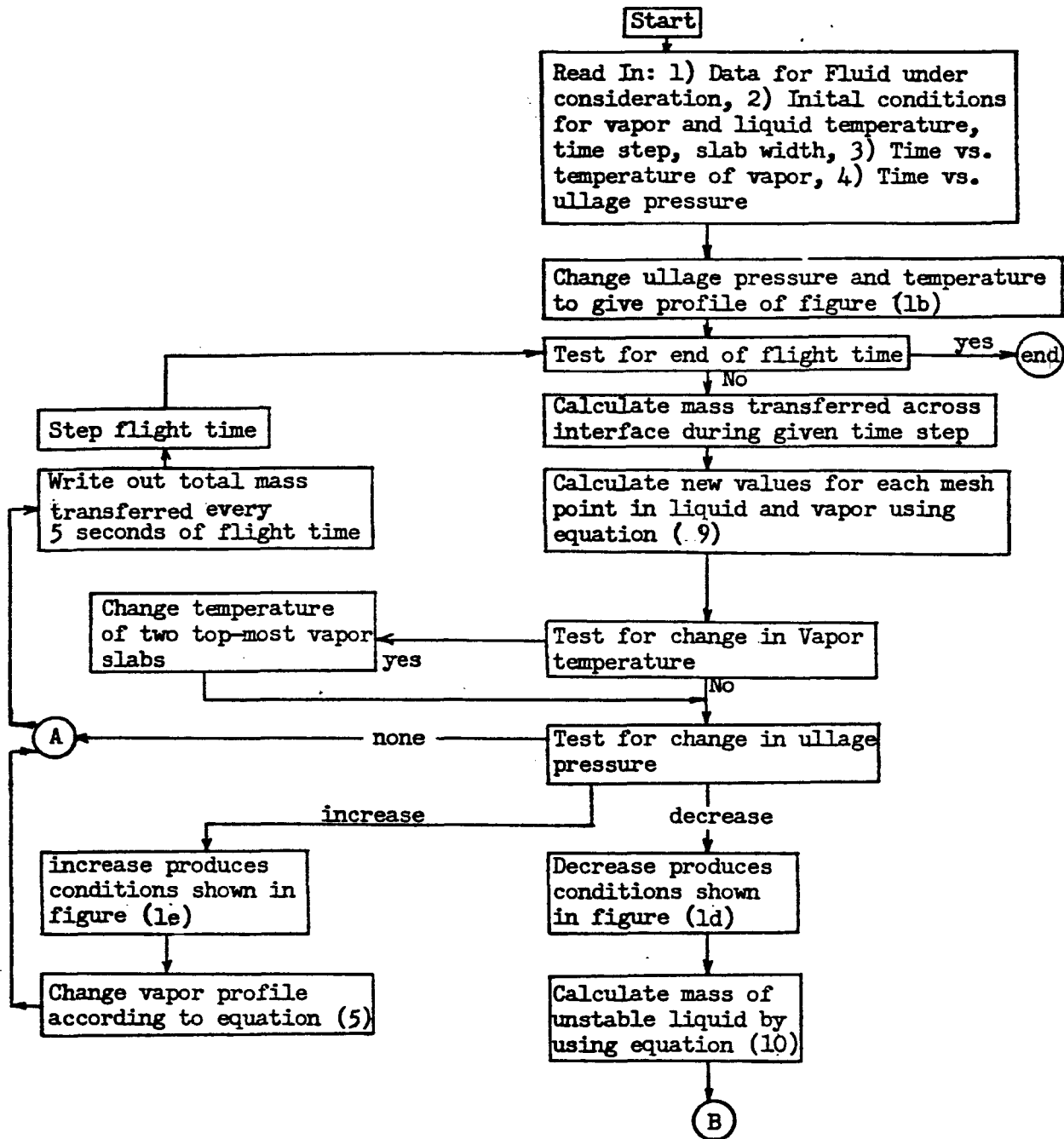


Figure 2 Flow Diagram

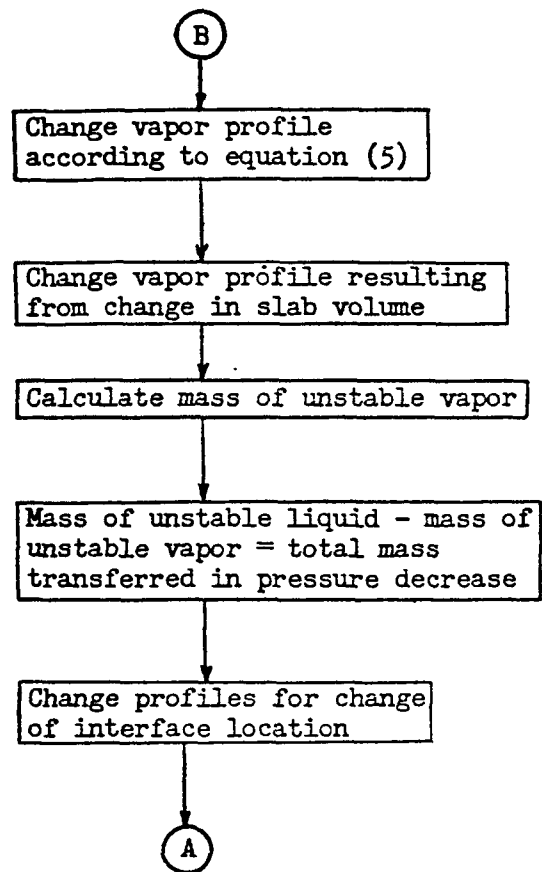


Figure 2 Flow Diagram (continued)

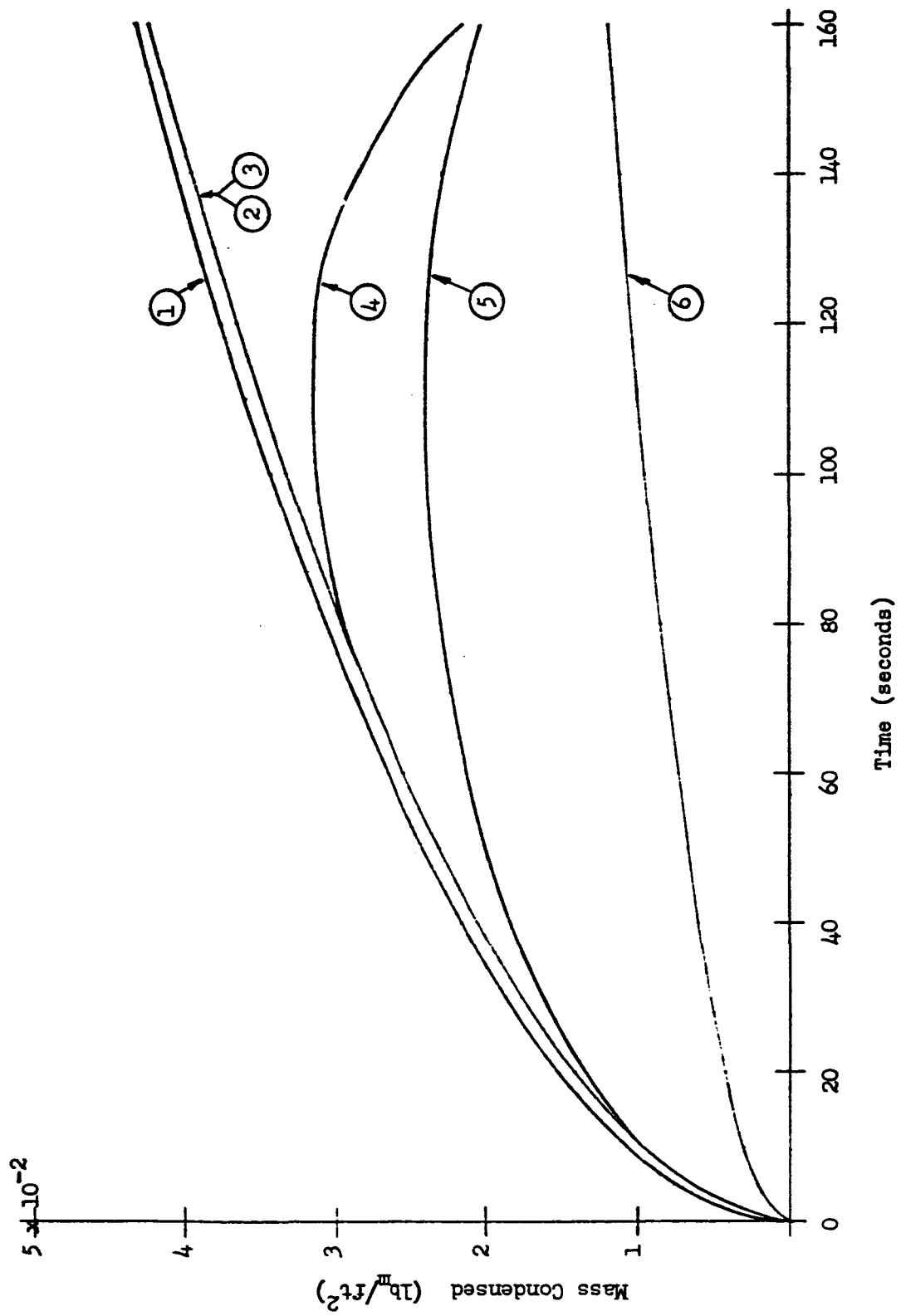


Figure 3 Mass Transfer Curves - Oxygen System

References

1. Thomas, P. D., and Morse, F. H., "Analytic Solution for the Phase Change in a Suddenly Pressurized Liquid - Vapor System," Advances in Cryogenic Engineering, Vol. 8, K. D. Timmerhaus (ed.), Plenum Press, Inc., New York (1963), pp. 550-562.
2. Knuth, E. L., "Evaporations and Condensations in One-Component Systems," ARS Journal, Vol. 32, 1962, pp. 1424-1426.
3. Yang, W. J., and Clark, J. A., "On the Application of the Source Theory to the Solution of Problems Involving Phase Change - Part 2," ASME Paper No. 63 - WA-116, presented at the ASME Winter Annual Meeting, Philadelphia, Pa. Nov. 17-22, 1963.
4. Yang, W. J., Larsen, P. S., and Clark, J. A., "Interfacial Heat and Mass Transfer in a Suddenly Pressurized, Binary Liquid - Vapor System," Paper to be presented at the 1964 ASME Winter Annual Meeting, New York, Nov. 29 - Dec. 4, 1964.

**DIMENSIONLESS MASS TRANSFER ALIGNMENT CHART
FOR SUDDENLY PRESSURIZED LIQUID-VAPOR SYSTEMS**

by

**John R. O'Loughlin*
The Boeing Company
New Orleans, Louisiana**

*** Associate Professor of Mechanical Engineering, Tulane University, New Orleans, Louisiana; consultant to The Boeing Company .**

DIMENSIONLESS MASS TRANSFER ALIGNMENT CHART
FOR SUDDENLY PRESSURIZED LIQUID-VAPOR SYSTEMS

John R. O'Loughlin *

Launch Systems Branch,
The Boeing Company,
New Orleans, La.

Abstract

An exact, closed form solution is available for the problem of interfacial mass transfer after the sudden pressurization of a saturated liquid-vapor system. Use of this solution, however, requires numerical work to find the root of a transcendental equation. In the present paper, this solution has been written in terms of dimensionless groups and displayed in the form of an alignment chart thereby eliminating the numerical work. This chart is valid for a wide range of fluids and pressurization conditions.

Introduction

A considerable amount of study has been devoted to the problem of mass transfer at the interface of a liquid-vapor system undergoing pressurization. Knowledge of such mass transfer is important in many applications particularly the pressurization of a cryogenic tank.

For a single component system, the work of Thomas and Morse (1) provides an exact solution to the following problem.

* Consultant, Propulsion/Mechanical Research; also Associate Professor of Mechanical Engineering, Tulane University.

- 1) Both liquid and vapor are initially saturated at a temperature T_1 .
- 2) Flow perpendicular to the interface is considered in the vapor but not in the liquid.
- 3) Both liquid and vapor are considered to be infinite in extent perpendicular to the interface.
- 4) At time zero, the ullage temperature is increased to T_3 and the ullage pressure to P_2 . Because of this pressure change, the interfacial temperature changes to T_2 which is the saturation temperature corresponding to P_2 .

The solution to the above problem, from the standpoint of interfacial mass transfer, requires finding the real root of the following equation as presented by Thomas and Morse.

$$\frac{k_v (T_2 - T_3)}{\sqrt{\alpha_v}} \frac{\exp\left\{\frac{\alpha_v}{P_v} \left(\frac{P_2}{P_v} Z\right)^2\right\}}{\operatorname{erfc}\left(\frac{P_2}{P_v} \sqrt{\frac{\alpha_v}{P_v}} Z\right)} + \frac{k_L (T_2 - T_1)}{\sqrt{\alpha_L}} \frac{\exp(-Z^2)}{(1 + \operatorname{erf} Z)} = \sqrt{\pi \alpha_L} \rho_L h Z \quad (1)$$

Since this is a transcendental equation, the real root must be found numerically. This can be done easily with the aid of an electronic computer. The disadvantage of this procedure is that the program must be run for each set of operating conditions and for each new fluid studied. To avoid this difficulty, Thomas and Morse also presented an approximate solution to this problem by an integral method. However, the accuracy of this approximate method decreases as the rate of mass transfer increases. It is exact only for zero mass transfer.

Technique

Both the necessity of using a computer program to find the real root of equation (1) for each new problem and the inaccuracy of the approximate integral method for large mass transfer rates can be avoided by use of an alignment chart. Equation (1) is first written in dimensionless form by dividing through by its right hand side.

$$\frac{C_1 \exp[-(C_3 z)^2]}{z \operatorname{erfc}(C_3 z)} + \frac{C_2 \exp(-z^2)}{z (1 + \operatorname{erf} z)} = 1 \quad (2)$$

where

$$C_1 = \frac{k_v (T_2 - T_3)}{\sqrt{\pi} \alpha_L \alpha_v \rho_L h} = \sqrt{\frac{\rho_v k_v C_{P_v} C_{P_L}}{\pi \rho_L k_L}} \frac{(T_2 - T_3)}{h} \quad (3)$$

$$C_2 = \frac{k_L (T_2 - T_1)}{\sqrt{\pi} \alpha_L \rho_L h} = \frac{C_{P_L} (T_2 - T_1)}{\sqrt{\pi} h} \quad (4)$$

$$C_3 = \frac{\rho_L \sqrt{\alpha_L}}{\rho_v \sqrt{\alpha_v}} = \sqrt{\frac{\rho_L k_L C_{P_L}}{\rho_v k_v C_{P_v}}} \quad (5)$$

From equation (2), it is apparent that the three dimensionless groups C_1 , C_2 and C_3 determine the value of z . The rate of mass transfer and the mass transferred until any time t are easily found once the value of z is known.

$$\dot{m} = - \rho_L \sqrt{\frac{\alpha_L}{t}} z \quad (6)$$

$$m = - 2 \rho_L \sqrt{\alpha_L t} z \quad (7)$$

Since a set of values for C_1 , C_2 and C_3 determines z , an alignment chart from which z could be read quickly for given C_1 , C_2 and C_3 would be of value. A technique for preparing such a chart is available in reference (2) for equations of the form

$$U(C_1) \cdot F_1(C_3, z) + V(C_2) F_2(z) = 1 \quad (8)$$

Equation (2) is of this form where

$$U(C_1) = C_1 \quad (9)$$

$$F_1(C_3, z) = \frac{\exp[-(C_3 z)^2]}{2 \operatorname{erfc}(C_3 z)} \quad (10)$$

$$V(C_2) = C_2 \quad (11)$$

$$F_2(z) = \frac{\exp(-z^2)}{z(1 + \operatorname{erf} z)} \quad (12)$$

Preparation of the chart requires prior calculation of the following quantities which provide the chart coordinates.

$$x = \frac{F_2(z)}{F_1(c_3, z) + F_2(z)} \quad (13)$$

$$y = \frac{1}{F_1(c_3, z) + F_2(z)} \quad (14)$$

For the present case, these coordinates take the form

$$x = \frac{\operatorname{erfc}(c_3, z)}{[\exp z^2(1 - c_3^2)][1 + \operatorname{erf} z] + \operatorname{erfc}(c_3, z)} \quad (15)$$

$$y = \frac{z [\operatorname{erfc}(c_3, z)] [1 + \operatorname{erf} z]}{\{\exp [-(c_3, z)^2]\} \{1 + \operatorname{erf} z\} + [\exp(-z^2)] [\operatorname{erfc}(c_3, z)]} \quad (16)$$

Equations (15) and (16) provide a set of (x,y) coordinates for given values of c_3 and z thereby locating a single point on the chart. A straightforward computer program was written to perform the calculations indicated by equations (15) and (16). Output of this program provided coordinates (x,y) from which the alignment chart, Figure 2, was prepared. The x and y axes are used for construction purposes and are shown on Figure 1. The y axis converts

to the C_1 and C_2 axes of the completed chart shown as Figure 2. The x axis is only used for construction and therefore is not shown on Figure 2.

An examination of the magnitudes of C_1 , C_2 and C_3 for cryogenics and various other fluids indicates that the following ranges should cover most problems of interest.

$$0 \leq C_1 \leq 10$$

$$0 \leq C_2 \leq 1.0$$

$$0 \leq C_3 \leq 200$$

Such a wide range for the variables C_1 and C_2 would normally require a large compression of those scales thereby causing a compression of the chart and loss of accuracy. This problem has been avoided by placing horizontal scales at right angles to the C_1 and C_2 scales. These horizontal scales are to be used for large values of C_1 and C_2 .

Use of the Chart

To calculate the mass transfer for a system as described in the Introduction, the following steps are required.

- 1) Calculate C_1 , C_2 and C_3 for the particular problem. It is suggested that the properties involved in these parameters be evaluated at an average temperature. That is, vapor properties at $(T_1 + T_3)/2$ and liquid properties at $(T_1 + T_2)/2$. It is reasonable to evaluate the heat of vaporization, h , at temperature T_2 .

- 2) If C_1 and C_2 are small enough to fall on the vertical C_1 and C_2 scales of Figure 2, these two points are connected by a straight line. At the point where this line intersects the value of C_3 from step (1), read z from the lines of constant z . Interpolation is frequently necessary on all scales. Once z is found, \dot{m} and m are calculated directly from equations (6) and (7) for any time.
- 3) Should C_1 or C_2 or both be large so as not to fall on the vertical scales of Figure 2, the chart can still be used to find z . Examination of Figure 1 indicates how this can be done through use of the horizontal scales drawn perpendicular to the C_1 and C_2 axes. Using similar triangles and Figure 1,

$$\frac{-C_1 + .06}{s} = \frac{-C_1 - .06}{r} \quad (17)$$

$$\frac{C_2 + .06}{1-r} = \frac{C_2 - .06}{1-s} \quad (18)$$

Solving these two equations for r and s yields

$$r = \frac{C_1 + .06}{C_1 - C_2} \quad (19)$$

$$s = \frac{C_1 - .06}{C_1 - C_2} \quad (20)$$

Now when C_1 or C_2 or both are beyond the vertical scales of Figure 2, those values can be used in equations (19) and (20) to calculate r and s . These two points are then connected by a straight line on Figure 2. At the point where this line intersects the value of C_3 of interest, z is read.

The conditions for zero mass transfer are found in reference (1) by setting $z = 0$ in equation (1). The result is

$$T_3 = T_2 + (T_2 - T_1) \frac{k_L}{k_v} \sqrt{\frac{\alpha_v}{\alpha_L}} \quad (21)$$

In terms of the parameters defined by equations (3) and (4), this equation can be written

$$C_1 = -C_2 \quad (22)$$

Thus, for the condition of zero mass transfer, there is a relation between C_1 and C_2 which does not involve C_3 . This is evident from Figure 2 also. That figure illustrates that for all C_3 , the lines of constant C_3 intersect at a single point for $z = 0$. This point is $x = 0.5$, $y = 0$ in Figure 1. Any straight line passed through this point on Figure 2 intersects a value of C_1 and C_2 (or r and s which can be converted to C_1 and C_2 by use of equations (17) and (18)) which satisfies equation (22).

Example Problem

Assume that one has calculated the parameters C_1 , C_2 and C_3 for a specific problem and that these values are -0.10, 0.04 and 75 respectively. Such values might be encountered with the oxygen system. The value of C_2 is on

the vertical scale of Figure 2. However, the value of C_1 is less than -0.06 and therefore equation (19) must be used. It yields $r = 0.286$. A straight line is now drawn through $C_2 = 0.04$ and $r = 0.286$. One must interpolate a $C_3 = 75$ line. This C_3 line and the previously drawn straight line intersect at a point. Interpolation with a graduated scale between the constant z lines on the large original of Figure 2 indicates that this point lies at $z = -0.00727$. This result could now be used in equations (6) and (7) to yield the mass transfer. The fact that z is negative is indicative of evaporation. A $z > 0$ means condensation.

As a check, substitute the above values of C_1 , C_2 , C_3 and z into the left hand side of equation (2). The result to slide rule accuracy is $6.55 - 5.55 = 1.00$ which checks the right hand side of that equation. This indicates that the z read from the chart is truly the root of equation (2) for the given C_1 , C_2 and C_3 .

Large Copies of Figure 2 Available

Large copies of the original of Figure 2 are available from the author.

Nomenclature

C_1, C_2 and C_3	defined by equations 3, 4 and 5
c_p	specific heat at constant pressure
h	heat of vaporization
k	thermal conductivity
\dot{m}	rate of interfacial mass transfer per unit area (mass/time-area)
m	interfacial mass transfer per unit area between $t = 0$ and any later time t (mass/area)
P_2	ullage pressure after pressurization

r, s	horizontal scales of alignment chart
t	time
T_1	initial saturation temperature of liquid and vapor
T_2	saturation temperature corresponding to P_2
T_3	ullage temperature after pressurization
x, y	coordinates used in construction of alignment chart
z	mass transfer parameter; $z > 0$ indicates condensation, $z < 0$ indicates evaporation
α	thermal diffusivity ($k/\rho c_p$)
ρ	density
$\text{erf } z = \frac{2}{\sqrt{\pi}} \int_0^z e^{-t^2} dt$	
$\text{erfc } z = 1 - \text{erf } z$	

Subscripts

L	liquid
V	vapor

References

1. Thomas, P. D., and Morse, F. H., "Analytic Solution for the Phase Change in a Suddenly Pressurized Liquid-Vapor System", Advances in Cryogenic Engineering, Vol. 8, K. D. Timmerhaus (ed.), Plenum Press, Inc., New York (1963), pp. 550-562.
2. Franklin, Phillip, "Graphical Representation of Functions," in Marks' Mechanical Engineers' Handbook, 6th ed., Theodore Baumeister (ed.), McGraw Hill Book Co., New York, (1958), pp. 2-85 to 2-91.

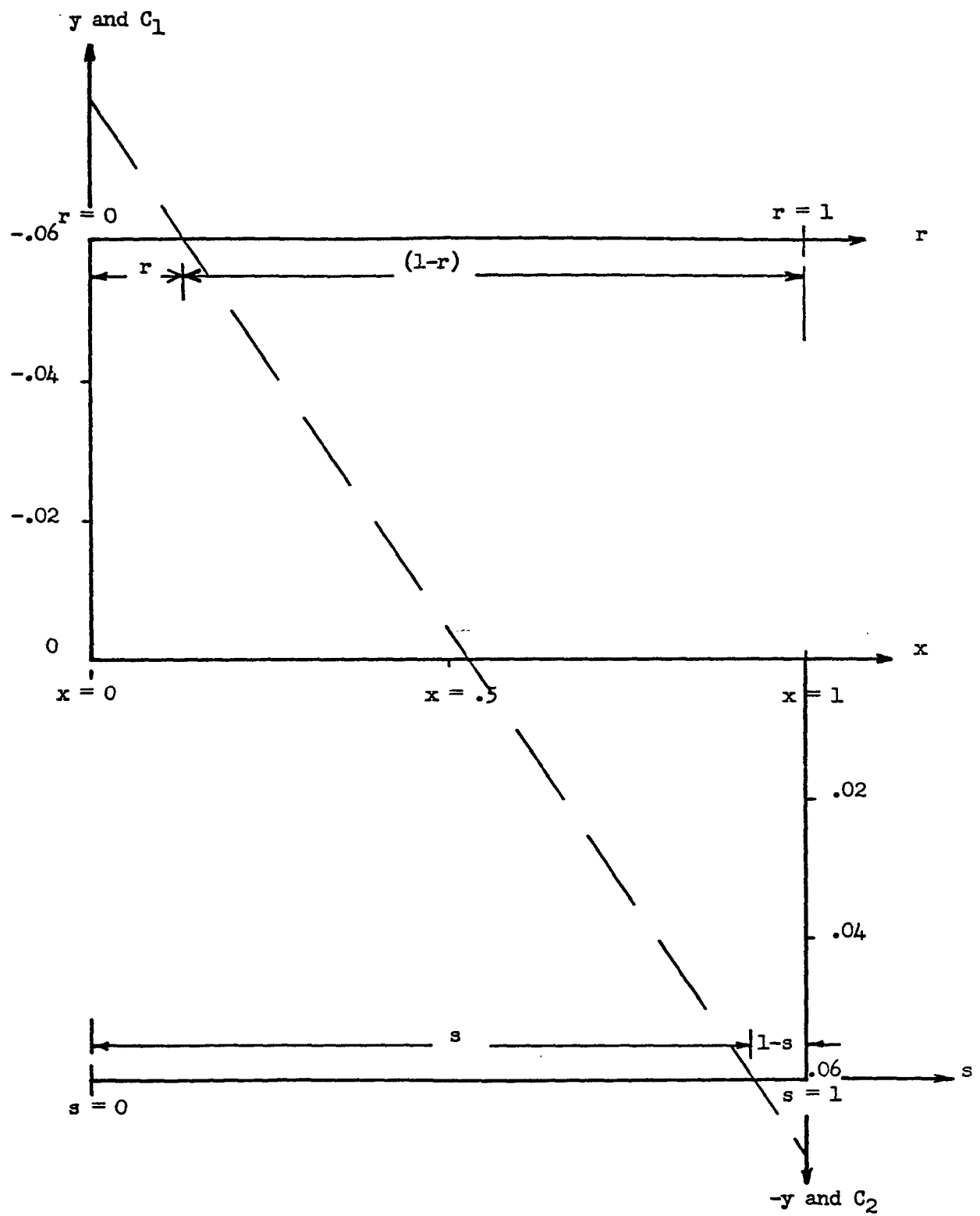


Figure 1 Construction of Alignment Chart

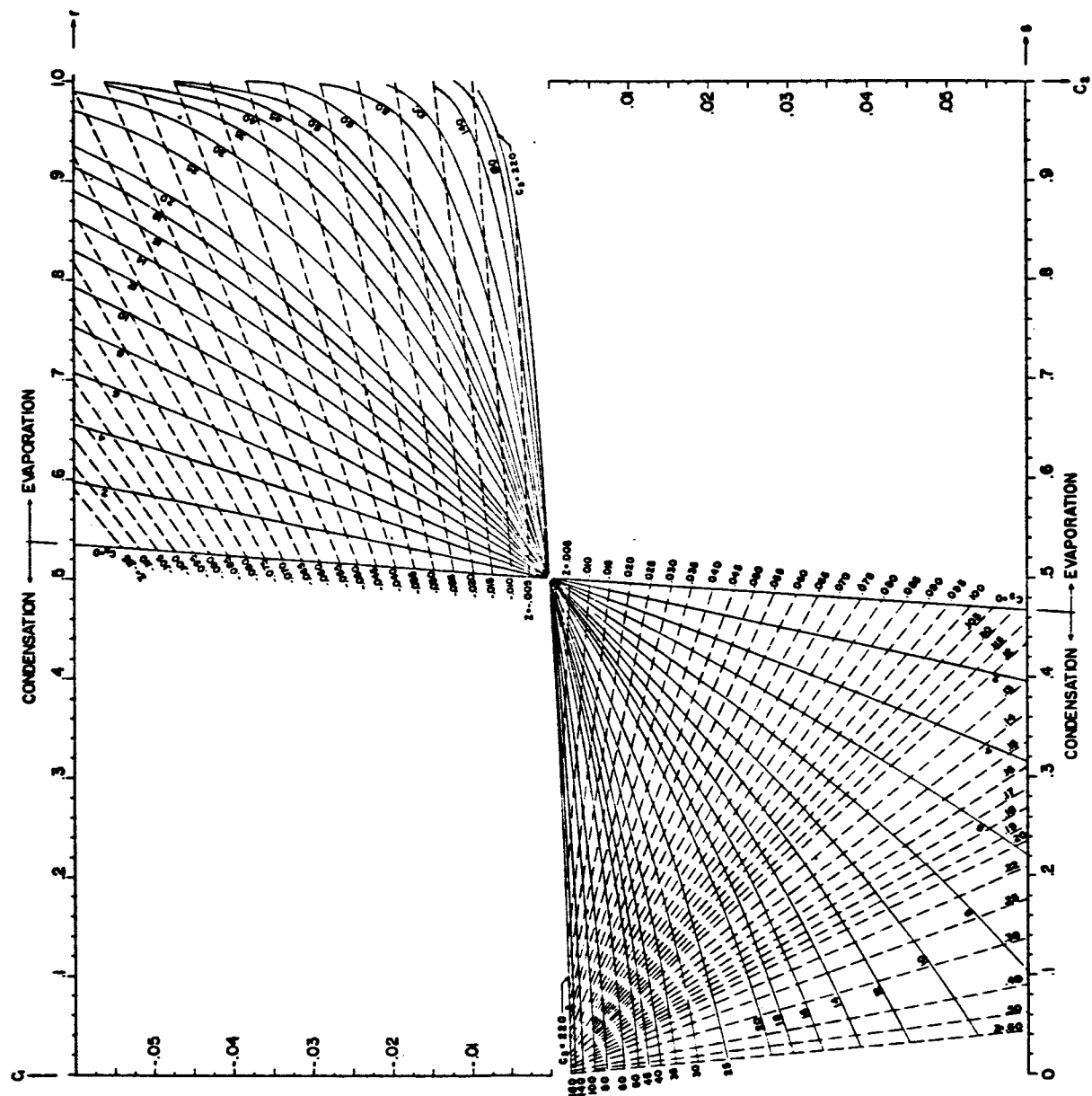


FIGURE 2 ALIGNMENT CHART

THERMAL ANALYSES AND DESIGN OF LIQUID
HYDROGEN TANK FLUID LINE FITTINGS

by

Joseph M. Fowler
The Boeing Company
Seattle, Washington

ABSTRACT

In this paper, the thermal analysis and design of liquid hydrogen tank fluid line fittings is discussed. The importance of including the radiation mode of heat transfer in the thermal analysis of fittings is emphasized. Some experimental data are included for comparison. The various parameters covered in the analysis are external boundary temperature, fitting penetration tube materials, overall fitting length, fitting configuration, and surface reflectance characteristics.

ACKNOWLEDGEMENTS

Boeing personnel who have contributed with many helpful discussions, editorial comments, and encouragements during the course of this study and preparation of the paper are D. K. Zimmerman, C. J. Hocevar, A. M. Scroggs, J. W. Straayer, D. H. Bartlett, D. L. Barclay, and C. V. Lindow.

Patrick J. Daly of the Boeing Math Services organization deserves special mention for handling all of the computer programming necessary to accomplish the analytical results.

CONTENTS

	<u>Page</u>
NOMENCLATURE	v
INTRODUCTION	1
FITTING CONFIGURATIONS AND STRUCTURAL DESIGN	1
THERMAL ANALYSIS METHODS	2
TEMPERATURE DISTRIBUTION AND HEAT FLOW RESULTS	6
CONCLUDING REMARKS	8
REFERENCES	10
ILLUSTRATIONS	11-27

NOMENCLATURE

A = area

K = apparent thermal conductivity

C.F. = compression factor, a constant that depends on the degree of compression of the multilayer insulation

F_{mn} = radiation shape factor between nodes m and n

\mathcal{F}_{mn} = gray body diffuse radiation factor between nodes m and n

σ = Stefan-Boltzmann constant

D = a determinant

ϵ = emittance

ρ = reflectance

T = absolute temperature

Q = heat flow rate

q = heat flow rate per unit area

INTRODUCTION

Fluid lines that penetrate the insulation of a liquid hydrogen propellant tank are media for undesired heat transfer to the propellant. The localized thermal energy introduced through line fittings of tanks can significantly influence propellant stratification patterns and tank pressurization requirements of high-performance space-storage systems. The published literature on the subject of cryogenic propellant storage has contained little information on the thermal design of tank fittings. In general, as was done in Reference 1, parametric studies of liquid hydrogen storage for space missions have considered heat flow through the tank fittings to be some assumed fixed percentage of the heat flow through the tank insulation.

Most reported detailed design studies of storage tanks have concentrated on minimizing the thermal conductance of fittings by reducing the solid conduction mode of heat transfer. However, heat transfer through some fitting configurations will not necessarily be minimized by this method.

It is the purpose of this paper to present results that show that infrared radiation within an evacuated fitting cavity can contribute a major portion of the total heat transfer through the fitting. As a result, surface reflective properties within the fitting and cavity geometry become important parameters in the thermal design of cryogenic tank fittings.

FITTING CONFIGURATIONS AND STRUCTURAL DESIGN

The tank fitting configurations considered in the thermal trade studies for this paper are presented in Figures 1 and 2. These fittings are configured for an RL-10 engine liquid hydrogen feed line and are designed for use with submerged, but externally removable, valves. Insulation consisting of alternate layers of glass fiber paper and aluminum foil is wrapped concentrically around the neck of each fitting. The penetration line materials assumed for purposes of making thermal trade studies are glass-reinforced epoxy with teflon liner, 6Al-4V titanium, and 304 stainless steel. These materials are chosen for their low conductance and high strength properties at cryogenic temperatures.

Two concentric tube penetrations for Configuration 1 are required so that a tool can be inserted to remove the valve from the tank without disturbing the vacuum conditions in the tank and neck insulations. In Configuration 2, the single fluid tube of 6.0-inch diameter is large enough for the tooling operation necessary to install or remove the valve. Presented in Table I are the tube wall thicknesses for each of the fittings based on strength requirements. The wall thicknesses for the outer 6.0-inch-diameter tube of Configuration 1 are designed by minimum gage* material requirements. The strength requirements for the fluid carrying lines of Configurations 1 and 2 are based on the following:

* Minimum gage values for thermal studies include the positive fabrication tolerance.

Internal pressure = 75 nominal + 100 surge = 175 psi

Ultimate factor of safety = 4.0

Yield factor of safety = 1.65

Proof to 1.5 times design pressure

Table I

FITTING STRUCTURAL REQUIREMENTS

	Length, L (in.)	Tube Wall Thickness					
		Fiberglass		Stainless Steel		Titanium	
		2.5- in. Dia.	6- in. Dia.	2.5- in. Dia.	6- in. Dia.	2.5- in. Dia.	6- in. Dia.
Configuration 1	8	0.040	0.033	0.010	0.010	0.010	0.010
	12	0.040	0.033	0.010	0.010	0.011	0.010
	16	0.040	0.033	0.012	0.010	0.013	0.010
Configuration 2	12	6-in. Dia.		6-in. Dia.		6-in. Dia.	
	16	0.075		0.014		0.0145	
	20						

The fiberglass tubes are strain critical, based on a limit of 0.233 percent allowed for the teflon liner. The 2.5-inch-diameter stainless steel and titanium tubes for Configuration 1 are designed by minimum gage requirements for the 8-inch length, but wall thicknesses increase with fitting length due to bending loads induced from assumed installation bolt torquing requirements. The stainless steel and titanium tube wall thicknesses for Configuration 2 are designed by ultimate pressure.

A third fitting shown in Figure 3 has been analyzed. This fitting, Configuration 3, was built and tested at Boeing to demonstrate the feasibility of a submerged-valve-type, low-conductance, fiberglass fitting. The wall thicknesses for Configuration 3 are shown in Figure 3 and are based on experimental thermal test requirements instead of the design conditions discussed above for Configurations 1 and 2. The fiberglass penetration tube of Configuration 3 is shown in Figure 4, along with a noncoated tube.

THERMAL ANALYSIS METHODS

Thermal models for Configurations 1 to 3 are presented in Figures 5 through 7, respectively. In the thermal models, the node points and thermal resistors between nodes are schematically described. Radiation and solid conduction are considered. Since the fittings are designed for use with submerged valves, vacuum conditions are assumed to exist within all cavities downstream of the

valves to achieve low heat-flow rates. A hard vacuum within the cavity is the proposed condition of operation in the space environment. For the ground hold condition, it may be expedient to purge the cavities with helium gas. This would greatly increase fitting heat-flow rate until the line is purged to the vacuum environment in space. Jakob, in Reference 2, presents an empirical correlation of data that can be used to estimate the convective heat-transfer rates in gaseous-filled enclosures.

It is assumed that the only heat flow through the insulated fitting necks of Configurations 1 and 2 is in a direction normal to the layers of insulation. The apparent thermal conductivity in the normal direction through the multilayer insulation is expressed by Equation (1) which was taken from Reference 1 and modified by including a compression factor (C. F.) on the conduction term.

$$K = 4.82 \times 10^{-6} + 1.5 \times 10^{-8} (\text{C.F.}) (T_o + T_i) + 5.46 \times 10^{-14} (T_o + T_i) (T_o^2 + T_i^2), \frac{\text{Btu}}{\text{ft hr } ^\circ\text{R}} \quad (1)$$

By using insulation on the necks of Configurations 1 and 2, such as aluminized mylar or aluminum foil carefully spliced with glass fiber paper, the longitudinal conduction can be kept to a minimum, and the physical model assumed will be closely approximated.

The insulation wrap about the fitting neck of Configuration 3 consisted of layers of 0.25-mil foil and glass paper. Therefore, a three-dimensional analysis of heat transfer within the multilayer insulation was considered for Configuration 3 by including in the thermal model a node pattern to account for conduction along the aluminum foil as well as normal to them.

Both conduction along the tube walls and radiation exchange throughout the evacuated cavities are accounted for in the analysis. Solid conduction between physically connected nodes was determined using the Fourier conduction equation and evaluating the thermal conductivity of the material at the mean temperature of the two nodes. The thermal conductivity versus temperature data used for the fitting materials in this analysis are presented in Figure 8. The values for aluminum, stainless steel, titanium, and fiberglass are taken from Reference 3, and the glass fibers data are those of Reference 4. Radiative heat exchange between the surface nodes within the cavities of the fittings is determined by using Hottel's method (Reference 5) for diffuse gray body radiation within an enclosure. In this case, the heat transferred by radiation between two nodes within an enclosure can be expressed as:

$$Q_{m-n} = A_m \mathcal{F}_{mn} (T_m^4 - T_n^4) \quad (2)$$

where

$$A_m \mathcal{F}_{mn} = \frac{\epsilon_n A_n}{(1 - \epsilon_n)} \frac{m D_n}{D} \quad (3)$$

$$\text{and } D = \begin{vmatrix} A_1 F_{11} - \frac{A_1}{\rho_1} & A_2 F_{21} & A_3 F_{31} & \dots & A_n F_{n1} \\ A_1 F_{12} & A_2 F_{22} - \frac{A_2}{\rho_2} & A_3 F_{32} & \dots & A_n F_{n2} \\ A_1 F_{13} & A_2 F_{23} & A_3 F_{33} - \frac{A_3}{\rho_3} & \dots & A_n F_{n3} \\ \vdots & \vdots & \vdots & \ddots & \vdots \\ A_1 F_{1n} & A_2 F_{2n} & A_3 F_{3n} & \dots & A_n F_{nn} - \frac{A_n}{\rho_n} \end{vmatrix}$$

${}_m D_n$ is formed by replacing the n th column of D by:

$$\begin{aligned} & - A_m F_{m1} \epsilon_m \\ & - A_m F_{m2} \epsilon_m \\ & - A_m F_{m3} \epsilon_m \\ & \vdots \\ & - A_m F_{mn} \epsilon_m \end{aligned}$$

The reflectance and emittance values for the fitting materials are listed in Table II. Since reflectance of a surface depends on a number of variables, e.g., direction, surface roughness, opaqueness, and incident energy wavelengths, the values listed in Table II are intended only to be representative of the materials used for the conditions of this analysis and not exact values. All surfaces are assumed to be opaque. The wavelengths of radiation to be considered fall in the infrared region of the spectrum since the highest temperature to be dealt with is 600°R.

Table II
MATERIAL SURFACE PROPERTIES

<u>Material</u>	<u>Reflectance</u>	<u>Emittance</u>
Fiberglass	0.10	0.90
Stainless Steel	0.60	0.40
Titanium	0.75	0.25
Aluminum	0.90 - 0.95	0.10 - 0.05

The valve cavity is represented in Thermal Models 1 and 2 by an effective emittance of $\epsilon_{\text{eff}} = 0.45$ for 2.5- and 4-inch-diameter disks, respectively. The value of effective emittance is determined by first solving Equation (3) to obtain the radiant interchange factors of a five-node model of the valve cavity and substituting them into Equation (4) below.

$$\epsilon_{\text{eff of opening}} = \frac{A_m \mathcal{F}_{m-o}}{\sigma} \quad (4)$$

At the opposite end of the fitting cavity, a similar representation of effective emittance for the downstream fluid line is made. By assuming that the fluid line extends beyond the fitting boundary for $L/D \geq 4.0$, the effective emittance of the opening will be independent of length and equal to $\epsilon_{\text{eff}} = 0.40$, as can be found in Reference 7. It should be pointed out that Equation (4) is valid only for an isothermal cavity. The entire valve cavity, which is assumed to be aluminum, is certain to be very nearly at the temperature of liquid hydrogen throughout. The downstream aluminum fluid line is, by assumption, isothermal with a temperature the same as the fixed external boundary temperature.

Solutions for the temperature distribution and the resulting heat flow through the fittings are determined using the Boeing Engineering Thermal Analyzer computer program. By iterative technique, the program solves the conduction and radiation equations for the nodal networks described in Figures 5, 6, and 7 until steady-state temperature conditions are attained. A separate program has been written to obtain rapid solutions of Equation (3). This solution is based on a matrix inversion routine programmed for the IBM 7094 computer. A typical 17-node enclosure requires 0.12 minute of computer time to obtain the resulting 256 "A \mathcal{F} " terms

In this analysis, diffuse emitting and reflecting surfaces are considered. It is recognized that diffuse scattering is more representative of materials such as fiberglass than it is for the high-reflectance, smooth-metal surfaces that generally exhibit specular characteristics. Since surfaces of all materials fall somewhere within the diffuse and specular range, it should be noted that the results in this paper represent the limiting case of purely diffuse surfaces. A general method of analysis for specularly reflecting surfaces had not yet been developed. Special geometric cases have been solved, including specular surfaces. These are reported in References 9, 10, and 11. However, the image analysis technique employed for obtaining solutions in References 9 through 11 would require a prohibitively large number of nodes for the geometry of the configurations studied herein.

The degree of error resulting from neglect of specular reflectance is believed to be small. There are a number of reasons for this argument. The first is that the sample problems presented in References 9 and 11 show that a variation in heat transfer, usually less than 10 percent, is the result of including specular properties in an otherwise all-diffuse analysis. A second reason is that the

specular surfaces have lower emittance values. The results presented in the next section of this paper show that radiation contributes more significantly to the total heat flow through fittings with materials of high rather than low emittance characteristics. Still another reason is that certain highly reflective metals, which might be used as surface coatings, are not entirely specular in the infrared region of the spectrum. As an example, in the investigation reported in Reference 8 it was concluded that polished gold exhibits reflectance characteristics that are more diffuse than specular in the far infrared.

TEMPERATURE DISTRIBUTION AND HEAT-FLOW RESULTS

TEMPERATURE DISTRIBUTIONS

The temperature distribution along a tube wall that penetrates cryogenic tank insulation becomes decidedly nonlinear when radiation, in addition to solid conduction, is considered in the analysis. Results that show this nonlinearity are presented in Figure 9. The multilayer insulation compression factor (C. F.) is 1.0 for obtaining these temperatures. In Figure 9, the difference in temperature between an analysis considering both radiation within the cavity and conduction and an analysis considering only conduction, increases with increasing external boundary temperature. This is the expected result since heat transfer by conduction is primarily dependent on the second power of the temperature difference while radiation is a fourth-power-dependent term.

In Figure 10, the analytically determined temperature distribution is compared with experimental data. These test data were obtained with five copper-constantan thermocouples bonded to the inside of the aluminized fiberglass tube wall of Configuration 3. The penetration was tested in the fitting of a Boeing, insulated, 19-inch-diameter liquid hydrogen tank. Except for one point, good agreement between experimental and theoretical temperature is found.

In Figure 11, the predicted steady-state temperatures for each node of Configuration 3 are presented. These temperatures are based on a C. F. of 50 for the thermal conductivity of insulation, Equation (1), in the direction normal to the layers. This factor is used to account for firm wrapping of the insulation about the fitting neck and atmospheric compression of the tank insulation by the soft outer shell. It can be seen in Figure 11 that, although large temperature gradients exist between layers, very small gradients occur along a layer due to the relative high conductance provided by the aluminum. For glass fiber paper and aluminum foil insulations of this type, it is very important to avoid short circuiting the foils either against the cold tank wall or the warm outer containment shell.

GAS-PURGED FITTING

Free-convection calculations for a helium-gas-filled enclosure, based on the geometry of Configuration 3, show that, at one atmosphere, the gas increases the heat transfer rate through the fitting by 33 Btu/hr. This calculation is for

boundary temperatures of 360 and 36°R and is based on the empirical equations presented in Reference 2, Pages 534 to 538. Tests of Configuration 3 at the above boundary temperatures resulted in an increased rate of heat transfer of 68 Btu/hr through the fitting when filled with helium gas (Reference 5). This difference between the predicted and experimental results can best be explained by the following:

- 1) The empirical data of Reference 2 were obtained for nonconducting walls.
- 2) The Grashof number for the test conditions is of the order of 4×10^8 , whereas the empirical equations are correlated with Grashof numbers ranging only as high as 0.11×10^8 .
- 3) The equations of Reference 2 do not account for radiation within the gas-filled enclosure.

HEAT FLOW THROUGH EVACUATED FITTINGS

Steady-state heat-flow rates for Configurations 1 and 2 are presented in Figures 12 through 14. The effects of external boundary temperature and overall fitting lengths are presented in Figures 12 and 13 for stainless steel and fiberglass tube penetrations in that order. The solid curves in these figures represent predicted heat flow rates considering both conduction and radiation in the analysis; whereas, the dashed curves represent rates considering only conduction throughout the fitting. Again, the deviation between the solid and dashed curves increases with increasing external boundary temperature, as was the case with temperature distributions. The influence of radiation in the analysis is more pronounced for the heat-flow results shown for Configuration 2 (fiberglass) and Configuration 1 (fiberglass; not shown) than for the penetration tube configurations with stainless steel and titanium (not shown).

A comparison of heat flow rates for Configurations 1 and 2 is presented in Figure 14. These data are based on a constant external boundary temperature of 400°R, which, according to detailed studies performed in Reference 12, is a representative liquid hydrogen tank outer shell mean temperature for a shrouded model in a 100-nautical-mile circular equatorial orbit around either the Moon or Earth. The lowest heat flow shown in Figure 14 is attained by using Configuration 1 with fiberglass penetration tubes. Both fittings approach a minimum and constant value of heat flow with increasing fitting lengths. The effect on fitting heat flow caused by penetration-tube material changes is more pronounced for fitting Configuration 1 than for Configuration 2. For this reason, Configuration 2 offers the lowest heat-flow rate for fittings longer than 10 inches, as shown in Figure 14, if penetrations of stainless steel are used. With titanium penetration tubes, Configuration 1 has the lowest heat-flow rate for lengths less than 13 inches, and Configuration 2 shows the lowest rate for lengths greater than 13 inches.

A vacuum deposition of aluminum on the walls of the fiberglass tubes reduces the emittance of the wall from 0.9 to of the order of 0.05. The small thickness of aluminum (200 to 1200 angstroms) has a negligible effect on conduction along the

tube. In Figure 15, the effect of wall emittance on heat flow through Configuration 2 is shown. It becomes evident that, as wall emittance approaches zero, heat flow through the fitting approaches the "conduction only" solution. Therefore, no matter what material is used for fitting construction, it is expedient to prepare the surfaces for the lowest emittance values possible.

Local heat-flow rates through Configuration 3 are presented in Figure 16. Since the fiberglass penetration-tube cavity for this fitting has surfaces coated with aluminum, little radiant energy is absorbed at the cold end of the tube. The major heat input for this fitting is by conduction along the stainless steel tube. Also, the results presented in Figure 16 show that penetration causes an increased heat flux through the tank insulation in the vicinity of the neck that decreases with distance away from the fitting. The glass fiber spacers against the tank wall are to prevent shorting out of the aluminum foils wrapped about the neck. The lower thermal resistance of these fiber insulators where the fitting joins the tank allows energy to be channeled out of the foil of the multilayer insulation. The heat-flow rate per unit area through the axisymmetric, two-dimensional tank multilayer insulation nodes is $1.57 \text{ Btu/ft}^2\text{-hr}$; for the one-dimensional set of insulation nodes, the value is $2.4 \text{ Btu/ft}^2\text{-hr}$. Additional nodes for the thermal model are probably necessary in order to determine the overall effect the fitting has on heat flow through the tank insulation. Care should be exercised to use radiation shielding, contact resistance, and low-conductance materials in the design of the insulation surrounding a fitting so that maximum thermal resistance will result for the overall tank insulation system.

CONCLUDING REMARKS

The results of the analysis presented in this paper show that the important parameters in thermal design of cryogenic tank fluid line fittings are both the conductive and radiative modes of heat transfer, fitting materials, surface reflectance, configuration, cavity vacuum condition, and external insulation. Fiberglass is the best material for tube penetrations considered in the investigation for obtaining low heat-flow rates through fittings. Additional reductions in heat flow for fiberglass tubes can be achieved by aluminum deposition and liner improvements. A Boeing development program that subjected fiberglass tubes with various liner materials to cyclic pressure testing at cryogenic temperatures has shown that a strain design allowable of 1.0 percent or slightly greater for H-film* liners on fiberglass tubes gives high reliability. This greater allowable strain will reduce the tube wall thickness required and, as a result, the heat-flow rate for the fiberglass fittings.

The importance of detailed thermal analysis and design for selection of tank fluid line fittings for a space propellant storage tank system is shown in Figure 17. A single Configuration 1 fitting with stainless steel penetration tubes will contribute a heat-flow rate approximately equal to 48 percent of the heat flow through the tank insulation. A tank with 300 square feet of surface area was chosen for illustration

* A Du Pont polyimide.

because in Reference 13 it was pointed out that, for a liquid hydrogen tank of that same surface area, at least three and possibly five fluid line penetrations would be required. With five of the above stainless steel penetration fittings on the tank described in Figure 17, the total penetration heat flow rate would be 240 percent of the insulation heating rate. However, by using Configuration 2 in the 16-inch length with an aluminized fiberglass tube, the total heat flow rate for five such fittings would be reduced to less than 75 percent of the insulation heating rate.

REFERENCES

1. Olivier, J. R. and W. M. McCombs, "Lunar Storage of Small Quantities of Cryogenic Fluids," NASA TR-4-42-2-D, January 21, 1964.
2. Jakob, M., Heat Transfer, Vol. I, John Wiley and Sons, New York, 1949.
3. Boeing Document D-16103-1, Thermophysical Properties of Materials.
4. Technical Documentary Report No. ML-TDR-64-5, Thermophysical Properties of Thermal Insulating Materials, Air Force Materials Laboratory Research and Technology Division, Air Force Systems Command, Wright-Patterson Air Force Base, Ohio, February 1964.
5. McAdams, W., Heat Transmission, 2nd ed., New York, McGraw-Hill Company, Inc., 1942.
6. Bartlett, D. H., The Boeing Company, Personal Communication, July 24, 1964.
7. Sparrow, E. M., U. L. Albers, and E. R. G. Eckert, "Thermal Radiation Characteristics of Cylindrical Enclosures," Trans. ASME, Journal of Heat Transfer, Series C, Vol. 84, 1962, pp. 73-81.
8. Harris, L. and P. Fowler, "Absorptance of Gold in the Far Infrared," Journal of the Optical Society of America, Vol. 51, No. 2, February 1961.
9. Eckert, E. R. G. and E. M. Sparrow, "Radiative Heat Exchange Between Surfaces with Specular Reflection," Int. Journal of Heat and Mass Transfer, Vol. 3, pp. 42-54, 1961.
10. Sparrow, E. M., E. R. G. Eckert, and V. K. Jonsson, "An Enclosure Theory for Radiative Exchange Between Specularly and Diffusely Reflecting Surfaces," ASME Transactions, November 1962.
11. Bobco, R. P., "Radiation Heat Transfer in Semigray Enclosures with Specularly and Diffusely Reflecting Surfaces," ASME Paper No. 63-AHGT-10.
12. Boeing Coordination Sheet 2-5522-2-8, "Propulsion Module Thermal Analysis," J. Gruber to C. P. Martin, December 18, 1964.
13. Swalley, F. E. and C. D. Nevins, "Practical Problems in Design of High Performance Multilayer Insulation System for Cryogenic Stages," Paper No. L-2, Cryogenic Engineering Conference, Philadelphia, Pennsylvania, 1964.

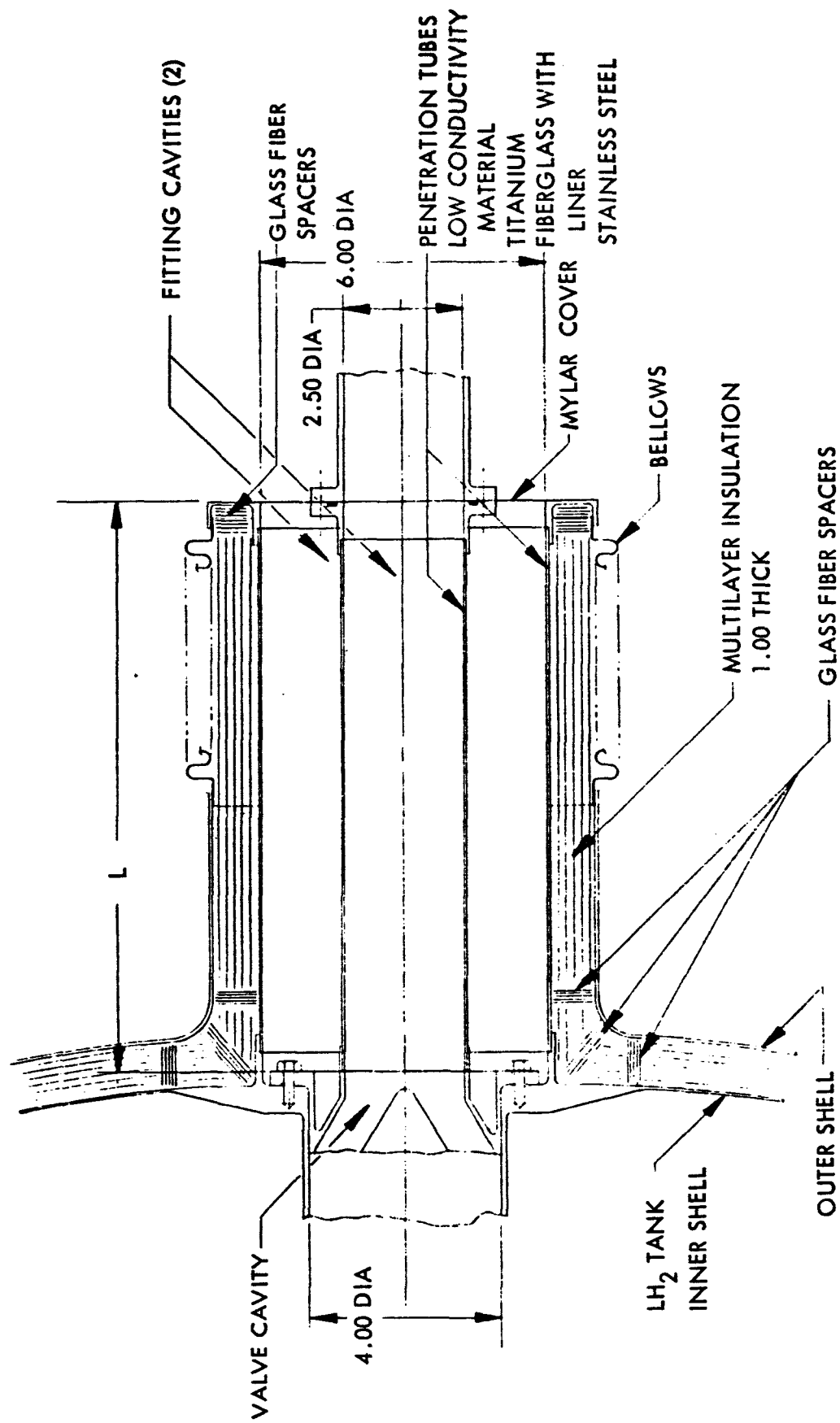


Figure 1: TANK PENETRATION FITTING MODEL, CONFIGURATION NO. 1

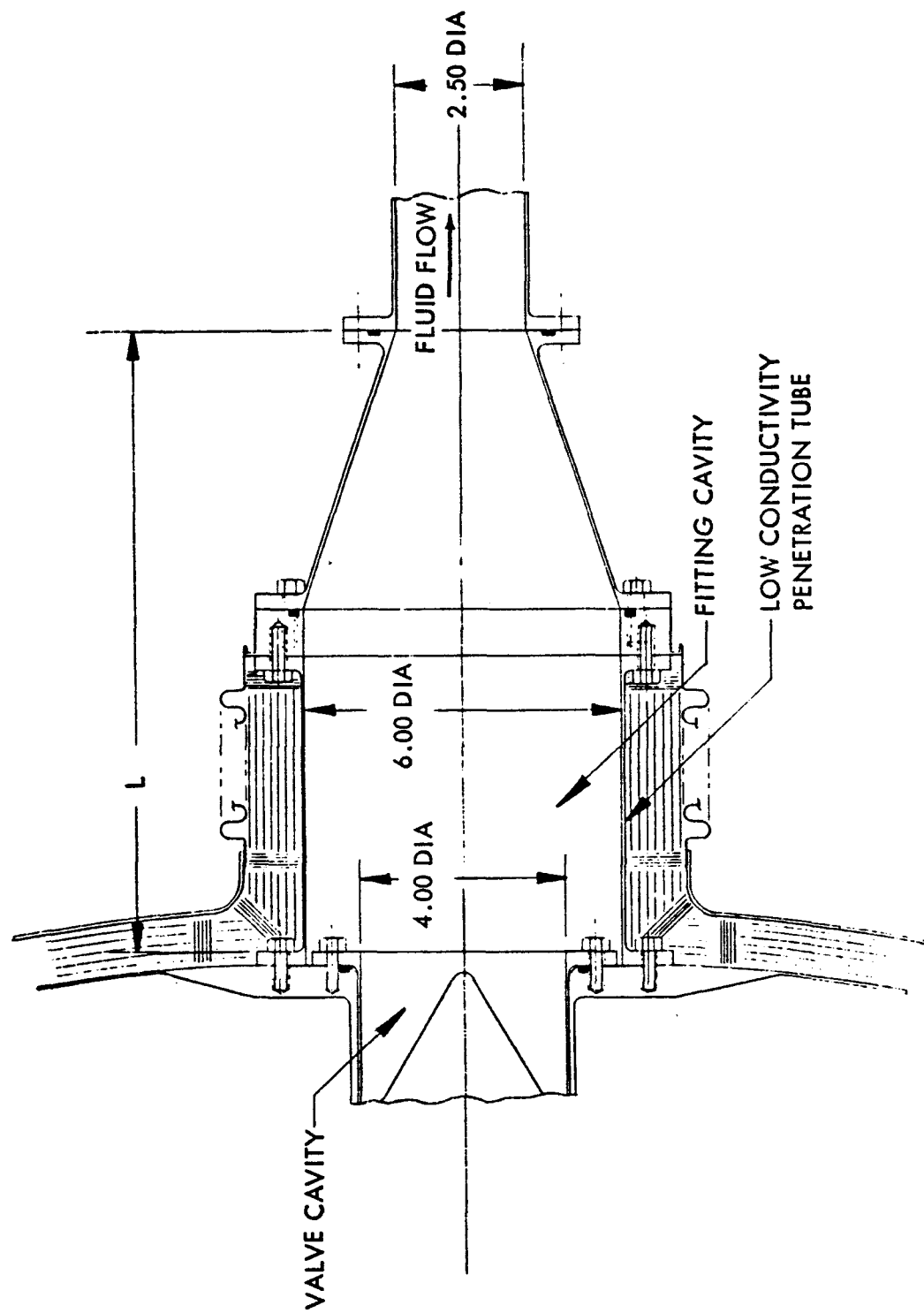


Figure 2: TANK PENETRATION FITTING MODEL, CONFIGURATION NO. 2

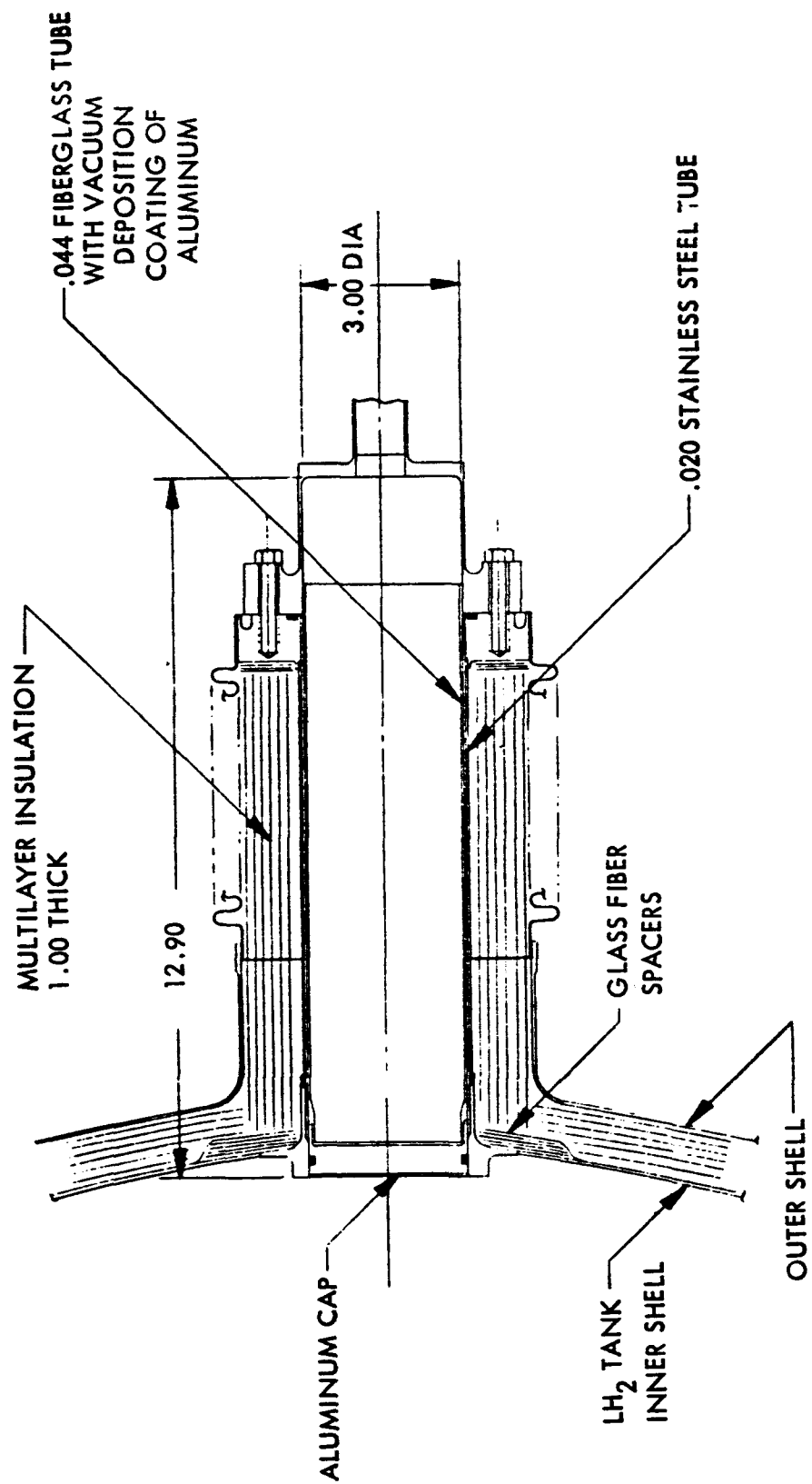


Figure 3: TANK PENETRATION FITTING MODEL, CONFIGURATION NO. 3

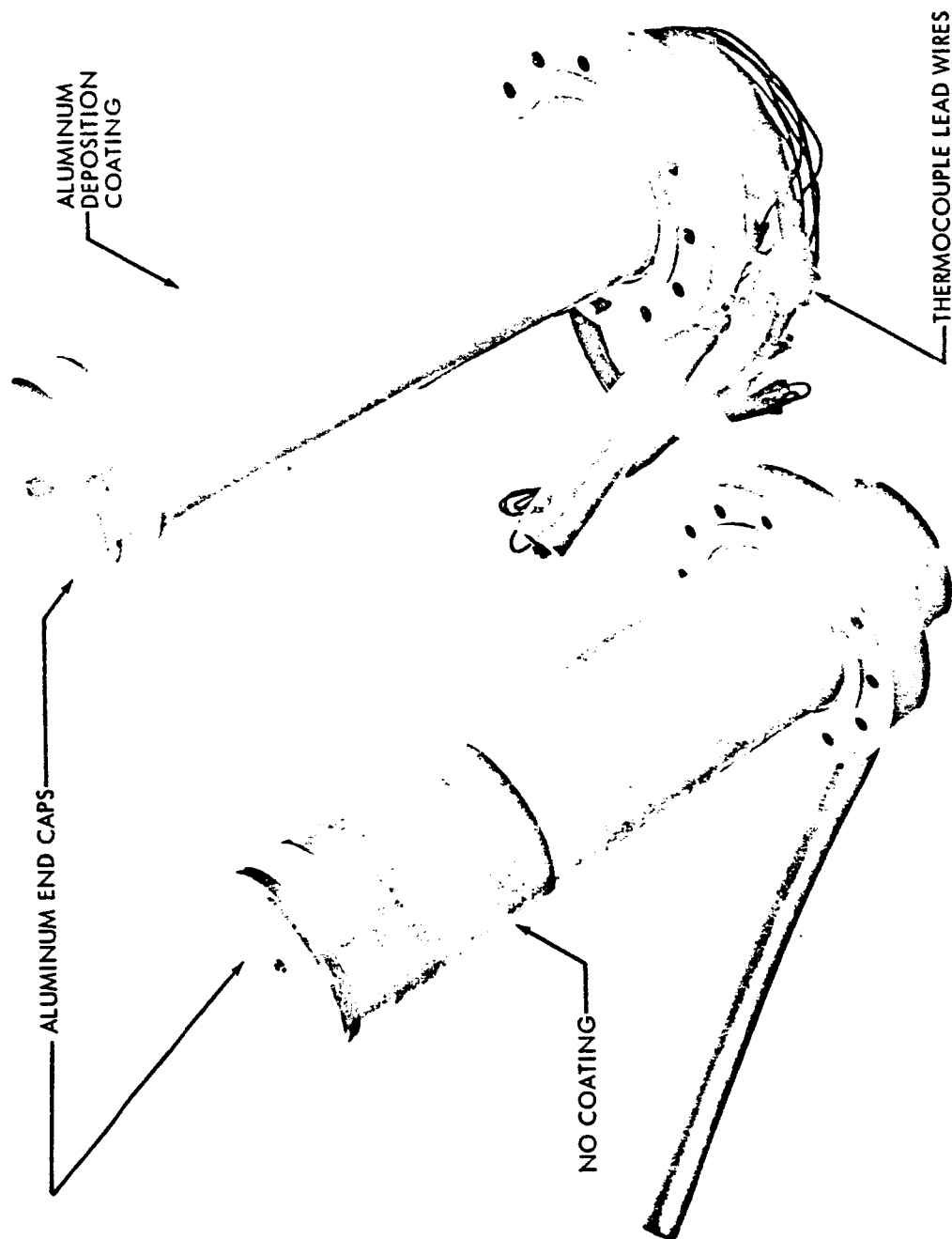


Figure 4: FIBERGLASS PENETRATION TUBES

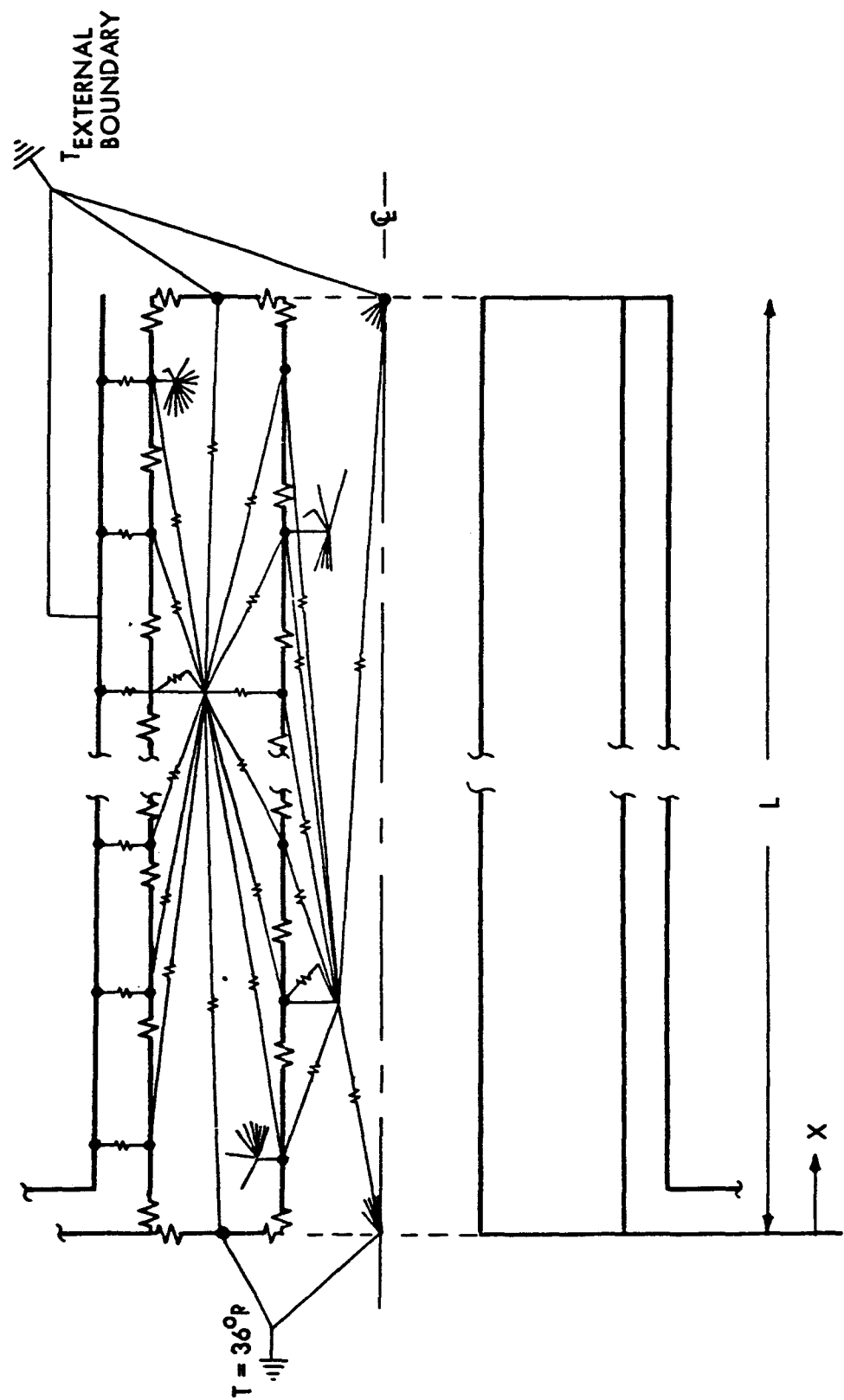


Figure 5: THERMAL MODEL OF CONFIGURATION NO. 1

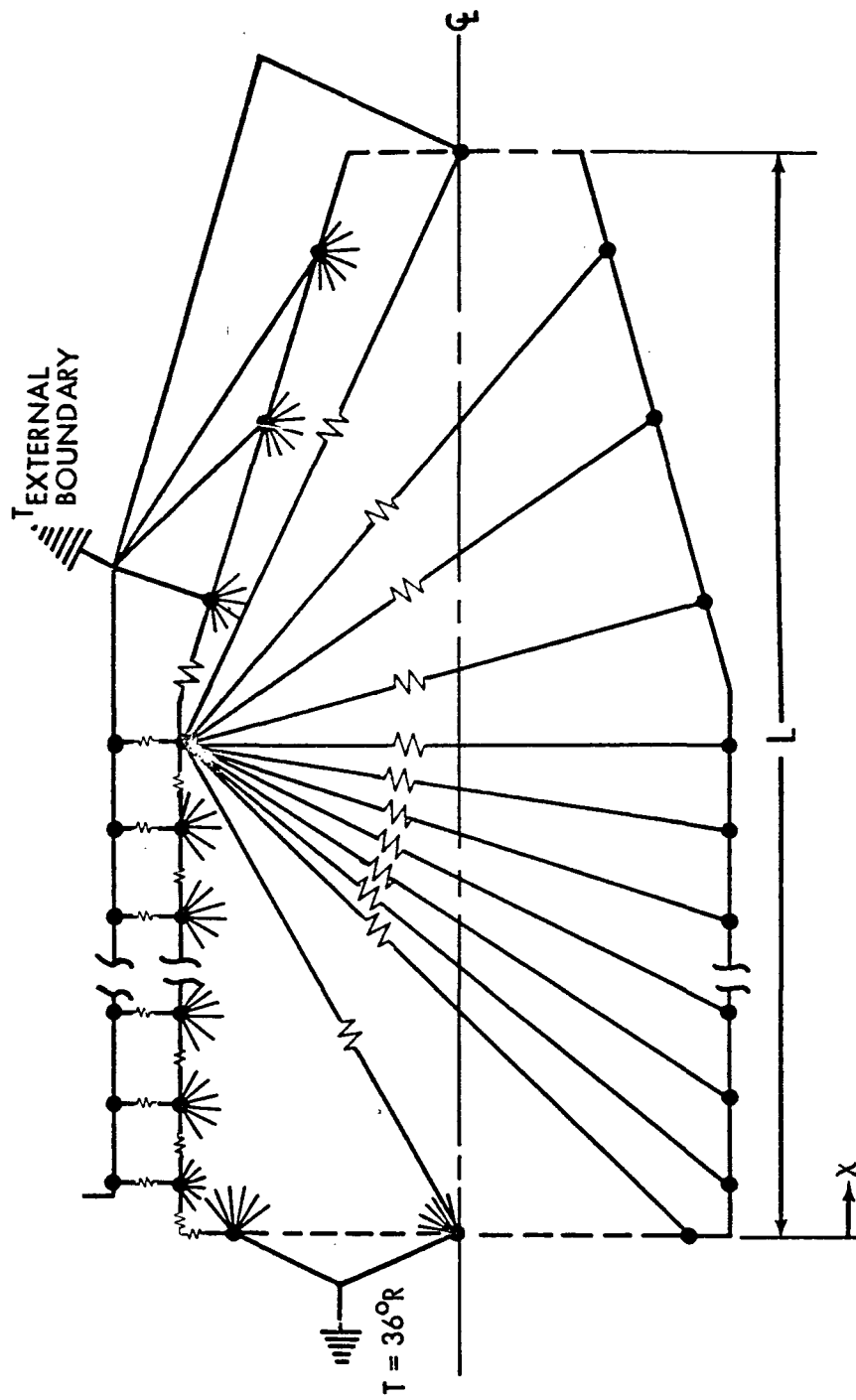


Figure 6: THERMAL MODEL OF CONFIGURATION NO. 2

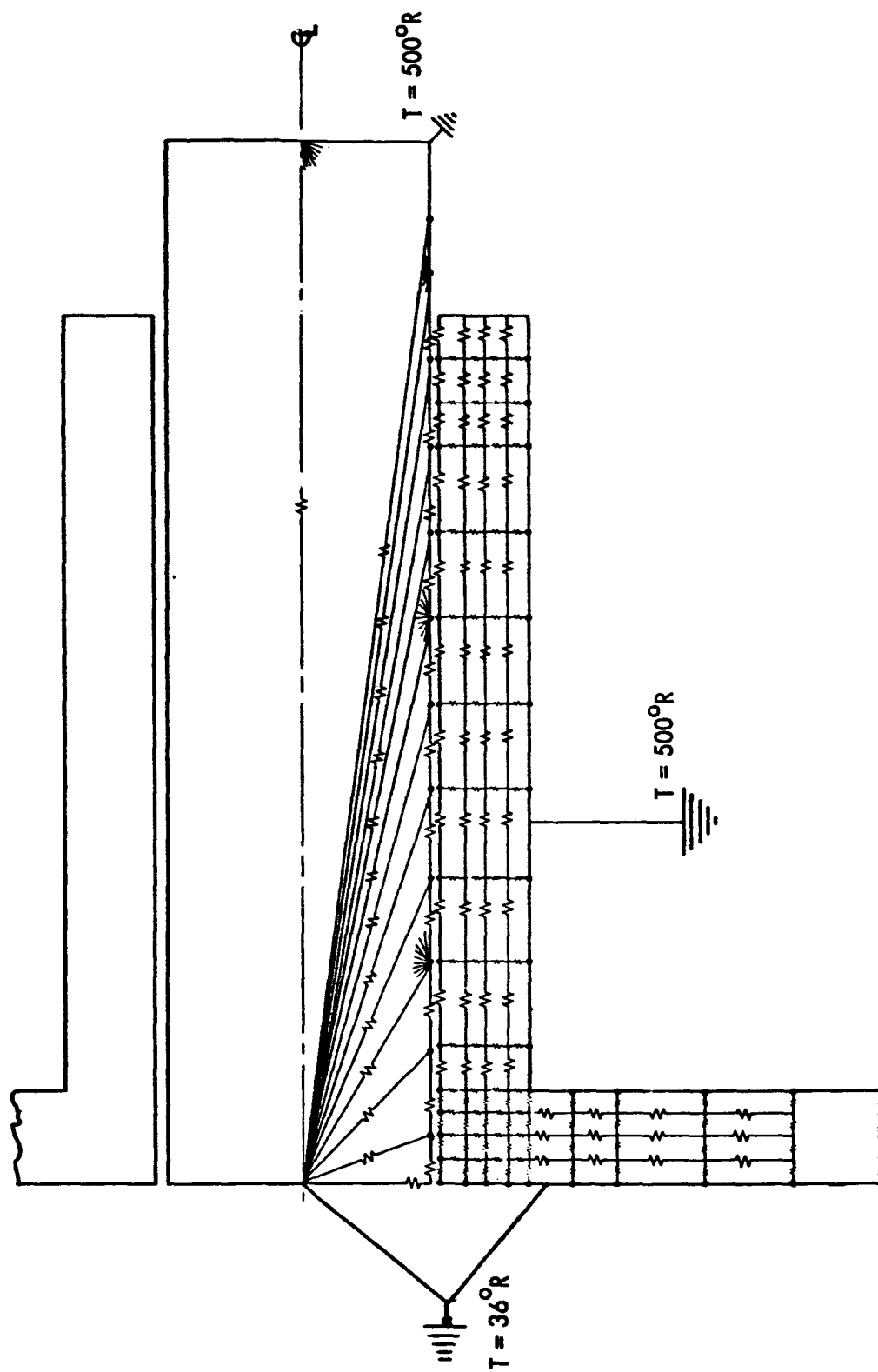


Figure 7: THERMAL MODEL OF CONFIGURATION NO. 3

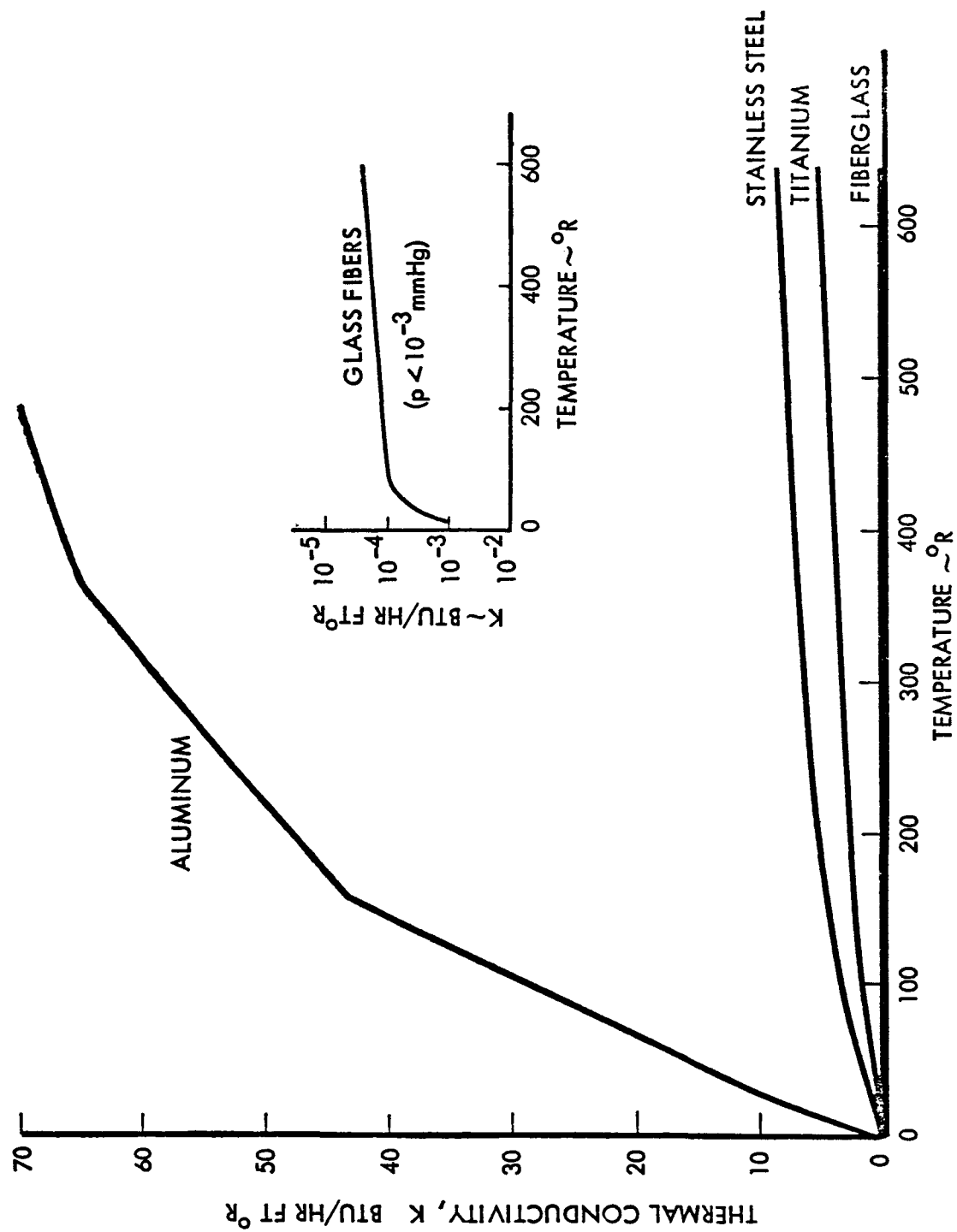


Figure 8: THERMAL CONDUCTIVITY OF FITTING MATERIALS

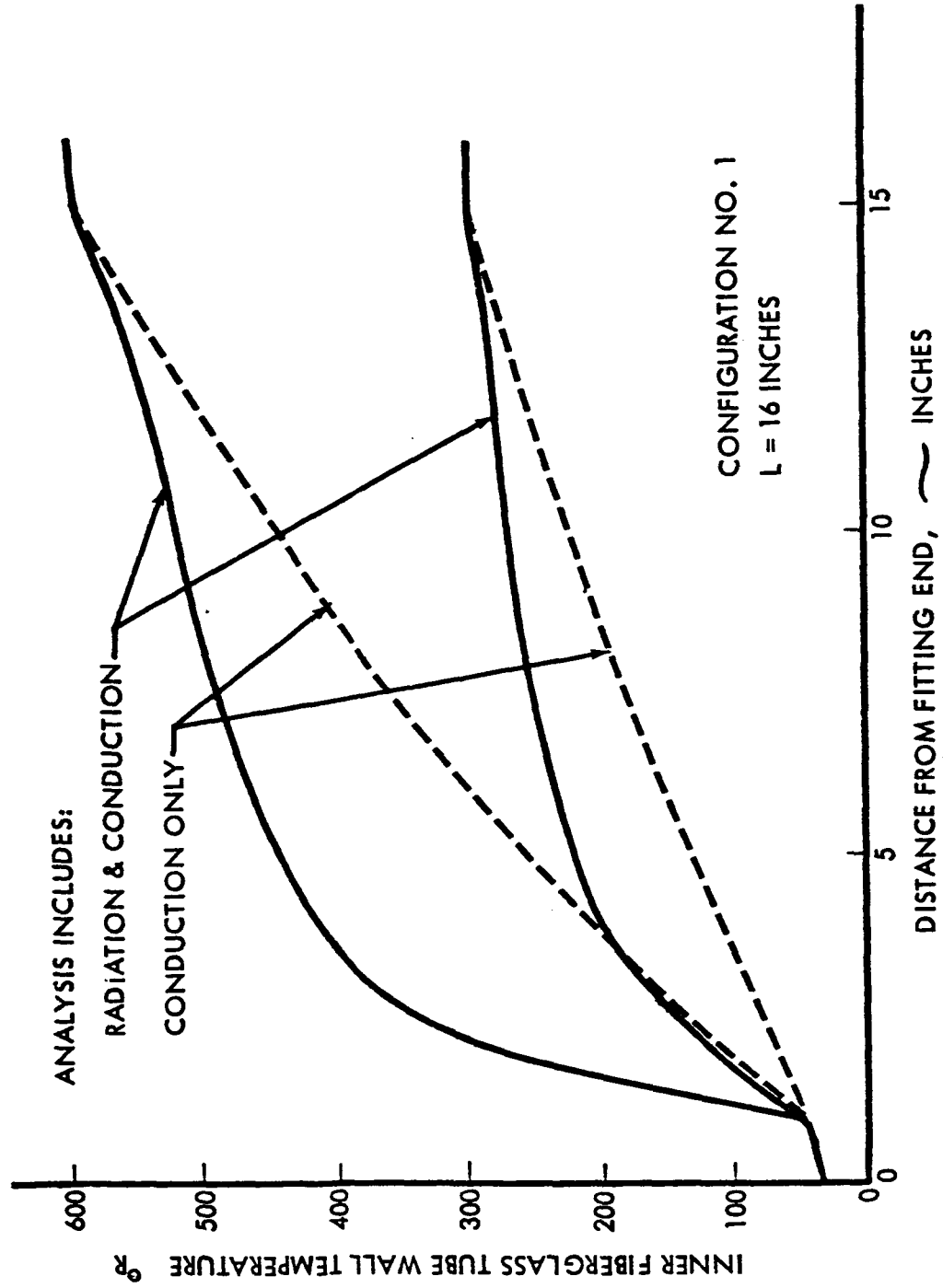


Figure 9: TEMPERATURE DISTRIBUTIONS FOR CONFIGURATION NO. 1

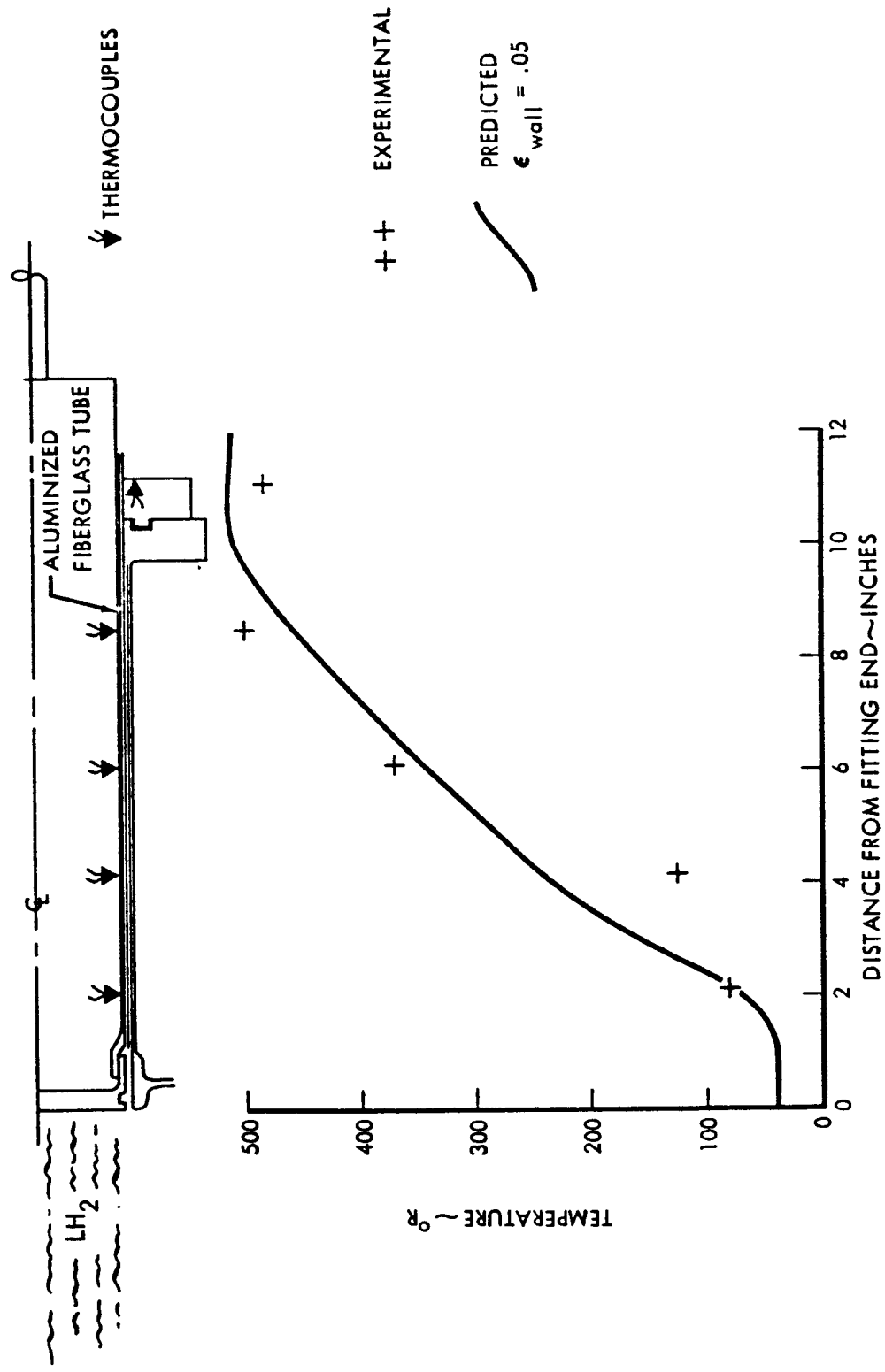


Figure 10: ALUMINIZED FIBERGLASS TUBE TEMPERATURES, CONFIGURATION NO. 3

Figure 11: STEADY STATE TEMPERATURES FOR FITTING, CONFIGURATION NO. 3

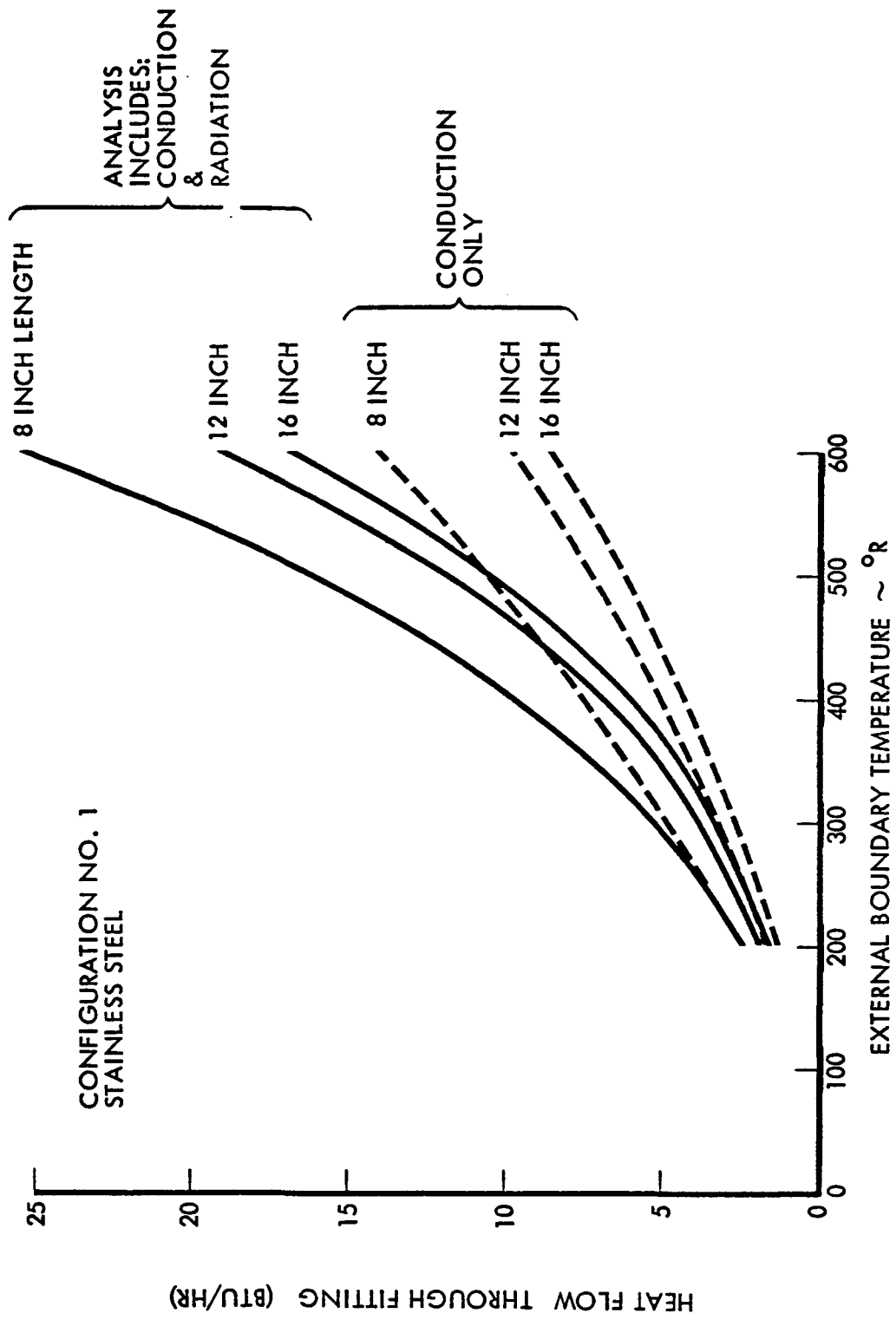


Figure 12: HEAT FLOW RATE FOR CONFIGURATION NO. 1 WITH STAINLESS STEEL TUBES

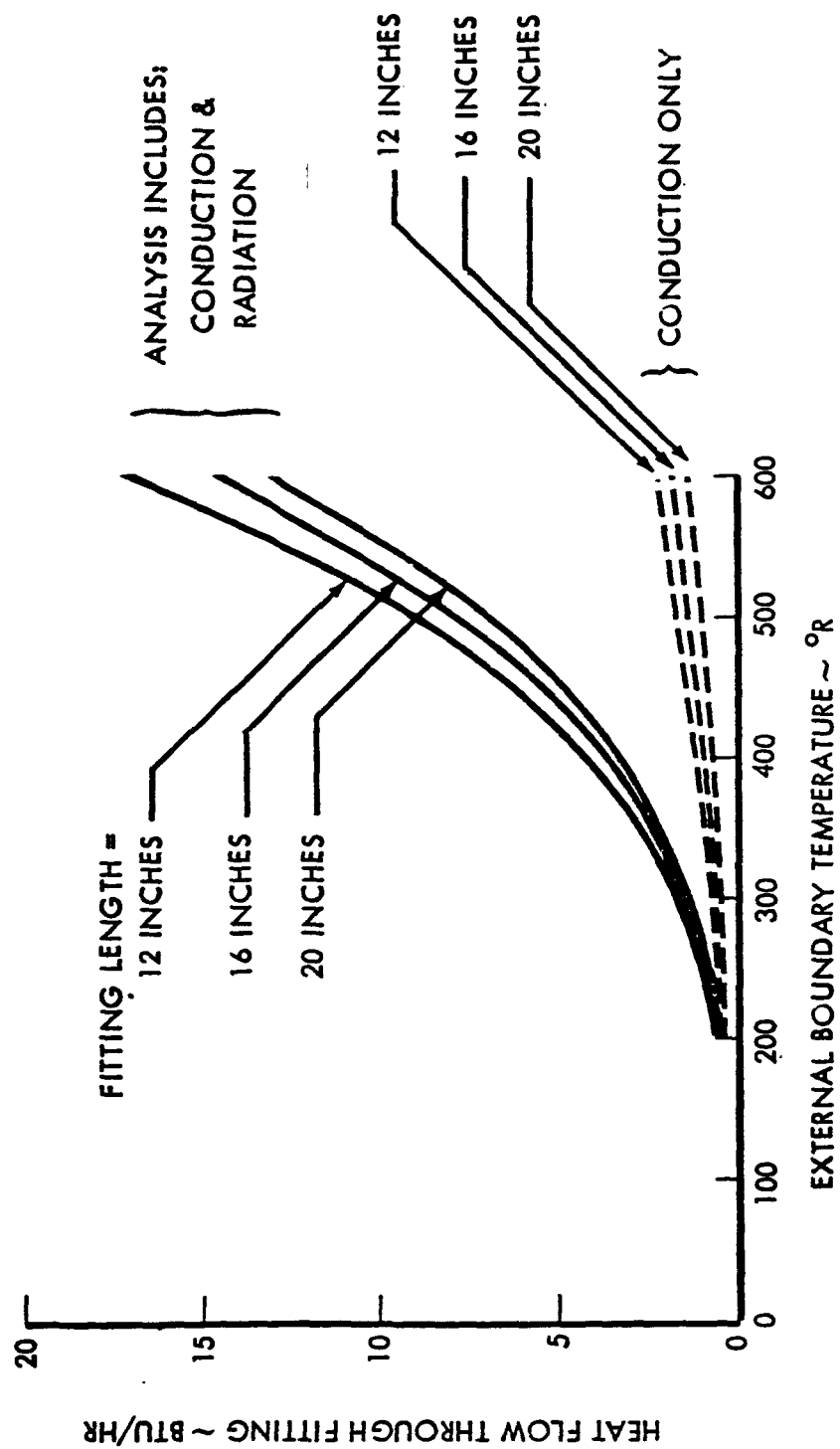


Figure 13: HEAT FLOW RATES FOR CONFIGURATION NO. 2 WITH FIBERGLASS TUBE

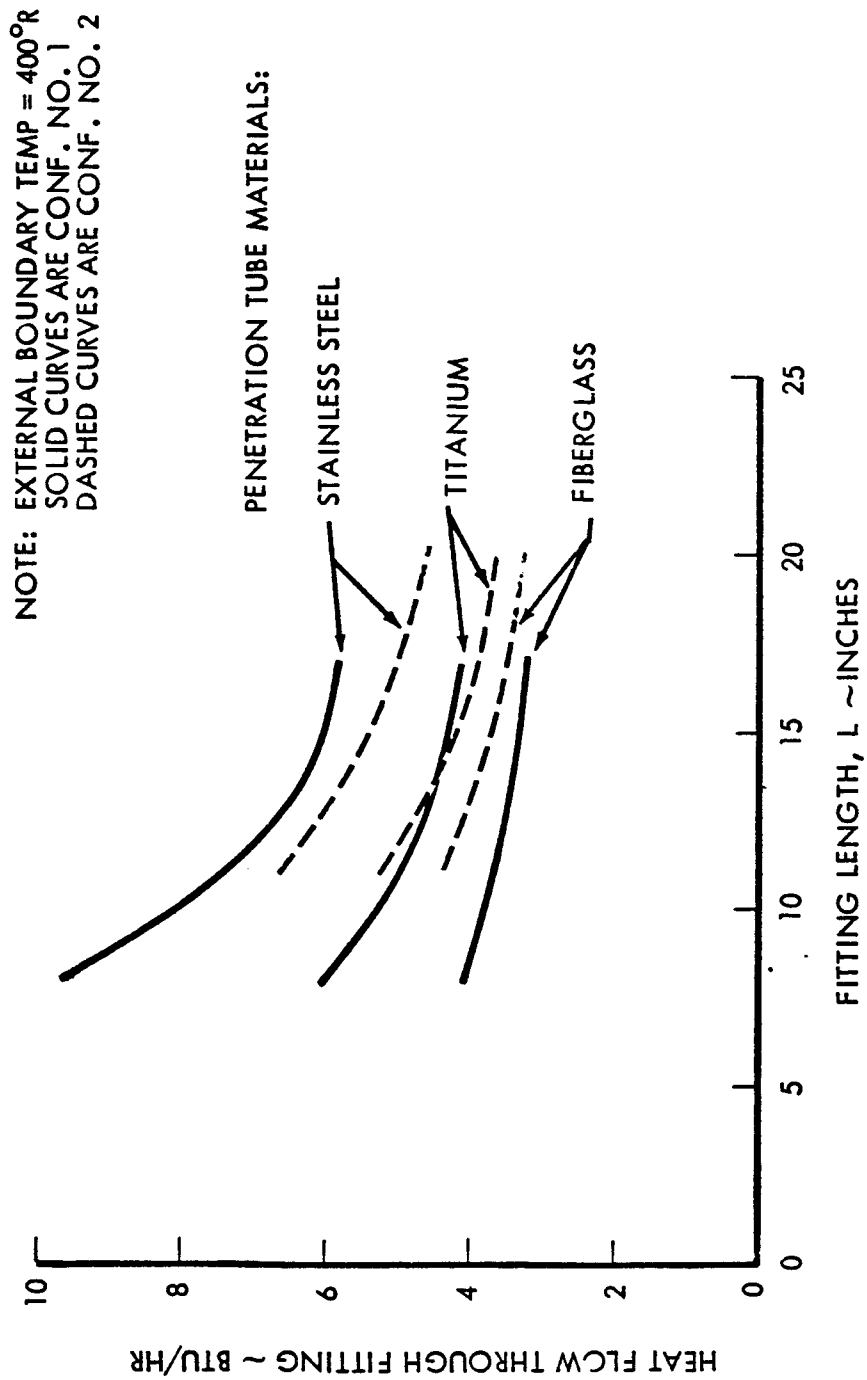


Figure 14: VARIATION OF HEAT FLOW RATE DETERMINED BY CONFIGURATION, MATERIALS, AND LENGTH OF TANK FITTING

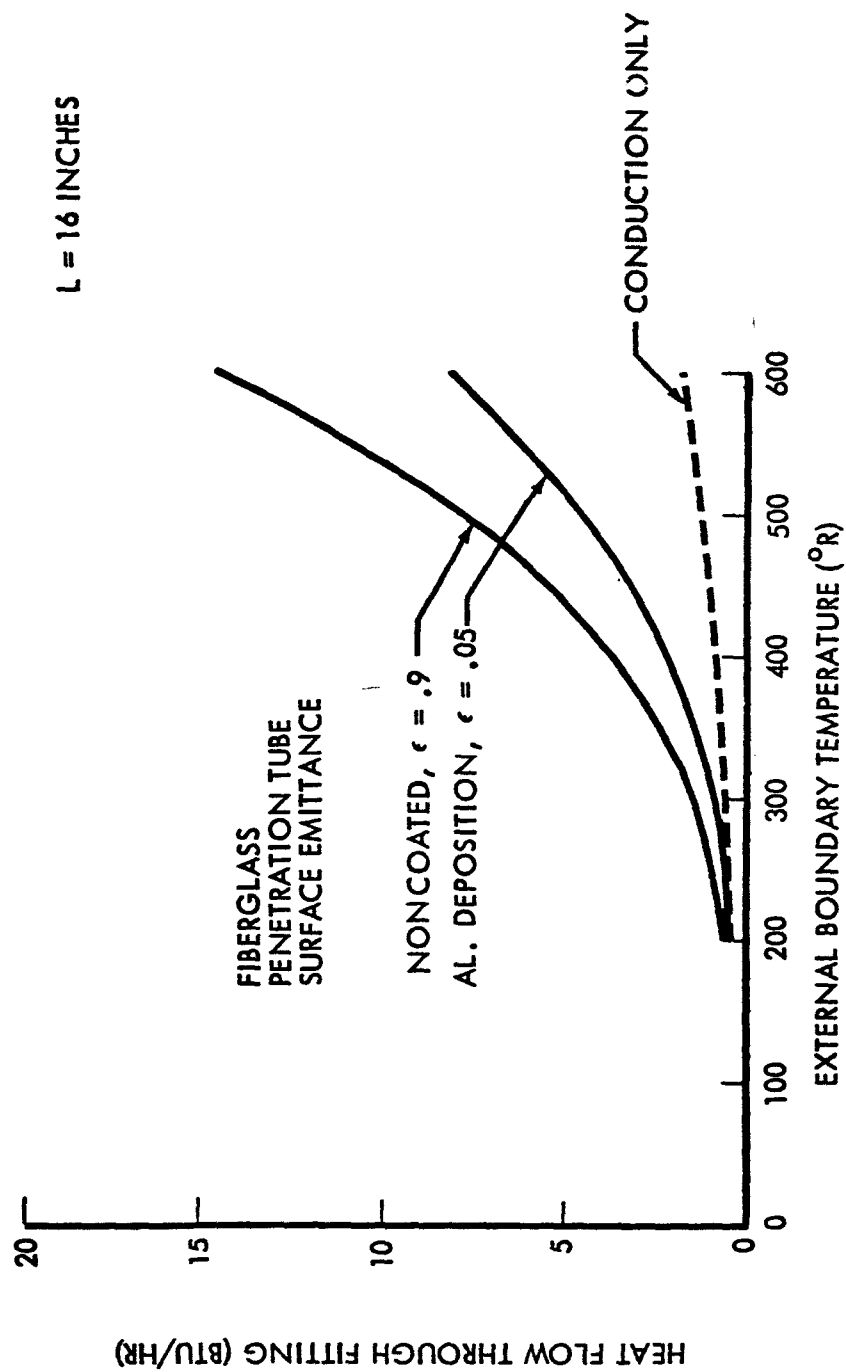


Figure 15: EMITTANCE EFFECT ON HEAT FLOW, CONFIGURATION NO. 2

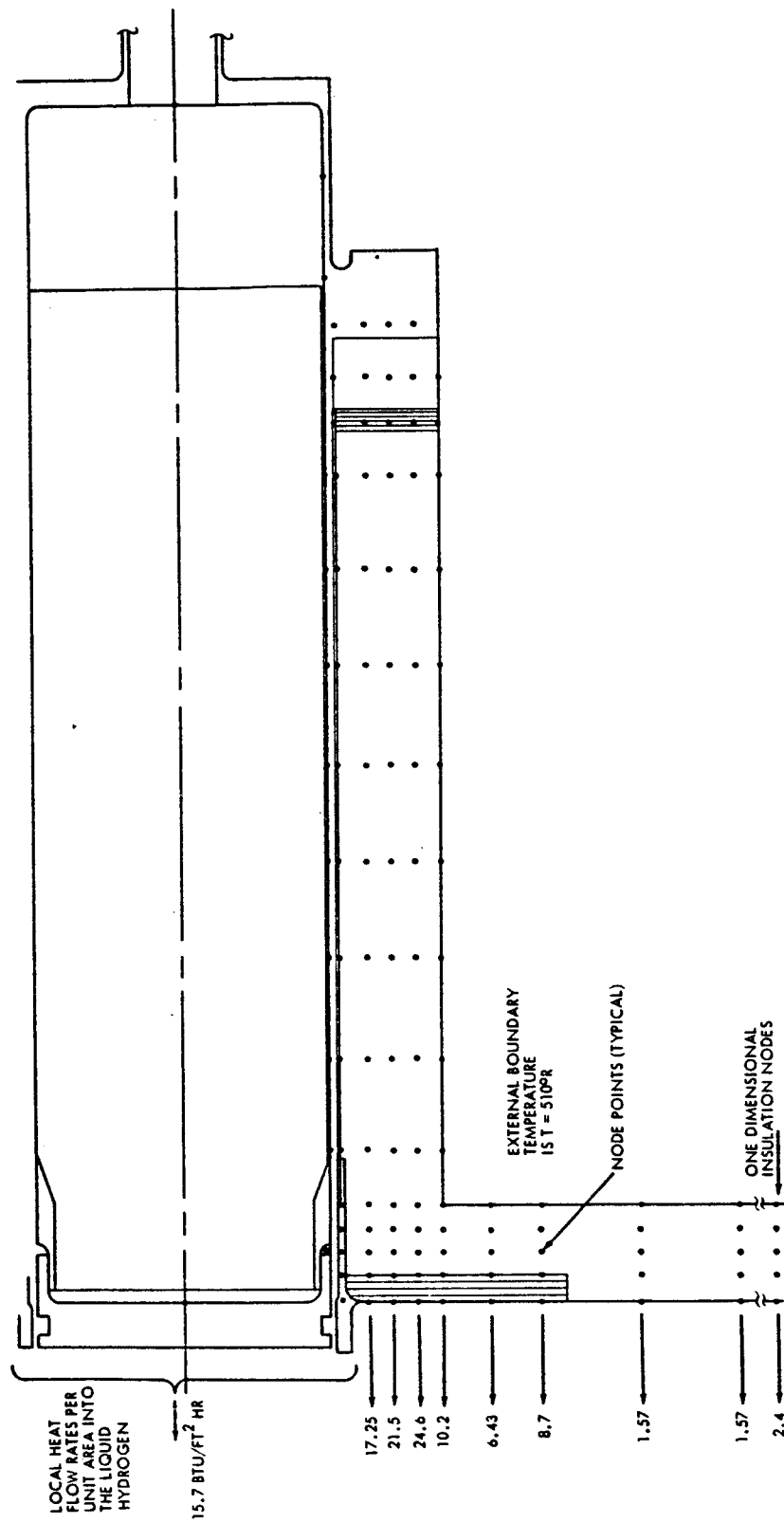


Figure 16: PREDICTED LOCAL HEAT TRANSFER RATES FOR FITTING, CONFIGURATION NO. 3

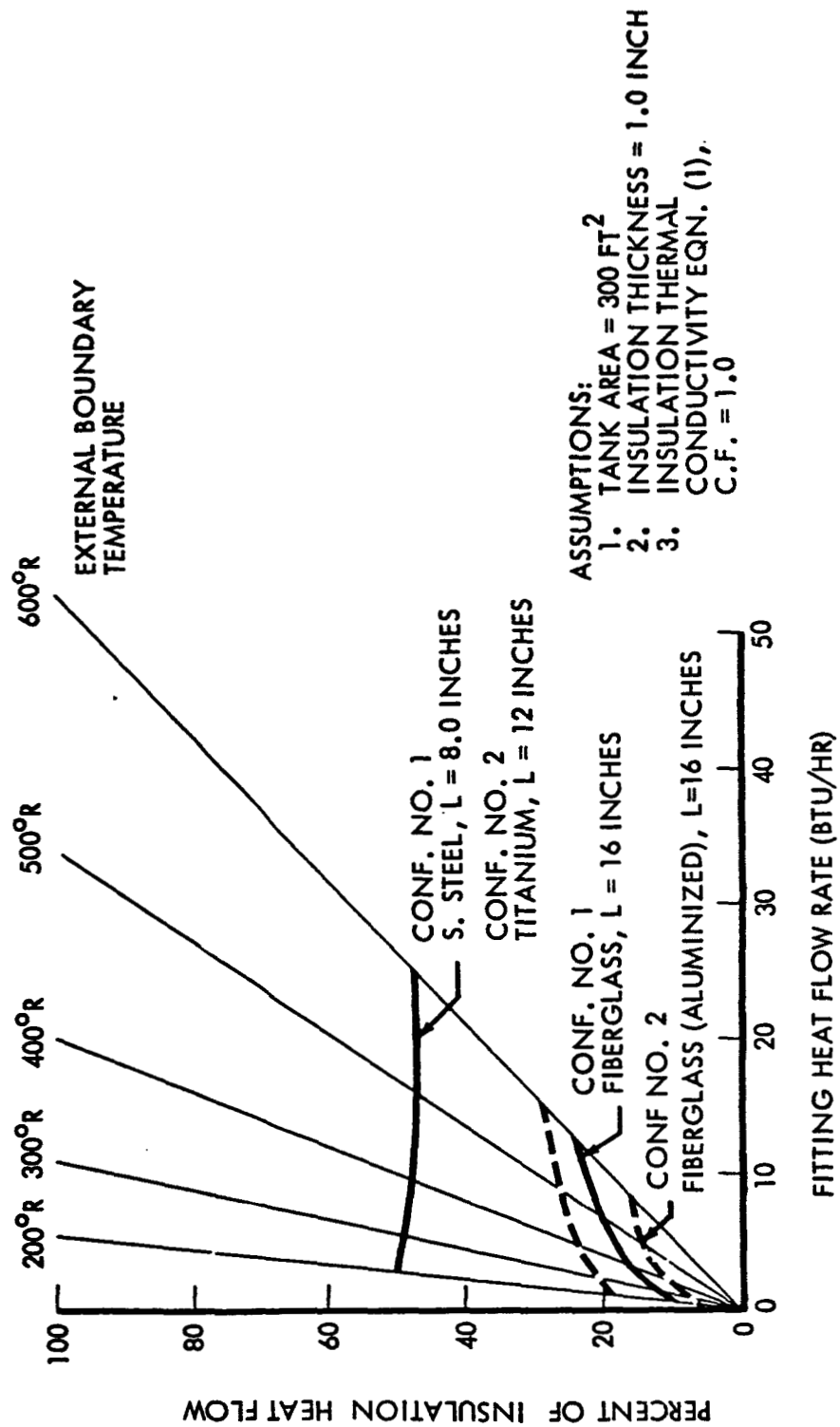


Figure 17: LIQUID HYDROGEN TANK FLUID LINE FITTING AND INSULATION HEAT FLOW RATE COMPARISONS

THERMAL DESIGN OF CRYOGENIC HEAT EXCHANGERS
FOR SPACE VEHICLE PRESSURIZATION SYSTEMS

J. H. Hargis¹ by
and H. A. Stokes²
Propulsion and Vehicle Engineering Laboratory
George C. Marshall Space Flight Center
Huntsville, Alabama

- ¹ Chemical Engineer, Brown Engineering Company, Inc., Huntsville
Alabama; MSFC Technical Support Contractor
² Mechanical Engineer, Chrysler Corporation, Huntsville, Alabama;
MSFC Technical Support Contractor

ABSTRACT

The thermodynamic problems associated with the design of cryogenic heat exchangers are discussed. Various recently developed heat transfer and pressure loss correlations are presented for both tube and shell side. Correlations are given for high Reynolds Numbers, large temperature differences, and heat transfer near the critical point. Certain special problems such as flow oscillations, carbon deposition, boiling heat transfer, and thermophysical properties are treated briefly.

THERMAL DESIGN OF CRYOGENIC HEAT EXCHANGERS FOR SPACE VEHICLE PRESSURIZATION SYSTEMS

INTRODUCTION

This paper presents correlations and other information obtained in the thermal design of heat exchangers for the pressurization systems of the Saturn vehicles. On this type of vehicle, pressurization of the propellant tanks is required to maintain a minimum NPSH at the propellant pumps. Heat exchangers are used to heat the pressurants and thus minimize gaseous residuals. Accurate thermal design is necessary to meet pressurization requirements without exceeding the maximum temperature fixed by structural and other limitations. A typical heat exchanger configuration is shown in Figure 1. The importance of the pressurant inlet temperature is illustrated by Figure 2, which shows the flow requirements for a typical propellant tank.

The pressurants consist of vaporized oxygen or hydrogen propellant or the inert gas, helium, which are forced through the heat exchanger tubes. LOX/RP-1 and LOX/H₂ combustion products are used as the heat source on the shell side. Nitrogen is often used on the tube side for test purposes.

For the heat exchangers considered, there are several difficult design problems as outlined below. The heat exchangers use helical coils, which complicate performance predictions. Reliable data for thermophysical properties are often limited. The large Reynolds numbers and high temperature differences exceed the range of most correlations. Carbon deposition occurs in units which use LOX/RP-1 combustion products. Condensation and/or solid formation can occur in units which use LOX/LH₂ combustion products. Flow oscillations have been experienced even at supercritical pressures. Due to lack of adequate information for the above problems, extensive experimental data is required for accurate heat exchanger design. The F-1*, J-2** and H-1*** heat exchangers were initially designed with excess heat transfer surface to cover the above uncertainties. After sufficient experimental data was obtained, design conditions in the F-1 unit were produced by bypassing the heat exchanger with a portion of the pressurant. In the case of the H-1 unit, a heat resistant coating was applied to the outside surface of the tubes. J-2 design conditions will be accomplished by plugging certain tubes and the possible use of a pressurant bypass.

* Saturn V, 1st Stage

** Saturn V, 2nd and 3rd Stages; Saturn IB 2nd Stage

*** Saturn I, 1st Stage; Saturn IB, 1st Stage

Most correlations presented in this paper were developed after initial design of these units.

Heat exchanger thermal design as discussed here is based on the heat transfer coefficients, the tube wall resistance, and the fouling factors combined to give the overall coefficient. The tube wall resistance is determined by the equation for heat flow through a cylinder. Heat transfer coefficients, pressure loss procedures, related thermophysical properties, and other problems are discussed below.

TUBE SIDE HEAT TRANSFER COEFFICIENTS

A number of investigations have been performed on single phase flow inside straight, round tubes. The best known are the Dittus-Boelter correlation based on bulk properties, the Colburn correlation based primarily on film properties, and the Sieder-Tate correlation based on bulk properties with a viscosity ratio correction. These equations are all limited to moderate temperature differences and produce significant errors near the critical temperature. Thus, the above equations are not adequate for most cryogenic applications. Corrections are necessary for fluid bulk temperature, tube wall to bulk temperature difference, entrance effects, etc. Tube side correlations used for design and data analyses are outlined below:

For hydrogen at supercritical pressures, the selected correlation is based on a report by Seader et al. (1) as follows:

$$(1) \quad (Nu)_b = 0.025 (Re)_b^{0.8} (Pr)_b^{0.4} (T_w/T_b)^{-0.55} \phi_1 \phi_2 \phi_3 \phi_4$$

Equation (1) is based on extensive experimental and analytical studies in conjunction with regenerative cooling of rocket nozzles. ϕ_1 , ϕ_2 , ϕ_3 , and ϕ_4 are corrections for bulk hydrogen temperature in the critical region, entrance effects, asymmetric heating, and surface roughness, respectively. These ϕ factors are discussed in Appendix A.

For oxygen at supercritical pressures, the selected correlation was developed at MSFC (2), based on the test data of Powell (3), as follows:

$$(2) \quad (Nu)_b = 0.023 (Re)_b^{0.8} (Pr)_b^{0.4} (T_w/T_b)^{-0.34} \phi_1 \phi_2$$

ϕ_1 and ϕ_2 are for bulk oxygen temperature and entrance effects, respectively. The ϕ factors are discussed in Appendix B.

For helium, nitrogen, and air at supercritical temperatures, the following selected equation is based on reports by Seader (4), McEligot, et al. (5), and Simoneau, et al. (6):

$$(3) \quad (St)_b = 0.025 (Re)_b^{-0.2} (Pr)_b^{-0.6} (T_w/T_b)^{-0.55}$$

Seader conducted an extensive literature survey for flow inside tubes in which several correlations were detailed. Equation (3) was obtained from Seader, but McEligot and Simoneau present similar results.

Several authors (7, 8, 9, and 10) have also presented data and/or correlations for helium, nitrogen, and air at supercritical temperatures based on a film or reference temperature. As outlined in a MSFC study (11), the results of the above writers can be reasonably correlated by:

$$(4) \quad (Nu)_r = 0.021 (Pr)_r^{0.4} (Re)_r^{0.8} (\rho_r/\rho_b)^{0.8}$$

Equation (4) was initially developed for a MSFC computer program, but equation (3) was later selected since it appears to have a better basis.

The limits of the above correlations vary widely as shown by the respective references. In some cases the limits are not specified. However, these equations are all of the same general type so that the limits are assumed to be the same for each equation. The limits are as follows:

$$1.5 \times 10^4 \leq Re \leq 3.7 \times 10^6, \quad 1.1 \leq (T_w/T_b) \leq 11.0, \quad \& \quad 0.7 \leq P_r \leq 120$$

Space vehicle pressurization system heat exchangers use helical coils. Both heat transfer and pressure loss in curved tubes are significantly greater than for a straight tube. In some cases the increase can be as much as 75 per cent. The above equations are all for straight tubes and must be corrected for a helical coil. The selected correction, initially developed by Ito (12) for pressure loss, was recently used by Seban and McLaughlin (13) to correlate heat transfer.

$$(5) \quad h/h_s = \left[\text{Re} (di/D)^2 \right]^{1/20}$$

$$\left[\text{Re} (di/D)^2 \right] > 6$$

The above equations are applicable only for single phase flow, but in some cases the pressurant experiences a phase change. Reliable forced convection boiling heat transfer correlations are limited. As a result, an extensive literature survey has been performed on boiling heat transfer for cryogenics by Seader et al. (14) for MSFC.

Figure 3 shows a comparison of computed performance with test data for a typical LOX heat exchanger. This comparison demonstrates that equation (2) presents significant corrections to the commonly used Dittus - Boelter equation.

SHELL SIDE HEAT TRANSFER COEFFICIENTS

The determination of the outside coefficient is complicated by the lack of correlations for helical coils in cylindrical ducts. It has been assumed the outside film will be essentially the same as that for cross-flow over straight, inline tubes. A limited study was performed at MSFC (15) of the better known references. The graphical results and correlations obtained are shown in FIG 4. Curves 1a, 2, and 3 of FIG 4 represent information given by McAdams (7). Curve 1b is based on the equation given by Gram et al. (16) assuming $F_h = 1$. Curve 4 is a modification of Dwyer et al.'s (17 & 18) correlation. Curves 5 through 9 show the results of Kays and London (19) which were also modified to conform with FIG 4. The data of McAdams, Gram, and Kays and London are based on gases, primarily air. The data of Dwyer was obtained from the flow of water over a single tube bank. Figure 4 is subject to the assumption that the tube matrix is ten rows in depth, and that the difference between film and bulk properties are negligible.

From the results of FIG 4, the following correlations were selected for the outside heat transfer coefficients:

$$(6) \quad (St)_b \times (Pr)_b^{2/3} = 0.33 F_h (Re)_b^{-0.4}$$

$$N = 10$$

$$2 \times 10^3 \leq Re_b \leq 1 \times 10^5$$

$$F_h = f(Re_b, X_l, X_t) \text{ as given by Gram, et al. (16)}$$

$$(7) \quad (St)_f \times (Pr)_f^{2/3} = 0.0325 (Re)_f^{-0.2}$$

$$N = 10$$

$$10^5 \leq Re \leq 10^6$$

At high Reynolds Numbers, $F_h = 1.0$ for most tube configurations. Corrections for N , which are about unity for most tube bundles, can be obtained from McAdams. Equation (6) is presented by Gram et al. and equation (7) is a modification of that used by Dwyer et al. to correlate their data. Of course both equations are limited to single phase fluids not near the critical point. Most of the test data appears to be for moderate ΔT 's between bulk fluid and the tube wall. Therefore, any corrections for large ΔT 's are yet to be determined. It is significant that the above heat transfer coefficients represent a mean value for the matrix. The importance of this is illustrated by the fact that Dwyer et al.'s tubes at the side walls gave coefficients about 15% greater than the average for the matrix.

PRESSURE LOSS CORRELATIONS

Friction pressure loss calculations are complicated by the effect of helical coiled tubes. The correlation selected was developed by Ito (12) as follows:

$$(8) \quad f_c / f_s = \left[Re \left(\frac{di}{D} \right)^2 \right]^{.05}$$

$$\left[Re \left(\frac{di}{D} \right)^2 \right] > 6$$

This curved tube friction factor replaces the straight tube friction factor normally used in pressure loss calculations. The straight tube friction factor can be determined by using the Colebrook equation (20) or a Moody diagram.

In some cases the oxygen pressurant used on the Saturn vehicles experiences a phase change. A correlation presented by Martinelli et al. (21) has been selected for two phase pressure loss calculations. A dimensionless term is used to evaluate a two phase correction factor as shown in Figure 5. The two phase pressure loss for turbulent flow of both liquid and vapor is the product of the pressure loss of the vapor component flowing alone and the two phase correction factor squared.

The static pressure loss in a heat exchanger includes the momentum loss, which is often significant. Since static pressure is normally specified for heat exchangers, it is important that momentum losses be determined. McAdams (7) presents a simplified method of computing the momentum pressure loss:

$$(9) \quad \Delta P_m = \frac{G^2}{g_c} (v_2 - v_1).$$

$$v_2/v_1 \leq 2.0$$

Shell side pressure loss is important due to its effect on turbine performance and shell side flow. The pressure loss procedures recommended by Kays and London (19) are currently used.

THERMOPHYSICAL PROPERTIES

Hydrogen, oxygen, and nitrogen are normally stored at subcritical temperatures and pressures; therefore, they pass through the region of the critical point when heated to a superheated temperature. Near the critical point, thermophysical properties vary considerably with temperature and pressure. This large property variation, especially specific heat, makes the use of finite difference procedures essential. Helium is used at supercritical conditions and does not pass through the critical region. Though considerable effort has been expended to obtain properties, data are still limited for the above fluids. The properties of the LOX/RP-1 and LOX/H₂ combustion products are also limited. The National Bureau of Standards (22, 23, 24, & 25) presents data for cryogenic fluids which are used as pressurants. The importance of properties is demonstrated by their use in the above correlations for heat transfer and pressure loss.

OTHER THERMAL DESIGN PROBLEMS

As outlined previously, analyses of heat exchangers which utilize LOX/RP-1 combustion products are complicated by carbon deposition. This carbon fouling is a function of total firing time, mixture ratio, dynamic pressure, etc. Preliminary carbon fouling correlations have been obtained as shown in Figures 6 and 7. Figure 6, by M. E. Nein, shows the importance of dynamic pressure and mixture ratio on carbon deposition. Figure 7 shows a correlation of some test data which illustrates the importance of accumulated firing time. These results were used for design and analysis of the F-1 unit but are not adequate for design in general. Efforts are continuing at MSFC to obtain better carbon fouling data.

Analyses of cryogenic heat exchangers using LOX/LH₂ combustion products are complicated by the possibility of condensation and/or solid formation. Efforts are being made to correlate these phenomena, however, at this time no reliable method has been obtained.

Another problem in heat exchanger design is oscillation of certain pressurants. Oscillations can affect system performance and cannot be tolerated. In the case of the F-1 heat exchanger, the GOX flow and pressure oscillated even though the operating to critical pressure ratio was about two (2). Oscillations can be controlled in some instances by orificing of the tube inlets. It is, however, frequently impossible to obtain the required pressurant flowrate range, due to excessive pressure loss. Though believed due to the large property changes near the critical point, the mechanism of oscillations are not clearly understood. Fundamental studies of oscillations are currently being performed for NASA by the General Electric Company (26) and the University of Miami (27).

CALCULATION METHODS

Due to the large temperature changes of cryogenic pressurants, the corresponding thermophysical properties vary significantly along the coil length. Because of this property variation, finite difference procedures are essential for accurate design. The coils are divided into a number of increments, and the properties, heat transfer coefficients, etc. are determined at local conditions. Design of heat exchangers by the incremental method is time consuming making computer solutions practical. Computer programs developed at MSFC will either design new heat exchangers or predict the performance of existing units.

CONCLUSIONS AND RECOMMENDATIONS

1. Heat exchanger design significantly affects both the pressurization system and vehicle payload by minimizing pressurant flow and gaseous residuals.

2. Corrections for most well known heat transfer correlations are necessary for analysis of cryogenic fluids in helical coils.

3. Equation (6) for low shell side Reynolds numbers should not be extrapolated beyond $Re = 10^5$. Adequate correlations for $Re > 1 \times 10^5$ are limited, therefore, more data is needed.

4. Complete and accurate thermophysical properties of cryogenics are especially important because of the large variations encountered. Due to these property variations, finite difference procedures are essential for design.

5. Although preliminary correlations for carbon deposition have been developed, they are limited to the conditions in certain Saturn LOX/RP-1 heat exchangers.

6. With test data, flow and pressure oscillations can be controlled by orifices, but a correlation capable of predicting oscillation limits during design is not available.

7. The correlations and other information presented in this paper represent significant improvement in cryogenic heat exchanger design. However, adequate correlations for carbon deposition, forced convection condensation, flow oscillations, etc. are not available. Therefore, test data is yet required to determine heat exchanger modifications in order to produce specified unit performance.

DEFINITION OF SYMBOLS AND UNITS

SYMBOL	DEFINITION	BRITISH UNITS	METRIC UNITS
C_p	Specific Heat	Btu/lb-°R	K Cal/Kg °K
d	Tube Diameter	ft	M
D	Coil Diameter	ft	M
f	Fraction factor		
F_h	Correction for Transverse and Longitudinal Pitch		
g_c	Gravitational Constant	$(lb_m) ft/sec^2$ (lb_f)	$\frac{Kg_m}{Kg_p} M/hr^2$
G	Mass Velocity	lb/ft ² hr	Kg/M ² hr
h	Film Coefficient	Btu/hr-°R-ft ²	K Cal/hr-°K M ²
j	(St) (Pr) ^{2/3} , Colburn Heat Transfer Factor		
k	Conductivity	Btu/hr-°R-ft ² /ft	K Cal/hr-°K-M ² /M
L	Length	ft	M
\dot{M}	Mass flow rate	lb/hr	Kg/hr
N	Number of tubes in direction of flow		
Nu	Nusselt Number, $\frac{hd}{k}$		
P	Static Pressure	lb/ft ²	Kp/M ²
q	Dynamic Pressure, $\frac{V^2 \rho}{2g_c(144)}$	lb/in ²	Kp/M ²
Pr	Prandtl Number, $\frac{C_p \mu}{k}$		

SYMBOL	DEFINITION	BRITISH UNITS	METRIC UNITS
Re	Reynolds Number, $\frac{\rho dV}{\mu}$		
R	Heat Transfer Resistance	ft ² °R-hr/Btu	M ² °K hr/C21
r	Actual Mixture Ratio		
S	Stoichiometric Mixture Ratio		
St	Stanton $\frac{h}{VC_p\rho}$ Number		
t	Time	Sec or hr	Sec or hr
T	Temperature	°R	°K
V	Velocity	ft/hr	M/hr
v	Specific Volume	ft ³ /lb	M ³ /Kg
X _l	Ratio of Pitch to Tube Diameter in Direction of Flow		
X _t	Ratio of Pitch to Tube Diameter Traverse to Direction of Flow		
X _{tt}	Dimensionless Ratio		
δ	Carbon Thickness	ft	M
ε	Surface Roughness	ft	M
μ	Viscosity	lb/ft-hr	Kg/M-hr
ρ	Density	lbs/ft ³	Kg/M ³
Φ	Two Phase Correction		
φ	Correction factors (see appendix A & B)-		

SUBSCRIPTS

DEFINITION

b	bulk
c	curved tube
f	film
i	inside
l	liquid
m	momentum
o	outside
r	film temperature determined by $T_r = T_i + 0.4 (T_{wi} - T_i)$
s	straight tube
v	vapor
w	wall

REFERENCES

1. J. D. Seader, W. S. Hines, J. R. McCarthy, et al., "Investigation of Cooling Problems at High Chamber Pressures," Rocketdyne Final Report, NASA Contract NAS8-4011, 1963.
2. M. E. Nein, "Oxygen Forced Convection Heat Transfer in the Region of the Critical Temperature at Super Critical Pressure," MSFC Memorandum, R-P&VE-PT-64-M-158, 1964.
3. W. B. Powell, "Heat Transfer to Fluids in the Region of the Critical Temperature," Ord 18, Jet Propulsion Laboratory Report No. 20-285, April 1956.
4. J. D. Seader, "Recent Developments in Turbulent Flow Heat Transfer Inside Tubes," Paper presented at the Southern California Section Meeting of the Institute of Chemical Engineers, Los Angeles, California, April 1964.
5. D. M. McEligot, P. M. Magee, and G. Leppert, "Effect of Large Temperature Gradients on Convective Heat Transfer: The Downstream Region," Transactions of the ASME, Journal of Heat Transfer, Paper No. 64-HT-12.
6. R. J. Simoneau and R. C. Hendricks, "A Simple Equation For Correlating Turbulent Heat Transfer to a Gas," presented at the AiChE-ASME Heat Transfer Conference, Cleveland, Ohio, August 9-12, 1964; ASME Paper No. 64-HT-36.
7. W. H. McAdams, "Heat Transmission," 3rd Edition, McGraw-Hill, New York, 1954.
8. R. G. Deissler and C. S. Eian, "Analytical and Experimental Investigation of Fully Developed Turbulent Flow of Air in a Smooth Tube With Heat Transfer With Variable Fluid Properties," NACA TN 2629.
9. M. F. Taylor and T. A. Kirchgessner, "Measurements of Heat Transfer and Friction Coefficients for Helium Flowing In a Tube at Surface Temperatures Up to 5900°R," ARS Journal, September, 1960

10. R. G. Deissler and A. F. Pressler, "Computed Reference Temperature for Turbulent Variable - Property Heat Transfer in a Tube for Several Common Gases, International Developments in Heat Transfer," Part III, Published by ASME, 1961.
11. J. H. Hargis, "Tube Side Heat Transfer Coefficients for High Temperature Differences Between Tube Wall and Fluid Bulk," MSFC Memorandum, R-P&VE-PTF-64-M-128, August, 1964.
12. H. Ito, "Friction Factors For Turbulent Flow In Curved Pipes," J. Basic Engineering, Trans. ASME, D, 81, June, 1959.
13. R. A. Seban and E. F. McLaughlin, "Heat Transfer In Tube Coils With Laminar and Turbulent Flow," Int. J. Heat Mass Transfer, Volume 6, pp 387-395, 1963.
14. J. D. Seader, L. A. Kalvinskis, and W. S. Miller, "Boiling Heat Transfer for Cryogenics," Rocketdyne Report, NASA Contract No. NAS8-5337, 1964.
15. J. H. Hargis, "Shell Side Heat Transfer Study For Inline And Staggered Tube Banks," MSFC Memorandum, M-P&VE-PT-410-63, September, 1963.
16. A. J. Gram, Jr., C. Mackey and E. S. Monroe, Jr., "Convection Heat Transfer and Pressure Drop of Air Flowing Across In-Line Tube Banks - Part II - Correlation of Data For Ten-row-deep Tube Banks," ASME Paper No. 56-A-127, Presented at the ASME Annual Meeting, New York, November 25-30, 1956.
17. O. E. Dwyer, et al., "Cross Flow of Water Through A Tube Bank At Reynolds Numbers Up To A Million," Industrial and Engineering Chemistry, Volume 48, No. 10, October, 1956.
18. O. E. Dwyer, et al., "Heat Transfer Rates For Cross Flow of Water Through A Tube Bank At High Reynolds Numbers," Brookhaven National Laboratory Report BNL 203, November, 1952.
19. W. M. Kays and A. L. London, "Compact Heat Exchangers," The National Press, Palo Alto, California, 1955.

20. V. L. Streeter, "Fluid Mechanics," 2nd Edition, McGraw - Hill, New York, 1958.
21. R. C. Martinelli, et al., "Isothermal Pressure Drop For Two-Phase Two-Component Flow in a Horizontal Pipe," Transactions of the ASME, February, 1944.
22. V. J. Johnson, "A Compendium of the Properties of Materials at Low Temperature (Phase I) Part II. Properties of Solids," by The National Bureau of Standards, Cryogenic Engineering Laboratory, WADD Technical Report 60-56, October, 1960.
23. V. J. Johnson, "A Compendium of the Properties of Materials At Low Temperature (Phase I) Part I. Properties of Fluids," By The National Bureau of Standards, Cryogenic Engineering Laboratory, WADD Technical Report 60-56, July 1960.
24. R. B. Stewart and V. J. Johnson, "A Compendium of the Properties of Materials at Low Temperature (Phase II)," by The National Bureau of Standards, Cryogenic Engineering Laboratory, WADD Technical Report 60-56.
25. "Fifth Progress Report to NASA On Cryogenic Research and Development For Period Ending March 31, 1962," The National Bureau of Standards Report 7246.
26. N. Zuber, "Investigation of the Nature of Cryogenic Fluid Flow Instabilities in Heat Exchangers," Study by General Electric under Contract No. NAS8-11422, currently in progress.
27. A. H. Stenning and T. N. Veziroglu, "Study of Boiling Flow Instability," Study by the University of Miami Under NASA Grant N_SG-424 currently in progress.

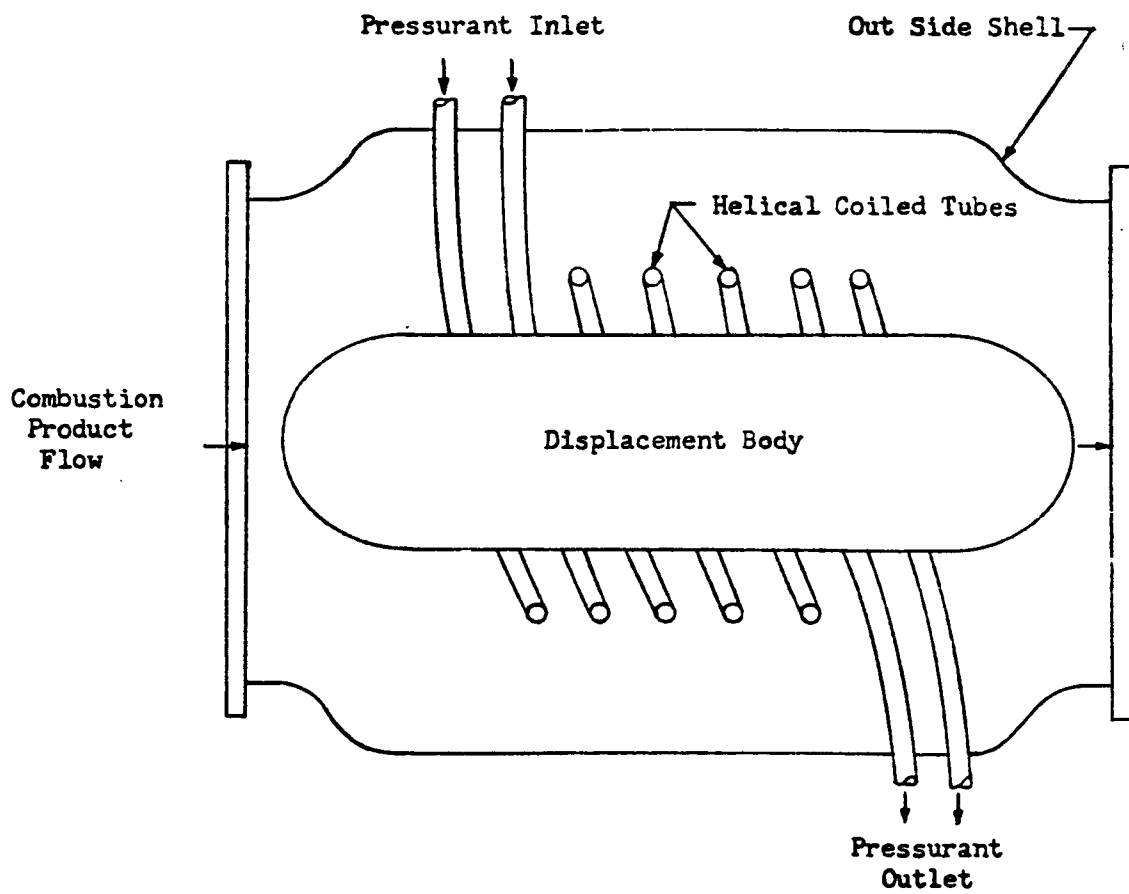


FIG 1 TYPICAL CONFIGURATION OF A SPACE VEHICLE PRESSURIZATION
SYSTEM HEAT EXCHANGER

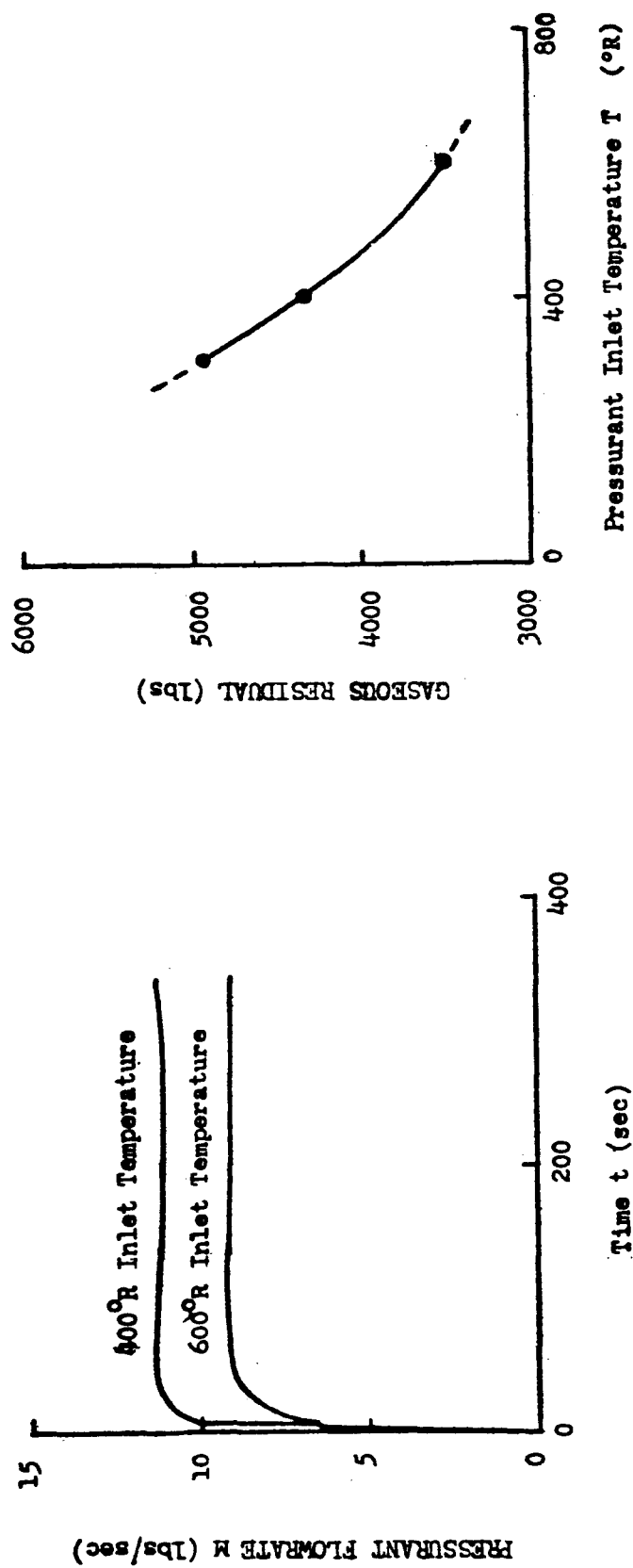


FIG. 2 TYPICAL FLOWRATE REQUIREMENTS AND GASEOUS RESIDUALS FOR VARIED PRESSURANT INLET TEMPERATURES

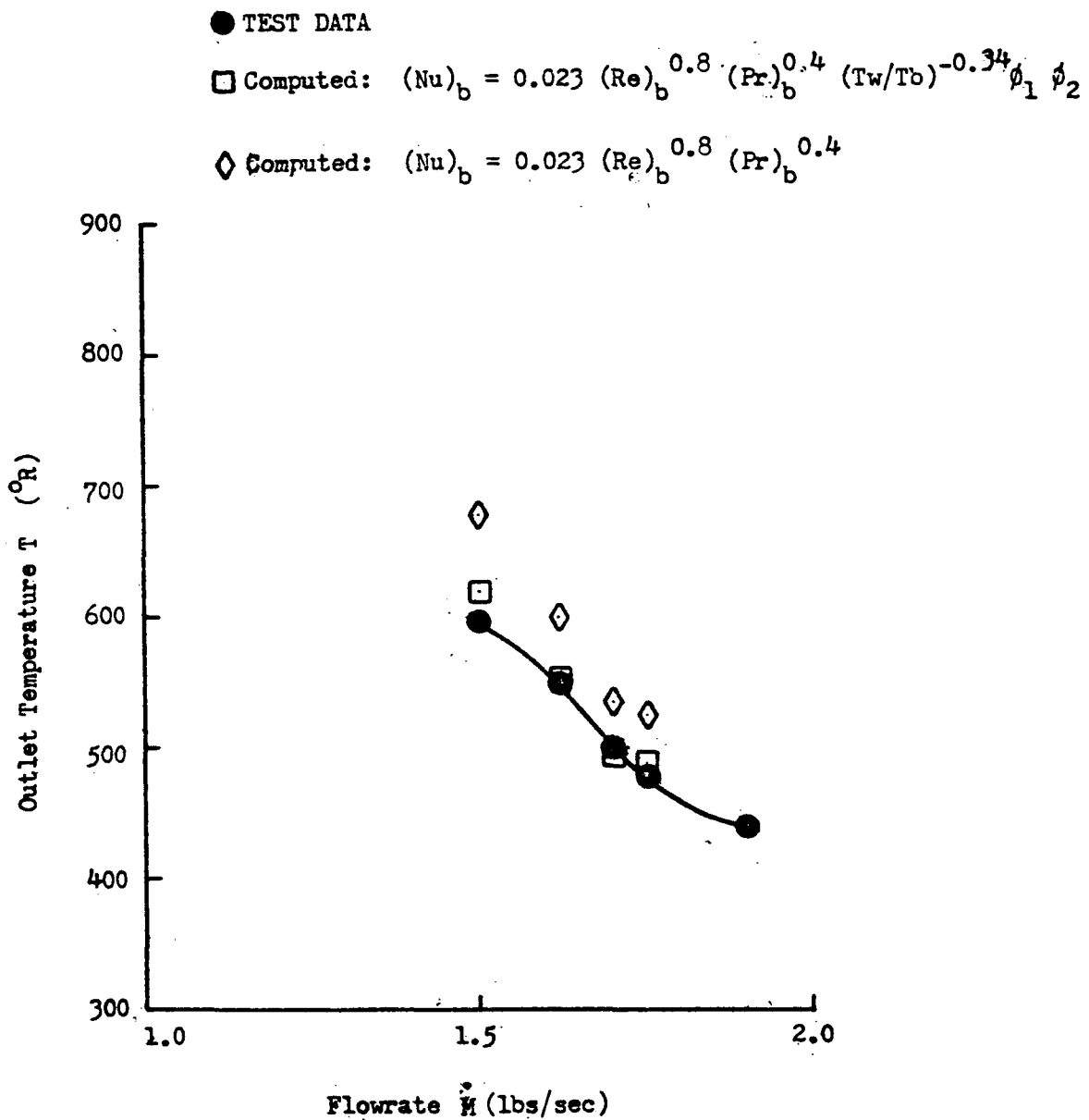


FIG. 3 COMPARISON OF TEST DATA AND COMPUTED PERFORMANCE PREDICTIONS FOR A TYPICAL LOX HEAT EXCHANGER

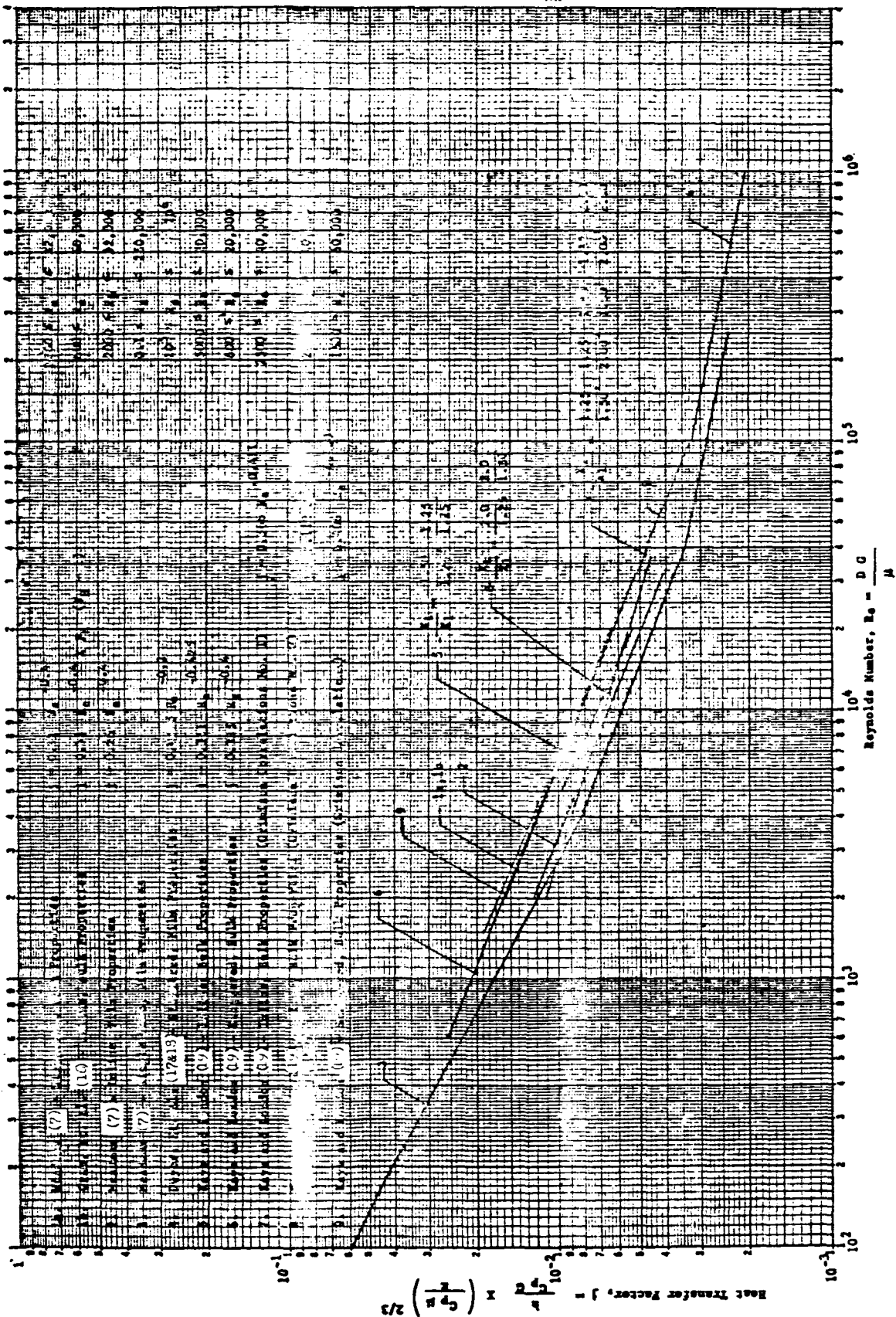


FIG 4 HEAT TRANSFER FACTOR, j , vs REYNOLDS NUMBER, Re , FOR STAGGERED AND INLINE TUBE BANKS

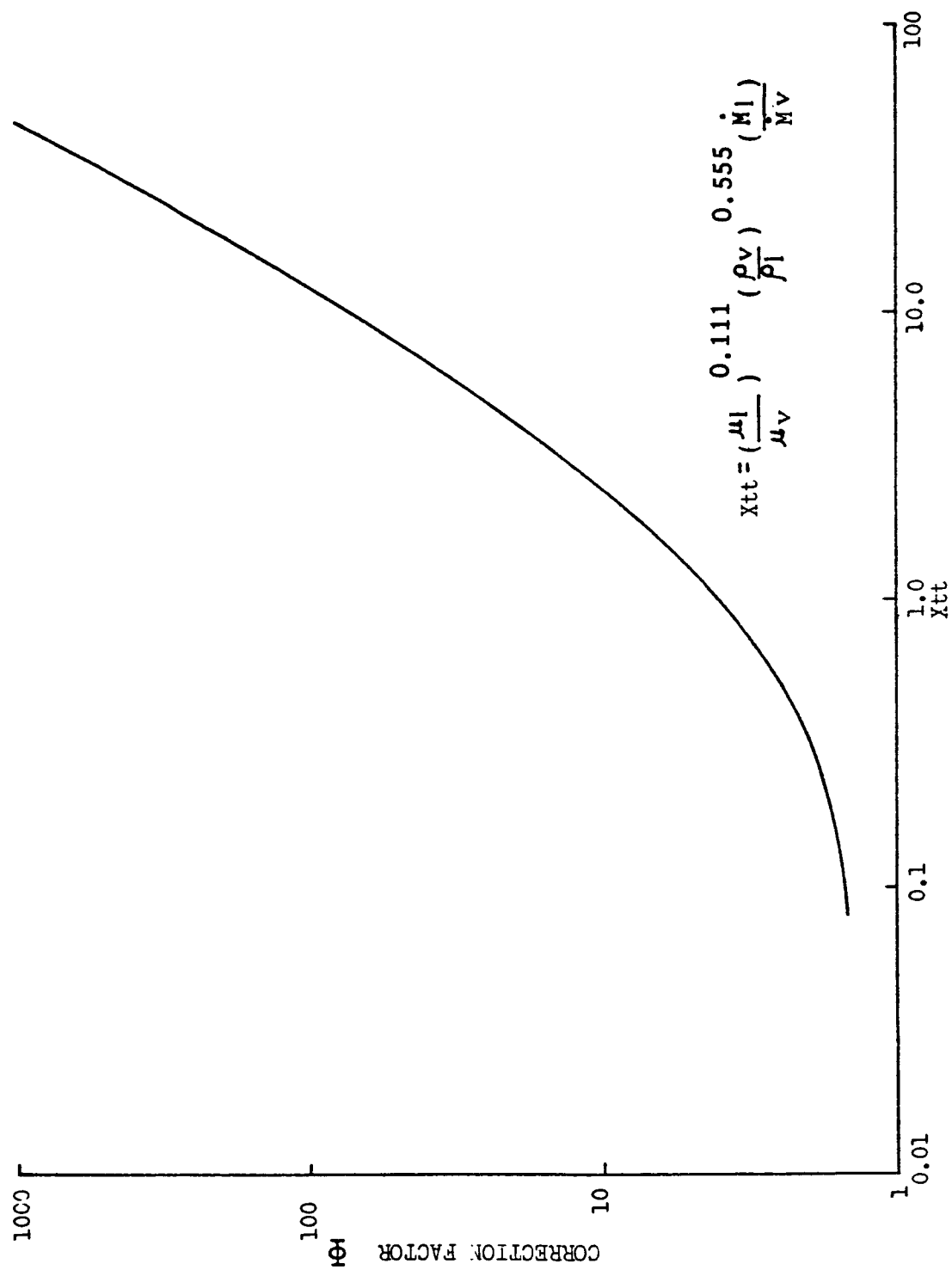


FIG. 5 TWO PHASE PRESSURE LOSS CORRECTION FACTOR

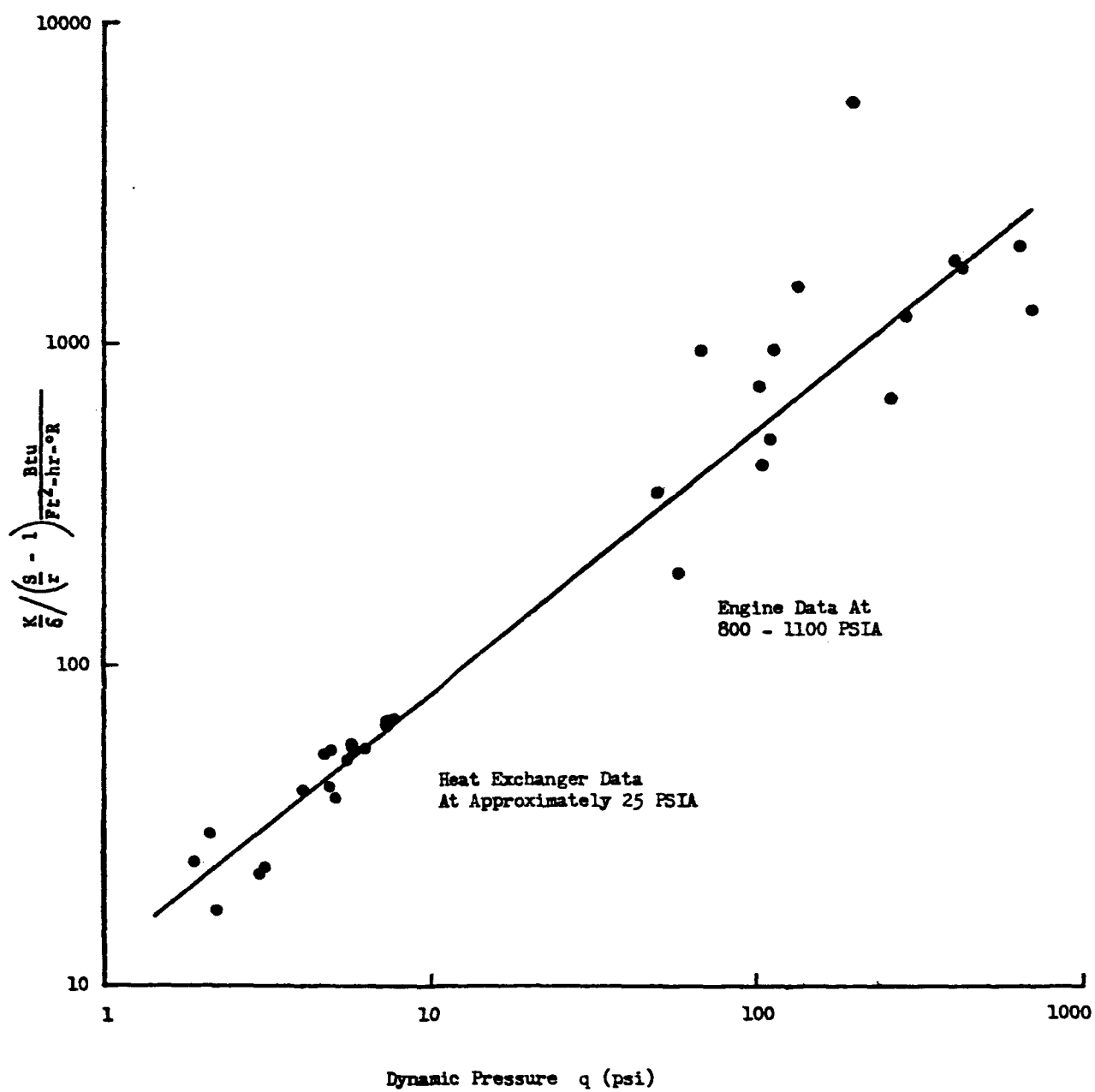


FIG. 6 PRELIMINARY CARBON RESISTANCE VS DYNAMIC PRESSURE AND MIXTURE RATIO

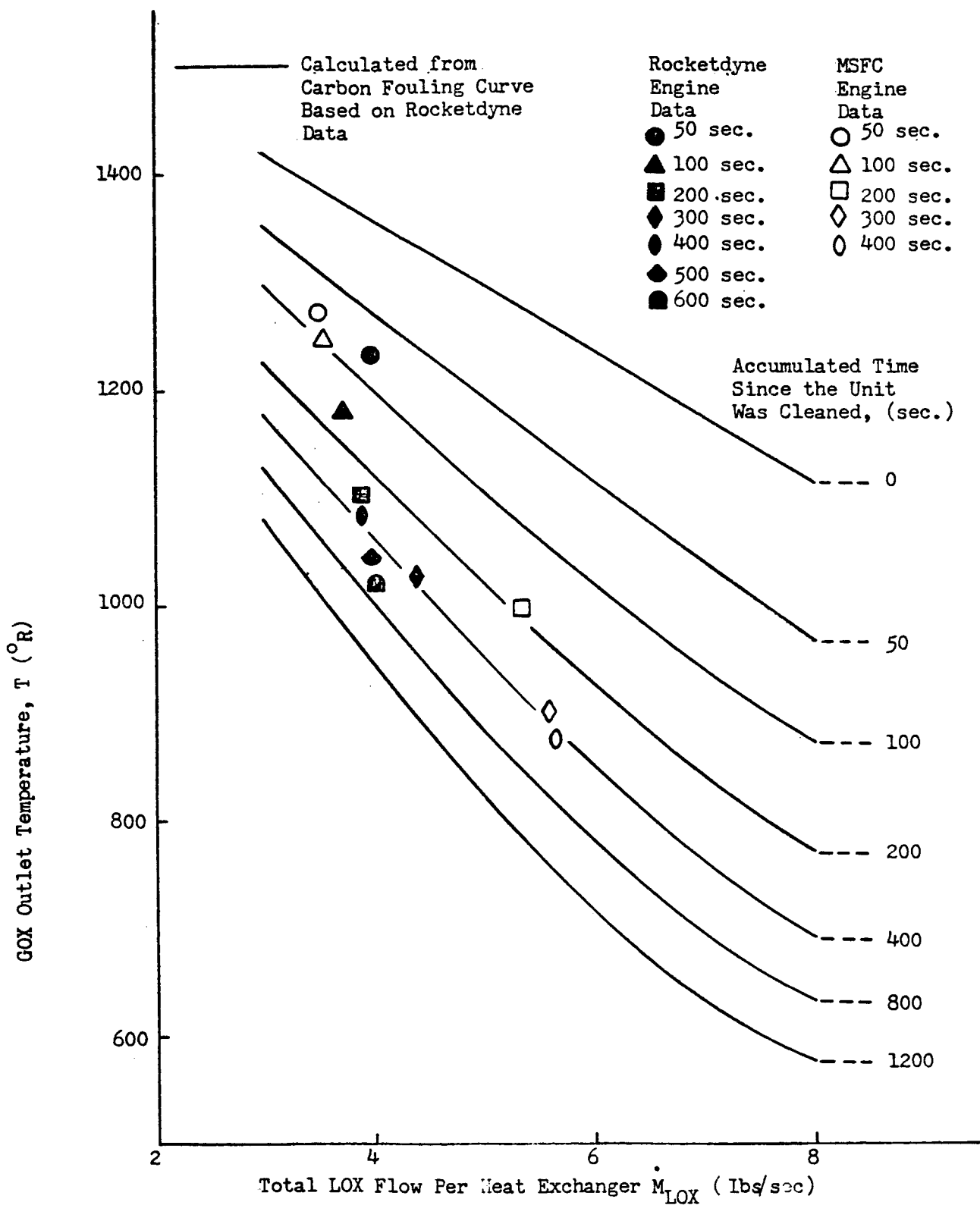


FIG. 7 GOX OUTLET TEMPERATURE VS LOX FLOWRATE FOR F-1 HEAT EXCHANGER

APPENDIX A

Ø FACTORS FOR TUBE SIDE HEAT TRANSFER CORRELATION OF HYDROGEN

$$Nu_b = 0.025(Re_b)^{0.8} (Pr_b)^{0.4} (T_w/T_b)^{-0.55} \phi_1 \phi_2 \phi_3 \phi_4$$

(1) ϕ_1 is a function of T_b as follows:

T_b (°R)	ϕ_1
40	1.0
50	1.0
60	0.38
70	0.51
80	0.70
90	0.80
100	0.92
110	0.96
>120	1.00

(2) $\phi_2 = 1 + d_i/L$, a correction for entrance effects.

(3) $\phi_3 = 0.90$ for $Re_b > 500,000$, a correction for asymmetric heating.

NOTE: Seader's corrections are recommended for regeneratively cooled high chamber pressure rocket engines. For the heat exchangers considered in this paper, $\phi_3 = 1.0$.

(4) $\phi_4 = 1 + 1000 (\epsilon/d_i) (\log_{10} Re_b - 5.625)$ for $\epsilon/d_i < 0.0005$;
 $Re_b > 500,000$, a surface roughness correction.

APPENDIX B

Ø FACTORS FOR TUBE SIDE HEAT TRANSFER CORRELATION OF OXYGEN

$$Nu_b = 0.023(Re)_b^{0.8} (Pr)_b^{0.4} (T_w/T_b)^{-0.34} \phi_1 \phi_2$$

(1) ϕ_1 is a function of T_b and T_w as follows:

ϕ_1 Correction Factor			
T_b ($^{\circ}R$)	T_w , ($^{\circ}R$)		
	600	1000	1800
200	1.3	0.95	—
278	0.58	0.42	0.32
300	0.68	0.556	0.434
350	0.836	0.764	0.655
400	1.0	1.0	1.0
> 400	1.0	1.0	1.0

$$(2) \phi_2 = \frac{1.48}{(L/d_i)^{0.1}} \text{ for } L/d_i \leq 50$$

$$\phi_2 = 1.0 \text{ for } L/d_i > 50$$

WEIGHT OPTIMIZATION OF A GAS GENERATOR/
HEAT EXCHANGER SUBSYSTEM DURING THE
INITIAL DESIGN OF A PRESSURIZATION SYSTEM:
TWO COMPUTER PROGRAMS

by

Wayne A. Muth
Martin-Marietta Corporation
Martin Company-Denver Division
Denver, Colorado

"WEIGHT OPTIMIZATION OF A GAS GENERATOR/HEAT EXCHANGER
SUBSYSTEM DURING THE INITIAL DESIGN OF A
PRESSURIZATION SYSTEM: TWO COMPUTER PROGRAMS"

by Wayne A. Muth, Assistant Research Scientist
Advanced Technology and
Development Section
Martin Company
Denver, Colorado

On 20 November 1963, a contract, NAS 3-2574, Advanced Pressurization System for Cryogenic Propellants was started by the Martin Company in conjunction with NASA Lewis. The program encompasses the analysis, design, development, fabrication, testing, and delivery of advanced pressurization systems for the propellant tankage of cryogenic propulsion systems for space vehicles.

One of the initial steps in the program involved the comparison of a large number of potential tank pressurization systems and methods. This first list of candidates was selected for consideration by mutual agreement between NASA and Martin. From these were to be selected a lesser number of candidate systems and methods which would subsequently undergo a detailed and rigorous analysis.

A system weight analysis comprised one of the major criteria by which these first candidates were to be compared. A number of the candidate systems included a gas generator/heat exchanger subsystem as a major element of the system. Thus, the need for an efficient calculation procedure for the determination of the optimum gas

generator/heat exchanger subsystem weight was subsequently identified. It was desired that the calculation procedure be relatively fast and easy to use yet sufficiently rigorous to yield subsystem weights which would be reliably accurate for this initial comparison of overall pressurization system weights. It was felt that a program suitable for use on the IBM 1620 digital computer would prove to be of particular value and efficiency.

Two computation approaches were developed. Both are basically similar in that they are referenced to the methods presented by Kays and London in their book, Compact Heat Exchangers.¹

1. The first computer program was generated for use in the initial screening of candidate systems. Emphasis lay in obtaining firm heat exchanger weight estimates for inclusion as part of the individual overall system weights. Trial calculations were made for heat exchangers of different configurations thereby permitting a tentative configuration choice to be made by direct comparison of heat exchanger weights.
2. A second computer program was developed later for the purpose of providing information in greater detail for initial design purposes. i.e., precise definition of the heat exchanger dimensions, flow velocity characteristics, and pressure drops for a particular configuration. This second program proved particularly useful as an in-house check against design data furnished by prospective vendors.

Each of the two computer programs is now discussed in detail. Following the discussion of the first program is a description of the manner in which gas generator weights were scaled and how the combined heat exchanger/gas generator subsystem weights were calculated. The paper is concluded with a brief discussion of calculations made during the course of the contract for which they were developed.

¹ Kays, W.M., and London, A.L., Compact Heat Exchangers.

McGraw-Hill. 1958.

FIRST COMPUTER PROGRAM

A number of alternative computation methods were examined and evaluated. It was deemed important that the usual assumption (1) that the heat capacities of the two fluids be constant, and (2) that the overall heat transfer coefficient be constant, should be avoided. This ruled out the classical "log-mean temperature difference" method per se. The method selected, however, was similar in principle. Rather than calculating a mean temperature difference (i.e., log-mean), the instantaneous temperature difference between hot and cold fluids is calculated for only a small increment of heat exchanger surface. This procedure is repeated until a specified final temperature is reached. The incremental lengths of heat exchanger surface are then summed to yield a total value for the surface required.

Consider Figure 1. This is the conventional plot of temperature history as a function of surface area, ... i.e., the two curves trace the respective temperature of the hot and cold fluids during travel through the exchanger. As drawn, the curves are applicable to parallel flow. (Analogous figures can be drawn for counter-flow and cross-flow cases.) The calculation procedure is comprised of four steps:

1) Initial input to the program

- a) cold fluid flow rate -- \dot{m}_c
- b) initial cold fluid temperature -- T_{c0}
- c) final cold fluid temperature -- T_{cf}
- d) hot fluid flow rate -- \dot{m}_h
- e) initial hot fluid temperature -- T_{h0}
- f) a value for the amount by which T_{h0} is to be decremented for any given step -- ΔT_h , and T_{h0}

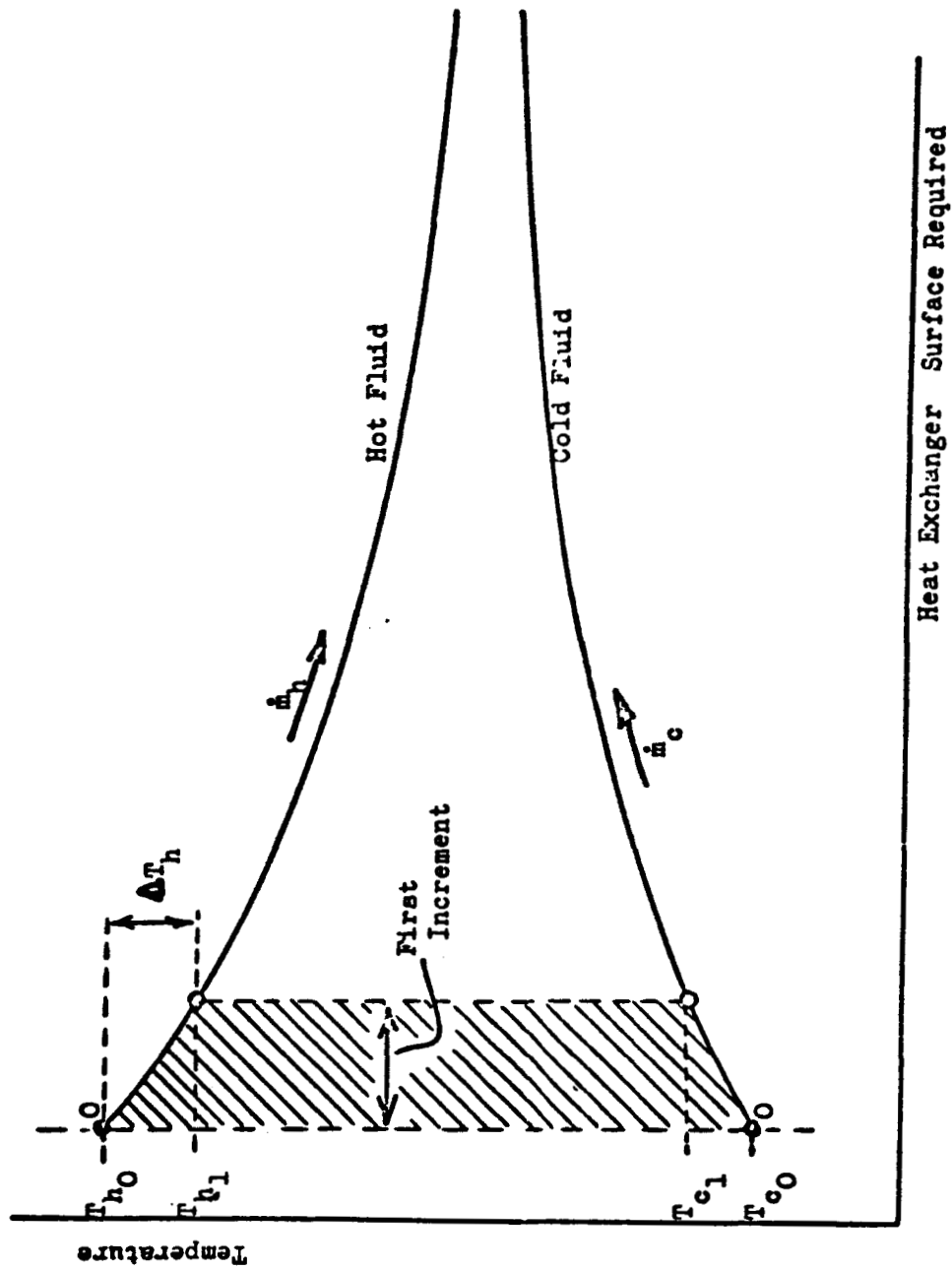


Fig. 1 Temperature Profile Along The Length
of a Parallel Heat Exchanger

- g) certain required physical properties and parameters such as specific heat, viscosity, and thermal conductivity (as functions of temperature) for both fluids, and the inside and outside tube diameters.

Items (a), (b) and (c) are dictated by the requirements of the pressurization system, (d) is an arbitrary trial value, (e) is dictated by restrictions on the gas generator outlet temperature, and (f) is arbitrary (usually 100°R).

2) Calculations over the first increment (shaded area in

Figure 1):

- a) T_{h1} is set as $T_{h0} - \Delta T_h$
- b) The heat made available for transfer over the first increment is

$$q_{h0 \rightarrow 1} = (\dot{m}_h) \left(c_{p_{h0 \rightarrow 1}} \right) \left(T_{h0} - T_{h1} \right) \left[\text{BTU} \right]$$

where $c_{p_{h0 \rightarrow 1}}$ is the instantaneous constant pressure heat capacity of the hot fluid evaluated at the mean temperature, $1/2 \left(T_{h0} + T_{h1} \right)$.

- c) The heat transferred to the cold fluid is assumed equal to that liberated by the hot fluid (an arbitrary loss may also be considered if desired):

$$q_{c0 \rightarrow 1} = q_{h0 \rightarrow 1}$$

Also

$$q_{c0 \rightarrow 1} = (\dot{m}_c) \left(c_{p_{c0 \rightarrow 1}} \right) \left(T_{c1} - T_{c0} \right)$$

Rearranging, T_{c_1} is calculated directly

$$T_{c_1} = \left[\frac{q_{c_{0 \rightarrow 1}}}{\dot{m}_c (c_{p_{c_{0 \rightarrow 1}}})} \right] + T_{c_0}$$

where $c_{p_{c_{0 \rightarrow 1}}}$ is evaluated (for convenience) at temperature T_{c_0} .

- d) For the increment under discussion, the basic heat transfer relation for a surface heat exchanger is applied as

$$Q_{0 \rightarrow 1} = U_{0 \rightarrow 1} A_{0 \rightarrow 1} \Delta T_{0 \rightarrow 1} = q_{h_{0 \rightarrow 1}} = q_{c_{0 \rightarrow 1}}$$

where $U_{0 \rightarrow 1}$ is the overall heat transfer coefficient for the increment $0 \rightarrow 1$, $A_{0 \rightarrow 1}$ is the heat transfer area, and $\Delta T_{0 \rightarrow 1}$ is the mean temperature difference between hot and cold fluids.

Examining individual terms,

$$U_{0 \rightarrow 1} = 1 / \left(1/h_{i_{0 \rightarrow 1}} + 1/h_{o_{0 \rightarrow 1}} \right)$$

where $h_{i_{0 \rightarrow 1}}$ is the convective film coefficient for the inside of the tube, $h_{o_{0 \rightarrow 1}}$ for the outside (Note: the

term recognizing conduction through the tube wall can be neglected for the thin wall tubes that are normally used).

The mean temperature difference over the increment is

$$\begin{aligned} \Delta T_{0 \rightarrow 1} &= 1/2 (T_{h_0} + T_{h_1}) - 1/2 (T_{c_1} + T_{c_0}) \\ &= 1/2 (T_{h_0} + T_{h_1} - T_{c_1} - T_{c_0}). \end{aligned}$$

The surface area of the heat exchanger is

$$A_{0 \rightarrow 1} = (\pi)(\text{tube diameter})(\text{tube length}_{0 \rightarrow 1})$$

Thus, the incremental tube length is expressed in functional notation as:

$$\text{tube length}_{0 \rightarrow 1} = f\left(T_{h_0}, T_{h_1}, T_{c_0}, T_{c_1}, \text{tube diameter}, h_{i_{0 \rightarrow 1}}, h_{o_{0 \rightarrow 1}}, q_{h_{0 \rightarrow 1}}\right)$$

All independent variables are now known except $h_{i_{0 \rightarrow 1}}$ and $h_{o_{0 \rightarrow 1}}$. These are evaluated in the computer program by use of the general term

$$(\text{Stanton No.})(\text{Prandtl No.})^{2/3} = g(\text{Reynolds No.})$$

The value for $g(\text{Reynolds No.})$ is obtained from figures presented in reference 1 (c.f. figures 40 through 106 for flow external to the tubes, figures 29 through 32 for flow inside the tubes). These figures pertain to a series of heat exchangers employing differently oriented tubes, in various shapes and configurations. For any such choice of heat exchanger components, entry into the figures at the appropriate value of Reynolds number (based on a prior hand calculation or a selected range) yields the value for $g(\text{Reynolds Number})$.

The left side is rewritten as

$$\left(\frac{h}{c_p \rho V} \left(\frac{c_p \mu}{k}\right)^{2/3}\right) = \frac{h \mu^{2/3}}{c_p^{1/3} \rho V k^{2/3}} = \left(\frac{h \mu^{2/3}}{c_p^{1/3} k^{2/3}}\right) \left(\frac{1}{\rho V}\right)$$

$$\left(\frac{h \mu^{2/3}}{c_p^{1/3} k^{2/3}}\right) \left(\frac{\text{tube diameter}}{(\text{Reynolds\#}) \mu}\right) = \frac{(h) (\text{tube diameter})}{(c_p^{1/3})(k^{2/3})(\mu^{1/3})(\text{Reynolds\#})}$$

Thus, $h_{i \rightarrow 1}$ and $h_{o \rightarrow 1}$ are each evaluated by the

general expression

$$h = \frac{(c_p^{1/3})(k^{2/3})(\mu^{1/3})(\text{Reynolds No.}) (g(\text{Reynolds No.}))}{(\text{tube diameter})}$$

where the properties c_p , k , and μ are evaluated for the respective fluids at the respective film temperatures and the parameter $g(\text{Reynolds Number})$ is obtained from the figures of reference 1. Each of the two film temperatures is assumed to be the mean between wall and bulk temperature; the wall temperature is assumed to be the mean between hot and cold fluid temperature.

3) Calculations over remaining increments

The procedures applied to the first increment are successively repeated over a series of additional increments until the desired value for T_{c_f} is reached. Incremental tube lengths are summed to yield overall length.

4) Repeated Trials .

Sample results are shown in Figure 2. Curves A represent the fluid temperature profiles which would be found if a relatively high value of hot fluid flow rate, \dot{m}_h , were selected in the first attempt at computation. Curves B, represent the profiles if too low a flow rate were chosen (and are invalid since T_{c_f} was not reached). Successive trials yield the families of curves C which represent valid solutions for the problem. When a satisfactory solution has been obtained, the weight of the heat exchanger tube bundle is calculated (by hand) directly from the value of heat exchanger tube length determined

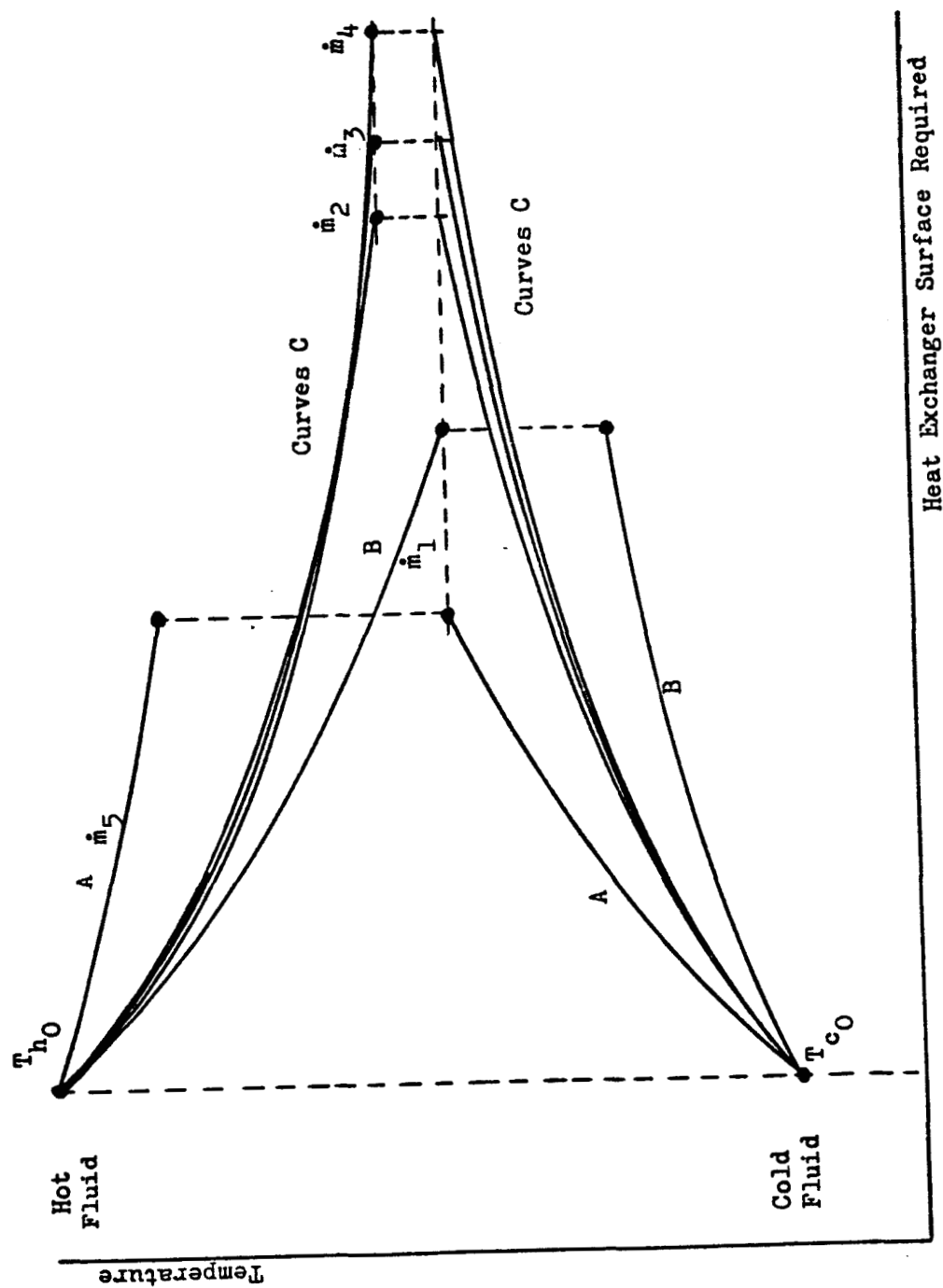


Fig. 2 Heat Exchanger Heat Transfer Characteristics.

by the program. Total heat exchanger weight (including case and header) is then determined either by empirical scaling from an existing similar heat exchanger or by directly summing the weight of these metal components needed to physically enclose the tube bundle.

The FORTRAN listing of this program is presented in Figure 3. The flow diagram for the program is given in Figure 4.

GAS GENERATOR WEIGHT SCALING AND CALCULATION OF COMBINED SYSTEM WEIGHT

Considering weight of heat exchanger alone, it is seen that weights always become successively lower as higher values of hot gas flow rate are considered. On the other hand, as the hot gas flow rate increases, the weight of the gas generator and gas generator propellant increases. Hence, weight optimization of the combined heat exchanger-gas generator subsystem is the pertinent consideration rather than the weight of either system alone.

The gas generator hardware weight is arbitrarily scaled for the gas generator as

$$W_{\text{gg hardware}} = \left(\sqrt[4]{\frac{\dot{m}_h \text{ (lb/sec)}}{0.0417}} \right) (8) \text{ [lbs]}$$

This empirical scaling expression was derived with primary reference to a H_2/O_2 gas generator manufactured by Sundstrand Aviation of Denver. The Sundstrand unit weighs eight pounds and has a throughflow of 0.0417 lb/sec. The scaling expression is based on the assumption that as flow rate is altered, only the cross-sectional area is changed, the length of the gas generator and the flow velocity remaining constant. The scaling expression is felt to be realistic for flow rates of one pound per second or less but would be overly conservative at high flow rates.

```

C      DIGITAL COMPUTER PROGRAM NO. 1 --- ADVANCED PRESSURIZATION SYSTEMS
C
C      CONTRACT -- MARTIN COMPANY, DENVER COLORADO
C      DIMENSION KODE(6),X(4),CH(4,20),XMH(4,30),CONH(4,30),XLENG(4,6)
C      DIMENSION KEY(4),C(4,6),XNUC(30),CCNC(30),CPCOL(30)
C
1  FORMAT(5I4)
5  FORMAT(4F10.0)
5  FORMAT(I3,F4.0,F8.0,2F8.2,2F4.2,F6.2)
16  FORMAT(I5,3X,I2F6.0)
19  FORMAT(20X,F20.0,2I6)
304  FORMAT(14X,2H (+5.0,2H ))
411  FORMAT(/,17H FIGURE NUMBER IS, I4)
416  FORMAT(20X,4F10.0)
900  FORMAT (I3,4F10.0,2F7.3)
C
C      VARIABLE NAMES DEFINED AS FOLLOWS....KODE=FIGURE NUMBER FROM KAYS
C      AND LONDON BOOK DESCRIBING THE HEAT EXCHANGER (SIX VALUES MAX)....
C      XMOLE FRACTION OF HOT GAS CONSTITUENTS, FIRST ARGUMENT DESCRIBES
C      CONSTITUENT, SECOND ARGUMENT SPECIFIES TEMPERATURE....
C      XMU=VISCOSITY, HOT GAS (ARGUMENTS AS ON CH)....CONH=THERMAL
C      CONDUCTIVITY (ARGUMENTS AS ON CH)....XLENG=HEAT EXCHANGER LENGTH
C      IN FEET....REY=REYNOLDS NUMBER (ANY FOUR VALUES)....C=DIMENSIONLESS
C      HEAT TRANSFER PARAMETER AS TAKEN FROM FIGURES IN KAYS AND LONDON
C      ....XNUC,CCNC,CPCOL ARE, RESPECTIVELY, VISCOSITY, CONDUCTIVITY, AND
C      SPECIFIC HEAT FOR COLD GAS (FUNCTS. OF TEMP)....NGGPC=NO. OF HOT
C      GAS CONSTITUENTS....WDRF=NO. OF REYNOLDS NO. VALUES TO BE USED
C      ....NO=16=NUMBER OF DIFFERENT HT XR CONFIGURATIONS BEING
C      CONSIDERED....DOUTS, DINS, RESPECTIVELY = OUTSIDE AND INSIDE HT XR
C      TUBE DIAMETERS (INCHES)....C2=DUMMY VARIABLE....NO=ANY ARBITRARY
C      REFERENCE NUMBER FOR CURRENT COMPUTER RUN....QLOSS=PERCENT OF HEAT
C      AVAILABLE FOR TRANSFER TO COLD FLUID WHICH IS NOT TRANSFERRED....
C      TH, TC (HESPY) = CURRENT VALUES OF HOT AND COLD GAS TEMPS....
C      THEND, TCEND (HESPY) = FINAL DESIRED HOT AND COLD FLUID TEMPS....
C      UTHOT=INCREMENT ON HOT GAS TEMP OVER ONE COMPUTATION INTERVAL....
C      WDUHT, WDUOTC (HESPY)=HOT AND COLD FLUID MASS FLOW RATES....
C      XMH=HOT GAS MOLECULAR WEIGHT....ICAD=COLD GAS TEMP FOR AN
C      ADIABATIC HT XR....INO=ITERATION NUMBER....QCSUM=SUMMATION OF HEAT
C      ENERGY TRANSFERRED....BMUP,XKHOT,CPH (HESPY)=CURRENT VALUES OF
C      HOT FLUID VISCOSITY, CONDUCTIVITY, AND SPECIFIC HEAT....DQ, NQTOC=

```

Fig. 3 FORTRAN Listing, First Computer Program

Reproduced from
best available copy.

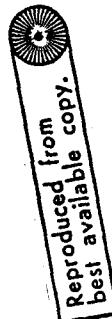

```

UTCAD=00/(WOUTC*CPC)
TH=TH+JTHOT
TC=TC+JTCOL
IF (TC-TCEND) 41,41,40
40 DELTH=PUTC*CPH*(TCEND-TC+JTCOL)/(WDOH*CPH*(1.-OLOSS/100.))
TH=TH+JTHOT-UFLTH
TC=TCEND
DO=WDOTH*CPH*DELTH
DQTOC=06*(1.-OLOSS/100.)
UTCAU=00/(WOUTC*CPC)
41 WCSUM=WCSUM + DQTOC
INU=INU + 1
PRINT 9,INU,OLOSS,TH,TC
TCAD1=TCAD1 + UTCAD
PRINT 399,TCAD1
WUOT=DJ*5500./(TH-TC)
CPH=U.
LTEMP= (A.*TC + TH)*.0025 + .63
JTEMP=(Z.*TH + TC)*.0025 + .63
DO 12 I=1,NCGPC
CPH=CPH+X(I)*CH(I,JTEMP)/XMMH
WUOH=XUOH+X(I)*XUOH(I,JTEMP)
12 AKUOT=XKHOT+X(I)*CONH(I,JTEMP)
DASEC=(CPCOL(LTEMP)*XUJC(LTEMP))*333*CONC(LTEMP)**.667*12.
DASEH=(CPH*PMMH)**.333*XKHOT**.667*12.
DO 20 J=1,NOFIG
PRINT 411,KOUE(J)
DO 415 I=1,MOREY
NIEPASEC*REY(I)*C(I,J)/PINS
NO=BASEH*REY(I)*C(I,J)/NOITS
UE1./(1./HU + 1./HI)
415 ALNG(I,J)=XLFG(I,J) + WUOT/(U*C2)
20 PRINT 416,XLNG(I,J)
50 IF (TC-TCEND) 50,35,35
35 PRINT 19,OLSUM
GO TO 4
END

```

*

Fig. 3 (continued)



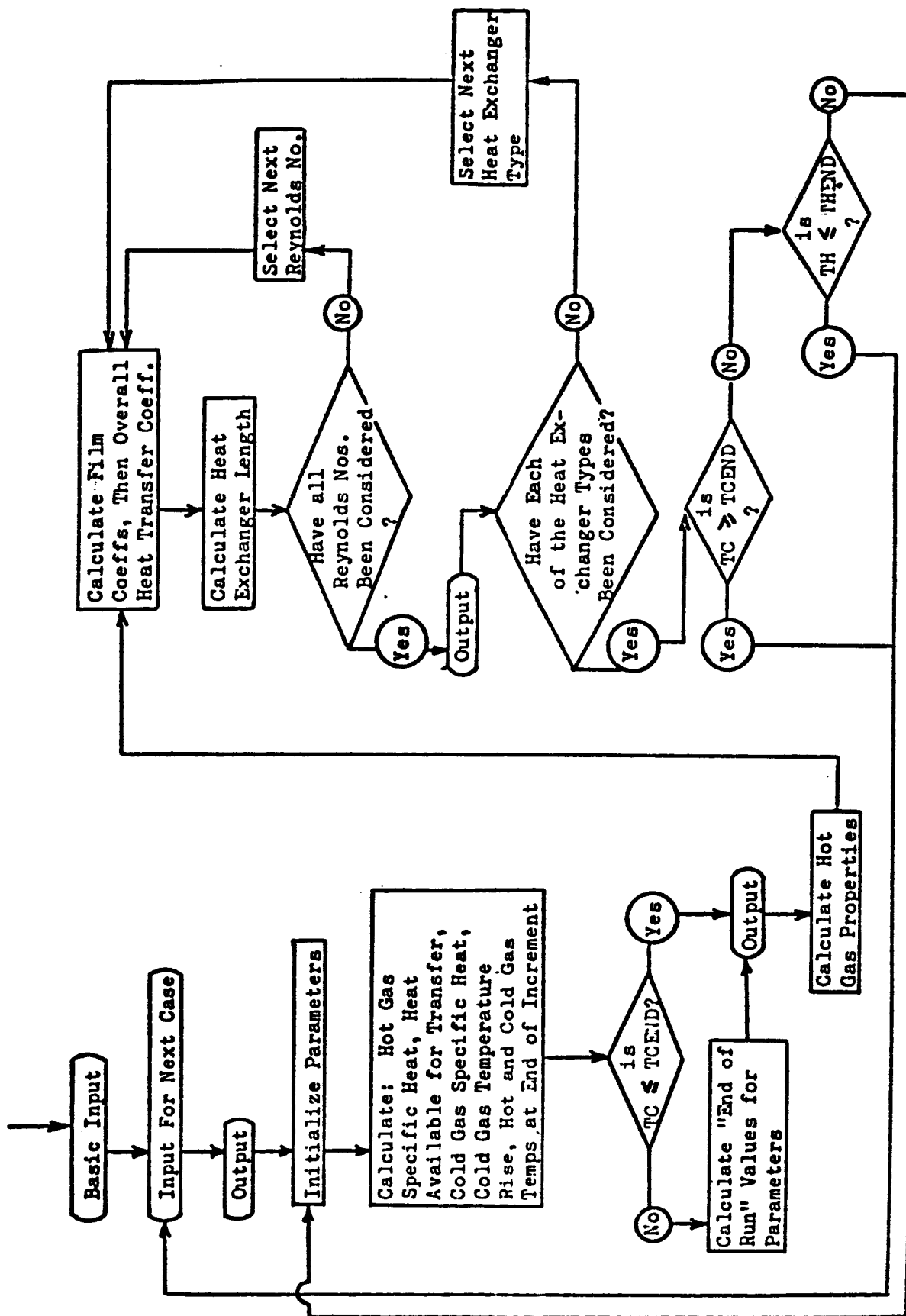


Fig. 4 Flow Diagram, First Computer Program

The overall subsystem (including gas generator propellant) thus has a weight equal to

$$\left(\begin{array}{c} \text{heat exchanger weight} \\ \text{at a given } \dot{m}_h \end{array} \right) + \left(\begin{array}{c} \text{gas generator weight} \\ \text{for this } \dot{m}_h \end{array} \right) + \underbrace{\left(\frac{\dot{m}_h}{\dot{m}_c} \right) (m_c)}_{\text{gas generator propellant weight}}$$

where \dot{m}_h = hot gas flow rate, lb/sec,

\dot{m}_c = cold gas (i.e., pressurant) flow rate, lb/sec,

and m_c = total pressurant required for the mission.

(Note that the third term of this relation implies that the hot gas and cold gas flow concurrently.)

As employed in the development studies under the present contract, a concurrent effort had by this time established certain paired trial values for \dot{m}_c and m_c which could be expected to bracket those values which would exist for the optimum (i.e., lightest weight) overall pressurization system. Taking one of these pairs of \dot{m}_c and m_c values, the subsystem weight was established by the equation above for trial values of \dot{m}_h . Side-by-side comparison at a series of \dot{m}_h values then identified the optimum choice of \dot{m}_h for the particular values of \dot{m}_c and m_c used. It must be borne in mind that the lowest overall pressurization system weight need not necessarily go hand-in-hand with the lightest heat exchanger/gas generator subsystem. One trial value each for \dot{m}_c and m_c with the associated trial values of \dot{m}_h yield one data point, viz. a value to be included in the weight summation for the overall system. Additional trials on \dot{m}_c , m_c , and \dot{m}_h for a series of heat exchanger configurations then permit the lightest overall system weight to be identified.

SECOND COMPUTER PROGRAM

The second program was developed to provide detailed information which would be useful for initial component design and for in-house confirmation of designs submitted by vendors. The logic of the second program differs from the first as follows:

- 1) Thermal and transport properties for both the cold and hot gases are evaluated at their respective mean temperatures* (where each mean temperature is simply the arithmetic mean between inlet and outlet temperature), i.e., a step-wise integration method is not employed as in the first program.
- 2) A "best" value of hot gas flow rate is calculated in place of the previous trial-and-error hot gas flow rates. This is calculated as

$$\dot{m}_{\text{hot}} = \dot{m}_{\text{cold}} c_{p_{\text{cold, avg}}} \Delta T_{\text{cold}} / c_{p_{\text{hot, avg}}} \Delta T_{\text{hot}}$$

where \dot{m} = gas flow rate,

$c_{p_{\dots \text{avg}}}$ = specific heat evaluated at the respective mean temperature,

and ΔT = absolute value of the temperature change during flow through the heat exchanger.

- 3) Reynolds numbers for the hot and cold gases are calculated.
- 4) Mach number is calculated at four stations in the heat exchanger (hot inlet and exit, cold inlet and exit).
- 5) Pressure drops within the heat exchanger are computed.

* A more restrictive assumption recognizing the difference in temperature history patterns for parallel flow, counter-flow, and cross-flow heat exchangers would have been desirable at this point but would have necessitated putting the program on a larger computer. This was not desired due to the relatively more favorable turn-around time for problem solving on the 1620 machine.

The method used (and sequential steps followed) in the second program are as follows:

- 1) Descriptive system parameters are input to the program.

For both the hot and cold gases, the input specifies the inlet pressure, molecular weight, and inlet temperature. For the cold gas only, the mass flow rate and the desired temperature at the heat exchanger outlet are specified. The amount by which the hot gas temperature at the heat exchanger outlet exceeds that for the cold gas is specified. For the particular heat exchanger under consideration, input parameters include the hot and cold gas side hydraulic diameters and the cross-sectional flow areas for an arbitrary one cubic foot tube bundle. Further descriptive parameters -- each for a one cubic foot tube bundle -- specify heat exchanger surface area, number of tubes, and tube bundle weight. Both the dimensionless heat transfer parameter and also a pressure drop (friction) parameter -- from figures 29-32 and 40-106 in reference 1 -- are specified by inputting (for each) the coefficients A and B which depict straight line fits to the figure curves in the form

$$\ln y = A \ln x + B.$$

(This permits use of values for the parameters corresponding to the Reynolds numbers calculated by the program.)

A value for the number of "heat transfer units" (NTU's) is also required and is obtained, as appropriate, from one of the figures 2-13 in reference 1 or may also be calculated

by the expression

$$N = \frac{\Delta T_g}{\overline{\Delta T_m}}$$

where ΔT_g = hot gas temperature change through the heat exchanger
and $\overline{\Delta T_m}$ is the log-mean temperature difference between
the two fluids.

- 2) Tables of transport and thermal properties are input as functions of temperature,
- 3) An arbitrary tube bundle size of one cubic foot is selected as a first try upon which subsequent iterations are based,
- 4) Hotside and coldside mean temperatures are calculated,
- 5) Hotside mean specific heat is calculated,
- 6) Calculations are made for sonic velocity $\left(= \sqrt{\gamma gRT} \right)$, density (from perfect gas law), flow velocity (from continuity equation), MACH number (from the definition), and Reynolds number (from the definition). The film coefficients, h , for hotside and coldside gases are calculated from the figures in reference 1 following the approach used in the first computer program,
- 7) The overall heat transfer coefficient is computed as

$$U_{\text{overall}} = 1 / \left(1/h_{\text{inside}} + 1/h_{\text{outside}} \right)$$

- 8) A new value for the required heat transfer surface area, A_{new} , is calculated by the expression .

$$A_{\text{new}} = \frac{(N)(\dot{m}_h)(c_{p_h})(3600)}{U_{\text{overall}}}$$

$$\left[\text{ft}^2 \right] = \left[\frac{\text{--} \mid \text{lb} \mid \text{BTU} \mid \text{sec} \mid \text{hr-ft}^2\text{-R}}{\text{--} \mid \text{sec} \mid \text{lbR} \mid \text{hr} \mid \text{BTU}} \right]$$

where N = the number of "heat transfer units",

\dot{m}_h = hot gas flow rate,

c_{p_h} = mean specific heat of the hot gas,

U = overall heat transfer coefficient.

- 9) The newly calculated value of required surface area is compared to the surface area displayed by the arbitrary one cubic foot tube bundle. If the two agree to within $\pm 2\%$, the calculation ceases and descriptive information concerning the heat exchanger is output.

If there is not an agreement to within 2%, a new iteration beginning with Step 6 is undertaken after first adjusting the heat exchanger dimensions to reflect the most recently calculated value of required surface area, A_{new} . This adjustment of dimensions is considered in only two of the three dimensions, viz. the two normal to the hot gas flow path. Thus the tube bundle considered in the next iteration is caused to have a heat transfer surface area identically equal to that which is required (as calculated in the previous iteration).

Iteration is repeated until the values of required surface area agree to within 2% from one iteration to the next.

The FORTRAN listing of the program is shown in Figure 5.

The flow diagram is shown in Figure 6. A sample output from the program is shown in Figure 7.

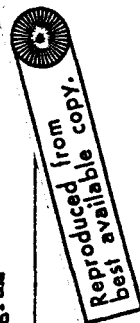
```

C DIGITAL COMPUTER PROGRAM NO. 2 --- ADVANCED PRESSURIZATION SYSTEMS
C CONTRACT -- MARTIN COMPANY, DENVER COLORADO
C
C DIMENSION HA(2),FR(2),FA(2),FR(2),VISC(2,19),CP(2,19),COND(2,19)
C DIMENSION WOUT(2),T(2),RHO(2),TMEAN(2),V(2),REFY(2),CAPRA(2),BASE(2)
C DIMENSION FILM(2),XMW(2),FIN(2),HYDIA(2),CROSS(2),SONIC(4),ZMACH(4)
C DIMENSION IDUM(2),FF(2),DELP(2)
C
C101 FORMAT (7E9.4)
C102 FORMAT (F9.0,F10.3,3X,FP.0,FA.2,/)
C104 FORMAT (4X,5H AREA,5X,5HCP,5HOUT,5X,7HMDOUT,5X,5HNOT 5X,5HMDNOTCOLD)
C105 FORMAT (14H HT XR WEIGHT=F12.0,19H LBS. 6G WEIGHT=F 6.1,5H LRS.)
C106 FORMAT (17H HT XR DIMENSIONS,F12.1,2H X,F12.1,1H X 12.(ALL INCHES))
C108 FORMAT (//,11H FIGURE NO.,F6.0,/)
C111 FORMAT (10F6.0)
C112 FORMAT (32H MACH NOS. PUT IN HOT OUT,21H COLD IN COLD OUT)
C113 FORMAT (11X,4F10.3)
C114 FORMAT (20H PRESSURE DROP (PSI).....HOT,F9.1,5H COLD,F9.1,////)
C115 FORMAT (30H AVO. RETARDS NOS. (HOT/COLD).....,F10.0,2H /,F10.0)
C116 FORMAT (29H PRESSURE DROP NOT CALCULATED)
C
C SUBSCRIPT 1 IS FOR HOT FLUID 2 IS FOR COLD FLUID
C (1,1) AND (2,1) RESPECTIVELY, REFER TO STREAM 1 (HOT) OR 2 (COLD)
C AT TEMPERATURE OF 1*100 (RANKINE)
C
C VISC=VISCOSITY (LB/HR-FT) CP=SP. HEAT (BTU/LR-R)
C COND=THERMAL CONDUCTIVITY (BTU/HR-FT-F) VELOCITY (FT/SEC)
C RHO=DENSITY (LB/CUBIC FT) HYDRAULIC DIA IN INCHES
C ANTU=NUMBER OF HEAT TRANSFER UNITS WHERE AREA IS IN SQ.FT.
C FILM = VALUES FOR THE FILM COEFFICIENTS IN BTU/HR-FT-F
C U IS THE OVERALL HT XFR COEFFICIENT
C CAPRA(LR-RTU/SEC-LB-R) = MASS FLOW RATE TIMES SPECIFIC HEAT
C CROSS(1) AND (2) ARE FLOW CROSS-SECTION AREAS FOR HOT AND COLD RESPY. ..
C (UNITS ARE SQ FT)
C
C PIN(1) AND PIN(2) ARE INLET PRESSURES IN PSI
C IDELT IS DELTA TEMP BETWEEN HOT AND COLD STREAMS AT EXIT OF HT XR
C AREF=SURFACE AREA (SQFT) FOR A ONE CUBIC FOOT HT XR TUBE BUNDLE

```

*

Fig. 5 FORTRAN Listing, Second Computer Program



```

C      T(1)=HOT GAS INLET TEMP. TO HT XR, T(2) IS COLD...
C      TTANK=TEMP OF PRESSURANT GAS DELIVERED AT HT XR OUTLET
C      WOUT=MASS FLOW RATES OF FLUIDS...JMEAN=MEAN TEMPERATURES...
C      XAW=FLUID MOLECULAR WEIGHTS...ZMACH=MACH NUMBER VALUES
C      CLUGE=SCALING FACTOR FOR WEIGHT OF HT XR AS FUNCT OF TUBE BUNDLE
C      WEIGHT...IDEL=DIFFERENCE IN HOT AND COLD FLUID TEMPS AT HT XR
C      EXIT...DEL=PERDUMMY VARIABLE FOR PRESSURE DROP...
C      REFWT=WEIGHT (LBS) OF A ONE CUBIC FOOT TUBE BUNDLE
C      REFWENO. OF TUBES IN ONE CUBIC FOOT TUBE BUNDLE
C      XHOF=FIGURE NO. FROM KAYS AND LONDON...ACRIG=HT XR SURFACE AREA
C      (FEET) AT START OF THE CALCULATION...AREAN=FWLY CALCULATED VALUE
C      OF REQUIRED SURFACE AREA (FT)...XWTE=HT XR WEIGHT (LBS)...
C      XDIME=HT XR DIMENSION (INCHES)...GWT=EGAS GENERATOR WEIGHT (LBS)
C      FOLLOWING ARE DUMMY VARIABLES...FF, IDIM, FASE, DHCOL, DENOM, SPHT1
C
C      FURTHER INFORMATION...FA AND FB ARE THE CONSTANTS IN THE EQUATION
C      FORN T=AX + B REPRESENTING THE FITTED STRAIGHT LINE FOR THE
C      DIMENSIONLESS HEAT TRANSFER PARAMETER LISTED IN FIGURES IN KAYS
C      AND LONDON BOOK...FA AND FB, DITTO, FOR FRICTION (PRESSURE
C      DROP) PARAMETER
C
C      FOR ADDITIONAL INFORMATION ON VARIABLE NAMES, SEE FLOW DIAGRAM
C
C      DO 1 I=1,19
C      1 READ 101,VISC(1,1),CP(1,1),COND(1,1),VISC(2,1),CP(2,1),COND(2,1)
C      READ 111,FA(2),FB(2),HA(2),HB(2)
C      IF=2.71d2818
C
C      A NEW CASE ALWAYS STARTS WITH A NEW SET OF CARDS AT STATEMENT 12
C
C      12 READ 111,XMW(1),XMH(2),CLUGE,PIN(1),PIN(2),IDELT,T(1),T(2),TTANK,CASE
C      READ 111,FA(1),FB(1),HA(1),HB(1),CROSS(1),AREFR,HYDIA(1),XNTU
C      READ 111,CROSS(2),HYDIA(2),REFWT,REFNT,WDOT(2),XNOF

```

*

Fig. 5 (continued)



```

AOKIG=AREFK
TMEAN(1)=(T(1) + TTANK + TDELT)*.5
TMEAN(2)=(T(2) + TTANK)*.5
TDUM(1)=TTANK + TDELT
TDUM(2)=TTANK
K=1MEAN(1)/100.
U=1MEAN(2)/100.
712 LHCOL=NDOT(2)*CP(2,J)*(TTANK - T(2))
KKK=TTANK/100. + .02
KLL=T(1)/100. + .02
DENOM=KLL - KKK + 1
SPH1EU.
DO 13 I=KKK,KLL
13 SPT1=SPH1I + CP(1,I)
SPH1=SPH1I/DENOM
WDOT(1)=LHCOL/(SPH1*(T(1) - TTANK - TDELT))
SONIC(1)=HOT IN. (2)=COLD IN. (3)=HOT OUT, (4)=COLD OUT
20 DO 2 I=1,2
SONIC(I)=(69592./XMW(I)*T(I))**.5
SONIC(I+2)=(69592./XMW(I)*TDUM(I))**.5
KHU(I)=PIN(I)*XMW(I)/(10.73*TMEAN(I))
V(1)=WDOT(1)/(RHU(I)*CROSS(I))
ZMACH(I)=V(I)*T(I) /TMEAN(I)/SONIC(I)
ZMACH(I+2)=V(I)*TDUM(I) /TMEAN(I)/SONIC(I+2)
UJJ=TMEAN(1)/100.
REY(I)=300.*HYDIA(I)*RHU(I)*V(I)/VISC(I ,JJJ)
CAPRA(I)=WDOT(1)*CP(I ,JJJ)
BASE(I)=(CP(I ,JJJ)*VISC(I ,JJJ))**.333*CONF(I ,JJJ)**.667*12.
2 FILM(I)=BASE(I)*REY(I)*F**(HA(I)*(LOG(REY(I))+HH(I))/HYDIA(I)
U=1./(1./FILM(1) + 1./FILM(2))
6066 AREAN=ANTJ*CAPRA(1)*3600./FILM(2)

```

*

Fig. 5 (continued)

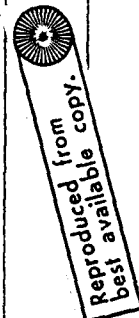



```

      IF (AREAN - AREFN) 5,11,6
      5 IF (AREAN - AREFN*.94) 10,11,11
      6 IF (AREAN - AREFN*1.02) 11,11,10
C
C      EXIT TO STM 11 IMPLIES SATISFACTORY SOLUTION HAS BEEN OBTAINED....EXIT TO
C      STM 10 IMPLIES ANOTHER ITERATION IS REQUIRED
C
      10 CROSS(1)=CROSS(1) * (AREFN/AREAN) **.5
      CROSS(2)=CROSS(2)*(AREFN/AREAN)
      AREFN=AREAN
      GO TO 20
      11 XRW=CROSS*PEFWT*AREAN/AORIG
      XDIM=12.*(AREAN/AORIG)**.5
      GGWT=((WDOT(1)/0.0416)**.05)*A.0
C      CALCULATE PRESSURE DROPS
      DO 25 I=1,2
      IF (FA(I)) 012,013,012
      013 PRINT 014
      GO TO 25
      012 RE(I)=2.*(FA(I)*LOG(REY(I)) + FA(I)
      UELP(I)=RW(I)*V(I)**2*FF(1) / (HYDRA(I)*772.)
      25 CONTINUE
      UELP(1)=UEL(I)*XDIM/12.
      PRINT 108,XNOF
      PRINT 104
      PRINT 103,AREAN,SPHT1,WDOT(1),CP(2,J),T(1),WDOT(2)
      PRINT 105,XRW,GGWT
      PRINT 106,XDIM,XDIM
      PRINT 112
      PRINT 113,ZMACH(1),ZMACH(3),ZMACH(2),ZMACH(4)
      PRINT 115,REY(1),REY(2)
      PRINT 114,UEL(1),UEL(2)
      GO TO 12
      END

```

Fig. 5 (continued)



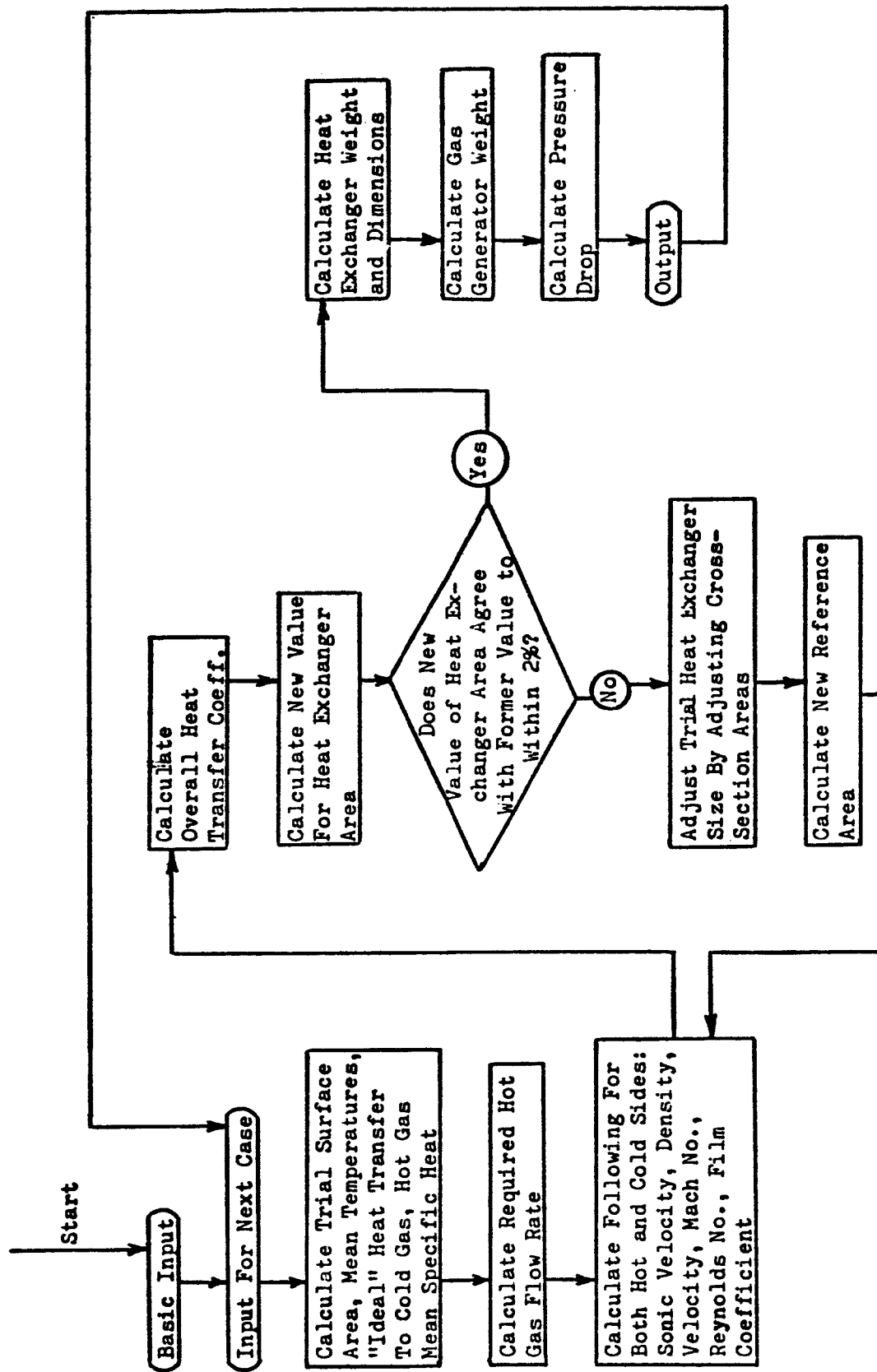


Fig. 6 Flow Diagram, Second Computer Program

FIGURE NO. 92.

AREA	CPHOT	MOOTHOT	CPCOLD	THOT	MDOTCOLD
93.	1.721	3.645	1.250	1660.	5.00

HT XR WEIGHT=	97. LBS.	GG WEIGHT=	74.8 LBS
HT XR DIMENSIONS	9.8 X		9.8 X 12. (ALL INCHES)
MACH NOS.	HOT IN	HOT OUT	COLD IN COLD OUT
	.130	.095	.008 .039

AVG. REYNOLDS NOS. (HOT/COLD)..... 10676. / 162810.

PRESSURE DROP NOT CALCULATED

Fig. 7 Sample Output, Second Computer Program

DISCUSSION

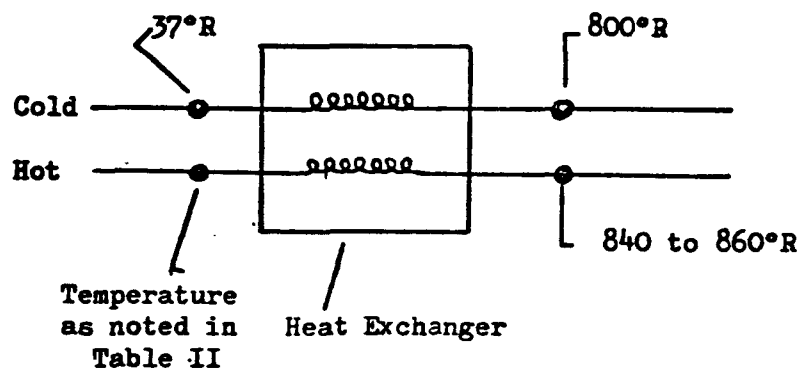
Close agreement exists between typical results obtained by either of the two programs noted and information quoted by a prospective vendor* (see Table I below).

Table I - Comparison of Heat Exchanger Computation Methods...For Helium at 5 lb/sec Flow Rate, from 37°R to 800°R...Hot Gas Entering at 1660°R

	Hot Gas Flow Rate	Heat Exchanger Weight	Dimensions
First Program	3.60 lb/sec	110 lbs	--
Second Program	3.645	97	10" x 10" x 12"
Vendor Data	3.62	90	10" x 10" x 12"

The first of the two programs was also employed to compare the performance of various prospective gas generator propellant combinations wherein the hot gas from the gas generator is used directly as the hot fluid in a simple heat exchanger. Any desired hot gas composition and temperature could be considered by the program.

The heat exchanger which was considered in the comparison is as shown below. The results which were obtained are shown in Table II.



* The calculation method employed by the prospective vendor is from Katz, et al. Correlation of Heat Transfer and Pressure Drop for Air Flowing Across Banks of Finned Tubes. University of Michigan Engineering Research Institute Report No. 30, December 1954.

Table II - Comparison of Prospective Gas Generator Propellant Combinations

Gas Generator Propellants	Hot Gas Inlet Temperature	Required Hot Gas Flow Rate for a Helium Flow Rate of 0.95 lb/sec
H_2/O_2	1800°R	0.55 lb/sec
50% N_2H_4 -50% UDMH/ N_2O_4	2060°R	1.02 lb/sec
N_2H_4 Decomposition	2460°R	0.82 lb/sec
N_2H_4 Decomposition	2060°R	1.09 lb/sec
50% N_2H_4 -50% UDMH/ H_2O_2	1822°R	1.26 lb/sec

Results were as had been anticipated. Combustion products from an H_2/O_2 gas generator operating below 2000°R contain 80 to 85% H_2 , the remainder H_2O . It was the relatively much higher heat capacity of the H_2 to which the higher performance could be attributed. Because of the higher heat capacity, a lesser product flow rate is thereby required through the heat exchanger. The results from this use of the computer program constituted one consideration which aided in identifying an H_2/O_2 gas generator as being a particularly sound choice for the pressurization systems being considered (H_2 and O_2 were to be the onboard main engine propellants as well).

It has not been intended that prospective users of either of the programs discussed in this paper necessarily adopt these methods in their present exact form. Variations of the methods might be more attractive for use in certain other, closely allied (but not identical) applications. The particular merit in both of the programs discussed is felt to lie in their ease of use and their fast production time on any of the small digital computers presently in use.

ADDENDUM -- SAMPLE INPUT PARAMETERS FOR SECOND COMPUTER PROGRAM

These values are suggested as sample inputs to the program. Entry into the table vertically is in accordance with the figure number from Kays and London. Values for HA and HB are for the laminar flow portion of the curves. The value for XNTU must be calculated for the specific case at hand.

DISCLAIMER ... Inputs corresponding to figure 92 only have been run on the computer program and appear to be satisfactory. The remaining have not been checked out.

	Figure No. from Kays & London					
	92	93	94	95	96	97
XNOF	92	93	94	95	96	97
FA (1)	- .06379	- .15274	- .16569	Not Given	- .22887	- .22553
FB (1)	-2.91287	-2.08318	-1.89225	Not Given	-1.55714	-1.63765
HA (1)	- .49939	- .35410	- .39429	- .12368	- .36079	- .36848
HB (1)	- .97313	-1.96022	-1.54503	-2.54972	-1.76752	-1.80436
TDELT	80. —————→					
FA (2)	- .20906 —————→					
FB (2)	- .98543 —————→					
HA (2)	- .43054 —————→					
HB (2)	- .92719 —————→					
CROSS (2)	.10318	.10318	.13059	.10318	.15624	.15624
CROSS (1)	0.538	.524	.494	.510	.449	.443
AREFR	140.0	163.	136.	209.	82.	98.7
HYDIA (2)	.32	.32	.36	.32	.575	.575
HYDIA (1)	.1848	.1545	.1742	.1171	.2628	.2156
REFNT	184.6	184.6	184.6	184.6	86.5	86.5
REFWT	72.68	82.45	72.53	92.84	35.22	38.97

DIGITAL COMPUTER ANALYSIS OF
PNEUMATIC PRESSURE REGULATOR DYNAMICS
by

James G. Absalom
Rocketdyne

A Division of North American Aviation, Inc.
Canoga Park, California

244
PAGE INTENTIONALLY BLANK

DIGITAL COMPUTER ANALYSIS OF
PNEUMATIC PRESSURE REGULATOR DYNAMICS

by

James G. Absalom

Rocketdyne
A Division of North American Aviation, Inc.
Canoga Park, California

ABSTRACT

This paper reviews the use of simplified programming for digital computers in the analytic solution of dynamic problems associated with pneumatic pressure regulating systems. Techniques are presented for setting up computer programs which realize the advantages of numerical computations in obtaining repeatable quantitative results from mathematical models which are more complete and exact than those which are practicable for other analytic methods.

For illustration, a digital computer analysis of a typical pneumatic pressure regulator is developed. Nonlinear and discontinuous equations are used in describing reversible flowrates, friction, displacement limits, deadband, and impact and rebound of mechanical elements. Programming techniques for iterative solutions are discussed. Results are presented in tabular form and in the form of reproductions of cathode-ray tube displays of pressures and displacements as time functions.

INTRODUCTION

The dynamic problems associated with pressure regulating systems in general and pneumatic pressure regulators in particular are of continuing concern in system and component design. Accurate prediction of dynamic stability, transient response, and steady-state performance is invaluable in minimizing problems encountered in developing new hardware or in adapting existing components for new applications.

Manual computation methods, supplemented by the use of analog computers, are in general use for dynamic analysis. These techniques, however, are severely limited in describing nonlinearities and discontinuities. Manual computations are usually limited to completely linearized mathematical models of physical systems. Analog computations are frequently semilinearized within available computer equipment limitations, and repeatability in the results is limited by the accuracy and drift characteristics of the analogy and its electrical components. The limitations inherent in analyzing a physical system by employing another physical system encourage the use of other techniques.

Simplified methods for programming digital computers now offer engineers the advantages of repeatable numerical computations. Data are obtained from mathematical descriptions which are more rigorous than those dictated by other analytic methods. In addition to the advantages of completeness, accuracy, and repeatability, digital computer programs can be easily stored for future use and for modification in setting up new similar programs. A printed listing of a digital program is readily understood by others familiar with programming, and programs can usually be used at any computer facility having similar equipment.

This paper reviews the use of simplified programming for digital computers in the analytic solution of dynamic problems. The particular problems associated with pneumatic pressure regulators serve as examples.

DISCUSSION

FORTRAN

A digital computer is designed to operate in response to a special code, or "machine language," which differs for each type of computer. A programmed set of instructions for a step-by-step procedure to be followed by a computer must be in the machine language for that particular computer.

The FORTRAN (FORMula TRANslation) System was developed to enable engineers to state in simple language, resembling familiar algebraic notation, the steps to be executed. A FORTRAN Compiler translates a FORTRAN language program into an efficient machine language program, thereby relieving the engineer of a considerable amount of clerical work and minimizing human errors by relegating the detailed mechanics of coding to the Compiler.

Engineers concerned with design synthesis and analysis problems can readily acquaint themselves with the FORTRAN System. The use of digital computers as an analytic tool is thereby made available to analysts who are not computer programming specialists.

SAMPLE COMPONENT (FLOWING DASHPOT)

A nonlinear mathematical model of a simple component will be developed and analyzed as an introduction to the application of the FORTRAN System. Analysis of a complete pneumatic pressure regulator will follow.

Figure 1 is a schematic of a cylinder with gas flow from supply pressure (P_S) through an orifice of effective flow area (C_1A_1) to cylinder pressure (P_C), and gas flow from cylinder pressure (P_C) to ambient pressure (P_A) through an orifice of effective flow area (C_2A_2). A piston in the cylinder, of cross-sectional area (A_P), is biased against a stop by a spring with installed load (F_S) and spring rate (Y_S). The piston can be displaced by an external force (F_A), assisted by ambient pressure.

Figure 1 includes conventional notation with subscripts denoting specific locations of parameters and variables. This notation requires conversion to FORTRAN notation.

FORTRAN NOTATION

The FORTRAN alphabet includes only upper case letters, and subscripts cannot be used. Associative and meaningful notation, however, can be devised.

The letters ϕ and Z are slashed to distinguish them from the symbols for 0 (zero) and 2 (two). An asterisk indicates multiplication, and a slash indicates division, while parentheses are used as in algebra.

The conventional notation of Fig. 1 is converted to FORTRAN notation as follows:

$PS = P_S =$ supply pressure (psia)
 $PC = P_C =$ cylinder pressure (psia)
 $PA = P_A =$ ambient pressure (psia)
 $FS = F_S =$ spring installed force (lb)
 $YS = Y_S =$ spring rate (lb/in.)
 $AP = A_P =$ piston area (in.²)

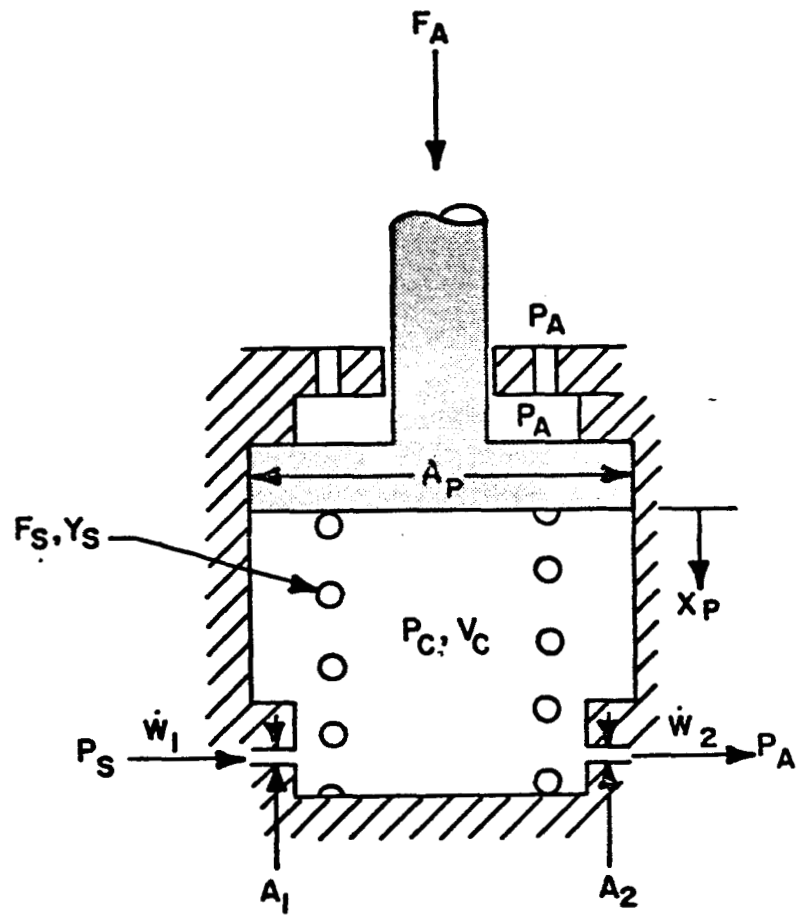


Figure 1. Schematic Flowing Dashpot

$$C1 \cdot A1 = C_1 \cdot A_1 = \text{effective inlet orifice area (in.}^2\text{)}$$

$$C2 \cdot A2 = C_2 \cdot A_2 = \text{effective exit orifice area (in.}^2\text{)}$$

$$VC = V_C = \text{cylinder volume (in.}^3\text{)}$$

$$XP = X_P = \text{piston displacement (in.)}$$

$$XD\phi TP = \dot{X}_P = dX/dt = \text{piston velocity (in./sec)}$$

$$XDD\phi TP = \ddot{X}_P = d^2X/dt^2 = \text{piston acceleration (in./sec}^2\text{)}$$

$$WD\phi T1 = \dot{w}_1 = \text{inlet gas flow (lb/sec)}$$

$$WD\phi T2 = \dot{w}_2 = \text{exit gas flow (lb/sec)}$$

BASIC EQUATIONS

The basic equations to be used in setting up a mathematical model of Fig. 1 are, in algebraic notation:

$$I \quad P \cdot V = W \cdot R \cdot \text{TEMP}$$

$$II \quad dP/dt = dW/dt \cdot R \cdot \text{TEMP}/V + dX/dt \cdot P \cdot A/V$$

$$III \quad dW/dt = C \cdot A \cdot P \cdot S/\sqrt{R \cdot \text{TEMP}}$$

$$IV \quad d^2X/dt^2 = F/m$$

$$V \quad dX/dt = \int (d^2X/dt^2 \cdot dt) = \int d(dX/dt)/dt \cdot dt$$

$$VI \quad X = \int (dX/dt \cdot dt)$$

Equation I is the perfect gas equation of state.

Equation II is the derivative of Eq. I, substituting $dV/dt = A(dX/dt)$, and describes the time rate of change of pressure caused by mass entering or discharging from a volume, and includes a pumping term if the volume is changing with time. The temperature derivative is assumed negligible.

Equation III is the nozzle isentropic flow equation, corrected for an orifice description.

Equation IV is Newton's second law of motion. Eq. V and VI are integrals of Eq. IV.

FORTTRAN PROGRAMMING

Having established a schematic of the system to be analyzed, with appropriate notation for the system parameters and variables, a FORTRAN Program can now be written, using the basic equations in a manner suitable for iterative computations.

In general, the approach is as follows:

1. State parameters and initial conditions
2. Compute forces
3. Compute accelerations
4. Integrate accelerations to obtain velocities
5. Integrate velocities to obtain displacements
6. Compute flowrates
7. Compute rates of change of pressures resulting from flowrates and pumping
8. Compute pressures
9. Increase TIME by one increment of time
10. Print output data or store for cathode-ray-tube display
11. Return to Step 2 and repeat Steps 2 through 11 until TIME = FINIS

Knowing all conditions which exist in the system initially (at Step 1), a set of forces are computed which correspond to the existing pressures and displacements. Instantaneous accelerations corresponding to the force distribution are then

computed. Next, the velocities are computed which will be obtained when the initial velocities are known, and the newly computed accelerations are maintained for a very small increment of time. The corresponding new displacements at the end of the time increment are then computed knowing the previous displacements and the computed values of acceleration and velocity. Pressures at the beginning of the time increment now being known, the corresponding flowrates are then computed. Using the most recently computed flowrates and velocities, rates of change of pressures are now computed. The pressures at the beginning of time increment and the rates of change of pressures during the time increment are now known, so the pressures existing at the end of the time increment are now computed. The value of TIME which existed at the beginning of the set of incremental computations is then increased by one increment of time. The desired output data can then be printed, or stored for a cathode-ray-tube display. The values existing at the end of the time increment (Step 11) become the initial values for the next set of computations beginning at Step 2. Steps 2 through 11 are repeated until TIME equals FINIS, the programmed end of the computer run.

When the time increment selected is small enough that a repeat computer run with a greater time increment produces essentially identical output, the time increment selected is conservatively small, and the iterative technique is not introducing computation errors.

A FORTRAN program is first written manually on code sheets, of which Fig. 2 is typical. Two lines on the code sheet, with an arbitrarily selected identification number, are used for each instruction in the program. Each instruction on the code sheets is then keypunched on a separate card, and the identification numbers become card sequence numbers.

When a deck of keypunched cards comprising a FORTRAN program is submitted for a computer run, a FORTRAN Compiler translates the FORTRAN source deck, and a new deck is keypunched in machine language for computer use.

FORTRAN CODE SHEET

DECK NO. DASH PROGRAMMER ABSA/LOM DATE PAGE 4 of 8 JOB NO.

FOR COMMENT STATEMENT NUMBER	FORTRAN STATEMENT			IDENTIFICATION
	90	00	73	
C1	COMPUTE PISTON ACCCELERATION, VEL	ATIN, VEL		
	CITY AND POSITION			4100
100	XDDPTP=(FA- /WP	FS-(PC-PA)*AP-VS*XP)*G		4200
	XDDPTP=XDDPTP	1+XDDPTP*T		4300
	XP=XP1+XDDPTP	PI*T+XDDPTP*T**2/2.		4400
C1				4500
C1	LIMIT PISTON POSITION			4510
	IF(XP-XP9)270,260,260			4515
260	XP=XP9			4520
	XDDPTP=0.			4521
	XDDPTP=0.			4522
270	CONTINUE			4525
C1				4600

Figure 3 presents a listing of a FORTRAN program capable of describing the performance of a mathematical model of the simple system of Fig. 1. The column of numbers at the righthand side of each page of the listing identifies the arbitrarily selected card sequence numbers which are used for machine sorting of the source deck. Card numbers are selected with sufficient spacing to permit additional instructions on keypunched cards to be added to a program as it is being refined.

Statements preceded by the code letter "C" are comment statements inserted for information only. The Compiler ignores these in translating from FORTRAN to machine language, and they do not appear as program instructions.

DEVELOPING SPECIFIC EQUATIONS

Analysis of the dynamic performance of a mathematical model of the scheme of Fig. 1 follows the general approach previously outlined.

The sum of the forces acting on the piston is described by the differential equation

$$W_P/g \cdot d^2X_P/dt^2 + B \cdot dX_P/dt + Y_S \cdot X_P = F_A - F_S - (P_C - P_A) A_P$$

or

$$W_P/g \cdot \ddot{X}_P + B \cdot \dot{X}_P + Y_S \cdot X_P = F_A - F_S - (P_C - P_A) A_P$$

Assuming the viscous damping coefficient B to be negligible, the preceding equation can be rewritten in FORTRAN notation as

$$WP \cdot XDD \cdot TP / G + YS \cdot XP = FA - FS - (PC - PA) \cdot AP$$

FLOWING DASHPOT ANALYSIS

+ INDICATES ADDITION
 - INDICATES SUBTRACTION
 * INDICATES MULTIPLICATION
 ** INDICATES RAISING TO A POWER
 / INDICATES DIVISION
 = INDICATES EQUAL TO
 GO TO 100 INDICATES GO DIRECTLY
 IF(A-B)100,200,300 INDICATES GO
 TO STATEMENT
 SORTF INDICATES TAKING A SQUARE

AT TIME=ZERO
PISTON DISPLACEMENT XP=ZERO
STEADY STATE FLOW ESTABLISHED FROM PS TC PC TO PA
STEP INPUT IN APPLIED FORCE FA
AS TIME INCREASES FROM ZERO
SUPPLY PRESSURE PS AND APPLIED FORCE FA MAINTAINED CONSTANT
PISTON POSITION XP AND CYLINDER PRESSURE PC VARY WITH TIME

0000000350
000000060
000000070
000000075
000000080
000000100
000000102
000000104
000000110
000000120
000000130
000000140
000000150
000000160
000000200
000000210
000000220
000000230
000000250
000000260
000000270
000000280
000000290
000000600
000000602
000000604
000000620
000000630
000000640
000000650
000000670
000000700
000000710
000000720
000000730
000000740
000000750

Figure 3. Flowing Dashpot Analysis

FLOWING DASHPOT ANALYSIS

```

C  HARDWARE DIMENSIONAL PARAMETERS
CC=.67
A1=.CC12
A2=.CC30
AP=2.
VCG=3.
FS=1C.
YS=30.
WP=5.
XP9=1.

C  T=.CCCC2
FINIS=.1

C  INITIAL CONDITIONS
PS=1C0.
PA=14.7
PC=PS*A1/A2
PC1=PC
WDGT1=.CCC73
WDGT2=WDGT1
FA=120.
XP=C.
XDOTP=0.
XDDOTP=0.

C  GAS DATA AND CONSTANTS FOR FLOW FUNCTIONS
G=386.
XK=1.66
R=463C.
TEMP=53C.
C1=2.0*G/12.*XK/(XK-1.)
C2=2./XK
C3=(XK+1.)/XK
C4=SQR TF(R/12.*TEMP)
RCR=(2./(XK+1.))*((XK/(XK-1.))
SCR=SQR TF(G/12.*XK*(2./(XK+1.))*((XK+1.)/(XK-1.)))

C
C
00001000
00001090
00001100
00001200
00001300
00001350
00001400
00001500
00001600
00001700
00001702
00001710
00001712
00001800
00001900
00002000
00002100
00002200
00002210
00002220
00002230
00002300
00002400
00002500
00002600
00002700
00002800
00002900
00003000
00003100
00003200
00003300
00003400
00003500
00003600
00003700
00003800
00003850
00003925

```

Figure 3. (Continued)

```

258      C      PRINT COLUMN HEADINGS FOR OUTPUT DATA      00003977
      C      WRITE OUTPUT TAPE 6,80,TIME,PS,FA,XP,XD0TP,PC,WD0T1,WD0T2 00003980
      80 FORMAT(IH1,4X4HTIME,7X2HPS,7X2HFA,7X2HXP,4X5HWD0TP,3X6HXC0TP,7X2HWD0T2,7X2HWD0T1,7X2HWD0T2)
      1PC 4X5HWD0T1,4X5HWD0T2/F9.5,2F9.2,1F9.4,3F9.2,2F9.5/) 00003984
      C      C      00004000
      C      COMPUTE PISTON ACCELERATION, VELOCITY AND POSITION
      100 XD0TP=(FA-FS-(PC-PA)*AP-YS*XP)*G/WP      00004100
      XD0TP=XD0TP1+XD0TP*T      00004200
      XP=XP1+XD0TP1*T+XD0TP*T*T/2.      00004300
      C      C      00004400
      C      LIMIT PISTON POSITION
      IF(XP-XP9)270,260,260      00004500
      260 XP=XP9      00004510
      XD0TP=C.      00004515
      XD0TP=0.      00004520
      270 CONTINUE      00004521
      C      C      00004522
      C      COMPUTE FLOW RATES      00004525
      RR1=PC/PS      00004600
      IF(RR1-RCR)140,140,145      00004700
      145 S1=SQRT((C1-ABS(F(RR1)*C2-RR1)*C3))      00004800
      GO TO 150      00004900
      140 S1=SCR      00005000
      150 WD0T1=CC*A1*PS*S1/C4      00005100
      RR2=PA/PC      00005200
      IF(RR2-RCR)240,240,245      00005300
      245 S2=SQRT((C1-ABS(F(RR2)*C2-RR2)*C3))      00005400
      GO TO 250      00005500
      240 S2=SCR      00005600
      250 WD0T2=CC*A2*PC*S2/C4      00005700
      C      C      00005800
      C      COMPUTE TIME RATE OF CHANGE OF PRESSURE      00005900
      VC=VC0-AP*XP      00006000
      PD0TC=(WD0T1-WD0T2)*R*TEMP/VC+XD0TP*AP*PC/VC      00006100
      C      C      00006150
      C      COMPUTE PRESSURE      00006200
      PC=PC1+PD0TC*T      00006300
      C      C      00006400
      C      C      00006500
      C      C      00006525
      C      C      00006550

```

Figure 3. (Continued)

FLOWING DASHPOT ANALYSIS

```

C   VARIABLES FOR BEGINNING OF NEXT ITERATION
XDDTP1=XDDTP
XP1=XP
PC1=PC
TIME1=TIME
C   INCREMENT TIME
C   TIME=TIME1+T
C   COUNT NUMBER OF ITERATIONS
C   COUNT=COUNT+1.
IF(COUNT-50.)310,300,300
300 COUNT=C.
WRITE OUTPUT TAPE 6,90,TIME,PS,FA,XP,XDCTP,XDDCTP,PC,WDDT1,WDDT2
90 FORMAT(F9.5,2F9.2,1F9.4,3F9.2,2F9.5)
310 CONTINUE
C   RETURN TO BEGINNING OF COMPUTATION LOOP
C   IF(TIME-FINIS)100,900,900
900 CALL EXIT
END(1,0,0,0,0,1,0,0,1,0,0,0,0,0)
00006600
00006700
00006800
00006900
00006910
00007000
00007100
00007200
00007250
00007260
00007300
00007400
00007500
00007600
00007700
00007800
00007850
00007860
00007900
00008000

```

Figure 3. (Continued)

From which the piston acceleration becomes

$$XDD\phi TP = (FA - FS - (PC - PA) * AP - YS * XP) * G/WP$$

For a small increment of time (T), the velocity at the end of the time increment can be described as

$$dX_P/dt = (dX_P/dt)_1 + d^2X_P/dt^2 \cdot T$$

or

$$\dot{\dot{X}}_P = (\dot{X}_P)_1 + (\dot{\dot{X}}_P) \cdot T$$

where

$(\dot{X}_P)_1$ = the velocity at the beginning of the time increment

$\dot{\dot{X}}_P$ = the acceleration during the time increment.

In FORTRAN notation the equation for velocity at the end of a time increment (T) becomes

$$XD\phi TP = XD\phi TP1 + XDD\phi TP * T$$

The displacement at the end of a small increment of time (T) can be described as

$$X_P = (X_P)_1 + (\dot{X}_P)_1 \cdot T + (\dot{\dot{X}}_P) \cdot T^2/2$$

where $(X_P)_1$ is the displacement at the beginning of the time increment, and other terms are as previously defined.

In FORTRAN notation the displacement equation becomes

$$XP = XP1 + XD\delta TP1 * T + (XDD\delta TP * T ** 2)/2.0$$

Weight flowrate of gas into the cylinder from supply pressure (P_S) to cylinder pressure (P_C) through orifice area (A_1) is described by

$$\dot{w}_1 = (C_1 \cdot A_1 \cdot P_S \cdot S_1) / \sqrt{R \cdot \text{TEMP}/12}$$

where

- \dot{w}_1 = weight flowrate (lb/sec)
- C_1 = orifice flow coefficient
- A_1 = orifice geometric flow area (in.²)
- P_S = supply pressure (psia)
- S_1 = $f(P_C/P_S)$ (ft^{1/2}/sec)
- R = specific gas constant (in./°R)
- TEMP = temperature (°R)

The flow function (S_1) for subsonic flow is defined by

$$S_1 = \sqrt{2gk/k-1 \left[(P_C/P_S)^{2/k} - (P_C/P_S)^{(k+1)/k} \right]}$$

where

- g = gravitational constant (ft/sec²)
- k = ratio of specific heats (-)

The flow function (S_1) for sonic flow is defined by the same expression except that P_C/P_S becomes a constant at the critical pressure ratio $((P_C/P_S)_C)$ where

$$(P_C/P_S)_C = (2/(k+1))^{k/(k-1)}$$

Weight flowrate of gas from cylinder pressure (P_C) to ambient pressure (P_A) through orifice area (A_2) is described by

$$\dot{w}_2 = (C_2 \cdot A_2 \cdot P_C \cdot S_2) / \sqrt{R \cdot \text{TEMP}/12}$$

For simplicity, an isothermal case is assumed with cylinder gas temperature equal to supply gas temperature.

The time rate of change of pressure in the cylinder (dP_C/dt) is described as

$$\dot{P}_C = (\dot{w}_1 - \dot{w}_2) \cdot R \cdot \text{TEMP}/V_C + \dot{X}_P \cdot A_P \cdot P_C/V_C$$

which in FORTRAN notation becomes

$$PDOTC = (WDOT1 - WDOT2) * R * \text{TEMP}/VC + XDOTP * AP * PC/VC$$

For a small increment of time (T) the pressure at the end of the time increment can be described by

$$P_C = (P_C)_1 + (\dot{P}_C) \cdot T$$

where

$(P_C)_1$ = pressure at the beginning of the time increment

\dot{P}_C = time rate of change of pressure

In FORTRAN notation the cylinder pressure is described by

$$PC = PC1 + PD\phi TC * T$$

If TIME1 is the time (in seconds) at the beginning of a time increment (T), the time at the end of the time increment is

$$TIME = TIME1 + T$$

These are all the basic equations, in FORTRAN notation, required for an analysis of the scheme shown in Fig. 1. Using these equations, the program listed in Fig. 3 can be set up.

PROGRAMMING SPECIFIC EQUATIONS

The program of Fig. 3 is not intended as an example of sophisticated programming techniques which experienced programmers develop, but is designed to illustrate the basic simplicity of this powerful analytic method and the close association between FORTRAN statements and their algebraic counterparts.

Commonly used symbols are defined on the first page of the program listing, and the operating conditions for the computer run are stated. All statements on the first page are comment statements preceded by the code letter C.

The first step in the computation procedure assigns numerical values to the symbols representing hardware dimensional parameters.

The second step assigns numerical values for the initial conditions of certain variables. The initial value for cylinder pressure (PC) is computed for the condition of steady-state flow from PS to PC to PA. Throughout the program there are no statements which modify the initial values for supply pressure (PS), ambient pressure (PA), or external force (FA). There are modifying statements for piston position (XP), flow terms, and cylinder pressure (PC). The program is therefore set up to determine the response of XP and PC to a step input in FA at time equal to zero.

The next step assigns values for the gravitational constant (G), the ratio of gas specific heats ($XK = k = C_p/C_v$), the specific gas constant (R) and the gas temperature ($TEMP$). Constants are then computed for later use in computing flow functions. RCR is the critical pressure ratio, while SCR is the flow function (S) for sonic flow at pressure ratios below critical. Computing SCR requires taking the square root of an expression. The symbol $SQRTF$ is a FORTRAN symbol directing the computer to obtain the square root of the expression which follows the symbol. The next step involves format statements for printing column headings for a tabulation of the program output data.

The preceding steps provide the computer with information which it will store.

Starting with card number 4200, the program begins computations which will be repeated for each increment of time. The number 100 which preceded the statement for computing acceleration is an arbitrarily selected statement number. The computer performs the operations indicated by each statement in the sequence in which the cards are numbered, unless otherwise instructed. As directed by card numbers 4200, 4300, and 4400, numerical values for piston acceleration, velocity, and position are computed in that order. Piston position is then limited by an "IF statement." If piston position (XP) minus maximum piston position ($XP9$) is negative (piston not fully stroked), the computer is directed to statement number 270 and continues. If ($XP - XP9$) is zero or positive (piston fully stroked), the computer is directed to statement 260, XP is set equal to $XP9$, the acceleration and velocity are set equal to zero, and the computer continues.

Flowrates are then computed. The constants $C1$, $C2$, $C3$, and $C4$ were computed previously to simplify the flow computations. Computing the flow function ($S_1 = f(P_C/P_S)$) requires taking the square root of an expression. Card number 5000 illustrates the manner in which this type of computation is directed.

Pressure rate of change and a new pressure are then computed, and values needed for the next iteration are reidentified for storage.

Time is incremented. Counting statements call for printing one line of tabulated data each time 50 iterations are performed. This technique reduces the amount of data printout while permitting the use of a very small time increment. With an iteration time increment of 0.000020 seconds, the print-out interval is 0.00100 seconds.

Card 7900 directs the computer to return to statement 100 (card 4200) if TIME is less than FINIS and to end the computations if TIME is equal to FINIS.

The results of a computer run are printed in the tabulation of Fig. 4. At TIME equal to zero the initial values are printed. As TIME progresses, the piston position (XP) varies from its initial at-rest position to its fully stroked position. Velocity and acceleration vary during stroking and become zero when the piston is fully stroked as described by discontinuous equations. The corresponding changes in cylinder pressure (PC) and in the two weight flowrates are tabulated. It will be noted that incoming flow ($WD/\Delta t_1$), described by a nonlinear flow equation, passes from the sonic flow regime to the subsonic flow regime as PC/PS changes with pumping. It will also be noted that as cylinder pressure (PC) is pumped by the piston to oppose displacement, a condition is obtained at which the piston decelerates in the presence of a forward velocity. When forward momentum is overcome, the piston velocity reverses until PC decays sufficiently to again reverse the net acceleration force.

Breakaway friction forces could be added by means of additional IF statements which add breakaway friction to the piston force balance to oppose impending displacement if the velocity is zero, and if the sum of all other forces exceeds the friction force. If the velocity is zero, and if the sum of all other forces is less than the breakaway friction, then the net force is set at zero, i.e., static friction can resist the driving forces but cannot become a driving force.

TIME	PS	FA	XP	XDDTIP	XDDQELP	PC	WEO11	WDO12
0.00000	100.00	120.00	0.	0.	0.	40.00	0.00073	0.00073
0.00100	100.00	120.00	0.0023	4.58	4571.37	40.06	0.00073	0.00073
0.00200	100.00	120.00	0.0052	9.13	4527.74	40.25	0.00073	0.00074
0.00300	100.00	120.00	0.0205	13.63	4454.86	40.55	0.00073	0.00074
0.00400	100.00	120.00	0.0364	18.03	4352.61	40.98	0.00073	0.00075
0.00500	100.00	120.00	0.0566	22.32	4220.77	41.53	0.00073	0.00076
0.00600	100.00	120.00	0.0810	26.46	4058.93	42.22	0.00073	0.00077
0.00700	100.00	120.00	0.1094	30.42	3866.56	43.04	0.00073	0.00079
0.00800	100.00	120.00	0.1417	34.18	3642.96	44.01	0.00073	0.00080
0.00900	100.00	120.00	0.1777	37.69	3387.29	45.13	0.00073	0.00082
0.01000	100.00	120.00	0.2170	40.94	3098.53	46.42	0.00073	0.00085
0.01100	100.00	120.00	0.2595	43.87	2775.53	47.88	0.00073	0.00087
0.01200	100.00	120.00	0.3047	46.47	2417.00	49.52	0.00073	0.00090
0.01300	100.00	120.00	0.3523	48.69	2021.63	51.38	0.00073	0.00094
0.01400	100.00	120.00	0.4019	50.49	1588.22	53.44	0.00073	0.00098
0.01500	100.00	120.00	0.4531	51.84	1115.74	55.74	0.00072	0.00102
0.01600	100.00	120.00	0.5054	52.70	603.59	58.28	0.00072	0.00106
0.01700	100.00	120.00	0.5583	53.02	51.92	61.06	0.00071	0.00112
0.01800	100.00	120.00	0.6113	52.78	-537.90	64.09	0.00070	0.00117
0.01900	100.00	120.00	0.6637	51.92	-1162.61	67.36	0.00068	0.00123
0.02000	100.00	120.00	0.7149	50.43	-1816.17	70.83	0.00066	0.00129
0.02100	100.00	120.00	0.7643	48.27	-2488.70	74.44	0.00063	0.00136
0.02200	100.00	120.00	0.8112	45.44	-3165.25	78.12	0.00060	0.00143
0.02300	100.00	120.00	0.8550	41.93	-3824.81	81.73	0.00056	0.00149
0.02400	100.00	120.00	0.8949	37.79	-4439.84	85.11	0.00051	0.00155
0.02500	100.00	120.00	0.9304	33.07	-4977.21	88.04	0.00047	0.00161
0.02600	100.00	120.00	0.9609	27.86	-5401.18	90.31	0.00042	0.00165
0.02700	100.00	120.00	0.9860	22.31	-5678.89	91.72	0.00040	0.00168
0.02800	100.00	120.00	0.9997	-1.71	-5621.00	91.04	0.00041	0.00167
0.02900	100.00	120.00	0.9953	-7.04	-5041.65	87.34	0.00048	0.00160
0.03000	100.00	120.00	0.9859	-11.75	-4363.82	83.22	0.00054	0.00152
0.03100	100.00	120.00	0.9720	-15.78	-3684.81	78.89	0.00059	0.00144
0.03200	100.00	120.00	0.9545	-19.11	-2976.61	74.57	0.00063	0.00136
0.03300	100.00	120.00	0.9341	-21.73	-2283.89	70.39	0.00066	0.00129
0.03400	100.00	120.00	0.9113	-23.67	-1623.87	66.46	0.00068	0.00122
0.03500	100.00	120.00	0.8869	-24.98	-1007.29	62.84	0.00070	0.00115
0.03600	100.00	120.00	0.8616	-25.69	-439.84	59.56	0.00071	0.00109
0.03700	100.00	120.00	0.8357	-25.86	76.35	56.61	0.00072	0.00104
0.03800	100.00	120.00	0.8100	-25.54	541.50	53.99	0.00073	0.00099
0.03900	100.00	120.00	0.7848	-24.79	957.22	51.68	0.00073	0.00095
0.04000	100.00	120.00	0.7605	-23.64	1325.86	49.66	0.00073	0.00091
0.04100	100.00	120.00	0.7376	-22.14	1650.03	47.91	0.00073	0.00088
0.04200	100.00	120.00	0.7164	-20.35	1932.31	46.41	0.00073	0.00085

Figure 4. Computer Runs

0.04300	100.00	120.00	0.6970	-18.29	2175.07	45.13	0.00073	0.00083
0.04400	100.00	120.00	0.6799	-16.00	2380.53	44.06	0.00073	0.00081
0.04500	100.00	120.00	0.6651	-13.53	2550.70	43.18	0.00073	0.00079
0.04600	100.00	120.00	0.6529	-10.91	2687.32	42.49	0.00073	0.00078
0.04700	100.00	120.00	0.6433	-8.17	2791.91	41.96	0.00073	0.00077
0.04800	100.00	120.00	0.6365	-5.33	2865.71	41.58	0.00073	0.00076
0.04900	100.00	120.00	0.6327	-2.44	2909.76	41.36	0.00073	0.00076
0.05000	100.00	120.00	0.6317	0.48	2924.87	41.28	0.00073	0.00075
0.05100	100.00	120.00	0.6336	3.40	2911.68	41.34	0.00073	0.00076
0.05200	100.00	120.00	0.6385	6.29	2870.62	41.54	0.00073	0.00076
0.05300	100.00	120.00	0.6462	9.13	2802.00	41.87	0.00073	0.00077
0.05400	100.00	120.00	0.6567	11.88	2705.98	42.34	0.00073	0.00077
0.05500	100.00	120.00	0.6699	14.53	2582.58	42.94	0.00073	0.00078
0.05600	100.00	120.00	0.6857	17.04	2431.76	43.69	0.00073	0.00080
0.05700	100.00	120.00	0.7039	19.38	2253.39	44.57	0.00073	0.00081
0.05800	100.00	120.00	0.7244	21.53	2047.32	45.60	0.00073	0.00083
0.05900	100.00	120.00	0.7469	23.46	1813.43	46.78	0.00073	0.00085
0.06000	100.00	120.00	0.7712	25.14	1551.69	48.12	0.00073	0.00088
0.06100	100.00	120.00	0.7971	26.55	1262.29	49.61	0.00073	0.00091
0.06200	100.00	120.00	0.8242	27.65	945.84	51.25	0.00073	0.00094
0.06300	100.00	120.00	0.8523	28.43	603.64	53.05	0.00073	0.00097
0.06400	100.00	120.00	0.8809	28.84	237.86	54.99	0.00073	0.00100
0.06500	100.00	120.00	0.9098	28.89	-148.13	57.06	0.00072	0.00104
0.06600	100.00	120.00	0.9386	28.53	-549.37	59.23	0.00072	0.00108
0.06700	100.00	120.00	0.9668	27.78	-958.95	61.46	0.00071	0.00112
0.06800	100.00	120.00	0.9940	26.61	-1367.58	63.70	0.00070	0.00116
0.06900	100.00	120.00	0.9596	-1.06	-1321.44	63.24	0.00070	0.00116
0.07000	100.00	120.00	0.9979	-2.28	-1118.17	61.95	0.00071	0.00113
0.07100	100.00	120.00	0.9951	-3.29	-903.91	60.60	0.00071	0.00111
0.07200	100.00	120.00	0.9914	-4.08	-684.60	59.23	0.00072	0.00108
0.07300	100.00	120.00	0.9870	-4.65	-465.56	57.88	0.00072	0.00106
0.07400	100.00	120.00	0.9822	-5.01	-251.36	56.57	0.00072	0.00103
0.07500	100.00	120.00	0.9771	-5.15	-45.83	55.31	0.00073	0.00101
0.07600	100.00	120.00	0.9719	-5.10	147.98	54.14	0.00073	0.00099
0.07700	100.00	120.00	0.9669	-4.86	327.67	53.05	0.00073	0.00097
0.07800	100.00	120.00	0.9623	-4.45	491.44	52.06	0.00073	0.00095
0.07900	100.00	120.00	0.9581	-3.88	637.97	51.18	0.00073	0.00094
0.08000	100.00	120.00	0.9546	-3.17	766.37	50.40	0.00073	0.00092
0.08100	100.00	120.00	0.9518	-2.35	876.06	49.74	0.00073	0.00091
0.08200	100.00	120.00	0.9459	-1.42	966.69	49.18	0.00073	0.00090
0.08300	100.00	120.00	0.9490	-0.42	1038.16	48.73	0.00073	0.00089
0.08400	100.00	120.00	0.9491	0.65	1090.47	48.40	0.00073	0.00088
0.08500	100.00	120.00	0.9503	1.76	1123.77	48.16	0.00073	0.00088
0.08600	100.00	120.00	0.9526	2.89	1138.30	48.04	0.00073	0.00088

Figure 4. (Continued)

0.08700	100.00	120.00	0.9561	4.03	1134.41	48.01	0.00073	0.00088
0.08800	100.00	120.00	0.9606	5.15	1112.54	48.09	0.00073	0.00088
0.08900	100.00	120.00	0.9663	6.24	1073.20	48.26	0.00073	0.00088
0.09000	100.00	120.00	0.9731	7.29	1017.03	48.52	0.00073	0.00089
0.09100	100.00	120.00	0.9809	8.27	944.76	48.88	0.00073	0.00089
0.09200	100.00	120.00	0.9896	9.17	857.27	49.32	0.00073	0.00090
0.09300	100.00	120.00	0.9992	9.98	755.65	49.83	0.00073	0.00091
0.09400	100.00	120.00	1.0000	0.	0.	49.46	0.00073	0.00090
0.09500	100.00	120.00	1.0000	0.	0.	49.04	0.00073	0.00090
0.09600	100.00	120.00	1.0000	0.	0.	48.65	0.00073	0.00089
0.09700	100.00	120.00	1.0000	0.	0.	48.27	0.00073	0.00088
0.09800	100.00	120.00	1.0000	0.	0.	47.90	0.00073	0.00088
0.09900	100.00	120.00	1.0000	0.	0.	47.56	0.00073	0.00087
0.10000	100.00	120.00	1.0000	0.	0.	47.22	0.00073	0.00086
**PRINTING=			279 LINES	**PUNCHING=	22 CARDS	**CRT=	0-35MM	0-9 INCH

Figure 4. (Continued)

Sliding friction could be added by IF statements which add friction to the piston force balance to oppose velocity if velocity is not zero.

Elastic rebound of the piston from its stops could be added by IF statements which state that if the piston touches a stop while moving, the resulting velocity will have two components. One component will be in the direction away from the stop with a value equal to the coefficient of restitution times the approach velocity. The other component will be the acceleration component. Whether or not the piston rebounds depends on the magnitudes of the approach and rebound components.

PNEUMATIC PRESSURE REGULATOR

The analytic method discussed for the simple component of Fig. 1 will now be extended for an analysis of the dynamics of a model of a pilot-controlled pneumatic pressure regulator.

Figure 5 is a schematic diagram of the regulator. Flow through the regulator is controlled by the normally closed main valve which is positioned by a diaphragm actuator biased by a belleville spring. The main valve diaphragm actuator senses pressure (P_{R1}) near the regulator outlet port and a controlled reference pressure (P_{C1}). Under steady-state flowing conditions the actuator positions the main valve to maintain a force balance in which regulator discharge pressure is lower than the controlled reference pressure by an amount determined by the spring bias and by P_{S1} acting on the valve cross section. The reference pressure is maintained by a simple, normally open, force-balance, bleed-regulator pilot valve. The bleed regulator accepts flow from P_{S1} to P_C , and modulates to maintain P_C equal to a preset value above ambient pressure (P_A). A flow path communicates P_C with P_{C1} , and P_{C1} with P_{R1} . Under conditions of initial pressurization, flow is established through the normally open pilot valve from P_{S1} to P_C , from P_C to P_{C1} and from P_{C1} to P_{R1} . When P_{C1} increases

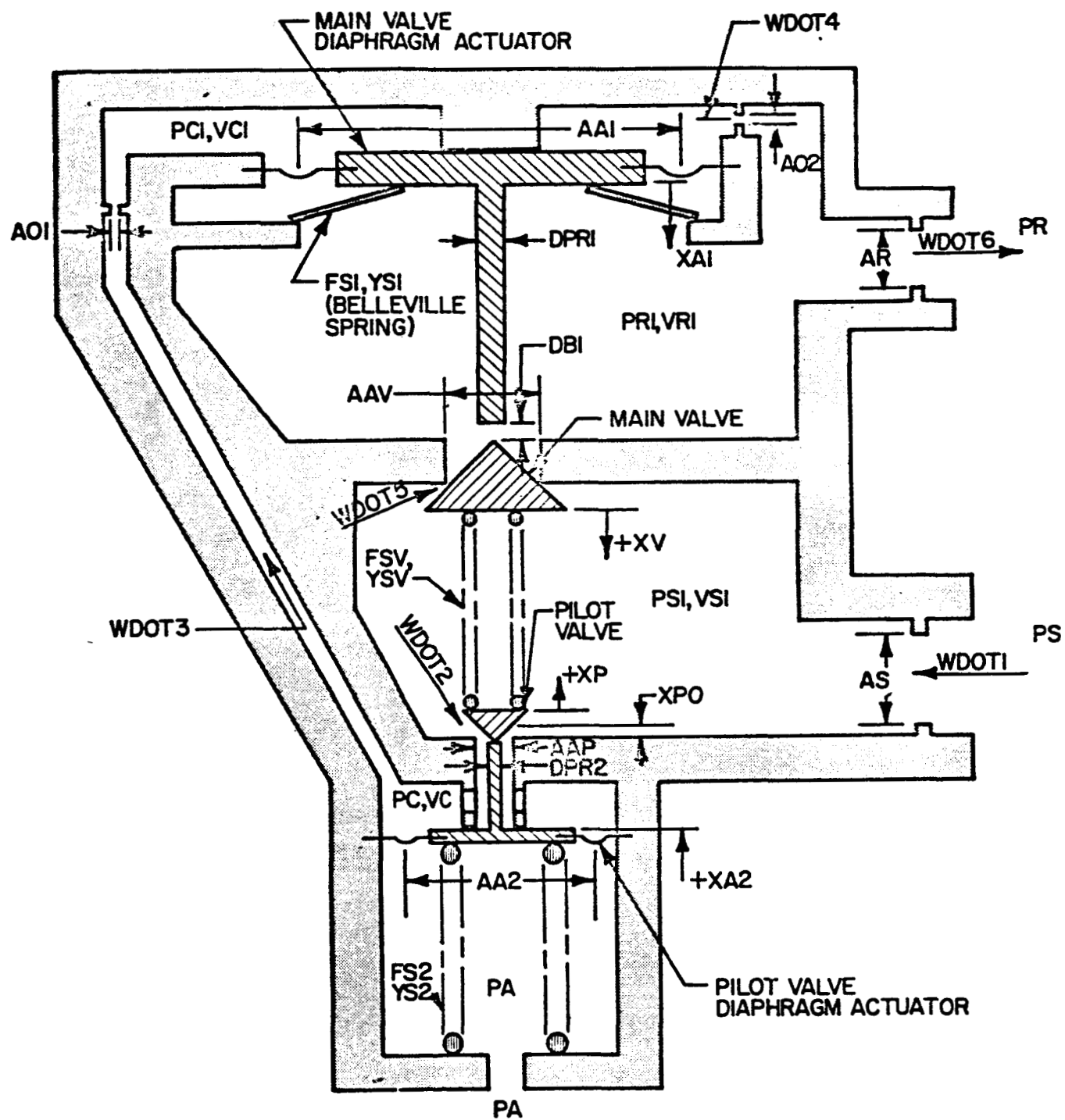


Figure 5. Schematic of Pressure Regulator

sufficiently to crack the main valve, flow is established from PS1 to P1, and from P1 to PR. When PC increases to overpower the bleed regulator spring force, the pilot valve closes. When P1 increases to unbalance the main valve actuator in the closing direction, the regulator locks up, and flow is terminated. When a flow demand results in a decrease in PR, and consequently in P1, flow is again established from PC1 to P1, and the main valve opens for flow from PS1 to P1. A reduction in PC1 and in PC actuates the bleed regulator to maintain the preset value for PC. Steady-state flow conditions are attained when force balances are established to maintain PC at its nominal preset value, PC1 slightly less than PC, and P1 slightly less than PC1. When flow demand is terminated, the regulator locks up with pressures PC, PC1, and P1 equalizing with PR.

In a pneumatic pressure regulating system the pressurizing time lags, force interactions, inertia effects, and friction effects introduce dynamics which affect stability and response. The equations describing flow are nonlinear and reversible. Friction and valve position limits introduce discontinuities in the describing equations.

Figure 6 presents a listing of a FORTRAN program set up to determine the response of a mathematical model of the regulator of Fig. 5. Initially the regulator is in its normal condition, and a step input in supply pressure (PS) is applied. Initial pressurization of the regulator and a downstream volume is described. At a programmed time a flow demand is applied, and steady-state flow conditions are established. Flow demand is then terminated.

In this program a more sophisticated approach is used for flexibility in usage and for minimizing computer running time. The complete program includes a main program and subprograms BF~~OR~~RCE, FL~~OW~~, and CRT. The main program includes the input data and directs the functioning of the subprograms. Subroutine BF~~OR~~RCE is called by the main program to compute the instantaneous belleville spring force as a function of the spring geometry and displacement. Subroutine FL~~OW~~

Figure 6. Fortran Program to Determine Response of Mathematical Model

5717 PILOT OPERATED GAS PRESSURE REGULATOR

```

C      STEP1=TIME AT WHICH STEP FLOW DEMAND IS APPLIED (SEC.)
C      STEP2=TIME AT WHICH FLOW DEMAND IS TERMINATED (SEC.)
C      STOP=PROGRAMMED TIME FOR END OF TABULATED DATA PRINTOUT (SEC.)
C      SUMF1,SUMF2,SUMFV,ETC.=SUMS OF FORCES (LB.)
C      T=TIME INCREMENT PER ITERATION (SEC.)
C      TAPE1,TAPE2=COMPUTER TAPES ASSIGNED FOR CRT DATA STORAGE
C      TIME=REAL TIME (SEC.)
C      TFMP=GAS TEMPERATURE (DEGREES RANKINE)
C      VS1,VC,VCL,VRI,VR=VOLUMES ASSOCIATED WITH PS1,VC,ETC. (IN. CUBED)
C      VS10,VCO,VCI0,ETC.=INITIAL VOLUMES (IN. CUBED)
C      WDOT1,WDOT2,ETC.=WEIGHT FLOW RATES OF GAS (LB./SEC.)
C      XA1=MAIN VALVE ACTUATOR DISPLACEMENT FROM STOP (IN.)
C      XA2=PILOT VALVE ACTUATOR DISPLACEMENT FROM STOP (IN.)
C      XP=PILOT VALVE DISPLACEMENT FROM SEAT (IN.)
C      XPDOT=PILOT VALVE VELOCITY (IN./SEC.)
C      XPO=PILOT VALVE DISPLACEMENT AS INSTALLED (IN.)
C      XV=MAIN VALVE DISPLACEMENT FROM SEAT (IN.)
C      XVDOT=MAIN VALVE VELOCITY (IN./SEC.)
C      XA19,XA29,XP9,XV9=MAXIMUM DISPLACEMENTS (IN.)
C      XK=RATIO OF GAS SPECIFIC HEATS
C      XT=BELLEVILLE SPRING THICKNESS (IN.)
C      YS1,YS2,YSV=SPRING RATES (LB./IN.)

COMMON C1,C2,C3,C4,C5,RGR,SCR
COMMON DR0,DB1,BFHT,XT,E,GAMMA,BIHT
DIMENSION X(100),Y1(100,4),Y2(100,2)

C      1 READ INPUT TAPE 5,10,XK,R,TEMP
C      READ INPUT TAPE 5,10,T,PRINT,STOP,FINES,PS
C      READ INPUT TAPE 5,10,STEP1,STEP2,DEMAND
C      READ INPUT TAPE 5,10,DB1,XV9,XP9,XA19,XA29,XPO
C      READ INPUT TAPE 5,10,VS1,VCO,VCI0,VR10,VR
C      READ INPUT TAPE 5,10,DS,DR,D01,D02,D1,D2,DV,DP
C      READ INPUT TAPE 5,10,FS2,YS2,FSV,YSV
C      READ INPUT TAPE 5,10,DPR1,DPR2
C      READ INPUT TAPE 5,10,W1,W2,DAMP1,DAMP2,FF1,FF2
C      READ INPUT TAPE 5,10,DR0,DB1,BFHT,XT,E,GAMMA,BIHT
C      10 FORMAT(6E12.5)

```

Figure 6. (Continued)

5717 PILOT OPERATED GAS PRESSURE REGULATOR

```

20 FORMAT(1H1 4X4HTIME 6X3HFS1 6X3HPS1 5X2HPC 4X3HPC1 4X3HPR1 5X2HPR 00001550
   13X5HWDOT2 3X5HWDOT3 3X5HWDOT4 3X5HWDOT5 3X5HWDOT6 6X2HXP 6X2HXV) 00001555
50 FORMAT(F9.5,2F9.2,4F7.2,7F8.4) 00001600
53 FORMAT(1H1 40H *****INPUT DATA*****//) 00001601
55 FORMAT(15X2HXK 16X1HR 13X4HTEMP/3F17.2//) 00001603
57 FORMAT(16X1HT 12X5HPRINT 13X4HSTOP 12X5HFINIS 15X2HPS/5F17.6//) 00001604
58 FORMAT(12X5HSTEP1 12X5HSTEP2 11X6HDEMAND/3F17.5//) 00001605
59 FORMAT(14X3HFS2 14X3HYS2 14X3HFSV 14X3HYSV/4F17.2//) 00001607
60 FORMAT(/15X2HDS 15X2HDR 14X3HDO1 14X3HDO2 15X2HDI 15X2HD2/6F17.5//00001610
   115X2HDV 15X2HDP/2F17.5//) 00001612
61 FORMAT(/14X3HDI 14X3HXV9 14X3HXP9 13X4HXA19 13X4HXA29 14X3HXP0/6F00001615
   117.5//) 00001616
63 FORMAT(/14X3HVS1 14X3HVC0 13X4HVC10 13X4HVR10 15X2HVR/5F17.2//) 00001618
65 FORMAT(13X4HDP1 13X4HDP2/2F17.4//) 00001620
73 FORMAT(15X2HW1 15X2HW2 12X5HDAMP1 12X5HDAMP2 14X3HFF1 14X3HFF2/6F100001627
   17.2//) 00001628
75 FORMAT(14X3HDO 14X3HDO1 13X4HBFHT 15X2HXT 16X1HE 12X5HGAMMA/6F17.00001630
   14//13X4HBIHT/F17.4//) 00001631
00001650
00001750
00001755
00001800
00001810
00001820
00001830
00001840
00001842
00001855
00001860
00001865
00001870
00001875
00001880
00001885
00001890
00001895
00001900
00001911
00001913

```

C.
C
C

COMPUTE CONSTANTS

```

G=386.
PI=3.1415927
PI4=PI/4.
T2=T/2.
T22=T*2/2.
STOP=MIN1F(STOP,FINIS-3.*T)
CV=.67
C1=2.*G/12.*XK/(XK-1.)
C2=2./XK
C3=(XK+1.)/XK
C4=SQR TF(R/12.*TEMP)
C5=XK
RCR=(2./(XK+1.))*XK/(XK-1.)
SCR=SQR TF(G/12.*XK*(2./(XK+1.))*XK/(XK-1.))
RT=R*TEMP
C5RT=C5*RT
TF INIS=FINIS-T
XMASS1=W1/G

```

Figure 6. (Continued)

5717 PILOT OPERATED GAS PRESSURE REGULATOR

```

00001914
00001915
00001920
00001925
00001930
00001932
00001933
00001934
00001936
00001940
00001945
00001947
00001948
00001949
00001990
00002000
00002100
00002200
00002300
00002400
00002490
00002500
00002600
00002700
00002800
00002900
00002910
00002915
00002917
00002919
00002930
00002932
00002934
00002936
00002990
00003000
00003005
00003100
00003200

XMASS2=W2/G
XA1MAX=MIN1F(XA19,XV9+DB1)

WRITE OUTPUT TAPE 6,53
WRITE OUTPUT TAPE 6,55,XK,R,TEMP
WRITE OUTPUT TAPE 6,57,T,PRINT,STOP,FINIS,PS
WRITE OUTPUT TAPE 6,58,STEP1,STEP2,DEMAND
WRITE OUTPUT TAPE 6,61,DB1,XV9,XP9,XA19,XA29,XPO
WRITE OUTPUT TAPE 6,63,VSI,VCO,VC10,VR10,VR
WRITE OUTPUT TAPE 6,60,DS,DR,D01,D02,D1,D2,DV,DP
WRITE OUTPUT TAPE 6,59,FS2,Y52,FSV,YSV
WRITE OUTPUT TAPE 6,65,DPR1,DPR2
WRITE OUTPUT TAPE 6,73,W1,W2,DAMP1,DAMP2,FF1,FF2
WRITE OUTPUT TAPE 6,75,DBO,DBI,BFHT,XI,E,GAMMA,BIHT

COMPUTE FIXED FLOW AREAS
AS=CV*PI4*DS**2
AR=CV*PI4*DR**2
AO1=CV*PI4*D01**2
AO2=CV*PI4*D02**2

COMPUTE PRESSURIZED AREAS
AA1=PI4*D1**2
AA2=PI4*D2**2
AAV=PI4*DV**2
AAP=PI4*Dp**2

COMPUTE PUSH ROD CROSS-SECTION AREAS
APR2=PI4*DPR2**2
APR1=PI4*DPR1**2

COMPUTE MAXIMUM VALVE FLOW AREAS
AVMAX=CV*(AAV-APR1)
APMAX=CV*(AAP-APR2)

INITIAL CONDITIONS
TIME=0.
WDOT1=0.
WDOT2=0.

```

Figure 6. (Continued)

```

WDOT3=0.
WDOT4=0.
WDOT5=0.
WDOT6=0.
DOT6=0.
WDOT7=0.
PA=14.7
PSI=PA
PC=PA
PC1=PA
PR1=PA
PR=PA
PS1DOT=0.
PCDOT=0.
PC1DOT=0.
PR1DOT=0.
PRDOT=0.
XV=0.
XP=XP0
XA1=0.
X1=0.
VEL1=0.
X1DOT=0.
X2DOT=0.
XA2=0.
X1DOT=0.
X2DOT=0.
XA1DOT=0.
XA2DOT=0.
AV=MINIF(.707*CV*P[*DV*XV,AVMAX])
X1DOT1=0.
X2DOT1=0.
AP=MINIF(.707*CV*P[*DP*XP,APMAX])
FS1=BFORCE(TIME,XA1)

C
C
CONSTANTS AND INITIAL CONDITIONS FOR CRT AND FOR DATA PRINTOUT
JQQ=1.
XJQQ=JQQ
NN=0
00003300
00003400
00003500
00003600
00003610
00003650
00004300
00004400
00004500
00004600
00004700
00004750
00004800
00004900
00005000
00005100
00005150
00005600
00005700
00005800
00005840
00005850
00005860
00005870
00005900
00005901
00005902
00005903
00005904
00005905
00005906
00005907
00005910
00005912
00005926
00005927
00005928
00005929
00005930

```

Figure 6. (Continued)

5717 PILOT OPERATED GAS PRESSURE REGULATOR

```

130 XA1=X1
    X1DOT=VEL1
    IF(XA1)201,201,203
201 X1DDOT=0.
    X1DOT=0.
    GO TO 215
203 IF(XA1-XA1MAX)215,201,201
215 X1DOT1=X1DOT
    XA1DOT=X1DOT
C
C   COMPUTE PILOT VALVE AND ACTUATOR POSITIONS
X2DDOT=((PC-PA)*AA2-FS2-YS2*XA2-DAMP2*X2DOT-FF2*ABSF(X2DOT)/X2DOT)/XMASS2
1/XMASS2
X2DOT=X2DOT1+X2DDOT*T
XA2=XA2+X2DOT1*T+X2DDOT*T22
XA2=MAX1F(MIN1F(XA2,XA29),0.)
XP=((PC-PS1)*AAP-FSV+YSV*XP0)/YSV
XP=MAX1F(MIN1F(XP,XP9),0.)
IF(XA2-XP0+XP)160,170,170
160 X2DDOT=((PC-PA)*AA2-FS2-YS2*XA2-DAMP2*X2DOT-FF2*ABSF(X2DOT)/X2DOT+
1(PS1-PC)*AAP+FSV+YSV*(XV-XP0+XP))/XMASS2
X2DOT=X2DOT1+X2DDOT*T
XA2=XA2+X2DOT1*T+X2DDOT*T22
XA2=MAX1F(MIN1F(XA2,XP0),0.)
XP=MAX1F(XP0-XA2,0.)
IF(XA2-XP0)170,251,251
170 IF(XA2)251,251,253
251 X2DOT=0.
    X2DDOT=0.
    GO TO 265
253 IF(XA2-XA29)265,251,251
265 X2DOT1=X2DOT
    XA2DOT=X2DOT
C
C   COMPUTE VARIABLE VOLUMES
VC=VCO+AA2*XA2
VC1=VC10+AA1*XA1
VR1=VR10-AA1*XA1
C

```

Figure 6. (Continued)

5717 PILOT OPERATED GAS PRESSURE REGULATOR

```

C      COMPUTE PDOT COEFFICIENTS
C5RTS1=C5RT/VS1
C5RTC=C5RT/VC
C5RTC1=C5RT/VC1
C5RTR1=C5RT/VR1
C5RTR=C5RT/VR

C      COMPUTE VARIABLE FLOW AREAS
AV=MIN1F(.707*CV*PI*DV**XV,AVMAX)
AP=MIN1F(.707*CV*PI*DP**XP,APMAX)

C      COMPUTE GAS FLOW RATES
WDOT1=FLOW(PS,PS1,AS)
WDOT2=FLOW(PS1,PC,AP)
WDOT3=FLOW(PC,PC1,A01)
WDOT4=FLOW(PC1,PR1,A02)
WDOT5=FLOW(PS1,PR1,AV)
WDOT6=FLOW(PR1,PR,AR)
WDOT6=(WDOT6+WDOT6)/2.
DOT6=WDOT6
IF (TIME-STEP1) 300,310,310
300 WDOT7=0.
GO TO 340
310 IF (TIME-STEP2) 320,330,330
320 WDOT7=DEMAND
GO TO 340
330 WDOT7=0.
340 CONTINUE

C      COMPUTE ISENTROPIC RATES OF CHANGE OF PRESSURES
PSIDOT=C5RTS1*(WDOT1-WDOT2-WDOT5)
PCDOT=C5RTC*(WDOT2-WDOT3-PC*AA2*XA2DOT/RT)
PC1DOT=C5RTC1*(WDOT3-WDOT4-PC1*AA1*XA1DOT/RT)
PR1DOT=C5RTR1*(WDOT4+WDOT5-WDOT6+PR1*AA1*XA1DOT/RT)
PRDOT=C5RTR*(WDOT6-WDOT7)

C      COMPUTE PRESSURES
PS1=PS1+PSIDOT*T
PC=PC+PCDOT*T

```

Figure 6. (Continued)

```

PC1=PC1+PC1000*Y
PR1=PR1+PR1000*Y
PR=PR+PR000*Y

C
C
C
X(M)=TIME
COUNT=COUNT+1.
TIME=TIME+T
IF(XMODF(M,JQQ))551,552,551
551 DO 5510 JJJ=1,4
5510 Y1(M,JJJ)=-50
DO 5520 JJJ=1,2
5520 Y2(M,JJJ)=-50
GO TO 553
552 CONTINUE
Y1(M,1)=PR-14.7
Y1(M,2)=PC-14.7
Y1(M,3)=PC1-14.7
Y1(M,4)=PR1-14.7
Y2(M,1)=XV
Y2(M,2)=XP
553 XN=XN+1.
IF(M-100)556,555,555
555 WRITE TAPE IT1,X,Y1
M=0
NN=NN+1
WRITE TAPE IT2,X,Y2
556 M=M+1
IF(COUNT-XLIM)432,562,562
562 COUNT=0.
IF(TIME-PRINT)432,560,560
560 IF(TIME-STOP)558,432,432
558 WRITE OUTPUT TAPE 6,50,TIME,FS1,PS1,PC,PC1,PR1,PR,WDOT2,WDOT3,WDOT5,WDOT6,XP,XV
14,WDOT5,WDOT6,XP,XV
432 IF(TIME-TFINIS)100,434,434
434 WRITE TAPE IT1,X,Y1
WRITE TAPE IT2,X,Y2
C
00011500
00011600
00011620
00011690
00011700
00011750
00012800
00012900
00012950
00013000
00013100
00013200
00013300
00013400
00013500
00013600
00013700
00013800
00013900
00014000
00014100
00014200
00014300
00014400
00014500
00014700
00014800
00014900
00015100
00015200
00015300
00015400
00015500
00015600
00015700
00015800
00015900
00016000
00016100

```

Figure 6. (Continued)

5717 PILOT OPERATED GAS PRESSURE REGULATOR

```
END FILE IT1
END FILE IT2
CALL CRT(XN,NW,TIME,TMIN,Y1,Y2,IT1,IT2)
GO TO 1
END(1,0,0,C,0,0,1,0,0,1,0,0,0,0,0)
```

```
00016200
00016300
00016400
00016500
```

Figure 6. (Continued)

is called by the main program to compute gas flow, sonic or subsonic, as a function of two pressures and an effective flow area. Subroutine CRT is called at the completion of a computer run for a cathode-ray-tube display of selected output data.

Interpreting the listing of Fig. 6 requires a more detail familiarity with FORTRAN notation than can be obtained from this brief presentation. Comment statements interspersed throughout the listing however, serve as guideposts in getting around the format jargon to the salient features of the program.

The program is written so that displacement, flow, and pressure transients occurring throughout the system are all computed for each small increment of time. For time increments in the order of 0.00002 seconds, the output data at any given time during a computer run can be treated as continuous data even though the computations proceed in step-by-step fashion.

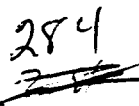
Typical output data, using the program of Fig. 6, is presented in Fig. 7 in the form of photographic reproductions of cathode-ray-tube displays of data stored during a complete run. This graphic presentation of the output data is frequently more useful and informative than a tabulated printout. Any desired variable can be selected for the CRT display.

Figure 7A lists the program input data for a typical computer run, while the two frames of Fig. 7B portray the output data. One frame shows pressures vs time, the other, displacements vs time. During initial pressurization with nitrogen gas, an oscillation in main valve position can also be detected in the pressure traces for PC1 and PR1 which show pumping effects. During initial pressurization of a 6 in.³ downstream volume, the regulated pressure overshoots the preset value of 280 psig. During flow demand, the regulated pressure decays, and the main valve opens prior to opening of the pilot valve, at which time the regulator modulates to control pressure. Oscillations in pilot valve

*****INPUT DATA*****

XK	R	TEMP	
1.40	662.40	530.00	
T	PRINT	STOP	PS
0.000020	0.	0.	5164.700012
STEP1	STEP2	DEMAND	
0.08000	0.19000	0.00630	
DB1	XV9	XP9	XA19
0.01000	0.04000	0.04000	0.05500
VS1	VC0	VC10	VR
1.00	0.50	0.50	1.75
DS	DR	DO1	DO2
0.17200	0.29700	0.06250	0.01350
DV	DP		DI
0.07500	0.02400		2.52000
FS2	YS2	FSV	YSV
145.00	375.00	1.00	10.00
DPR1	DPR2		
0.0200	0.0200		
W1	W2	DAMP1	DAMP2
0.07	0.13	1.00	1.00
DR0	DB1	BFHT	XT
2.0100	0.7400	0.0620	0.0220
RIHT			
0.0520			
			FF1
			10.00
			FF2
			5.00
			GAMMA
			0.3000

Figure 7. Input Data



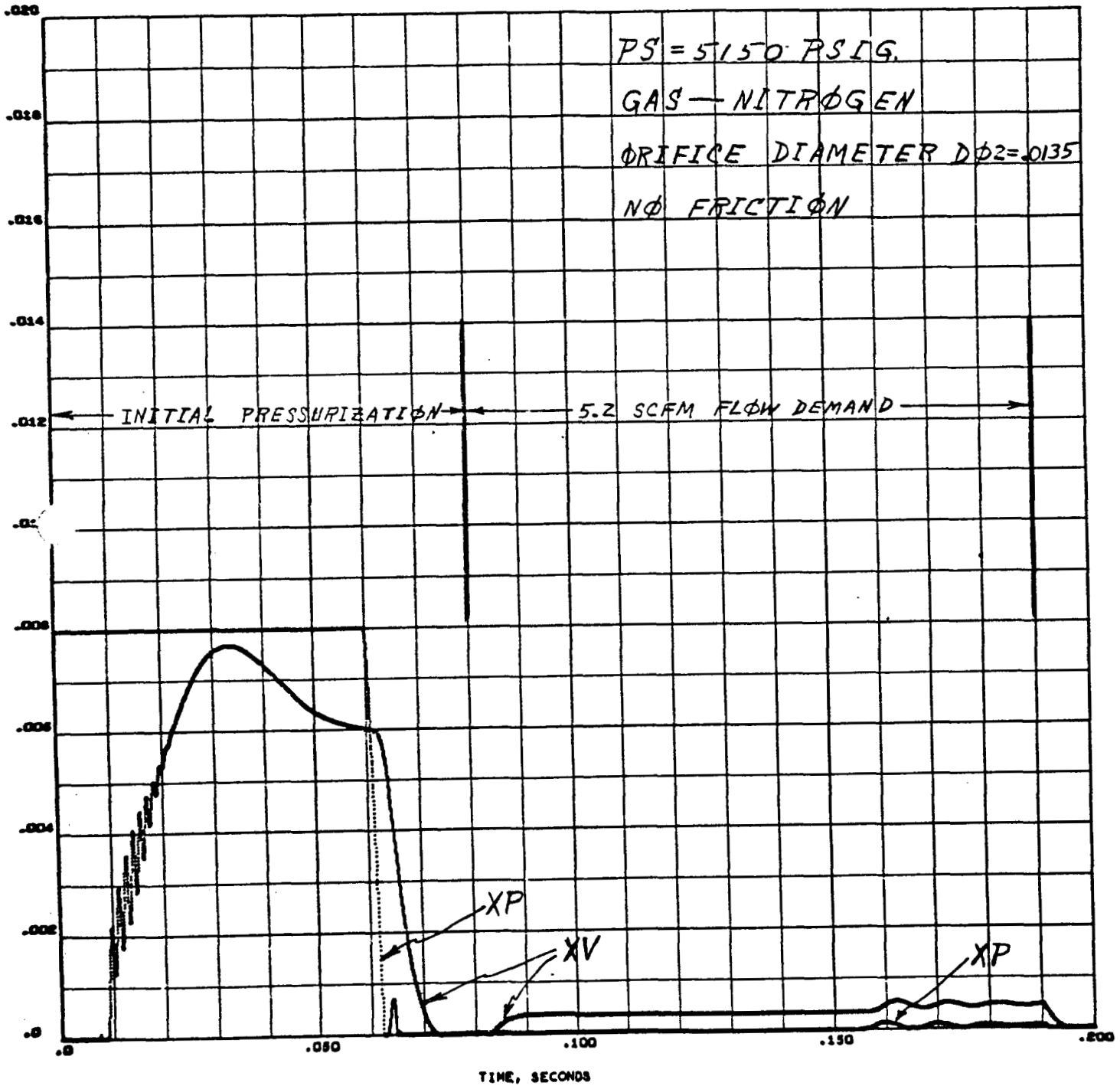


Figure 7. (Continued)

and main valve position are damping out when flow is terminated, and the regulator locks up. Had the run been continued with flow demand terminated, all pressures would converge because of bleed flow from PC1 to PR1.

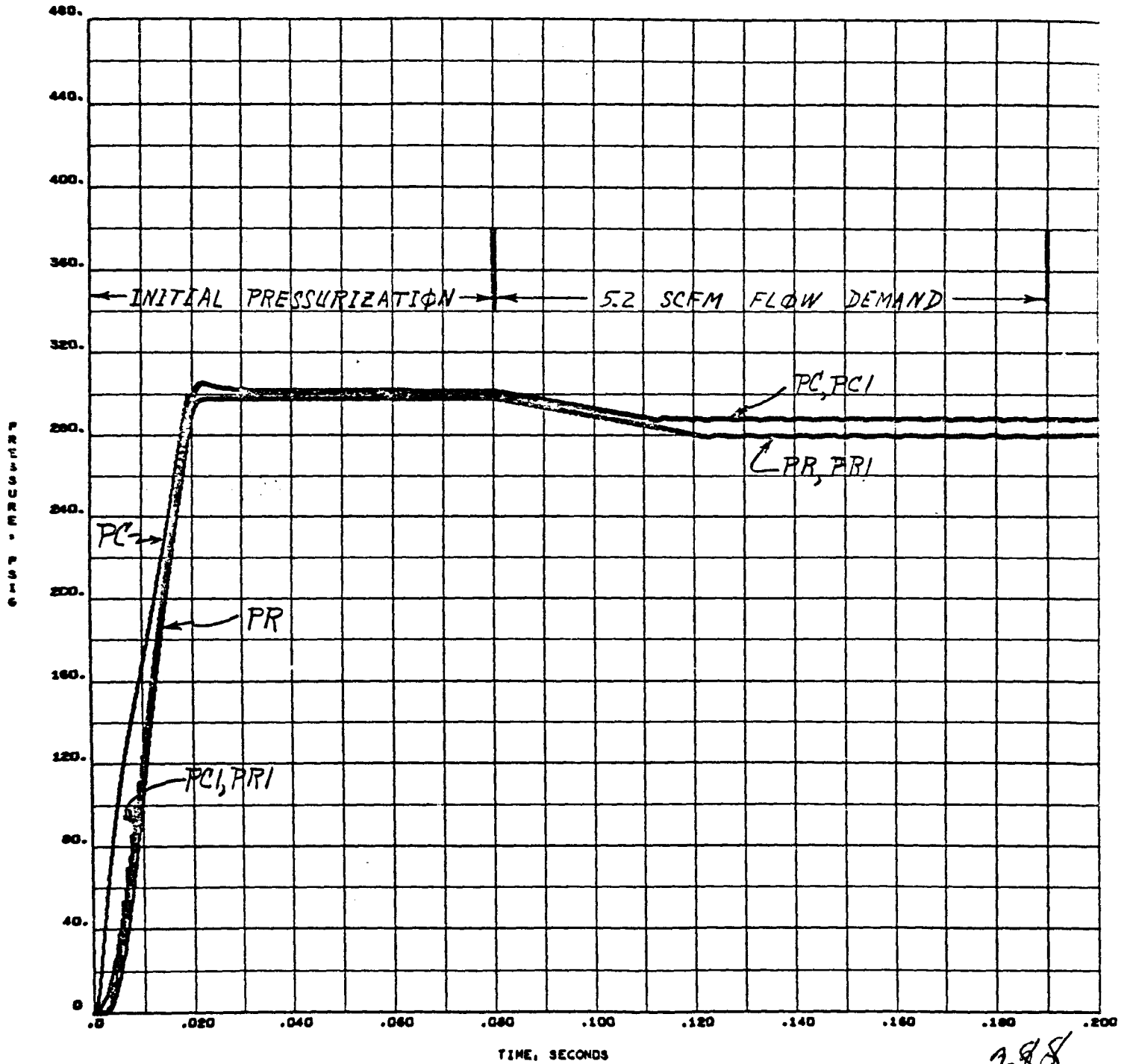
For computation purposes, all pressures are in PSIA. These are converted to PSIG for the CRT displays.

Figure 8 portrays the results of an identical run except for the use of helium as the pressurant. More rapid initial pressurization is accompanied by greater initial overshoot and more violent oscillation of the main valve. The regulator is more oscillatory with flow demand than in the similar run with nitrogen.

The computer run for Fig. 9 is the same as the run for Fig. 8 except that bleed orifice area ($A_{\phi 2}$) has been reduced by a factor of 2. This change has little effect on initial pressurization, but has a strong damping effect during flow demand.

The computer run for Fig. 10 is the same as the run for Fig. 9 except that 5 pounds of sliding friction has been added to the main valve actuator force balance, and the run time has been extended to 0.3 seconds. Since the actuator is biased by a belleville spring which must slide against the actuator and against the spring fixed base as the spring deflects, the inclusion of this friction force is realistic.

A comparison of Fig. 7 through 10 indicates the effects of the specific gas constant, the size of orifice area ($A_{\phi 2}$), and actuator friction. It is apparent that the configuration of Fig. 5 can be sized and tuned to conform with various sets of system requirements.



10000 POINTS

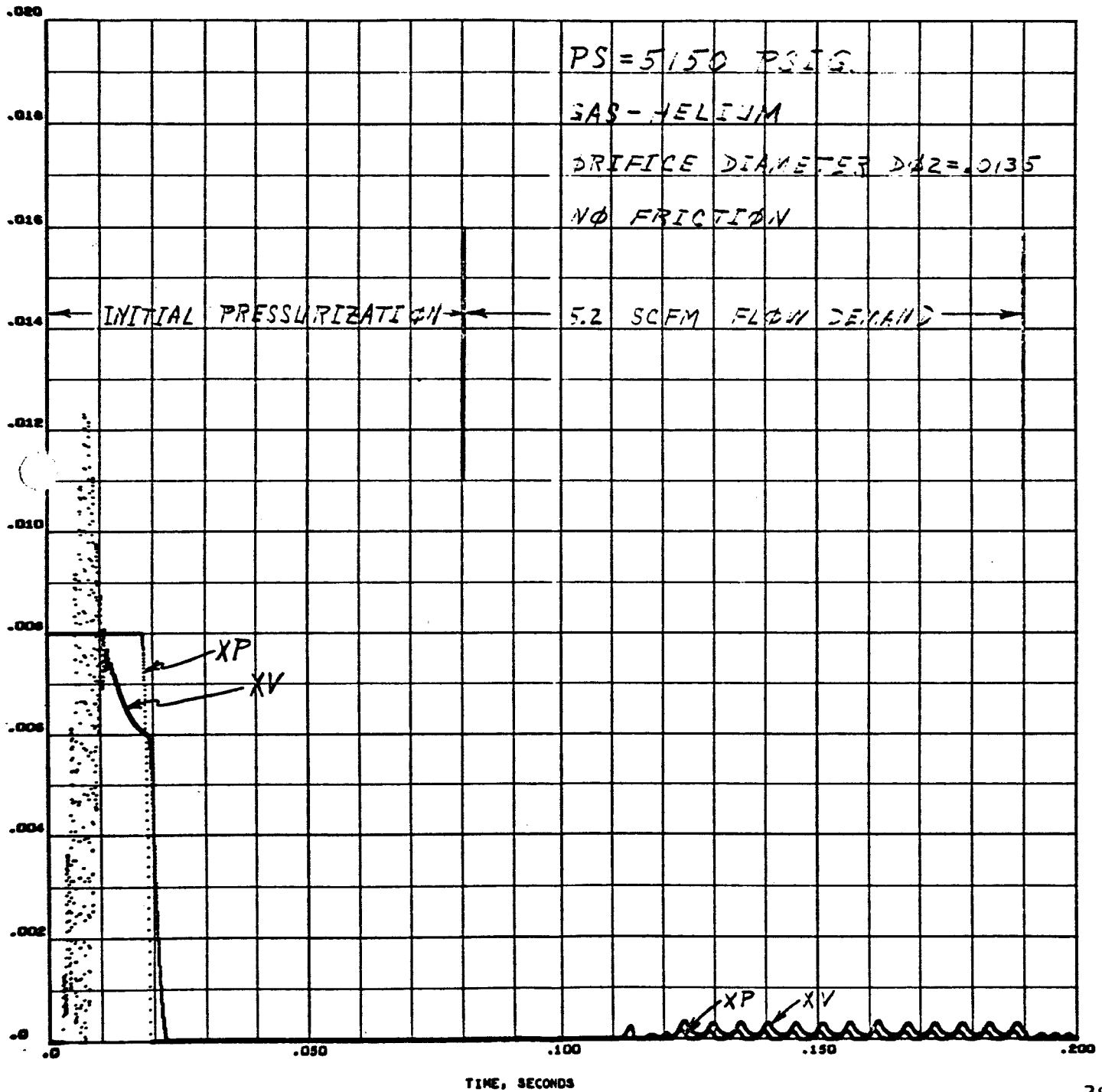
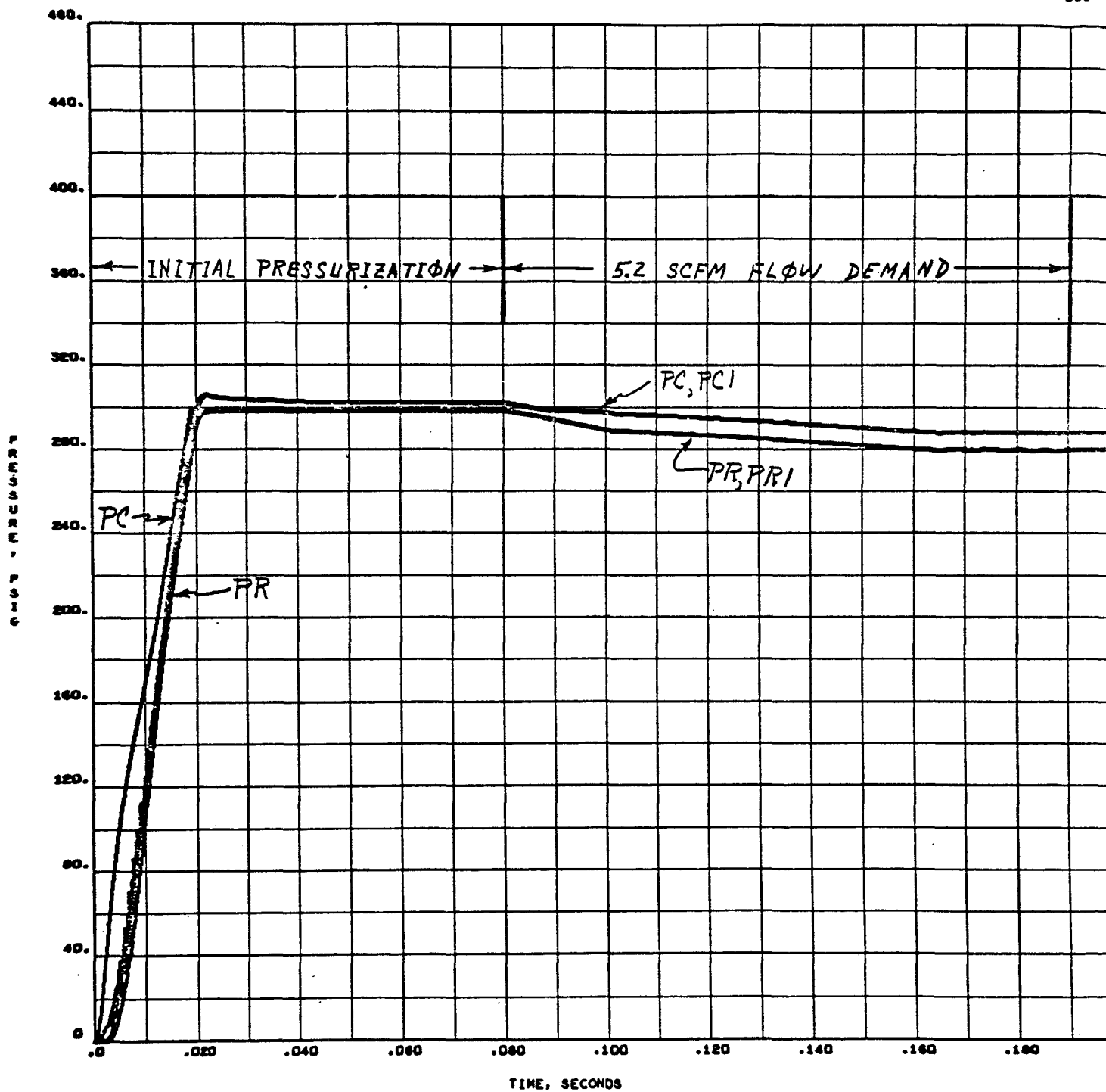
5457-23
004 000

Figure 8. Computer Run



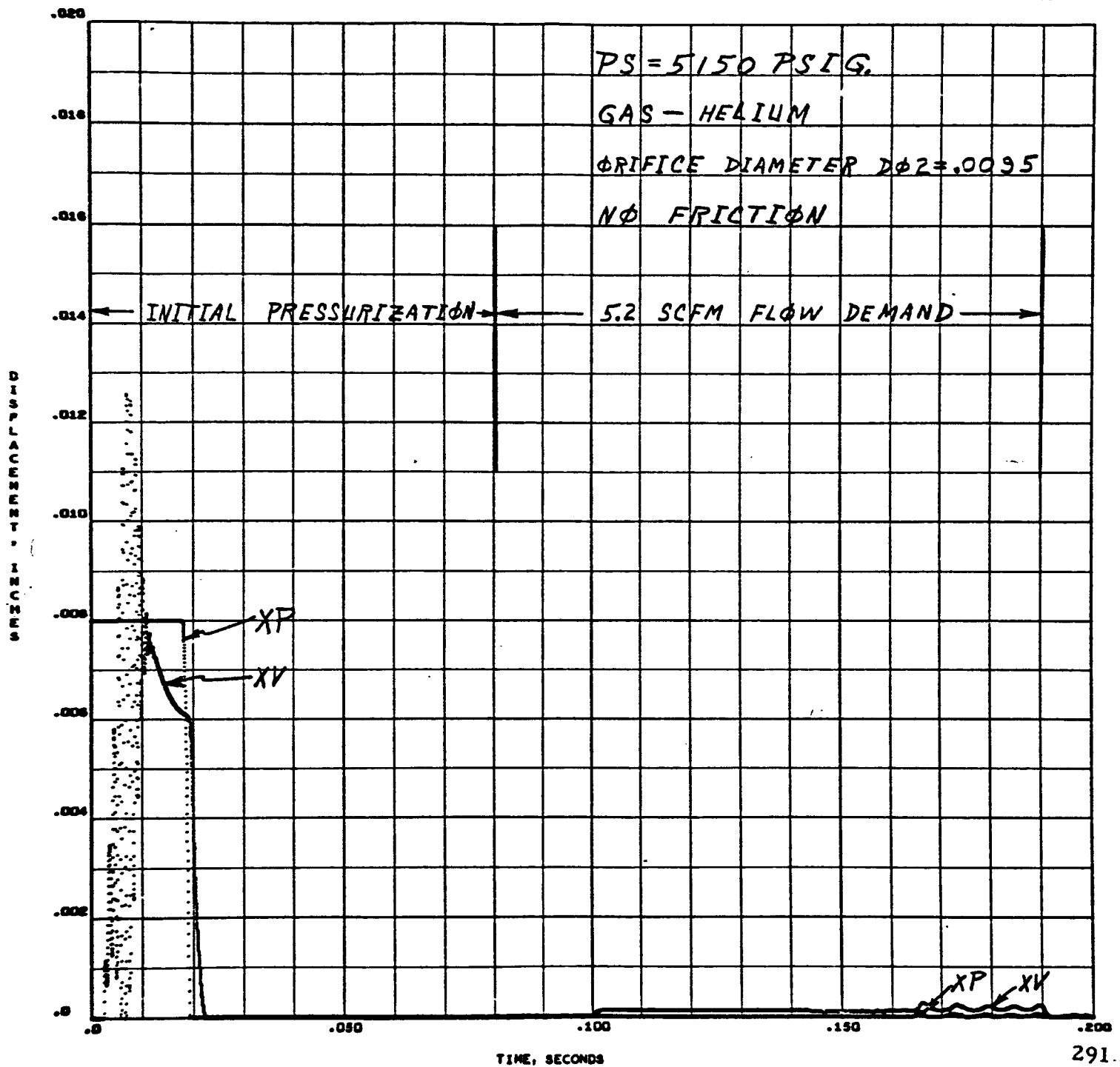
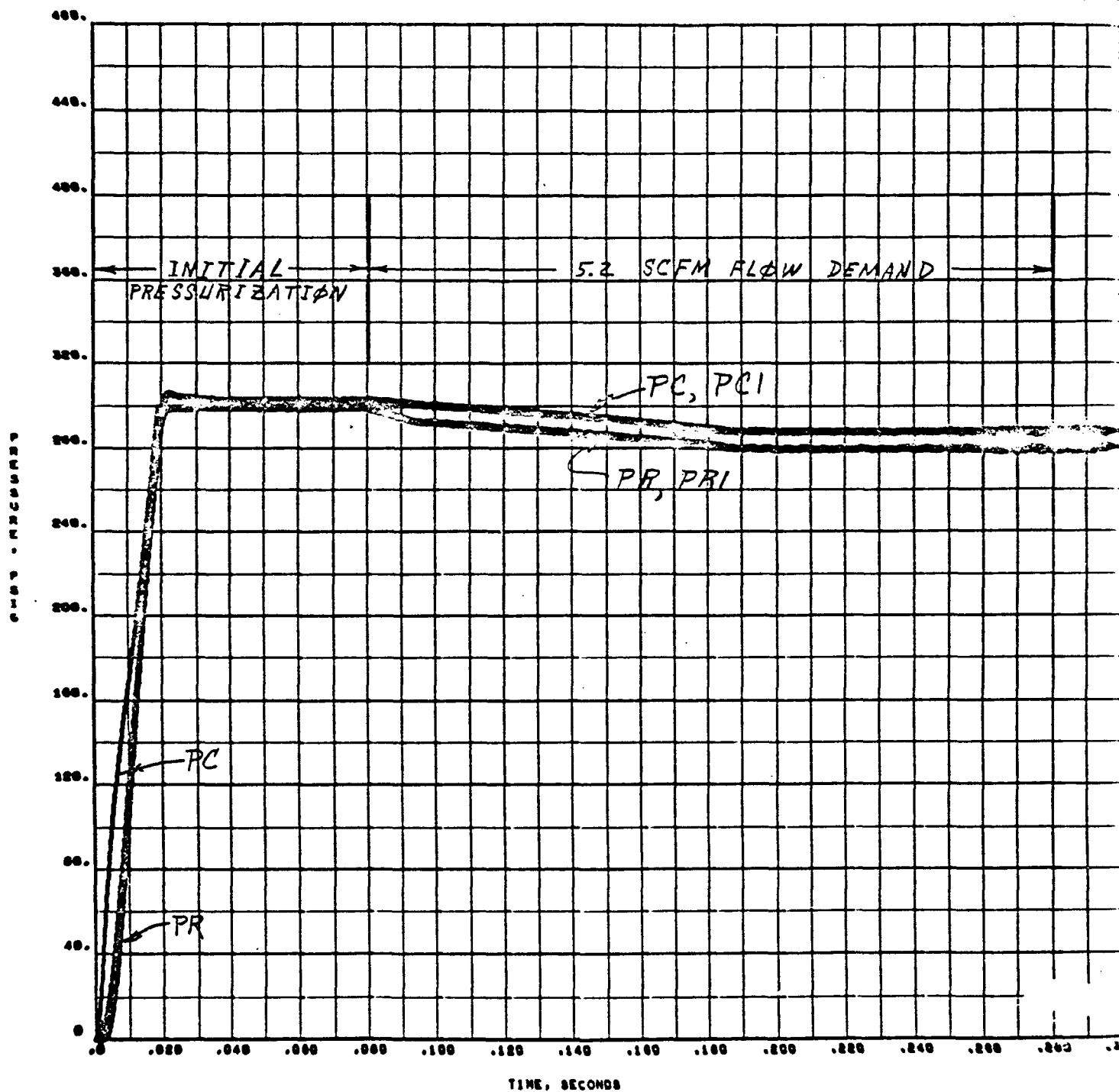


Figure 9. Computer Run



15000 POINTS

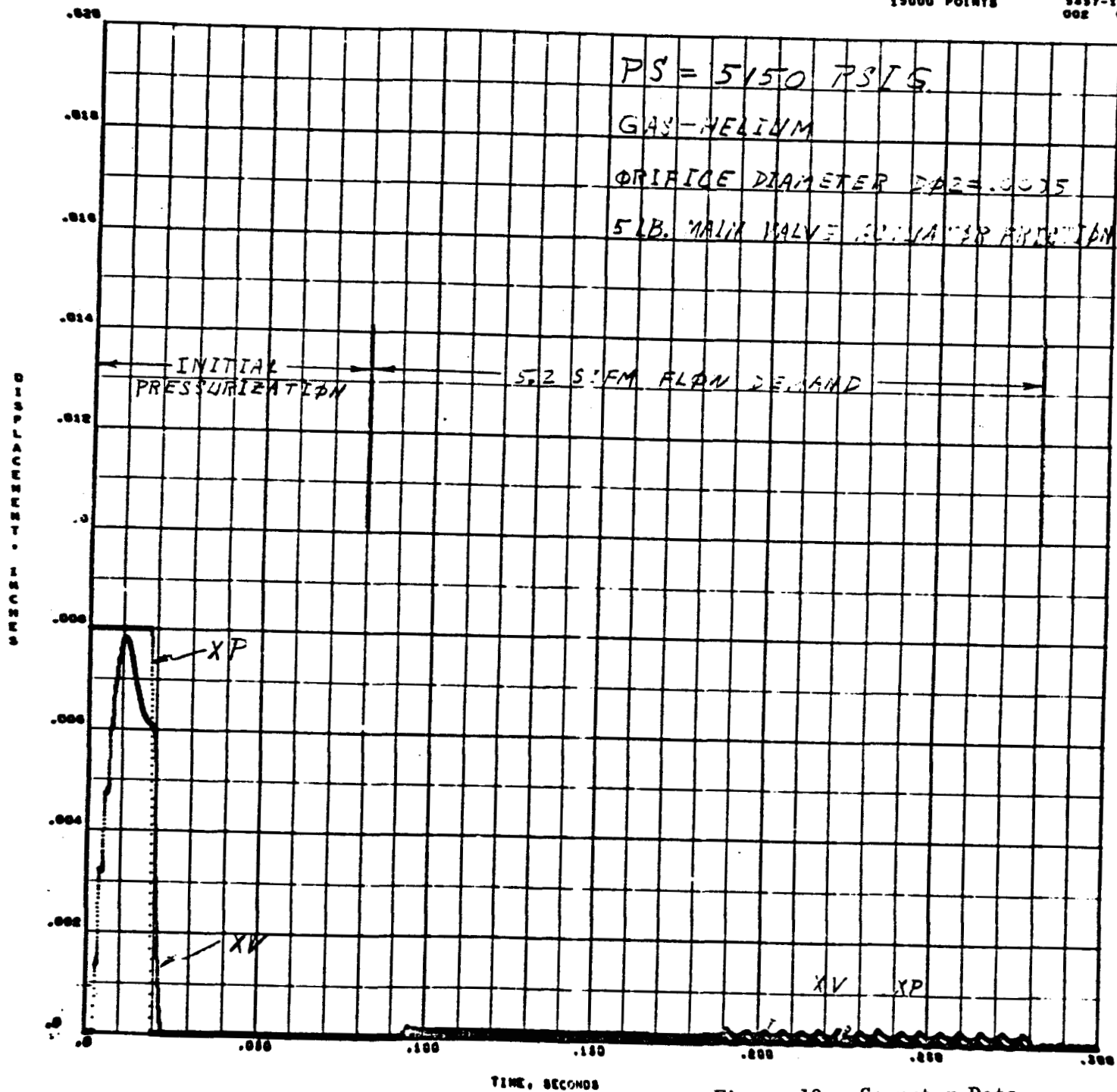
5457-17
002 000

Figure 10. Computer Data

The sample computer program can be used to extend the dynamic analysis to include the effects of supply pressure range, gas temperature, and downstream volume. The computer runs for Fig. 7 through 10 investigate the response to step inputs in supply pressure and flow demand. The response to other inputs can also be determined.

Figures 7 through 10 illustrate a convenient form of presentation of digital computer output data. In the upper righthand corner of Fig. 10 a statement "15,000 points" is printed. This is the number of discrete data points plotted for each of the six variables in the two frames of Fig. 10. In zones of fast transients, individual data points can be discerned. The data points merge to form continuous lines in zones of slow transients.

Dynamic analysis of the relatively simple scheme of Fig. 5 requires a mathematical model which includes six nonlinear and reversible gas flow descriptions. Accurate analysis of a complete pneumatic system which includes high pressure and low pressure relief valves as well as control valves, actuators, etc., would require many additional flow descriptions. A mathematical model for a pneumatic control system, for example, can easily include more than 100 flow terms.

In the program listed in Fig. 6, card numbers 10100 through 10600 call for subprogram FL ϕ W to compute flowrates. Flow can be positive or negative in direction, and sonic or subsonic in regime. Any number of additional flows can be computed using the same FL ϕ W subprogram, which is merely a computation procedure for the orifice-gas-flow equation producing exact results. In comparison, an accurate analogy requires a nonlinear function generator for each nonlinear reversible-flow description, and the number of function generators available is usually limited.

In a hydraulic system, nonlinear reversible flowrates can be computed using one subprogram based on an incompressible flow-orifice equation.

Card number 5994 in Fig. 6 calls for subprogram BFØRCE to compute an instantaneous belleville spring force. Any additional number of nonlinear belleville spring forces could be computed using the same subprogram.

A digital computer analysis of the simple scheme of Fig. 5 has been presented primarily for demonstration of a powerful analytic method which can be utilized by engineers with rudimentary FORTRAN training. The overwhelming advantages accruing to this method can best be appreciated when this method is successfully applied to complex systems which are beyond the scope of accurate analysis by other analytic methods.

SUMMARY

The purpose of this paper has been to review the application of FORTRAN programming and digital computers to the analytic solution of dynamic problems associated with pneumatic pressure regulators.

Although the general subject of dynamic analysis of nonlinear systems and complete details of the FORTRAN System cannot be encompassed in a single brief presentation, the intent of this paper is to emphasize the simplicity of a powerful analytic method which is available to engineers concerned with hardware and system dynamics.

Hopefully, the simple flowing dashpot program developed for illustration is sufficiently basic to indicate the ease with which nonlinearities and discontinuities can be handled in setting up and analyzing a mathematical model.

A program for analysis of a pneumatic pressure regulator has been included to present detailed programming techniques and to indicate the capacities of an iterative method.

SERVOMECHANISM APPROACH TO
FACILITY TANK PRESSURIZATION
by

Sanford M. Goldstein and Kurt J. Schurman
Rocketdyne
A Division of North American Aviation, Inc.
Canoga Park, California

SERVOMECHANISM APPROACH TO FACILITY TANK PRESSURIZATION

by

Sanford M. Goldstein and Kurt J. Schurman

ABSTRACT

This paper discusses the achievement of versatility in facility-tank pressure regulation through the use of servosystems. Methods of programming a tank-pressure profile and criteria for the selection of hardware are given, and a case study of the F-1 thrust chamber test stand is presented to demonstrate the correlations between analog simulation techniques and system operation.

DISCUSSION

ELECTROMECHANICAL VS MECHANICAL CONTROL

The need for versatility, accuracy of control, and convenience of operation in facility propellant tank pressure regulation has established the electromechanical servosystem as the basic control technique at Rocketdyne's propulsion field laboratories.

Mechanical pressure regulators, such as the pneumatic dome type (Fig. 1), are being used in this service, but they have two inherent drawbacks which restrict their application.

The first of these is caused by a variation in control-chamber volume with any sudden poppet position change. This results in a temporary differential between dome reference pressure and control chamber pressure. If the separation plate orifice which allows these pressures to equalize is too large, the regulator

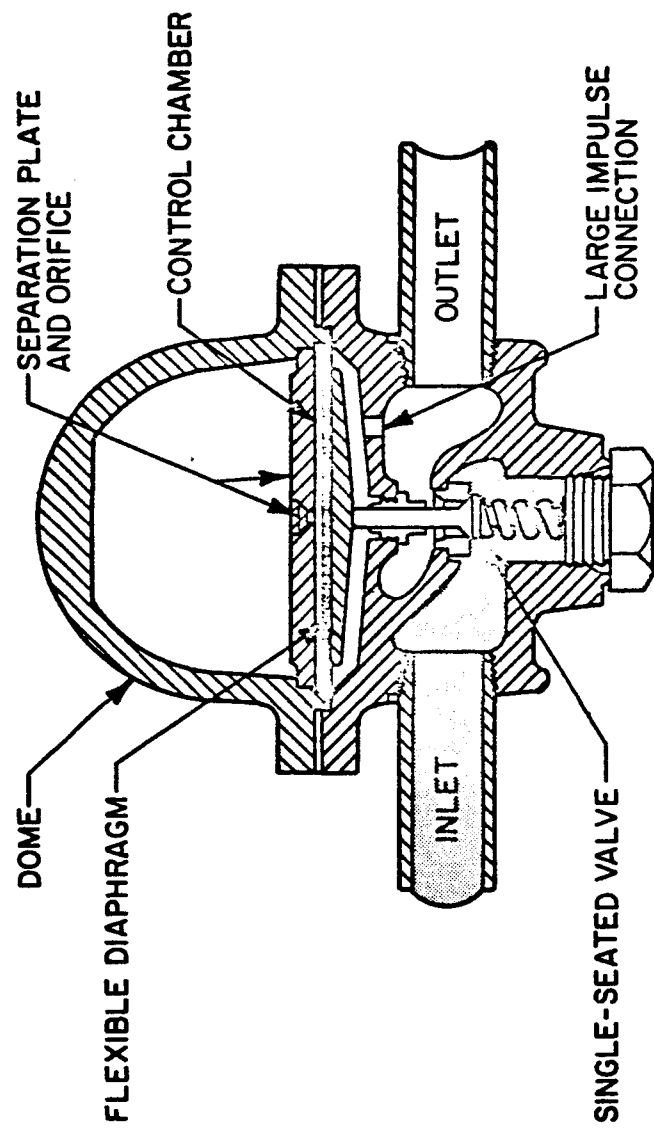


Figure 1. Typical Dome Pressure Regulator

has a tendency to chatter. For this reason, response of these valves is limited to approximately 1 cps. Secondly, the steady-state regulated pressure tends to increase because of a decrease in net seat force with supply-pressure decay in the storage vessel. For various regulators of one manufacturer, tests have shown an outlet-pressure rise per 100 psi inlet-pressure decay of between 0.65 and 5.5 psi on unbalanced designs, and 0.50 to 1.3 psi for balanced units.

A need to program or regulate injector or pump inlet pressures creates additional restrictions because of the need for overly long sensing lines. Since electro-mechanical servosystems can respond to logic circuitry, these pressurization systems may be readily incorporated into an integrated propellant conditioning system for automated engine testing.

As an example, in turbopump cavitation testing tank pressure must be varied in accordance with some predetermined curve. In this application, the propellant normally is recirculated from the run tank through the pump and a flow restriction back to the tank. The tank pressure undergoes a programmed decay until the net positive suction head at the pump inlet becomes low enough for cavitation to occur. The pump head drop is automatically monitored and used to initiate tank repressurization. To prevent pump damage, repressurization time must be minimized and, therefore, the regulator size may be as much as an order of magnitude larger than required for normal operation.

In another application, programming requirements specify a faster tank pressure decay than can normally result from propellant efflux. A vent valve servosystem is provided, and an on-off pressurizing control valve is used to supply pressurizing gas during periods when pressure decay caused by propellant efflux is greater than program requirements.

In applications where hydraulic oil supply is not provided, a high pressure (up to 5000 psi) pneumatic actuation system has been used for modulating valve* control. This system utilizes an industrial servovalve modified for GN_2 operation and has a frequency response somewhat lower (10 cps to 3 db point) than a hydraulic system.

*Equivalent terms often used are: throttling, regulating, or control valve

SYSTEM DESIGN PROCEDURES

When a request is received for a new tank pressurization system, a study is made of operating requirements to determine the suitability of mechanical regulation for the application. If it is determined that a servosystem is superior, a dual design and analysis approach is undertaken to minimize development time and costs. First, hardware is selected, and modulating valves can be sized in consideration of the effects outlined below. Then a complete system study is initiated to determine final system configuration and transient characteristics.

UNBALANCED VS BALANCED VALVES

The pressurizing gas storage vessels of facility test stands are normally high pressure and, hence, restrict the selection of a modulating valve to one that is capable of service at high inlet pressures (3000 psi and up). Commercially available valves may be categorized into unbalanced designs where the actuator may have to exert a large force to overcome those on the flow restricting elements of the valve, or balanced designs where this force unbalance is minimized.

Balanced valves are preferable since unbalanced valves:

1. Require use of larger actuators, hydraulic oil demand, accumulators, and servovalves with a resulting decrease in response time.
2. Exhibit a large load pressure drop (i.e., the pressure drop across the actuator piston) which makes the actuator, servovalve, and modulating valve combination nonlinear and thus limits the use of standard servosystem linear analysis techniques.

(Advantages and disadvantages of various types of modulating valve are listed in the Appendix.)

USEFUL DEFINITIONS FOR PROPERLY SIZING VALVES

To adequately size a valve for tank pressurization service, it becomes desirable to relate static and dynamic process requirements to valve characteristics. To this end, modulating valve gain (G_v) and control rangeability (C_r) are defined as follows:

$$G_v = \frac{\dot{W}_{\max}}{100} \left| \Delta P \text{ valve} = \text{constant} \right.$$

The maximum valve flow per percent stroke at a constant valve (ΔP).

$$C_r = \frac{\dot{W}_1}{\dot{W}_2} \left| \frac{d\dot{W}}{ds} = K G_v \right.$$

The maximum flow divided by the minimum flow over the range of stroke where the slope of the actual flow characteristic is within some tolerance (K) of the modulating valve gain (G_v).

The required G_v is determined by:

1. Predicted depletion of gas-storage-vessel pressure during test duration. The valve must be adequately sized to provide sufficient gas flow at minimum anticipated supply pressure.
2. Predicted pressure drop of the pressurizing lines and valves both upstream and downstream of the modulating valve. The line losses which may have considerable effect on valve sizing can be determined by the modified Darcy method and Moody chart or preferably by the Gas Dynamics method which indicates line choking.
3. A major factor in valve sizing is the specific propellant being handled and the working pressure range desired. If the propellant is storable or noncryogenic, then the pressurizing gas simply has to replace the tank propellant efflux on a volume basis. For cryogenic propellants, heat transfer, and mass transport effects, such as condensation, vaporization, and absorption are superimposed on the volume rule.

The minimum required flow (\dot{W}_2) arises from a standby mode where the system is in the operate configuration prior to run commencement, and tank pressure must be regulated with minimum ullage and no propellant efflux. During this period there can be system leakage and/or gas absorption which requires the modulating valve to be constantly throttling at low flowrates.

The slope tolerance (K) becomes a restriction on the degree of nonlinearity introduced into the closed-loop control system through the valve flow characteristic. An approximation to the limitation on K , for some systems, may be found by Lyapunov's direct method and Aizerman's conjecture (Ref. 1). Valve (K) can be determined from the actual valve flow characteristic at constant (ΔP). It then becomes possible to determine compatibility of a given valve and a given system or conversely the required system (G_v) and (C_r) can be imposed as design or selection requirements on the valve. Caution must be exercised in the application of this approach since in throttling service the valve (ΔP) is not constant, and the system nonlinearity is different than observed from the valve flow characteristic.

A TYPICAL SYSTEM

Figure 2 illustrates a typical tank pressure control system. The main components are:

1. Electronic controller
2. Servovalve (This is a pilot valve which responds proportionately to amplifier voltage and drives the modulating valve).
3. Modulating valve, actuation, and position feedback transducer.
4. Transducer (This senses tank pressure which is compared to desired reference pressure to the controller).

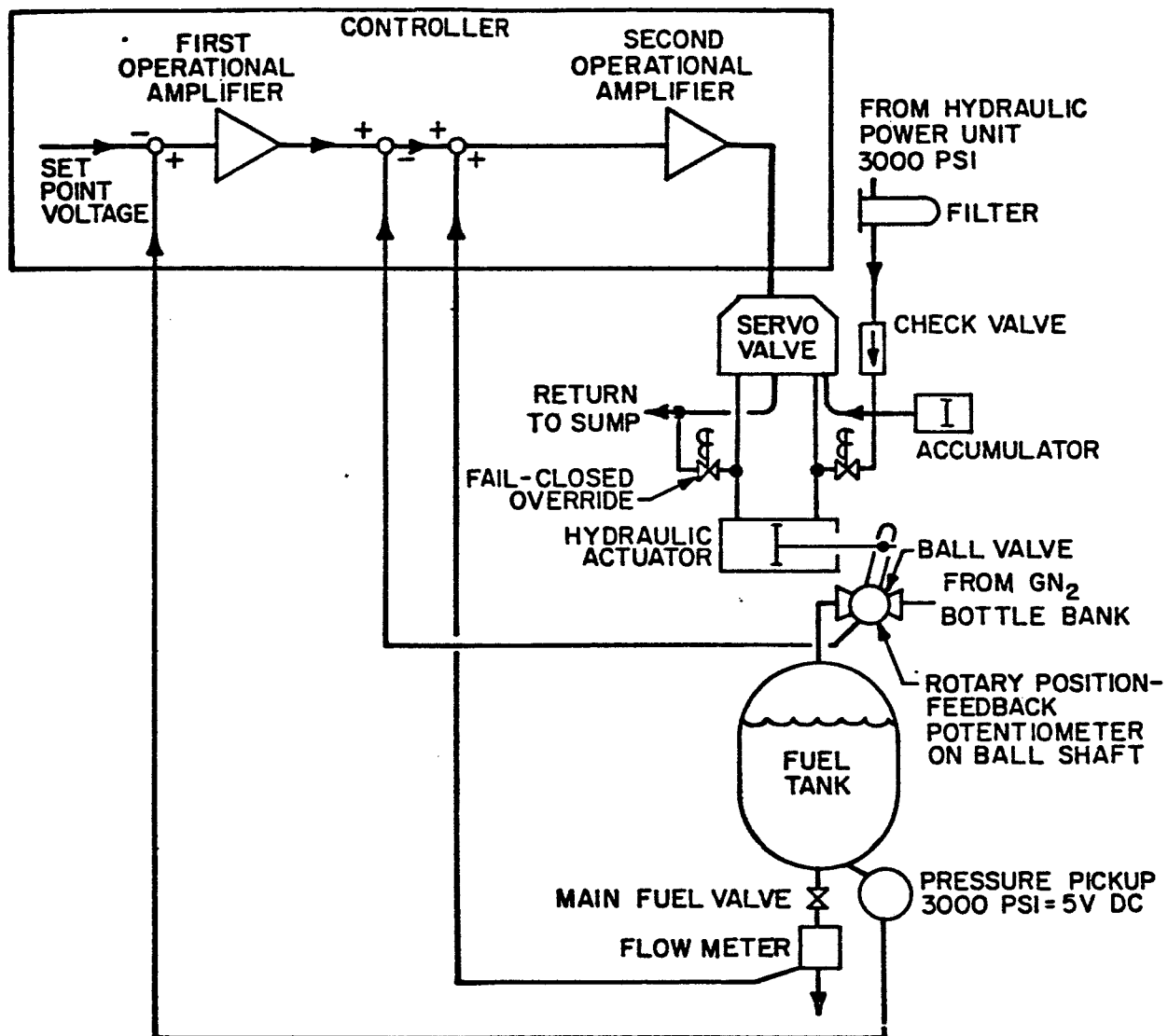


Figure 2. Electrohydraulic Pressurizing System

The controller consists of two solid-state operational amplifiers; its input is the pressure set point, and the output drives the servovalve for modulating valve positioning. Closed-loop control is provided by the valve-position transducer (inner loop) and by the tank pressure transducer. The servovalve consists of a polarized electrical torque motor and two stages of hydraulic power amplification. The first hydraulic stage (flapper stage) converts the electrical signal into a differential pressure driving the second stage sliding spool. Flow from the servovalve to the actuator is essentially proportional to spool position for constant supply pressure and modulating valve loading.

With the controller in the "operate" mode, tank pressure is sensed by a transducer and compared to a set point voltage proportional to the desired tank pressure. The resulting voltage difference is integrated by the first operational amplifier to generate a control signal voltage whose magnitude is dependent on both the magnitude of the difference (error) voltage and the length of time it exists. The control signal is amplified by the second operational amplifier and is the input to the servovalve for modulating valve actuation.

The modulating valve is mechanically linked to the position feedback transducer to produce a voltage proportional to the modulating valve position. This position voltage is fed back to the second operational amplifier in such a manner that it cancels the control voltage when the regulating valve has been positioned in such a way that the tank pressure is caused to approach the desired tank pressure registered at the set point.

A CASE STUDY

Fuel tank pressure on an F-1 thrust chamber stand at Edwards Rocket Site was controlled by a servosystem schematically (Fig. 2). Mixture ratio tolerances require fuel tank pressure to be within 30 psi of set point (1600 to 1800 psi) at the beginning of main stage, and within 15 psi 500 milliseconds later. In the start sequence, the fuel tank is prepressurized to approximately 125 psi

below set point. The modulating valve seats are retracted from the ball, and 100 milliseconds later the controller is switched to the operate mode. Following another 100 milliseconds delay, an opening signal is given to the main fuel valve.

Problems became apparent during a thrust chamber stability test program. A severe tank pressure dip of between 100 and 200 psi was prevalent during the fuel-flow start transient, and can be seen from Run 239 in Fig. 3. Because of the critical nature of the requirements, it was decided to develop an analog simulation and investigate system operation with regard to servovalve size, actuator size, flow-area trim, and controller compensation.

VALVE EQUATIONS

The equations describing ball-valve rotation as a function of servovoltage were derived by reference to Fig. 4, which shows the modulating valve actuation system and a schematic based on the following assumptions:

1. Hydraulic oil is incompressible.
2. Dynamic effects of servovalve supply lines may be disregarded because of the accumulator at the supply port.
3. Both actuators are identical and may be treated as a single unit with twice the piston area.
4. Viscous damping and friction in the actuator can be neglected.

Servovalves are four-way valves in which the hydraulic oil supply and return areas (A) are always equal and proportional to spool position and signal current.

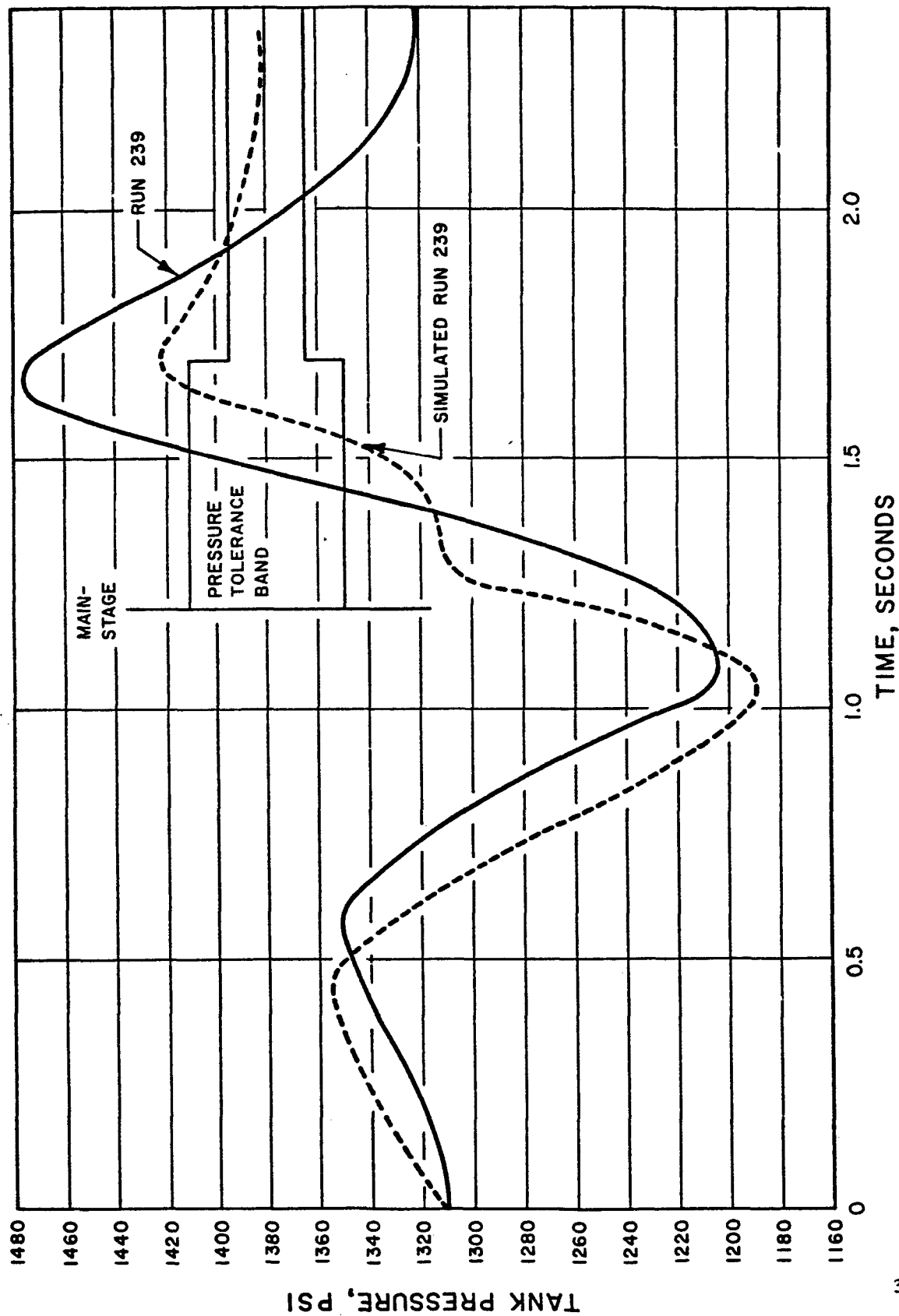


Figure 3. F-1 Thrust Chamber Stand Fuel Pressurizing System Tank Pressure

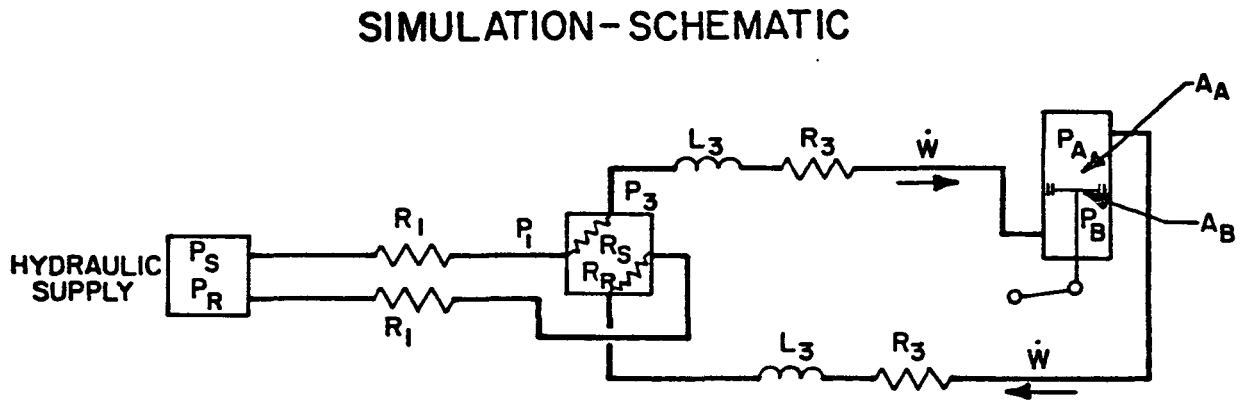
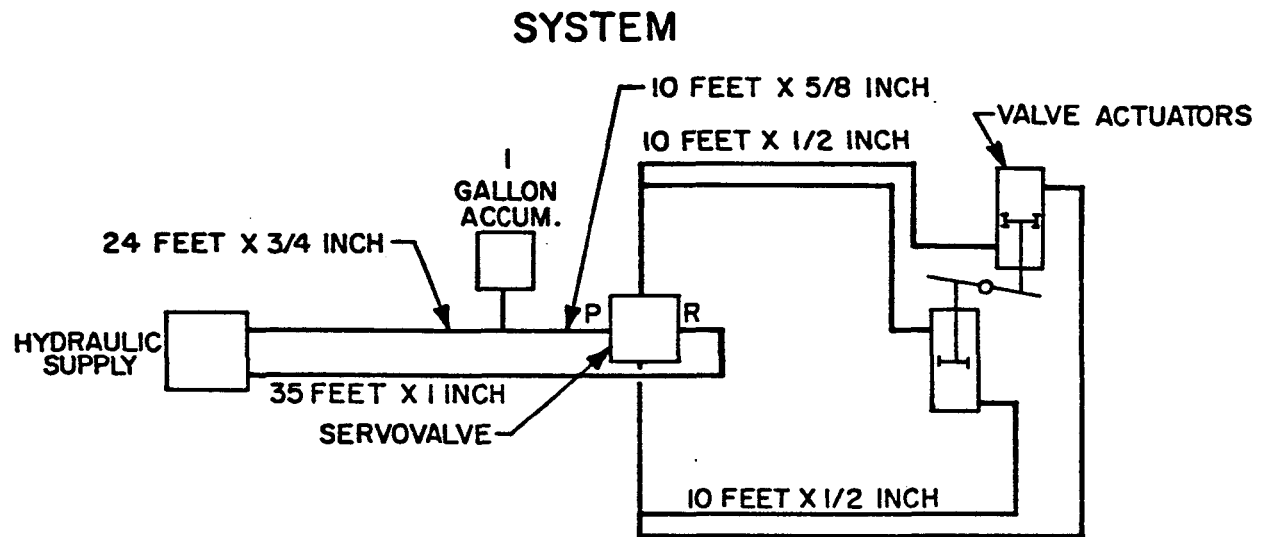


Figure 4. Modulating Valve Actuation System

The weight flowrate of hydraulic oil (\dot{W}) through the servovalve can be related to pressure drop by:

$$R_s \dot{W}^2 = P_1 - P_3 \quad (1)$$

where

$$R_s = \frac{1}{2gC^2 A^2 \gamma} = \frac{0.116}{A^2}$$

For symbols see page 320

The servovalve supply line pressure loss is:

$$R_1 \dot{W}^2 = P_s - P_1 \quad (2)$$

The pressure drop between the servovalve and actuator closing port is:

$$P_3 - P_B = L_3 \ddot{W} + R_3 \dot{W}^2 \quad (3)$$

where

R_3 and L_3 = effective resistance and inertia of the connecting line

The flowrate out of the opening port (\dot{W}) can be described as a function of piston velocity (\dot{X}):

$$\dot{W} = A_A \gamma \dot{X} \quad (4)$$

where

A_A = piston area in opening port

From Assumption 1, it can be seen that the flowrates into and out of the double acting cylinder differ by the ratio (k) of the areas on either side of the piston. Since the resistance and inertia of the pressurizing and return lines are approximately alike, it can be shown:

$$P_B = k^2 (P_s - P_A) \quad \text{Opening} \quad (5a)$$

$$P_B = P_s - k^2 P_A \quad \text{Closing} \quad (5b)$$

where

$$k = \frac{A_B}{A_A}$$

By introducing this k-ratio it is possible to simulate properly the pressure distribution caused by the area difference on the rod side of the pistons. The proper equation in Equation 5 was chosen in the mechanization by using the polarity of the servovoltage to actuate a relay.

When a ball valve is partially open, the pressure distribution inside the ball passageway is uneven and causes a considerable closing torque. This flow torque is zero when the valve is fully open or fully closed because of symmetry, and has a maximum at some intermediate ball position.

Angular acceleration of the ball is developed by the difference between the actuator and flow torques.

$$(P_A A_A - P_B A_B) l \cos (\theta - 45^\circ) = T_L + J_B \ddot{\theta} \quad (6)$$

$l \cos (\theta - 45^\circ)$ was approximated by an effective lever arm l' to yield

$$P_A = k P_B + \frac{T_L}{A_A l'} + \frac{J_B}{A_A l'} \ddot{\theta} \quad (7)$$

where

θ = ball rotation

T_L = load torque

The load torque (T_L) has been a major factor affecting response characteristics. In this study, the load torque vs ball position curve was determined on the basis of constant pressure at the valve inlet and simulated through use of a diode function generator.

The ball rotation was found to be approximately linear with actuator stroke:

$$\theta = k_1 X \quad (8)$$

Since the response of the servovalve is much faster than the modulating valve, it was assumed the servoflow area (A) was linear with current (i_s):

$$A = k_2 i_s \quad (9)$$

A lag exists between servovalve voltage (V_s) and current (i_s) because effective coil resistance (R_c) and inductance (L_{eff}):

$$V_s = i_s R_c + L_{eff} \frac{di_s}{dt} \quad (10)$$

The valve position feedback voltage (E_f) is linear with actuator stroke:

$$E_f = k_3 X = k_3 \theta$$

DESCRIBING EQUATIONS FOR FUEL TANK

In this system the fuel was noncryogenic, and the tank process equations were written on a volume-flow basis using perfect gas equations:

$$P_t = \frac{RT (M_o + \Delta M)}{V_o + \Delta V} \quad (11)$$

The initial mass of gas (M_o) in the ullage space (V_o) is:

$$M_o = \frac{P_o V_o}{RT_o} \quad (12)$$

The increase of mass in the ullage space can be found from pressurizing gas flowrates:

$$\Delta M = \int \frac{\dot{W}_{GN_2}}{g} dt \quad (13)$$

Ullage volume increase (ΔV) is found from fuel flowrates (\dot{W}_f):

$$\Delta V = \int \frac{\dot{W}_f}{\gamma} dt \quad (14)$$

The fuel-flow curve from the main-tank valve opening was plotted as a function of time and simulated with a diode function generator. This approach was felt justified, since it was the rate of change of fuel flow, not the steady value, that was found to have a major effect on pressure transients.

The pressurizing gas flowrate through the choked modulating valve is:

$$\dot{W}_{GN_2} = \frac{C A_R P_R S}{\sqrt{RT}} \quad (15)$$

where

S = a function of the modulating valve upstream to throat-pressure ratio
which for GN_2 under critical flow equals 3.88.

Valve flow area $A_R = f(\theta)$, and is zero until the ball is approximately 20 percent open and increases nonlinearly to maximum flow area at 90 degrees. A diode function generator was used for this simulation.

The pressure feedback transducer provides a voltage linear with pressure:

$$E_t = k_4 P_t \quad (16)$$

GN_2 FEED SYSTEM

Because of long length of feedline between the bottle bank and propellant tank, both line inertia and compressibility effects have to be considered. This is achieved by considering the total line to be made up of several sections each having a lumped inertia and compressibility factor (finite difference approach). The number of required sections is dictated by the frequency to which the overall model is to be described, and can be determined from the solution of a ladder network with similar end conditions (Ref. 2).

The solution to the ladder network as presented in this reference is:

$$\omega_r = \frac{2}{\sqrt{LC}} \sin \frac{r\pi}{2n} \quad r = 1, 2, 3, \dots \quad (17)$$

where

ω_r = resonant mode
L = lump inertia
C = lump capacitance

For small sine arguments, i.e., $\frac{r\pi}{2n} \leq \frac{\pi}{8}$, the above solution, for a fluid system, is in agreement with classical acoustic theory. This can be shown by substituting fluid equivalent inertia and capacitance in the above equation and considering

$$L = \frac{\ell}{Ag} \quad (18)$$

$$C = \frac{\ell Ag}{a^2} \quad (19)$$

where

ℓ = lump length
 A = duct area
 a = acoustic velocity in fluid media

$$\omega_r = \frac{2\pi a r}{2 \ell_T} \quad r = 1, 2, 3 \dots \quad (20)$$

where

ℓ_T = total line length = $n\ell$

Thus, for example, when $n = 8$, $r = 1$, and $n = 8$, $r = 2$

$$\frac{r\pi}{2n} \leq \frac{\pi}{8} \quad (21)$$

and

$$\omega_1 = \frac{2\pi a}{2 \ell_T}, \quad \omega_2 = \frac{2\pi a}{\ell_T} \quad (22)$$

which agree with acoustic theory.

For the GN_2 system studied, frequencies to the first acoustic mode were considered pertinent, requiring a four-section description of the feedline.

$$\frac{r\pi}{2n} \leq \frac{\pi}{8} \quad \text{and } r = 1 \quad (23)$$

$$\frac{\pi}{2n} \leq \frac{\pi}{8}, \quad n \geq 4 \quad (24)$$

Figure 5. Electrical Simulation of the Nonlinear Pressuring Pipe Conditions

The electronic controller has pressure and position amplifier transfer functions given by:

$$\frac{E_o}{E_t - E_s} = \frac{k_1 (\tau s + 1)}{s} \quad \text{and} \quad \frac{V_s}{E_o - E_f} = k_2 \quad (27)$$

where gain(k_1) is adjustable from unity to open loop gain of the operational amplifier (approximately 200,000), and the lead time constant (τ) can be set at any value between 0 and 0.8 second.

This simulation was performed on a Beckman Ease Model 1130 analog computer, and described nonlinear resistances by means of squaring circuits and actuation delays by relays driven from a time base.

In Fig. 3 correlation between this simulation and run data is shown by tank pressure curves for Run 239. The computer curve seems to exhibit slightly more damping than the real system by stabilizing in the tolerance bank after the second pressure overshoot which itself is lower than that in the physical system. At the completion of Run 239 the modulating valve was removed for service. Excessive friction between the ball and seats was found which may account for the discrepancy observed. It was felt correlation was close enough to provide information for optimizing system performance. Runs were made to find optimum controller gain and lead settings for 60, 40, 25, and 15 gpm servovalves. Indication was that use of a 60 gpm valve and controller settings of $k_1 = 4$ and $\tau = 0.8$ second would meet system requirements. Additional runs demonstrated that actuator size and modulator valve orifice adjustments would not further improve regulation.

Figure 6 shows correlating pressure traces for simulated and actual Run 245 which incorporated these changes.

The study further indicated that the initial buildup and subsequent decay of fuel flow caused by increasing thrust chamber pressure was the major factor causing pressure fluctuations. In view of the need for higher flowrates requested for the F-1 uprating program and the marginal manner in which present pressure

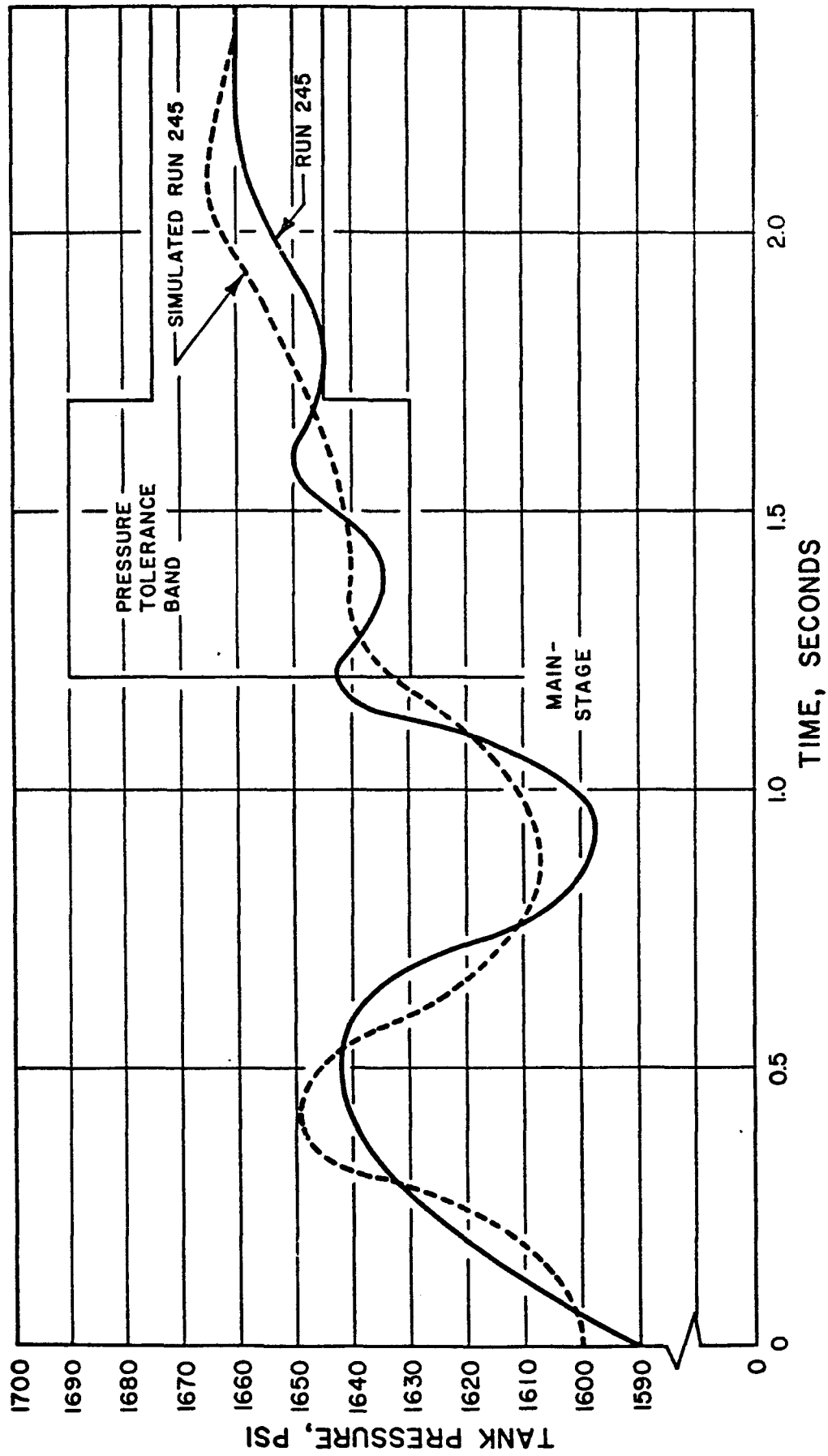


Figure 6. F-1 Thrust Chamber Stand Fuel Pressurizing System Tank Pressure

regulating requirements are met, it has been decided to investigate the additional use of fuel flow feedback (Fig. 2). The simulation has been changed so that the flow signal is differentiated and used to drive the modulating valve further open in anticipation of tank pressure decay. Figure 7 indicates that it may be possible to further improve the system so that it is within 10 psi of set point 900 milliseconds before mainstage.

•

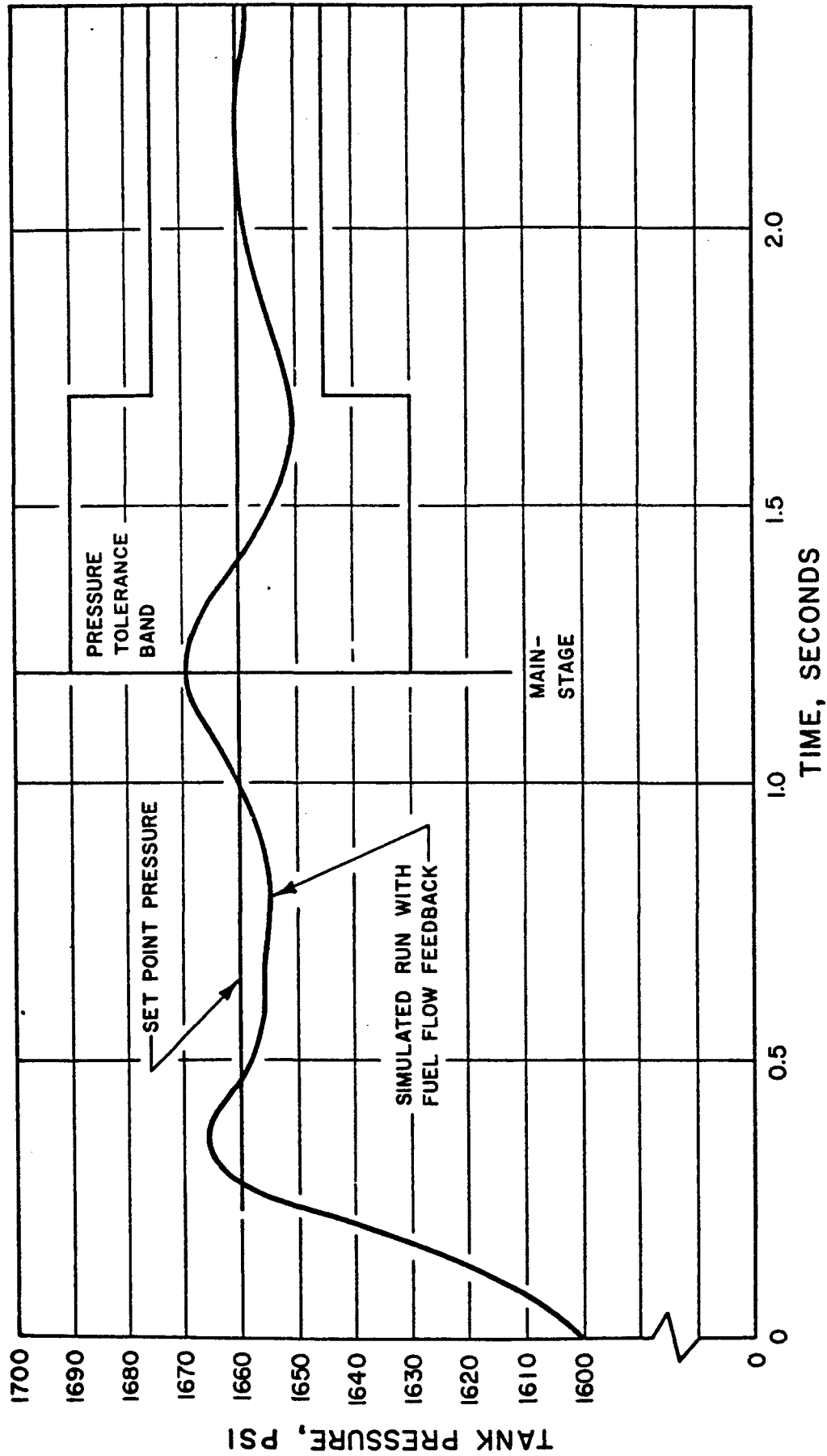


Figure 7. F-1 Thrust Chamber Stand Fuel Pressurizing System Tank Pressure (showing improvement)

APPENDIX

Comparison of several types of modulating valves* which have been used at Rocketdyne Test Facilities.

<u>Type of Valve</u>	<u>Advantages</u>	<u>Disadvantages</u>
Gate Valve	Large $\frac{c_v}{\text{size}}$ ratio	<ol style="list-style-type: none"> (1) Standard designs must be modified for modulating valve service. (2) Excessive friction creates large hysteresis and requires large actuator.
Butterfly	Large $\frac{c_v}{\text{size}}$ ratio	<ol style="list-style-type: none"> (1) Relatively large flow torque when partially open necessitates use of large actuators (2) Two packings which may cause external leakage with wear.
Ball Valve	Large $\frac{c_v}{\text{size}}$ ratio (Ball-valve regulators are in continuous reliable use at Rocketdyne Field Laboratories.)	<ol style="list-style-type: none"> (1) When partially open ball shaft torque is excessive and requires large actuators. (2) Rack and pinion actuator linkage is subject to wear and introduces backlash. (3) Pivoted linkage subjects linear position transducer to high-g loads (whipping) and requires use of flex lines for hydraulic oil supply and return which may contaminate oil with elastomeric particles. (4) Flow torque tends to close valve causing a nonlinear position response

*Equivalent terms often used are: throttling, regulating, or control valve

<u>Type of Valve</u>	<u>Advantages</u>	<u>Disadvantages</u>
Regulator with fluted in-line poppet	Designed for 5000 psig operating pressure. Medium $\frac{c_v}{\text{size}}$ ratio	Actuator is inside the valve itself and is therefore, inaccessible. Internal leakage is considerable, but not necessarily objectionable if a separate shutoff valve exists.
Single-poppet globe valve	Very good reliability. Commercially available up to 6000 psig operating pressure. Split body facilitates seat replacement. Minimum internal leakage because of soft seat. Poppet can be linear or any desired characteristic. (Ample experience with these valves at Rocketdyne Field Laboratories.)	Unbalanced poppet requires large actuator and large hydraulic oil supply. External split-body leakage may occur in cryogenic service. Small $\frac{c_v}{\text{size}}$ ratio
Balanced-plug angle valve (Fig. 8)	Small stem force. Small actuator. Minimum hydraulic oil demand. Minimum response time. Solid single-body design is a good safety feature. (Some experience was gathered at Santa Susana Field Laboratories which is encouraging from the standpoint of reliability.)	Two internal leakage paths (not necessarily objectionable if a separate shutoff valve exists). Valve seat replacement is difficult unless special treatment of the seat-ring thread prevents galling.

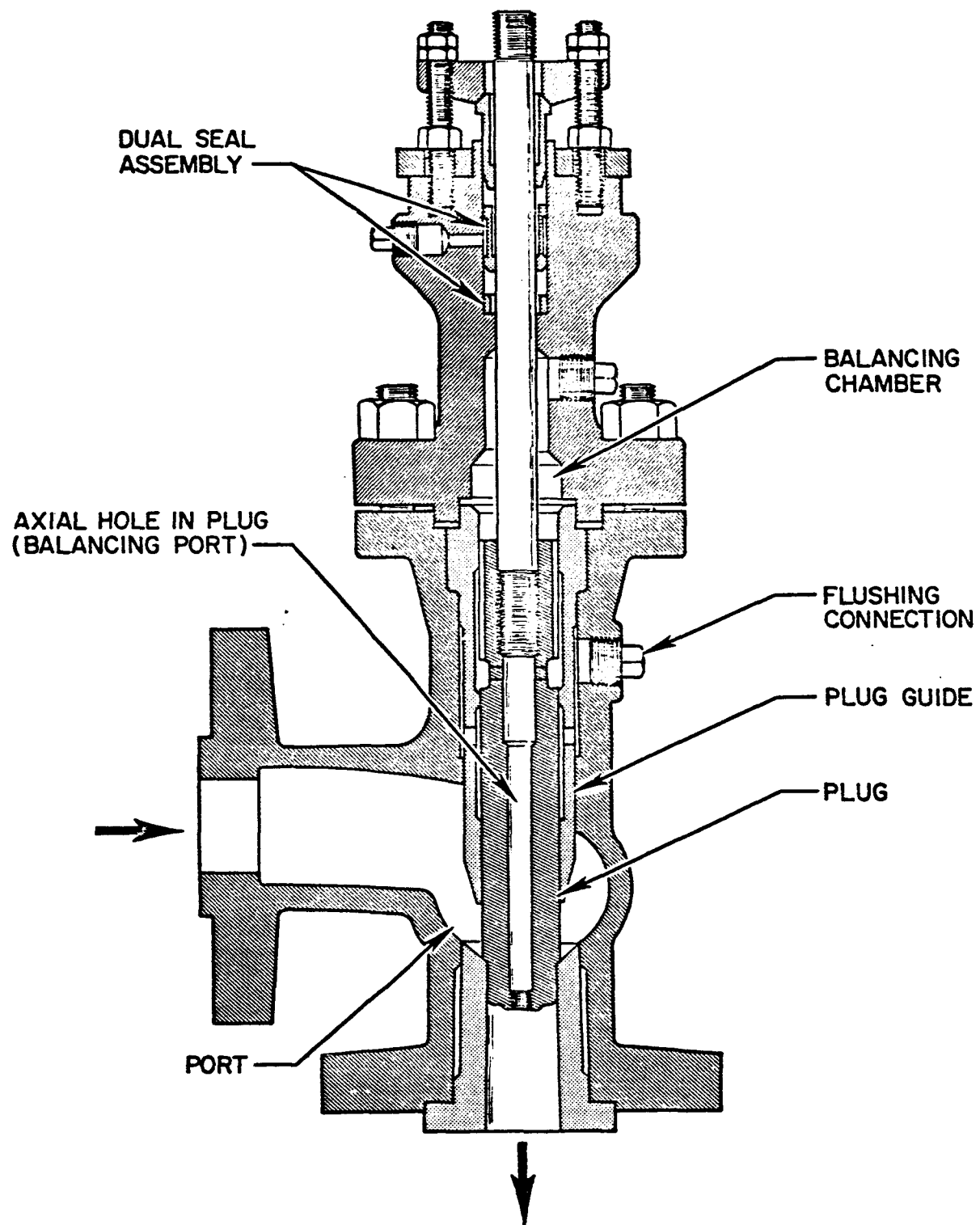


Figure 8. Balanced-Plug Angle Valve

NOMENCLATURE

A	= effective servovalve flow area (supply area equals return area), ft^2
A	= internal cross-sectional area of pressurizing pipe, ft^2
A_A	= annular piston area, near side (rod side), ft^2
A_B	= piston area, far side (no rod), ft^2
A_R	= throat area, modulating valve, ft^2
c	= hydraulic oil velocity in effective area A , ft/sec
C	= discharge coefficient
C	= lump capacitance of pressurizing pipe section
E_o	= controller output voltage
E_f	= valve position feedback voltage
E_t	= tank pressure transducer signal, volt
E_s	= set point voltage
g	= gravitational acceleration 32.2, ft/sec^2
GN_2	= gaseous nitrogen
i_s	= servovalve current, amperes
J_B	= mass momentum of inertia, moving ball-valve parts, $\text{ft lb}/\text{sec}^2$
k	= piston area ratio A_B/A_A
K	= gain
k_1, k_2, k_3, k_4	= proportionality constants
l	= lump length of pressurizing pipe section, feet
l	= length of ball lever arm, feet
l'	= effective ball lever arm, feet
l_T	= total length of pressurizing pipe, feet
L	= lump inertia of pressurizing pipe section
L_3	= hydraulic inertia of tubing between cylinder and servovalve
L_{eff}	= torque motor coil inductance, Henry
M_o	= initial gas mass in ullage, $\text{lb sec}^2/\text{ft}$
ΔM	= increase of gas mass in ullage, $\text{lb sec}/\text{ft}$

n	= number of lumped pressurizing pipe sections
P_o	= initial tank pressure, lb/ft^2 absolute
P_1	= servovalve inlet pressure, lb/ft^2 absolute
P_3	= servovalve return pressure, lb/ft^2 absolute
P_A	= pressure in "near" chamber of cylinder, lb/ft^2 absolute
P_B	= pressure in "far" chamber of cylinder, lb/ft^2 absolute
P_B	= pressure in gas pressure vessel, lb/ft^2 absolute
P_R	= modulating valve inlet pressure, lb/ft^2 absolute
P_s	= hydraulic oil supply pressure, lb/ft^2 absolute
P_t	= tank pressure, lb/ft^2 absolute
P_1, P_2, P_3	= pressure between lumped pipe sections, lb/ft^2 absolute
r	= integer designating first mode and harmonics
R	= gas constant, $\text{ft/}^\circ\text{R}$
R	= lump resistance of pressurizing pipe section
R_1, R_3	= hydraulic resistance of tubings between cylinder and servovalve
R_c	= torque motor coil resistance, ohm
R_s	= servovalve hydraulic resistance
R_{REG}	= modulating valve hydraulic resistance
s	= Laplace transform operator
S	= flow coefficient
t	= time, seconds
T	= average temperature in tank ullage, $^\circ\text{R}$
T_o	= initial temperature in tank ullage, $^\circ\text{R}$
T_L	= load torque (torque exerted on ball-shaft by flowing gas), ft lb
V_o	= initial ullage volume, ft^3
V_s	= servovalve voltage
ΔV	= ullage volume increase, ft^3/sec
\dot{W}_f	= fuel flowrate, lb/sec

\dot{W}	= weight flowrate, hydraulic oil, lb/sec
\dot{W}_{REG}	= weight flowrate through modulating valve, lb/sec
x	= piston stroke, feet
\dot{x}	= piston velocity, ft/sec

GREEK LETTERS

γ	= density, hydraulic oil or liquid fuel, lb/ft ³
θ	= ball angular position, radians
τ	= time constant
ω_r	= resonant mode, radians/sec
ω	= sonic velocity in fluid, ft/sec

REFERENCES

1. "Stability of Non Linear Control Systems by the Second Method of Lyapunov," AFMDC TR-61-6, Air Force Missile Development Center.
2. Pipes, Louis A.: Applied Mathematics for Engineers and Physicists, McGraw-Hill Book Company, Inc., 1958.

GENERAL REFERENCES

1. Beard, C. S.: "Basic Valve Types and Flow Characteristics," Instruments and Automation, 29, 490-502, March 1956.
2. Stoll, H. W.: "Selection of Control Valves Based on Process Dynamics," I.S.A. Preprint. 16-JA-61.
3. Rockwell, R. A.: "Valve Rangeability Instruments," Vol. 25, No. 8, August 1952.
4. Valstar, J. E.: "Sizing Valves for Maximum Flow and Control Rangeability," Control Engineering.
5. Gibson and Tuteur: Control System Components, McGraw-Hill Book Company, Inc. 1958.
6. Blackburn, Reethof, and Shearer: Fluid Power Control, John Wiley and Sons, Inc., 1960.
7. Malkin, I. G.: "Theory of the Stability of Motion," U.S. Atomic Energy Commission, AEC-TR-3352, Office of Technical Services, Department of Commerce Washington, D.C.

CRYOGENIC STORAGE OF HELIUM
FOR PROPELLANT TANK PRESSURIZATION

by
J. S. Tyler
AiResearch Manufacturing Company
9851 Sepulveda Boulevard
Los Angeles, California

SECTION I

INTRODUCTION

This paper has been prepared in response to many inquiries regarding the application of cryogenic helium storage to propellant tank pressurization systems. The high weight penalties associated with conventional helium storage systems have prompted the development of a Supercritical Helium Storage and Supply System for this application.

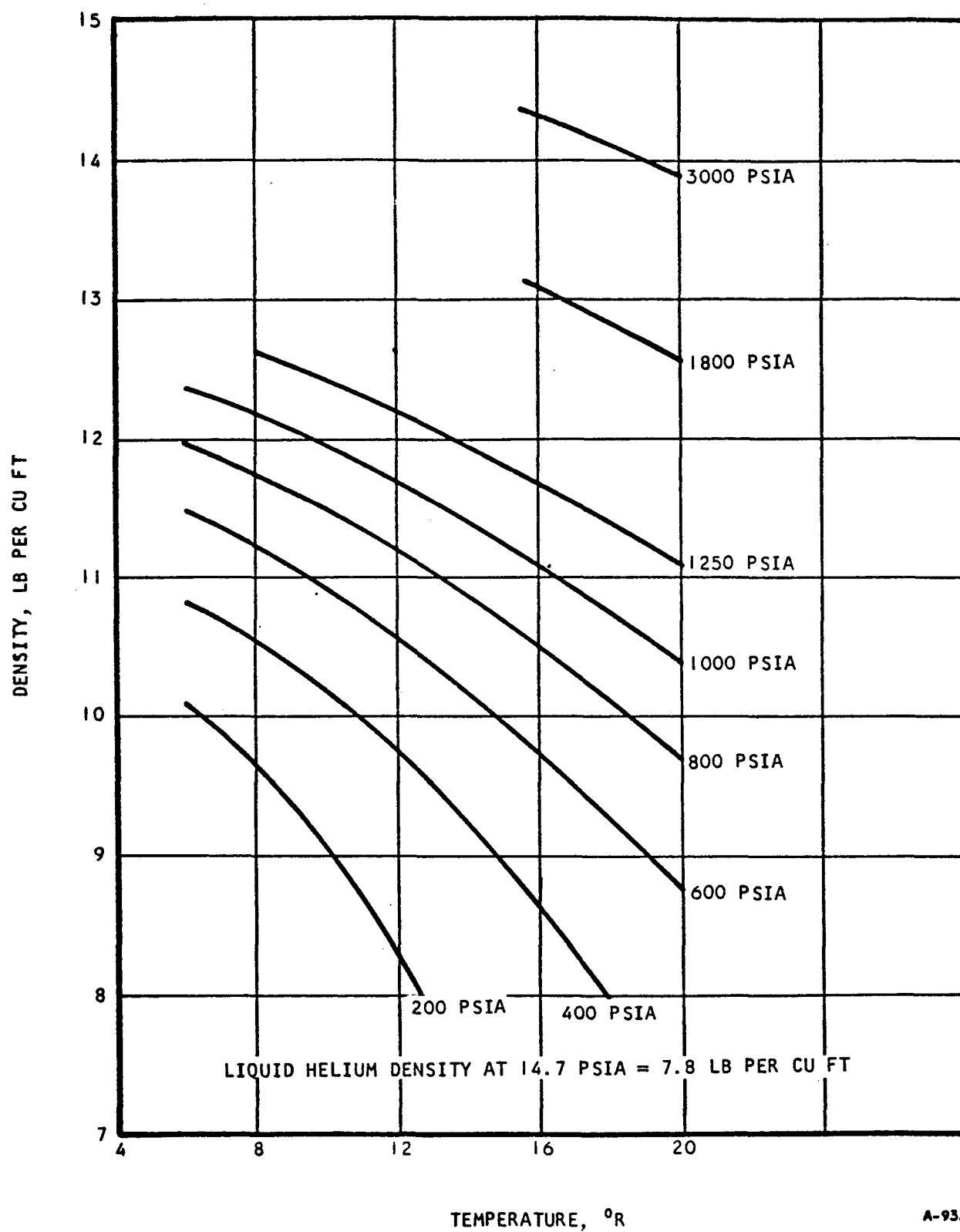
Storage of helium at extremely low temperatures and supercritical pressures yields fluid densities much greater than the liquid density. Figure 1 shows the range of densities possible with the supercritical helium concept. The fluid density selected for an optimized system is dependent upon the mission requirements. During both storage and fluid delivery, the helium is a single-phase fluid; thus, no two-phase problems are encountered during operation.

To date, missile and space vehicle propulsion systems have used either high-pressure gas storage or the more advantageous method of immersing the high-pressure storage vessel in a low-temperature propellant in order to increase densities and thus reduce weight penalties. This latter concept is limited, however, to applications in which a cryogenic fluid is utilized as the spacecraft propellant. Combining the advantages of both storage techniques, supercritical storage can provide the low tankage weight and volume possible with the cryogenic immersed-storage concept for applications where cryogenic propellants are not used or where immersion is not considered practical. Figure 2 provides a weight penalty comparison for the various helium storage systems.

Recent investigations have been made of helium storage requirements for cryogenic helium vessels leading to minimum weight and volume penalties. To maintain the required cryogenic helium temperatures, it is necessary to store the fluid in a vacuum-jacketed, superinsulated vessel that minimizes heat transfer from the ambient environment to the low-temperature helium. Recent state-of-the-art advances in flight-weight, high-performance cryogenic storage systems have made this achievement possible.

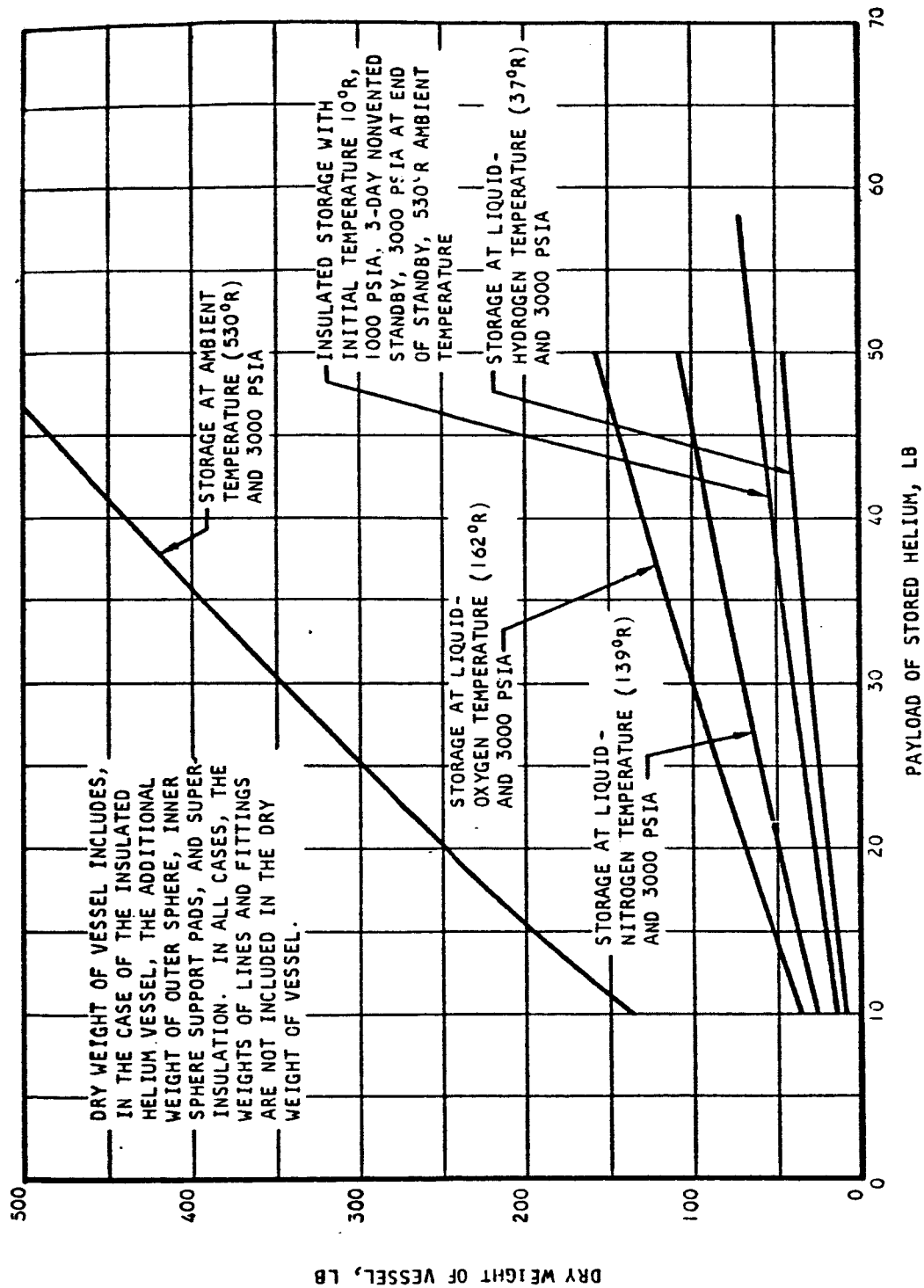
The concept described herein should thus be of interest to designers of propulsion systems for present and future spacecraft of extreme complexity for longer-duration missions, in which cryogenic propellants are not anticipated and the weight penalties associated with high-pressure gas storage are intolerable.

The balance of this report concerns a typical system and its operation. Emphasis is placed upon the fundamentals and techniques involved in design of a supercritical helium storage vessel.



A-9328

Figure 1. Helium Density



A-4945

Figure 2. Dry Weight of Vessel vs Payload of Stored Helium for Various Storage Temperature Conditions

SECTION 2

DESCRIPTION AND OPERATION OF SUPERCRITICAL CRYOGENIC-HELIUM STORAGE VESSELS

DESCRIPTION

A simplified schematic of a typical insulated vessel for supercritical cryogenic helium storage is shown in Figure 3. The vessel consists of concentric, spherical inner and outer shells, each fabricated from titanium alloy hemispheres welded together in an inert gas atmosphere. Five semirigid fiberglass support pads serve to separate the inner from the outer sphere. The annulus between the inner and the outer spheres is filled with a super-insulating material such as aluminized Mylar and is evacuated to approximately 10^{-5} mm Hg. Although for simplification the connections between the inner and outer spheres are shown as straight lines in Figure 3, they would actually be routed through the insulation to give a long heat-leak path. The lines are fabricated from titanium, which has exceptionally low thermal conductivity. The internal heat exchanger, located inside the inner sphere, consists of a tube attached to a copper sphere, which provides the extended surface required for efficient heat transfer.

OPERATION

A specially designed ground fill system is required to fill the cryogenic storage vessel. The ground fill system is capable of supplying liquid helium and high-pressure gaseous helium at 10°R or lower. Using the ground fill system, the flight vessel is first filled with liquid helium and then pressurized with 10°R high-pressure helium to the predetermined design fill pressure; maximum density storage is obtained by this method. The temperature and pressure measurements will indicate when the fill density is attained.

When the fill is completed, the storage vessel enters the standby phase. Standby is defined as the time between vessel fill and when fluid delivery will first be required. During standby, ambient heat leak through the vessel insulation and connecting lines causes the fluid storage pressure to rise. When the maximum storage or vent pressure is attained i.e., 3200 psi, further pressure buildup is prevented by venting through the high-pressure relief valve.

Helium delivery is started by opening the solenoid-operated shutoff valve. As fluid is withdrawn from the storage vessel, it passes through the external heat exchanger (No. 1) and the helium temperature is raised to approximately 500°R . The liquid propellant is an excellent heat source for this purpose. From the external heat exchanger, the warm helium enters the bypass control valve, where it is either diverted through the vessel internal heat exchanger or delivered to the supply line. The bypass control valve diverts the warm helium into the internal heat exchanger whenever the operating pressure drops below the operating pressure band. The warm helium gas flowing through the internal heat exchanger has the effect of warming the stored fluid in the

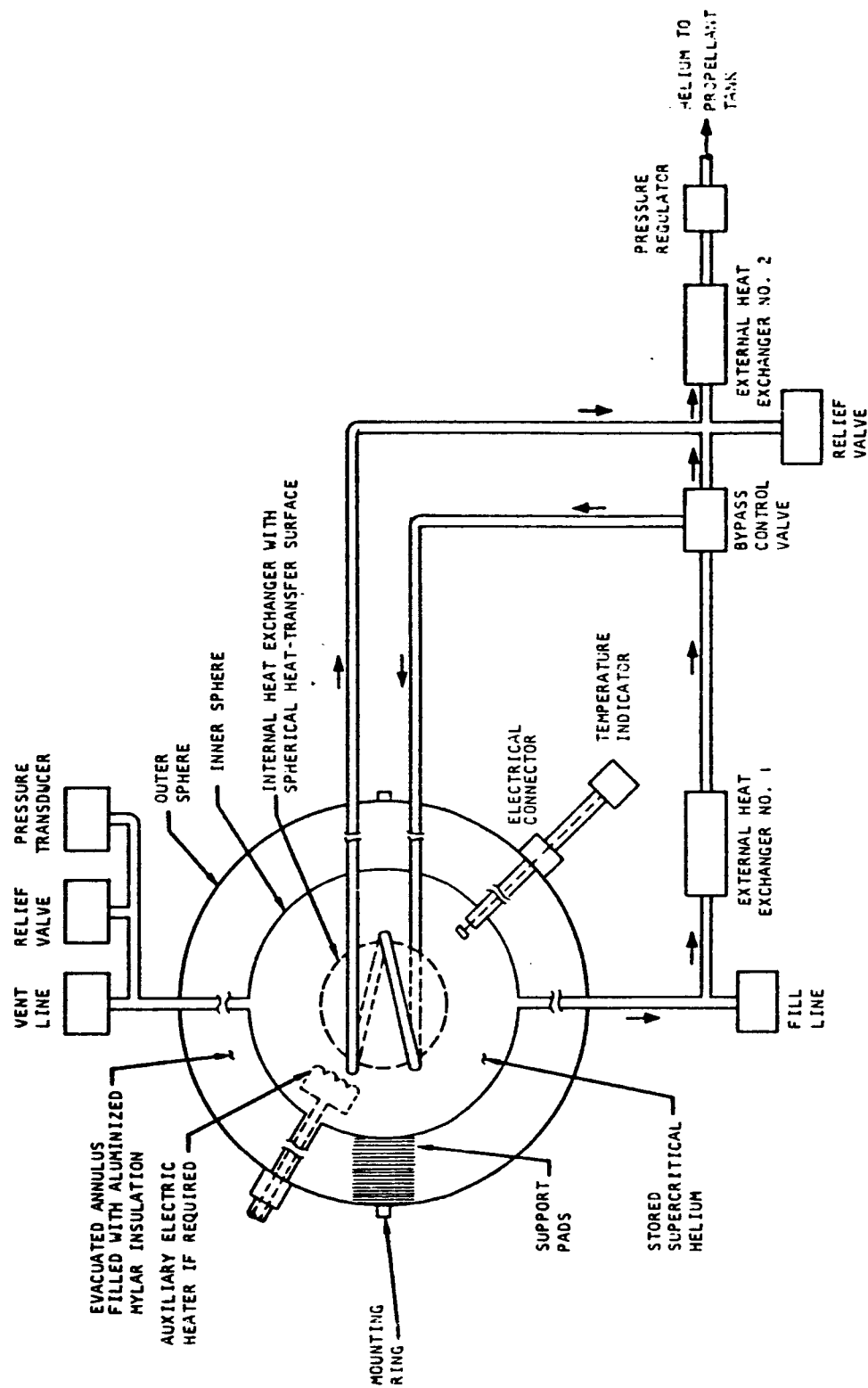


Figure 3. Simplified Schematic of Typical Supercritical-Helium Insulated Cryogenic Vessel

vessel and increasing the storage pressure. The cooled helium gas leaving the internal heat exchanger then passes through the external heat exchanger (No. 2), where it is again warmed to a suitable delivery temperature. Once the operating or storage pressure increases to the desired level, the bypass control valve directs the helium straight to the supply line, in certain designs, the bypass control valve can be eliminated, and all the delivery fluid is passed through the internal heat exchanger. The system pressure regulator controls the gas discharge pressure to the desired delivery pressure.

SECTION 3

TECHNICAL DISCUSSION

GENERAL

The design of a supercritical storage vessel falls into four general categories: thermodynamic design, heat-transfer considerations, structural and material considerations, and general design and weight optimization. Each of these areas must be carefully considered in order to design a minimum-weight, highly reliable pressurization system consistent with the most stringent design objectives.

This report considers only spherical vessels, because they represent the lightest configuration. The qualitative conclusions, however, are applicable to many other configurations.

THERMODYNAMIC DESIGN

The thermal design objective for a supercritical storage system is to provide an adequate insulation system that will enable the fluid to be stored for a specified standby period. Standby refers to the period after filling and capping, before delivery of the stored fluid is initiated. Two basic methods may be employed for accomplishing this objective.

The first method, nonvented standby, consists of filling the vessel with the amount of fluid required to accomplish the mission and designing the insulation so that the amount of heat transferred to the helium during the specified standby time does not exceed that amount which would cause the pressure to rise to the maximum allowable pressure before the pressurization system is operated.

In many instances where the standby time requirement is very long, it may be more feasible to fill the vessel with more fluid than would normally be necessary to meet mission requirements. The helium pressure is allowed to build up, and then the excess fluid is vented until the system is required for pressurization usage; this method is called vented standby. This concept should be used when the weight of the vented fluid combined with any resultant increase in tankage weight is less than the weight of the additional insulation that would be required to meet the nonvented standby requirement. The use of

vented standby, with the associated possibility of using the vented fluid to remove heat that is being transmitted through the insulation by means of a vapor cooled shield, will not be discussed further in this report. This method should be considered, however, when it is desirable to provide cryogenic helium storage for long-duration standby.

Fundamental Thermodynamic Equations

The thermodynamic characteristics and the resultant heat input and insulation requirements are determined by application of the first law of thermodynamics. For this development, the thermodynamic system considered consists of the mass of stored fluid at any time. The first law as applied to this system can be written as:

$$dE = \underline{q} - \underline{w} + E_a dm \quad (1)$$

where \underline{E} = total internal energy of the fluid in the vessel

\underline{q} = infinitesimal quantity of heat input to the system

\underline{w} = infinitesimal quantity of work

E_a = internal energy of the exit stream

m = total stored mass

Differentiation of the relation between enthalpy and internal energy results in:

$$dE = dH - PdV - VdP \quad (2)$$

where \underline{H} = total enthalpy

\underline{V} = total volume

P = vessel pressure

The work term in Equation (1) is given by:

$$\underline{w} = PdV - P V_a dm \quad (3)$$

where PdV = the work performed by the stored fluid due to a volume change.

$PV_a dm$ = the work performed on the fluid exiting from the vessel

Subscript "a" = the fluid properties of the exit stream in the event they vary from the state of the stored fluid mass

Combining Equations (1) and (3) results in

$$\underline{q} = dH - VdP - H_a dm \quad (4)$$

This equation can be integrated for evaluation of finite changes. For the case of a constant-volume storage vessel, the integrated form is

$$\underline{Q} = \underline{H}_2 - \underline{H}_1 - \underline{V} (P_2 - P_1) - \int_{m_1}^{m_2} H_a \, dm \quad (5)$$

where \underline{Q} = the quantity of total heat input over the finite time interval.

Equation (5) is the form of the first law that is most useful for design purposes.

Basic Considerations

For the case of nonvented standby, the mass of the stored fluid does not change, and Equation (5) becomes

$$\underline{Q} = \underline{H}_2 - \underline{H}_1 - \underline{V} (P_2 - P_1) \quad (6)$$

Due to the relationship between internal energy and enthalpy ($\underline{E} = \underline{H} - PV$), this equation can be written as

$$\underline{Q} = \underline{E}_2 - \underline{E}_1 \quad (7)$$

When put on a differential rate basis, Equation (7), can be written as

$$d\theta = \frac{d\underline{E}}{\underline{\dot{Q}}} \quad (8)$$

which, upon integration, yields

$$\theta = \int_{\underline{E}_1}^{\underline{E}_2} \frac{d\underline{E}}{\underline{\dot{Q}}} \quad (9)$$

where θ = the standby time

$\underline{\dot{Q}}$ = the ambient heat leak rate

To perform the indicated integration, the rate of heat transfer to the cryogen $\underline{\dot{Q}}$ must be expressed as a function of the internal energy of the stored fluid. Thus, in principle, a definite tank geometry must be considered and a transient heat transfer analysis conducted to compute the standby time.

In practice, this transient analysis is unnecessary for two reasons. First, the temperature change of the stored fluid during pressure buildup is moderate. Second, due to the characteristics of the terms which constitute $\underline{\dot{Q}}$, the heat transfer rate is only slightly affected by these moderate fluid temperature changes. Taking $\underline{\dot{Q}}$ as an average value, the standby time is given by:

$$\theta = \frac{\underline{E}_2 - \underline{E}_1}{\underline{\dot{Q}}}$$

The amount of thermal protection or insulation required to meet a specified standby time is a function of the initial fill state, the final state at the end of the standby period, and the quantity of fluid contained in the vessel. The total weight of fluid stored differs from the usable weight by the weight of residual fluid remaining in the tank at the end of the delivery period. The determination of residual will be discussed later. In order to maintain a common basis of comparison, all systems discussed in this report, except where specifically stated, will be designated for an initial fluid density of 11.4 lb per cu ft and an initial fill pressure of 1000 psia. The maximum operating pressure will be considered to be 3000 psia. Equation (6) can then be used to determine the total amount of heat transfer allowed, so that the standby time requirement can be met.

The actual fluid-state path followed during withdrawal is dependent on the initial pressure, the energy input to the system, and the flow schedule required to pressurize the propellant. Equation (5) can be used and integrated over the flow rate schedule to solve for the pressure, internal temperature, and time history of the fluid. From this relationship, it can be seen that the residual fluid remaining in the vessel may be calculated as a function of energy input to the fluid. Figure 4 shows a typical withdrawal path for a specified condition. This curve is presented as a typical example and should be used only as an indication of the behavior that may be expected from a supercritical helium system during fluid delivery. It is only after detailed mission requirements are analyzed that an optimum system may be designed to accomplish a particular end application.

HEAT-TRANSFER CONSIDERATIONS

The various modes of heat transfer to the inner vessel and important design features are discussed below. The insulation used is part of a weight-optimized system and must have high thermal efficiency and low weight. The type of insulation that has been shown to be consistent with these requirements, and is often referred to as superinsulation, consists of multiple layers of highly reflective radiation shields separated by a low-conductivity material.

The two promising kinds of superinsulation are: (1) layers of aluminized polyester film and (2) layers of aluminum foil separated by fiberglass paper. The low-conductivity material is the polyester film in the first, and the fiberglass paper in the second. Both of these insulation systems must be used in conjunction with a vacuum level of at least 10^{-4} mm Hg in order to minimize residual gas conduction. Under these circumstances, apparent thermal conductivities of these materials have been found by measurement to have ideal values of approximately 4×10^{-5} Btu-ft per hr-ft²-°R. This apparent thermal conductivity includes heat-transfer effects due to radiation, conduction, and convection (residual gas conduction). With an assumed thermal conductivity of 7.5×10^{-5} Btu per hr-ft-°R, Figure 5 shows the heat-transfer rate through the insulation as a function of the thickness for various vessel diameters.

Heat transfers through lines penetrating the annulus and the intravessel supports also contribute to heat transfer to the helium. These heat leaks can be calculated by Fourier's equation of heat conduction.

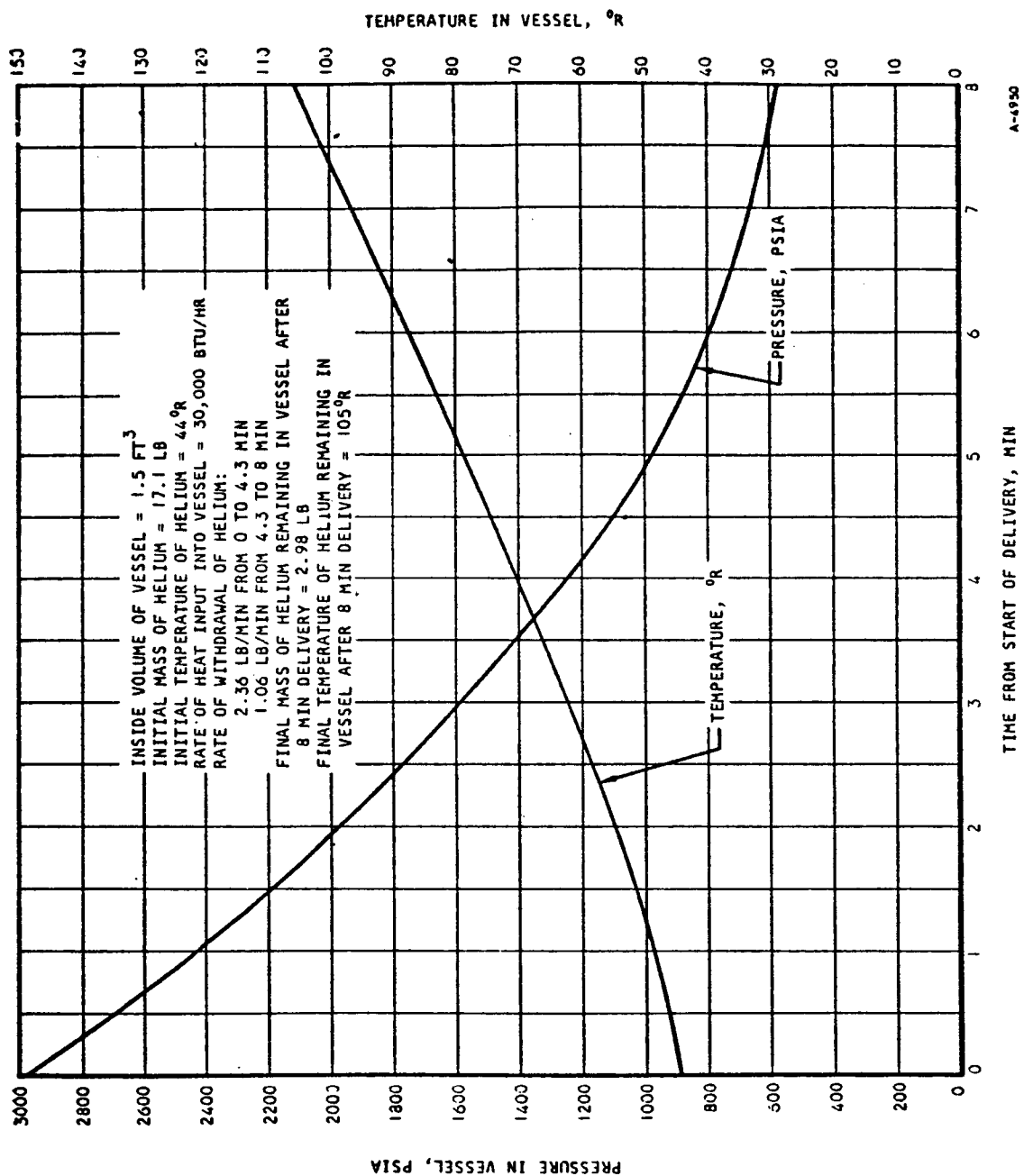
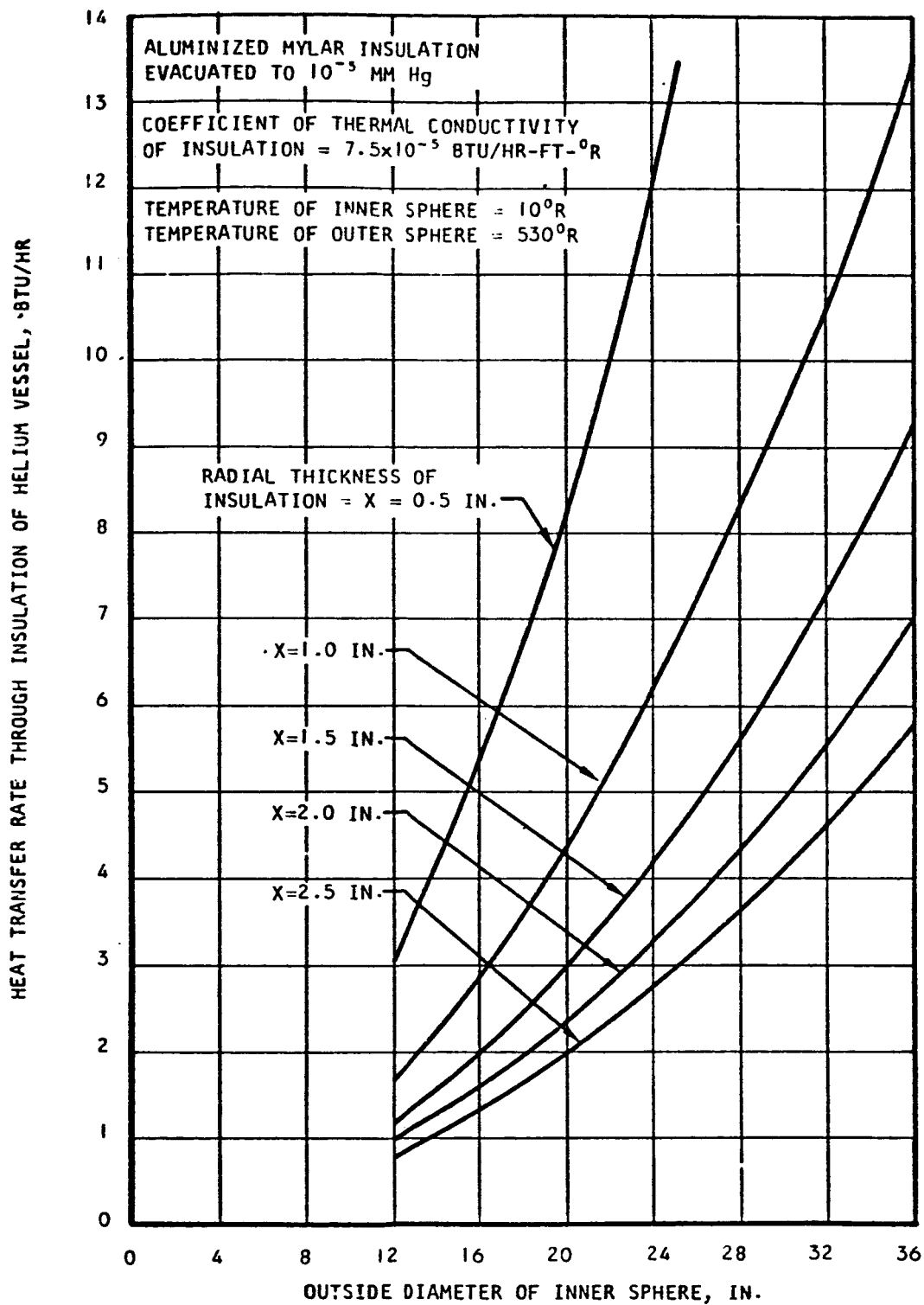


Figure 4. Typical Helium-Vessel Pressure and Temperature vs Time for Rapid Delivery Lasting 8 Min



A-4944

Figure 5. Heat-Transfer Rate Through Insulation of Helium Vessel vs Outside Diameter of Inner Sphere for Various Thicknesses of Evacuated Aluminized Mylar Insulation

As was stated in the previous section, fluid expulsion requires the simultaneous addition of energy. This addition of energy may be accomplished by electrical heat input, by simultaneous electrical heating combined with fluid-to-fluid heat transfer, or by fluid-to-fluid heat transfer alone.

The flow rates usually required for a pressurization system are generally so large that electrical power penalties preclude the use of electrical heating alone as the energy source. Fluid-to-fluid heat transfer is generally the most acceptable method for fluid expulsion. This method consists of the following steps: (1) fluid withdrawal is initiated and the fluid is diverted through an external heat exchanger, which transfers heat to the fluid; (2) the fluid is run back through a heat exchanger that is located inside the storage vessel; (3) the helium then leaves the storage vessel and flows into the propellant tank to initiate pressurization. Waste heat from the spacecraft or from some other heat source must be provided for the external warmup heat exchanger.

VESSEL DESIGN

Typical storage vessels for the supercritical helium consist of two concentric spherical shells separated by an evacuated insulation space. The inner vessel contains the cryogenic fluid at operational pressures and temperatures, and the outer vessel is exposed to ambient pressure and temperature.

An intershell support system is required to transmit loads between the shells. The design of the intershell mounts is extremely critical because a large percentage of the vessel heat leak is normally carried through these supports by direct conduction. The inherent difficulty is that the thermal insulation requirements demand minimal contact area between the tanks, yet large structural loads must be transmitted through the same supports. In addition, appreciable changes in radial clearance between the shells will occur because of the large temperature difference between the inner and outer tanks when cryogenic fluid is stored in the inner vessel. Despite the change in radial clearance, the intershell supports must continue to hold the inner shell rigidly in place without introducing appreciable local stresses. This recurring problem in the design of high-performance cryogenic tanks has led to the development of numerous support devices, ranging from stacked insulated washers to support rings on the inner and outer shells that are connected by rods, wires, or metal bands. These supports have the common disadvantages of intricate fabrication procedures, and transmittal and amplification of dynamic loads to the inner shells.

A novel method of support has already proved successful under severe vibration, shock, and thermal load conditions associated with the Project Gemini program. The annular space is largely filled with a non-load-carrying superinsulation. Support of the inner shell is accomplished by the use of equally spaced, compressed fiberglass pads. With the proper choice of pad density, size, and location, a suitable support can be designed to hold the inner shell for the various environmental shock and vibration loadings which may be encountered. The compressibility of the fiberglass support pads is sufficient to easily absorb the radial-clearance changes due to thermal

effects without loss in holding effect. Precompression of the pads results in an energized (self-strained) structural system. For a given vibratory loading, less cyclic deflection and, consequently, less incremental force is experienced by the supports. The resonant frequency of the inner shell mounting can be tuned by varying the stiffness or the compressibility of the fiberglass support pads; the maximum amplification factor is 2.0 to 3.0 at resonance. The inner shell structure then is isolated from the high g-level vibratory inputs at the high frequencies. Conversely, loadings due to the support pads on the outer shell support structure are materially less than those associated with more rigid inner-shell support methods.

Reinforcement rings are unnecessary for the inner shells. The pad loading on the inner shell is much lower than internal pressure loading, and the influence of pad loading tends to reduce membrane stresses in the shell with little or no bending. Pad precompression loads are designed so that they are low enough to preclude inner shell buckling when the inner vessel is not pressurized.

MATERIAL CONSIDERATIONS

Besides the tensile strength-to-density ratio, the problem of low-temperature brittleness is of critical importance in the selection of materials for cryogenic applications. There are several methods for evaluation of material toughness, often referred to in terms of resistance to brittle fracture (or notch sensitivity); these include determinations of tensile elongation value, notched-to-unnotched tensile strength ratio, energy required to initiate and propagate a crack, charpy V-notch tests, etc. In general, a combination of tensile elongation and notched-to-unnotched tensile strength ratio provides the information for the selection of the most suitable material.

After extensive studies, the titanium alloys Ti-TAl-4V ELI and Ti-5Al-2.5 Sn ELI appear best suited for the inner shells, since they have the highest strength-to-density ratios at cryogenic temperatures. For the outer shell, either titanium or aluminum are considered the best metals. Titanium is generally selected because of better fatigue characteristics and manufacturing compatibility.

WEIGHT OPTIMIZATION

To arrive at the minimum weight design for a supercritical cryogenic tank, it is necessary to investigate all the environmental and performance requirements, the various combinations of design parameters which will meet these requirements, and the effect of these combinations of design parameters on the total tank weight. The requirements fall into the following categories:

- a. Usable fluid weight
- b. Standby time
- c. Buildup time
- d. Delivery pressures

- e. Vibration levels
- f. Acceleration levels
- g. Shock levels
- h. Temperature levels
- i. Electrical power characteristics

In designing to meet these requirements, the following general parameters can be varied:

- a. Fill pressure
- b. Residual density
- c. Fluid weight vented
- d. Percent of initial fill
- e. Vent pressure
- f. Minimum operating pressure
- g. Internal heater on and off pressure
- h. Pressure decay path

Selection of a combination of these parameters will define the details of a tank design which includes the items which contribute to the weight. These details will include:

- a. Fluid fill weight
- b. Internal heater and quantity gauge configuration
- c. Inner shell diameter and thickness
- d. Interwall support configuration
- e. Interwall line configurations
- f. Insulation configuration
- g. Outer shell diameter and thickness
- h. External support configuration

There is a complex relationship between the tank requirements, the general design parameters, and the design details. Generally speaking, a change in one variable will result in changes in many of the design details, and a change in one of the design details will affect conformance to a number of the requirements.

Because these quantities involve such complex interrelationships, a meaningful optimization procedure must treat upon all of them simultaneously. If it were possible to establish an overall functional relationship between the filled tank weight and all the variables, then they could be treated simultaneously by analytical means with LaGrange multipliers. It has not been found possible to obtain such an expression without making unrealistic

assumptions about its form, so that the analysis ceases to have practical value. An alternate method is available which permits these variable to be considered simultaneously without this disadvantage.

The method utilized is based on the use of digital computer techniques, rather than analytical techniques. A program is used that selects the combination of design parameters which result in the lowest total weight, without assuming any parametric relationships between the various quantities. This is accomplished by first determining the total weight for the tank corresponding to selected combinations of design parameters which satisfy the tank requirements and then selecting the combination which yields the lowest total weight. In arriving at these weights, the program considers the fluid thermodynamics, the system heat transfer, the stress analysis of the shells and supports, and the constraints which manufacturing considerations place upon the design. The combinations of design parameters are chosen to cover a range sufficient including all the combinations which might yield the minimum weight tank.

The sequence of operations involved in this program is as follows: A set of design parameters is chosen based on a system which increments the parameters one at a time in a manner to assure that all possible combinations will occur. With this set of parameters, the volume and weight of the fluid fill can be derived. The weight and volume of the capacitance gauge and internal heat transfer surface can then be found. The diameter thickness, and weight of the inner shell can then be determined. These items represent all the weight supported by the fiberglass pads; therefore, the required pad area can then be found.

The allowable heat transfer rate during standby can be obtained from the required standby time, fluid properties, and design parameters being used. With this information, plus the pad area and inner vessel dimension, it is possible to determine the insulation thickness needed to meet the standby requirement. The outer shell diameter is then fixed, and its thickness and weight can be calculated. At this point, the total weight supported by the external ring is known, and the ring size and weight can be found. This defines a tank which will satisfy the standby requirements. The predicted performance of this tank is then compared to the requirements imposed by the mission flow profile. If it does not satisfy these requirements, the program returns to the appropriate point in the previous calculation and redesigns the tank so as to meet these requirements. When a tank has been found that satisfies all of the requirements, its total weight is compared to the total weight of the tanks calculated for different combinations of design parameters. The design parameters for the lightest three tanks are stored, and the next set of design parameters is chosen; the whole process is then repeated. When all the combinations of design parameters have been considered, the characteristics of the lightest three tanks are printed out. The number of combinations considered can run into the thousands for a complex set of requirements.

Once this minimum weight configuration has been established, the effects of variations in the design parameters can be investigated to determine the weight penalty associated with these changes. This permits tradeoffs involving factors, other than tank weight, to be made in a quantitative manner.